Author:
Plastow, Ian

Title:
The development and application of computational methods for the design of aircraft fuel systems.

UNIVERSITY OF BRISTOL
DEPARTMENT OF AEROSPACE ENGINEERING

THE DEVELOPMENT AND APPLICATION OF COMPUTATIONAL METHODS FOR THE DESIGN OF AIRCRAFT FUEL SYSTEMS

Ian Plastow BEng

July 1994

A thesis submitted to the University of Bristol in accordance with the requirements for the degree of Doctor of Philosophy in the Faculty of Engineering

DEDICATION

This thesis is dedicated to Michelle my wife, and the memory of Peter Plastow my father.

TABLE OF CONTENTS

LIST OF TABLES

LIST OF FIGURES

SUMMARY

Aircraft fuel systems have traditionally been analysed and designed using graphical methods and relied heavily on test rigs for flight clearance. Even with the advancements of the aircraft fuel systems themselves the methods of design and analysis have changed little from those used on early aircraft. This research considers the analysis and design of aircraft fuel systems using computational methods through the application and development of commercial software. Three software packages have been selected and used throughout this research. Flowmaster and Bath*fp* network analysis packages which provide a means of analysing the fuel system for both steady state and dynamic operation. Star-CD a Computational Fluid Dynamics package which provides a means of modelling the operation of individual components. A programme of testing of combining 'Y' junctions has also been undertaken. This testing serves two purposes. It provides a means of validating Star-CD to the modelling of component losses, particularly combining 'Y' junctions, and allows data available on combining 'Y' junctions to be extended to included angles of 30°.

Consideration is given as to how Flowmaster and Bath*fp* model the components and conditions which are specific to aircraft fuel systems, or have a specialised application for aircraft fuel systems. Development of component models and methods within this research to enable aircraft fuel systems to be modelled by Flowmaster and Bath*fp* are presented.

The application of Flowmaster, Bath*fp* and the models developed within the research to the modelling and simulation of aircraft fuel systems is considered. A design procedure for aircraft fuel systems detailing the application of the three selected packages is presented.

The thesis is concluded with two case studies which illustrate the application of the three software packages to the simulation of aircraft fuel systems. These studies illustrate points made throughout the thesis.

The application of computational methods, and particularly the three selected software packages, to the design and analysis of the aircraft fuel system enables a greatly increased number of analyses to be undertaken in a reduced time scale. All three packages have shown good comparison of results to both test rig and flight data. Ultimately the application of computational methods to the design and analysis of aircraft fuel systems should result in a better quality, safer design, at a reduced cost.

ACKNOWLEDGEMENTS

Dr. D. A. Cowling for supervision of this project.

Dr. R. Stirling (formerly of Bristol University) for supervision at the start of this project.

British Aerospace Airbus Ltd., Fuel Systems Engineering Group.

British Aerospace Airbus Ltd., Systems Laboratory, in particular Messrs N. Shufflebotham and M. Purdie (now at British Aerospace Military Aircraft Ltd.), for their invaluable help with the test programme.

Dr. C. W. Richards of the Fluid Power Centre, The University of Bath, for his guidance on the development of models.

Mr. D. S. Miller of British Hydrodynamic Research (BHR), for his advice on the test programme.

The work reported herein was supported jointly by the Department of Trade and Industry and British Aerospace Airbus Ltd., Filton.

DECLARATION

The work presented herein was carried out solely by the author, under the supervision of Dr. D. A. Cowling, at the Department of Aerospace Engineering in the University of Bristol, in partial fulfilment of the requirements for the degree of Doctor of Philosophy.

The ideas and results are original except where otherwise acknowledged or referenced, and no part of this work has been submitted previously to any University, College or other academic institute.

The views expressed herein are those of the author and not of the University of Bristol.

Ian Plastow

NOMENCLATURE

A	Cross-sectional Area	m^2
A	Intercept of polynomial equation	
a	Acoustic velocity	m/s
B	First order constant of polynomial equation.	
C	Second order constant of polynomial equation	
C_d	Discharge coefficient	
D	Diameter	m
D	Third order constant of polynomial equation	
d	Diameter	m
E	Youngs Modulus	N/m^2
e	Wall Thickness	mm
f	Friction factor	
g	Gravitational constant	m/s^2
H	Total Head	m
H^*	Normalised pump head	
h	Static pressure	m
h_1	'Y' junction leg 1 inlet static head	m
h_{13}	'Y' junction static head loss leg 1 to 3	
h_2	'Y' junction leg 2 inlet static head	m
h_3	'Y' junction leg 3 outlet static head	m
K	Bulk Modulus	N/m^2
k	Loss Coefficient	
k_{13}	'Y' junction loss coefficient leg 1 to 3	
k_{23}	'Y' junction loss coefficient leg 2 to 3	

k_b	Branch pipe loss coefficient	
k_f	Forward loss coefficient	
k_i	Inlet loss coefficient	
k_o	Outlet loss coefficient	
k_r	Reverse loss coefficient	
k_{tp}	Through pipe loss coefficient	
l	Linear distance	m
L_1	Momentum Equation applied to Method of Characteristics	
L_2	Continuity Equation applied to Method of Characteristics	
M	Jet pump mass flow ratio	
l	Length scale	
N	Number of reach lengths	
N	Jet pump pressure ratio	
N^*	Normalised pump speed	
n	Nozzle rate of contraction	
P	Total pressure	bar, psi
p	Static pressure	bar, psi
p_i	Inlet pressure	bar, psi
p_{in}	Inlet static pressure	bar, psi
p_o	Outlet pressure	bar, psi
p_{out}	Outlet static pressure	bar, psi
p_{sur}	Surface pressure	bar, psi
Q^*	Normalised pump flow rate	
q	Volumetric flow rate	m^3/s, L/min, igph
q_{in}	Inlet volumetric flow rate	m^3/s, L/min, igph
q_{out}	Outlet volumetric flow rate	m^3/s, L/min, igph
R	Jet pump area ratio	

t	Time	sec
u	Velocity	m/s
u_1	'Y' Junction leg 1 inlet flow velocity	m/s
u_2	'Y' Junction leg 2 inlet flow velocity	m/s
u_3	'Y' Junction leg 3 outlet flow velocity	m/s
V	Volume	m^3, L
V_i	Initial volume of fluid	L
v	velocity	m/s
W_H	Suter head parameter	
W_M	Suter torque parameter	
x	x co-ordinate	
y	y co-ordinate	
z	height	m

Greek

ß	Bulk Modulus of Fluid	N/m^2
γ	Weighting factor	
Δh	Static head loss	m
Δp	Static pressure loss or rise	bar, psi
δx	Distance in x	m
ε	Strain	
η_d	Diffuser efficiency	
θ	Angle from normal	°
θ	Suter pump speed parameter	
λ	Multiplier applied to Characteristic Equations	
ρ	Fluid density	kg/m^3
Σ	Summation	
τ_o	Shear force	N/m^2

Subscripts, Superscripts, Dressings and Primes

.	Time derivative
i,j,k	Definition of CFD cell face positions
d	Jet pump diffuser
j	Jet pump motive flow nozzle
m	Jet pump mixing tube
s	Jet pump suction flow nozzle
1,2	Stations defining pressure and flow rate
30	30∘ 'Y' junction
30a	30∘ 'Y' junction for flow ratios of 0 to 1
60	60∘ 'Y' junction
90	90∘ 'Y' junction
120	120∘ 'Y' junction
150	150∘ 'Y' junction

CHAPTER 1

INTRODUCTION

Aircraft and their fuel systems have advanced significantly from early aircraft when fuel systems simply supplied fuel to the engines and there was little restriction on space and positioning of tanks. With the advancement in aerodynamic design and the introduction of the gas turbine engine there became a requirement for todays aircraft to travel further and faster. As a result, fuel systems have developed considerably from their predecessors. In line with this development has been the tightening of airworthiness safety requirements [1]. Todays aircraft fuel systems can be considered as highly complex fluid networks that not only supply fuel to the engine, but can also provide control of the position of the centre of gravity (cg) of the aircraft, provide wing bending relief and may aid in passive flutter alleviation during normal flight, and act as a heat sink to other systems. Typically a modern large transport aircraft's fuel system will contain in excess of thirty control valves, fifteen pumps and numerous specialised components, all of which are required to perform in both the heat of a tropical day (54°C) and the cold of the troposphere (–50°C).

Unlike the advancement of the fuel systems themselves, the methods of design and analysis have not advanced in the same manner and the methods of today are similar to those used on early aircraft. Research to date has been limited to very specific models that are required to yield results for a limited number of cases. They have been concerned only with analysis of the distribution of fuel and its effects on aircraft centre of gravity (cg) [2,3], and analysis of fuel temperatures [4,5]. None of the above development activities have been concerned with the modelling of the aircraft fuel system with respect to its pressures and flow rates.

The design of fuel systems currently relies heavily on experience gained from earlier aircraft programmes and test rig results. The analysis to verify the operation of the design has been based around steady state graphical methods. These methods are adequate for simple systems with a steady state response. When the size and complexity of today's aircraft fuel systems are considered, together with their analysis requirements, the application of these graphical methods is severely stretched. The number of analyses required to verify the system, both from an operational and safety point of view, are now very large. There is now an increasing requirement for the use of dynamic analysis of these systems, and the application of graphical methods to dynamic modelling is impractical.

Fuel system components are rarely available 'off the shelf', due to the stringent safety requirements and extremes of operation. Often the only performance data available is limited data from supplier testing. For some components, such as complex shaped junctions, this

performance data is not even available. In these circumstances the only means of obtaining this performance data is by costly rig testing, or approximating from other known components.

Thus, the need for a means of analysing the operation of the fuel system and the performance of components more efficiently and accurately is quite clear. The most efficient and accurate means are computational methods. In the past, the use of computational methods has not been possible due to the limited computing power available. With the recent advancements in computing this is no longer the case. This research has been undertaken to develop methods and procedures appropriate to the design and analysis of aircraft fuel systems [6,7].

The aim of this research is to provide the fuel system design engineer with a set of tools and methods which enable detailed design and simulation of the fuel system prior to testing and flight. These are divided into two types. Network analysis which provides a means of analysing the fuel system for both steady state and dynamic operation. This will ultimately lead to the modelling of the fuel system during a complete flight. The second type, component modelling, provides a means of evaluating the performance of the individual components, which will then be used within the network analysis methods.

Application of these tools enables analysis of the system to be carried out in a greatly reduced time scale, thus cutting the development time from concept to first flight. Through the use of simulation the fuel system design engineer will gain an increased understanding of the system's performance and be able to investigate different design alternatives. Ultimately this should result in significant cost savings plus an improved, safer design.

From the outset it was decided to base the research around commercially available software. This decision was made for a number of reasons. Firstly the methods and procedures developed from this research are to be used in an industrial design environment. As such they require a simple, yet comprehensive, user interface, so that the computational methods themselves do not hinder or obscure the design and analysis. This is best achieved with commercial software, which requires these features for it to be viable. Secondly, the use of commercial software takes advantage of the investment and knowledge incorporated in the software, particularly the user interface and component libraries. Thirdly, commercial software packages are flexible by nature and this is the requirement to model the diversity of operation and design for different aircraft types.

Structure of Thesis

The thesis begins by explaining the operation and characteristics of the various sub-systems which make up an aircraft fuel system. This is the basis of Chapter 2.

Chapter 3 considers network modelling. Throughout this research two analysis packages, Flowmaster and Bath*fp* have been used. This Chapter introduces these packages and explains the reasons for their selection. It gives a limited description of the theory used in each package and briefly describes their operation. The Chapter concludes with a summary of the various attributes and limitations of each method.

Chapter 4 considers component modelling. It outlines the various methods available for modelling components, and considers in more detail the application of Computational Fluid Dynamics (CFD). The CFD package used throughout this research, Star CD, is introduced, and a brief outline of its theory and operation given.

As part of this research a programme of testing of combining 'Y' junctions was undertaken. Chapter 5 contains the results of this work. The testing serves two purposes. It enables the data available on combining 'Y' junctions to be extended down to included angles of 30°, and provides a means of validating Star-CD for modelling component losses, in particular combining junctions. A description of the test work and the development of the CFD model is given along with a discussion of the applicability of both the test results and CFD results for the 30° 'Y' junction.

Flowmaster and Bath*fp* are the two packages used for network analysis. Chapter 6 considers how these two packages model the various components and conditions of fuel systems. It explains the development of models and methods within this research for the cases where no suitable model is available in the package.

Chapter 7 considers the application of the computational methods to the modelling and simulation of aircraft fuel systems. It considers the suitability of each package to various typical modelling requirements and explains the application of the packages to the design of the fuel system.

Chapter 8 concludes the thesis with two case studies which illustrate the application of the three chosen software packages to the simulation of aircraft fuel systems. They are used to not only illustrate the points made throughout the thesis but also to highlight, by practical example, typical problems that may be encountered.

CHAPTER 2

AIRCRAFT FUEL SYSTEMS

The aircraft fuel system can be defined as all aspects of the aircraft concerned with the storage and use of the fuel extending from the connection of the fuel pipe to the engine and Auxiliary Power Unit (APU).

An aircraft fuel system can be broken down into six main areas of operation.

- Fuel Storage.
- Refuel.
- Engine Feed.
- Fuel Transfer.
- Fuel Recirculation.
- Venting.

In this Chapter the requirements and design of each of these sub-systems is discussed to set the context for the material presented in the rest of the thesis.

2.1 Aviation Fuel

Aviation fuels are required to operate in temperatures which can range from the heat of a tropical country, 54°C, to a temperature of -50°C at 40,000ft and arctic conditions of -20°C.

The most widely used fuel for civil aircraft use is a kerosene based fuel to the American Society for Testing Materials specification ASTM D 1655 JETA. A similar fuel JETA-1 is also in common use and has a lower freeze point. A third type of fuel to the same specification is JETB which has a much lower freezing point but is not in wide usage and is only usually used in arctic conditions. However its use as a secondary fuel must be accounted for. The properties of all these fuels vary with altitude and temperature changes, and the operation of the fuel system and its components must be considered at all possible combinations of fuel, temperature and altitude. JETB can cause many penalties in the design due to its higher volatility at elevated temperatures, in many cases the critical design consideration being 'hot' JETB. Generally for all fuels increases in temperature and/or altitude reduce the performance of the components within the fuel system, and this is most marked with JETB. This is illustrated in Figure 2.1, which shows a typical pump characteristic for JETA at sea level and a temperature of 20°C and the degraded characteristic for JETB at 40,000ft and a temperature of +54°C, thus showing the extremes of performance.

2.2 Fuel Storage

2.2.1 Requirements

The fuel storage system is designed to store the amount of fuel necessary for the sector to be flown and measure the fuel quantity onboard at all times on the ground and in flight. Other possible requirements are the provision in the layout of the tanks for control of aircraft centre of gravity (cg), provide a heat sink capacity for other systems (covered in Section 2.6), supply bending relief and possibly aid in passive flutter alleviation during normal flight.

2.2.2 Tank Arrangements

The position and number of tanks can vary from a single tank in each wing, Figure 2.2, to a multi-tank arrangement, Figure 2.3. These can include more than one tank in the wing, and tanks in the fuselage and the tail plane. The inclusion of these tanks can be solely to increase the capacity and range, or for safety or structural reasons.

2.2.2.1 Wing Tanks

Wing tanks are found on the majority of aircraft and in the case of turboprop and some short range jet aircraft these may be the only type of tanks in use. Generally the wings will be sub-divided into two or more tanks for both safety and aerodynamic reasons. From a safety point of view this is important so that should a tank rupture all the fuel is not lost, or if the fuel in a tank becomes contaminated (for example with hydraulic fluid) the contamination is contained. Aerodynamic considerations can lead to the inclusion of a small outboard tank to allow for bending relief due to the aerodynamic forces causing an upwards bend on the wing tip. Ideally, the volume of these outboard tanks will be equal to the mandatary fuel reserves: bending relief is then supplied throughout the majority of flights. Provision can also be made to aid in passive flutter alleviation during normal flight with similar methods.

Wing tanks contain large volumes of fuel with large surface areas and small heads. Changes to aircraft attitude can cause movement of large quantities of fuel resulting in trim changes. Adequate baffling is required to restrict this movement sufficiently, yet allow the fuel level throughout the tank to remain constant. In the case of very large delta planforms, such as Concorde, unrestricted movement can cause structural failure and thus extensive subdivision of the tank is required. In the case of Concorde, subdivision into thirteen tanks was used, Figure 2.4.

2.2.2.2 Centre Tank

Centre tanks are generally positioned in the fuselage between the wings and are of a single tank construction. They can be extended to the belly fairings between the fuselage and wing when additional fuel capacity is required. They are usually found on long haul aircraft and are sometimes optional on medium haul aircraft to increase their range for intercontinental routes. Fuel from the centre tank is generally available to feed all engines. The engine feed system is usually arranged such that the centre tank fuel is the first to be depleted, because it is not used to aid the structural or aerodynamic characteristics of the aircraft. The fuel from the centre tank can be fed direct to the engines or transferred into engine feed tanks.

2.2.2.3 Trim Tank

When fitted, a trim tank is generally positioned in the tail plane, although it may be positioned in the fin as on the Super VC10. The additional capacity is not usually required to meet range performance, the fuel only being used for trim purposes where the additional moment arm of the fuel enables the negative incidence of the tail plane to be reduced.

2.2.2.4 Surge Tanks

Surge tanks are connected into the vent system and retain fuel spilling through the vent pipe, either at refuel overflow or during taxiing as explained in Section 2.7.

2.2.2.5 Additional Centre Tanks (ACT)

These tanks are generally placed in cargo bays, so reduce the cargo that can be carried. They are designed to fit into the space of standard cargo containers. They are not usually fitted as standard but at a customers request where range is more important than cargo capacity. The ACT's do not feed the engines directly but transfer their fuel into the other tanks as required.

2.3 Refuel

2.3.1 Requirements

The refuel system is required to fill all, or a specified number of the aircraft fuel tanks within a designated time, whilst maintaining system pressures below a value to ensure structural integrity. The time for refuel can vary from aircraft to aircraft but generally, for a commercial jet airliner is approximately thirty minutes when utilising all refuelling points.

2.3.2 Refuel System Design

Refuelling is nearly always carried out under pressure to enable the tanks to be filled in a specified period. The refuel rates of the individual tanks are designed so that each tank requires a different time to fill. This is because the quantity of fuel on board is dependent on the sector to be flown, and the distribution of the fuel to the tanks is dependent on the total quantity on board. This is illustrated in Figure 2.5 where the horizontal axis represents the total fuel mass on board and the vertical axis the mass of fuel in each tank. To achieve the required fuel distribution for all flight sectors the aircraft will have a phased refuel based on the distribution of Figure 2.5.

The quantity of fuel required for each tank is set either manually or by the aircrafts fuel computer (Section 2.8), and the tank inlet valves shut off when this quantity is reached. If the tank is being filled to capacity, a high level sensor may be used to shut the valve. In modern aircraft valve shut off is usually controlled by the aircraft's fuel computer (Section 2.8). The valve closure time is set between two and five seconds to keep any pressure surge to a minimum.

Hydro-carbon fuel can build up an electrostatic charge during distribution, so care is taken in the design of the refuel system to keep this to a minimum. Anti-static additives are commonly used, and these though not mandatory, reduce the ability of the fuel to maintain the charge. Electrostatic charges can also occur in fuel mist, and the charge is greatly increased by agitation of the mist. It is therefore important to ensure that the fuel is not sprayed into a tank. Too aid in this, the fuel usually enters the tank through diffusers (Figure 2.6), these are specialised components which allow the flow to enter the tank with the minimum of spray. This is achieved by the fuel exiting the diffuser through the large base area hence with a low flow rate and less tendency to cause spray. To further aid in reducing spray the diffusers are usually placed at low points in the tank so are quickly submerged. The diffusers may also be placed a distance apart (Figure 2.7), allowing any charge in the fuel on entering the tank to disperse before the two flows meet.

2.3.3 Refuel System Arrangements

There are two systems which can be used to distribute the fuel to the tanks, one using a refuel gallery and the second a manifold at the coupling, as illustrated in Figure 2.8. Refuel galleries have the advantage of requiring the minimum number of pipes and valves but can suffer from surge pressures, though these are reduced in magnitude due to the valve closure times outlined in Section 2.3.2. Manifold couplings do not suffer from surge pressure problems because the tank inlet valves are usually located near the refuel coupling, but require duplication of the system when couplings are on both sides of the aircraft as shown Figures 2.8b.

2.3.4 Refuel Coupling

The refuel coupling on the aircraft is of an international standard and nominally 2½" diameter. The refuelling hose is connected to the coupling by a bayonet type connection, which once connected allows self sealing valves on the aircraft and hose to be operated. These valves must be closed before the hose is disconnected, to prevent spillage of fuel.

The number of refuel couplings are to an extent dependent on the size of the aircraft. Large aircraft such as the Airbus A340 and Boeing 747 will require up to two couplings to achieve refuel within a reasonable time, but smaller aircraft such as the Airbus A320 or Boeing 737 will be adequately served with a single coupling. The aircraft is designed with a refuel coupling(s) on one side only, but the majority of airlines specify couplings on both sides for flexibility of operation.

2.3.5 Ground Equipment

All ground refuelling equipment supplies fuel to the aircraft at a maximum pressure of 50±5psi. It is required for the valves on the ground equipment to operate quicker than those on the aircraft to prevent pressure surges from the equipment reaching the aircraft. There is no international standard on this, but the large oil companies ensure their equipment meets this requirement so they are not held responsible for damage to the aircraft due to pressure surges from their equipment.

The delivery of this fuel to the aircraft can be from either hydrants on the apron or refuel tankers dependent on the facilities at the airport. Both systems have the necessary equipment to ensure the fuel is supplied to the aircraft at the correct pressure and flow rate.

2.4 Engine Feed

2.4.1 Requirements

The requirement of the engine feed system is to supply fuel to all engines at all times. This is a flight safety function so additional requirements are laid down by the Joint Airworthiness Regulations (JAR) JAR 25 851 to 961 and 991 [1]. The main requirements are summarised below.

- Each engine must have a separate feed system for independence.
- Engine feed to be maintained both during and after five seconds negative or zero gravity (g).

- After an engine(s) loss, all the remaining fuel is to be usable by the remaining engine(s).
- Fuel supply must be maintained to the engines if all normally generated electrical power is lost.
- Engine rotor burst should not destroy the feed system to the other engine(s) or result in the loss of fuel that would prevent the aircraft reaching an airport in the event of a diversion.
- An emergency standby pump shall be provided for each main pump.

2.4.2 Engine Feed System Types

Two principal engine feed systems are in general use to meet the above requirements. The first is a direct feed system with a main feed tank for each engine, and an alternate feed tank for each engine. The second system is a transfer system in which each engine has a single dedicated feed tank, alternate feed being taken from the feed tanks of other engines. In both types of system the feed tanks are generally wing tanks.

The direct feed system has been the preference in the USA, and the transfer system in Europe. Both methods have their advantages and disadvantages. The disadvantages of the direct feed systems are:

- They require a reliable automatic means to switch feed when one tank empties without inducing air.
- If more than one engine is fed from one tank, fuel contamination will affect more than one engine.
- They are heavier and more expensive than transfer systems, requiring additional pumps in the alternate feed tanks.

The disadvantages of transfer systems are:

- If the transfer systems fail there may be a large amount of unusable fuel, or a risk of tank overflow.
- They are more complex than direct feed systems.

2.4.3 Negative 'g' Protection

There are two principal methods of ensuring fuel supply during the mandatory five seconds of zero or negative 'g'. Both methods can be applied to the direct feed and transfer feed systems.

2.4.3.1 Collector Cells

This method is shown in Figure 2.9, in which the pumps are mounted in a collector cell in the main tanks in a position convenient for structural and other considerations such as rotor burst. The collector cell is maintained full, often by one or more jet pumps. The pumps used to supply the engines are simple centrifugal type with the fuel flowing directly into the impeller.

Negative 'g' protection is achieved by the volume of fuel in the collector cell ensuring that the flow to the engines will not uncover the pump inlets during the zero or negative 'g' manoeuvre as shown in Figure 2.9.

If electrical power is lost, feed to the engines is achieved by gravity through the pumps. If the pressure loss of the stationary pump is too great, a by-pass inlet located at the lowest point in the tank may be used. Negative 'g' protection is maintained during electrical power failure as long as the fuel level in the wing is above the top of the collector cell.

Collector cells may not be appropriate for aircraft which require the majority of their reserve fuel to be used for bending relief throughout normal flight. This is because fuel must be kept for both bending relief and to ensure sufficient is present in the collector cell to provide for five seconds of negative 'g' protection. In smaller aircraft this may significantly exceed the required reserve fuel adding to the weight. For this reason collector cells are usually found on large aircraft or smaller aircraft which do not require bending relief throughout normal flight.

2.4.3.2 Remote Entry Pumps

This arrangement is shown in Figure 2.10, in which the pumps are mounted in a suitable position for structural and other considerations, such as rotor burst, with their remote inlets at low points in the tank.

Negative 'g' protection is afforded by the amount of fuel already in the remote inlet pipe allowing the engines to run for the mandatary five seconds. To minimise the time for which inlets are uncovered they are spread fore and aft. The pumps are fitted with a positive reprime element, which enables rapid reprime and feed pipe pressurisation. The air which has entered the feed system is removed by an air release valve which will be designed to operate at any pressure. The design of this valve, shown in Figure 2.11, uses a ball which 'floats' thereby closing the valve when fuel is present.

During electrical power failure, feed to the engines is ensured through a gravity by-pass inlet located at the lowest point in the tank. Gravity feed is not generally provided through the pump, because remote inlets can suffer from icing on the inlet filter of the pipe as there will be no pump agitation at this point.

Negative 'g' protection using remote inlet pumps is complicated by the requirement for a positive reprime element on the engine feed pumps. For this reason they are only usually found on aircraft where collector cells are inappropriate.

2.4.4 Centre Tank Usage

If a centre tank is fitted its fuel is generally used first, because the centre tank fuel is only used to feed the engines and not for structural or aerodynamic reasons. The engine feed can either be taken from it directly, or it can be transferred into the main feed tank. If the centre tank is used to directly feed the engines, the centre tank pumps require greater head than the wing tank pumps to ensure engine feed is taken from the centre tank. This can be achieved using the same pumps in the wing and centre tank, with the wing tank pumps derated with pressure relief valves. Alternatively a different higher rated pump may be fitted.

2.5 Fuel Transfer

2.5.1 Requirements

The fuel transfer system is required to ensure that the fuel is distributed to the correct tanks so that:

- Engine feed tanks are always full.
- Tanks providing bending relief or flutter alleviation are kept full for the maximum possible time.
- The correct quantity of fuel is maintained in the trim tank to ensure the drag of the aircraft is kept to a minimum as described in Section 2.2.2.3.

2.5.2 Fuel Transfer Methods

There are four methods of transferring fuel between tanks:

- Mechanical Pumps.
- Jet Pumps.
- Tank Air Pressure.
- Gravity.

2.5.2.1 Centrifugal Pumps

Centrifugal pumps are only dependent on an electrical supply and easy to control. Although a simple low pressure pump may be satisfactory, usually the same type of pump as is used in the engine feed system is used for commonality, together with some means of derating the

pump. The main disadvantages of mechanical pumps are that they are heavy and expensive, and consume power.

2.5.2.2 Jet Pumps

A jet pump [8,9], Figure 2.12, is a pump which utilises a stream of fluid at a high pressure and flow rate to entrain a secondary fluid. It consists of a nozzle, a suction inlet, mixing tube and generally a diffuser. The primary fluid, commonly known as the motive flow, exits the nozzle into the mixing chamber. On meeting the slower secondary flow, commonly called the suction flow, a dragging action occurs at the boundaries of the two flows, resulting in a mixing of the two flows and momentum transfer. At the exit of the mixing tube the momentum of the two flows should be equal. The diffuser is used to recover static head.

The jet pumps use a bleed of fuel from the engine feed pumps for the motive flow. The capacity of the engine feed pumps is not usually increased for this bleed because they are sized for take off flows so have excess capacity in cruise. The advantages of jet pumps are that they are light, simple and do not require an additional power source. The disadvantages are their very low efficiency, generally not exceeding 35% and their dependence on the engine feed pumps. If these are inoperative, no motive flow is provided so the jet pumps are inoperative, and if demand on engine feed is high the jet pump performance degrades.

2.5.2.3 Gravity Transfer

This is a very simple system when the difference in heads is adequate to provide sufficient flow. There are a few possible problems to be aware of when using such a system.

- Transfer may not be possible at all attitudes, particularly in climb.
- The transfer rate will change as the delivery tank empties, particularly if the majority of the head difference is in the tank.
- If the two tanks are not connected to the same vent system, the air pressure can either increase or even decrease to an extent which will prevent fuel transfer.

Gravity transfer is commonly used for transfer of fuel from the trim tank to centre tank, and the outer wing tank to inner wing tank.

2.5.2.4 Tank Pressure Transfer

This method uses differential air pressure in tanks to transfer the fuel. It is not very often used within civil aircraft, but is very common in military aircraft. Its only application in civil aircraft is for transfer of fuel from additional centre tanks (ACTs) since it is neither convenient

or advisable to run power supplies. The ACTs are within the pressure hull of the aircraft so there internal pressure is kept below cabin pressure to minimise the risk of leakage. However the ACT is pressurised above the pressure of the tank they are transferring to. The air to pressurise the tank is taken from either the pneumatic system or directly from the cabin air with appropriate reduction of pressure.

2.6 Fuel Recirculation

2.6.1 Requirements

The requirement of the fuel recirculation system is to cool the Integral Drive Generators (IDG) oil with the engine feed fuel flow, and return any excess fuel used for cooling to the tank. The return flow to the tank will be controlled to ensure the temperature of the fuel remains within safe limits both during return and within the tank.

2.6.2 Operation of Recirculation System

Cooling of the IDG's on a modern commercial aircraft is achieved by using either air or fuel. The use of air cooling is costly in terms of drag and additional weight, whereas cooling by fuel recirculated to the tanks requires additional control of the temperature of the fuel. However in many cases this is preferred to the increase in drag.

Cooling is achieved by passing the fuel to the engines through a heat exchanger to allow the IDG oil to cool. The flow rate to the engine will be adequate to cool the IDG during take off but may be marginal for cruise conditions. At flight idle and during a long taxi out, when the fuel will be hot, the flow rate will be insufficient to provide the cooling required. At these times the flow rate to the engine is increased to allow the IDGs to cool and the excess flow is returned to the tanks. The returned fuel can be up to a temperature of 100°C which is around the limit for aluminium structures. Provision is therefore made to mix this with the colder fuel, and monitor and control the temperature by cycling the fuel recirculation on and off if required. The system will be designed for cooling with maximum electrical load on a long taxi out in hot climate.

2.7 Fuel Venting

2.7.1 Requirements

The requirements of the vent system are summarised below.

- To allow air to enter and leave the tanks without exceeding the pressures allowable in the tanks from structural or fuel system considerations. This is

to be achieved with the tanks filled to the required capacity and without spillage of any fuel in all normal operating conditions of aircraft attitude and acceleration.

- To prevent excessive pressure in the tanks in the event of refuelling systems or transfer systems failing to stop the flow at the required level.
- To discharge fuel safely from the aircraft should an overflow occur.
- To prevent ignition of vapour at the tank outlet propagating to the tanks.
- To maintain near equal pressure distribution in all tanks, and to allow fuel to move freely on change of attitude.

The following are secondary requirements.

- To prevent tank over pressure due to an internal pipe failure.
- To provide some tank pressurisation to reduce fuel vaporisation or assist the engine feed system when all pumps have failed.
- To ensure no spillage due to the accelerations experienced during a crash.
- To minimise fuel spillage during zero or negative g conditions.

2.7.2 Vent System Design

The vent system consists of a series of pipes connecting each tank to the atmosphere via the surge tank. The outlet from the surge tank is usually a flush fitting NACA intake designed to resist icing, Figure 2.13. This intake produces a small amount of ram air pressure (about 0.25psi in cruise) providing a small amount of tank pressurisation.

An adequate number of vent pipes have to be provided in each tank to ensure they are adequately vented to maintain pressures within structural limits. With changes of attitude and wing bend from ground to flight conditions vent inlets become covered in fuel, particularly when the tank is full, provision has to be made to ensure the fuel does not pass out of the aircraft at these times. This is usually provided by an 'air no fuel' valve at the pipe entrance. To meet the requirement of discharging fuel safely from the aircraft in the event of an overflow, at least one of the vents in the tank is required to be open ended. A rise is usually provided on this vent line to ensure fuel does not leave the tank when the vent inlet is covered due to fuel movement.

The surge tank is provided to retain any spillages of fuel through the vent system. The major causes of spillage are fuel spray during refuel, spillage during taxi turns when tanks are full, and the high aircraft pitch experienced during the climb–out after take off with full tanks.

Spilling continues until the manoeuvre is completed or the air space in the tank reaches the vent spilling the flow. The deceleration of an aborted take off can cause fuel spillage which can also spill out of the surge tank, leading to fuel spilling on hot brakes creating a risk of combustion. A flame trap may be fitted into the vent inlet to prevent propagation of the flame into the tanks.

2.8 Fuel System Computer

In modern commercial aircraft the control of the operation of the fuel system is generally by means of a fuel system computer. The operation of this computer can be broken down into two areas:

- Fuel Quantity Indication (FQI).
- Operational Control of Fuel System.

2.8.1 Fuel Quality Indication (FQI)

The FQI system measures the quantity of fuel within the individual tanks of the aircraft. This is usually achieved with probes situated throughout the tanks, the electrical capacitance of which is proportional to the height of fuel on the probe. Each of the probes has a volume of the tank allocated to it, Figure 2.14. For each of these allocated volumes, there is a volume–height relationship. From this data the volume of fuel in the tank is determined. In addition to the probes a densiometer is included within the tank to determine the density of the fuel. This is then used to output the fuel quantity as a mass to the flight crew.

2.8.2 Operational Control of Fuel System

This is concerned with monitoring and controlling the operation of the components of the fuel system such as valve and pumps. It receives data from the FQI on tank quantities, and from other on–board computers, data such as the position of the centre of gravity of the aircraft, the altitude, attitude, etc. Based on this information, the computer determines and signals the relevant position of valves and pump operation for all normal and failure combinations. The computer operation is defined in the form of a logic description. To give an indication of the operation of the computer on a modern large commercial aircraft such as the Airbus A330 and Boeing 777, the fuel control computer can have in excess of 150 inputs and control outputs.

CHAPTER 3

NETWORK SIMULATION

The aim of this Chapter is to introduce the requirements of network simulation within the fuel system modelling environment, and describe the methods of network simulation that have been selected and used throughout this research. The first part of this will be achieved by outlining the role of network simulation and explaining how a network and its associated components are considered within the framework of simulation. The second part is covered with a discussion of the selection of the methods employed, and a brief outline of their theories and operation. The Chapter is concluded with a summary of the various attributes and deficiencies of each of the methods used within this programme.

3.1 Role of Network Analysis

The fuel system and its sub-systems as outlined in Chapter 2 are all networks, so the methods outlined in this Chapter will be used extensively in their analysis. These will range from simple networks such as the recirculation system which consists of a single branch, through to the total fuel system which is complex and highly branched.

Due to the time consuming nature of the calculations, network simulation would traditionally only have been carried out in any detail on sub-systems for normal operation and in critical areas. This is due to the vast number of conditions and calculations that are required to be analysed to fulfil safety and operational requirements. The use of computer simulation enables these networks to be analysed more quickly, and for the system as a whole, allows flight profiles to be studied. Improved analysis efficiency also allows the study of the less critical areas of the system and hence improve design and reliability.

3.2 Network and Component Description for Simulation

The aim of network analysis is to determine the pressures and flow rates at various points within a network. A network is a system of components linked to form an open or closed loop circuit. For the purpose of network analysis, a component can be described by the equations and data governing its inlet and outlet pressure and flow rate. The pressure and flow rate of the components also provides the link, both mathematically and physically, between the components. In addition to the pressure and flow rate, data such as pump speed, valve position etc., may be calculated or required by the model. These variables may have an important effect on system behaviour or may be for monitoring purposes.

3.3 Selection of Packages

From the early stages of the research project it was decided not to develop a specific network analysis method but rather use commercial software packages. This takes advantage of the investment in user interfaces and component libraries. It was therefore necessary to consider the features and benefits of the network simulation packages available.

A network simulation tool for application to the modelling of fuel systems must enable networks to be analysed quickly and efficiently. It must have a simple but comprehensive user interface that can be quickly understood, yet not over burden an experienced user. It must also contain sufficient component models to enable a fuel system to be analysed effectively. It was anticipated from the outset that no commercial package would contain all of the necessary component models required for an aircraft fuel system. This is because aircraft fuel systems have unique operating conditions, Eg. changing 'g' vector, changing attitude of the analysis platform, changing tank geometries, changing fluid and atmospheric conditions etc. It was therefore a desirable feature for the packages to accept user defined component models. A major requirement of any package selected was that it should be easily integrated into an industrial design and analysis environment, its application being well beyond this research.

The requirements laid down for the selection of an appropriate commercial network analysis software package were as follows:

- A simple user interface which would enable network simulations to be quickly set up and analysed.
- A component library to cover all, or the majority, of the components required for simulation of an aircraft fuel system (Table 3.1).
- The ability to input user defined component models.

Two network analysis packages were selected, Flowmaster, developed by British Hydromechanics Research Association (BHRA) and marketed by Flowmaster UK Ltd., and Bath*fp* developed and marketed by Bath University. Flowmaster uses an iterative flow balancing method to solve the steady state equations of the system; its major strength is its library of components. Bath*fp* solves the dynamic equations of the system with numerical integration methods; its major strength is its component modelling techniques, these enable Bath*fp* to be adapted to the modelling of a wide range of systems. Initially the predecessor to Bath*fp*, HASP [10 to 13] was considered and rejected due to its cumbersome and complex user interface, which was not suitable to the industrial application. At the start of the project only Flowmaster was selected [14]. However with the development of Bath*fp* from HASP,

a package with a user interface of the same standard as Flowmaster was available, with the added advantage of good component modelling capabilities, so this was therefore also selected [15].

The development and application of the two packages was performed for two reasons, the first being to exploit the use of different solution techniques. For analyses which are of a safety critical nature both packages can be used to analyse the system, the two solutions providing cross validation. Secondly, neither could completely model an aircraft fuel system due to the uniqueness of its operational conditions and components, and the weakness of one package is generally one of the strengths of the other, so they both complement each other.

Both packages use very similar graphical user interfaces which enables any person competent with the use of one to quickly and easily gain experience of the other without the need for further in–depth training.

3.4 Theory

The pressure and flow rate can be defined in terms of a pressure loss and compressibility effects.

Pressure Loss

Pressure loss is defined as

$$\Delta P = \left[p_1 + \rho\frac{u_1^2}{2} \right] - \left[p_2 + \rho\frac{u_2^2}{2} \right] + \rho g \left[z_1 - z_2 \right] \qquad 3.1$$

Pressure loss in turbulent flow is proportional to (velocity)^2 [16] and can be written as:

$$\Delta P = k\rho\frac{u^2}{2} \qquad 3.2$$

where k is an empirical value relating the pressure loss to (velocity)^2 and is referred to as the loss coefficient.

Expanding equation 3.2 in terms of flow rate gives:

$$\Delta P = \frac{k\rho}{2A^2}q^2 \qquad 3.3$$

So that flow rate is given by:

$$q = \sqrt{\frac{2A^2\Delta P}{k\rho}} \qquad 3.4$$

Compressibility Effects

The rate of change of pressure due to compressibility effects is defined as:

$$\frac{dP}{dt} = \frac{\beta}{V}\sum q \qquad 3.5$$

Where ß is the bulk modulus of the fluid and V is a complaint volume in which dP/dt can be considered to be constant. From equation 3.5 flow rate is given by:

$$\sum q = \frac{V}{\beta}\dot{P} \qquad 3.6$$

For steady state conditions $\Sigma q = 0$.

3.4.1 Traditional Hand Calculations

These methods are restricted to the steady state solution of networks through solution of equation 3.3 with graphical methods. This is best illustrated through a simple example. If we take a simple non-branching system as shown below,

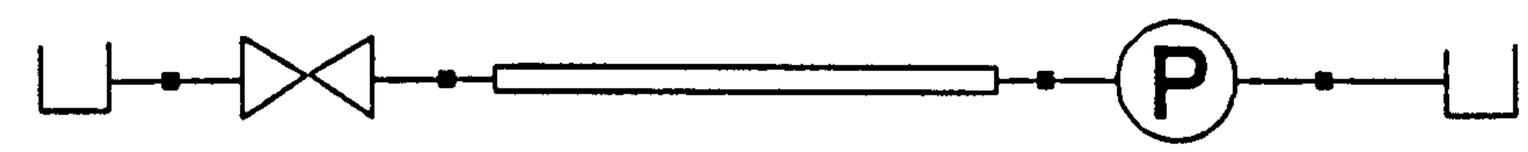

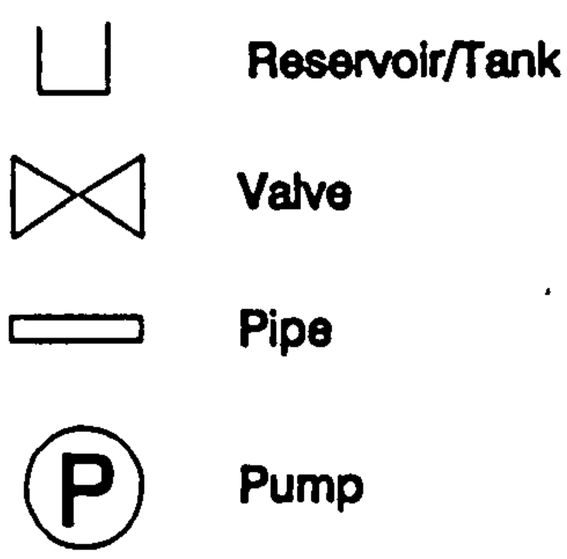

The above network consists of two reservoirs which define the boundaries of the system, a valve and pipe with associated loss coefficients, and a pump which provides additional pressure and flow rate to the system.

The pressure loss at a known flow rate can be determined for the pipe and valve from equation 3.3, and the loss for the total system by summation of the losses for each component.

$$\Delta P_{total} = \sum_{i=1}^{n} \Delta p_i \qquad 3.7$$

If this loss is calculated at various flow rates an appropriate system characteristic can be developed. This can be plotted with the pump characteristic and the operating point of the network determined, as shown in Figure 3.1. The flow rate and pressure rise required by the pump can be taken from this plot. Assuming the reservoirs have a constant pressure then this pressure can be used in conjunction with the flow rate determined from Figure 3.1 and equation 3.3 to determine the inlet and outlet pressure of each component.

If the network is branched, the solution cannot be obtained directly using the above method unless the flows in the branches are known. If not known then the flow rate for each branch must be estimated and checked by the above method, and then the process repeated until a stable solution is achieved. For highly branched networks this can be very time consuming.

3.4.2 Flowmaster

3.4.2.1 Iterative Solution Method

The equations and methods used by Flowmaster are the same as those for the traditional graphical methods outlined above, except the loss equation for the components are rewritten to solve for mass flow rate rather than volumetric flow rate.

Rewriting equation 3.4 in terms of mass flow rate gives:

$$\dot{m}^2 = \frac{2\rho A^2 \Delta P}{k} \qquad 3.8$$

Equations of the form of equation 3.8 are developed for all of the components within the network and expressed in matrix notation. These equations are then solved with the following procedure.

1. The mass flow rates are initialised to 1kg/s.
2. The loss coefficients k are determined for each component from the mass flow rates.
3. The pressures are solved for using Gaussian elimination.
4. The resulting pressures are used to update the mass flow rates and the process repeated from step 2.

This iterative process is halted when a stable solution has been achieved, or after one hundred iterations at which stage it is assumed the solution is unstable. This iteration process has been found to be stable for most applications. A few problems have been encountered where multiple solutions are present. These are discussed in detail in the first case study of Chapter 8.

The solution algorithm used within Flowmaster solves for the steady state conditions. To analyse flow changes in a network over a period of time (dynamic analysis) a series of steady state analyses are carried out at a user selected fixed size time step, with any time dependent properties of a component such as valve position, pump speed etc. adjusted as appropriate at each time step. Inertias and rates of change of pressure etc. are taken into account with approximations of the differential equations. Initial conditions for the dynamic analysis are obtained from a steady state initialisation, each time step uses the solution from the previous time step to initialise its solution. The analyses at each time step are restricted to twenty iterations. If solution is not achieved within this number of iterations a warning is given and the analysis continued. This approach, and in particular the fixed time step creates limitations on the application of Flowmaster to the study of time dependent events. This is discussed in detail in Chapter 7.

3.4.2.2 Discontinuity Handling

To aid in the understanding of discontinuity handling when applied to the iterative techniques of Flowmaster, it is appropriate to consider discontinuities as two types. The first are discontinuities of solution, for example a valve closing, and the second are discontinuities of data describing the components.

Discontinuities of solution can only occur with time dependent events. These discontinuities are taken into account through the size of the user defined time step. If this is defined too large the discontinuity will not be resolved and solution difficulties arise due to the rapid changes of state. For these cases where the solution fails a warning will be given. If the time step is the correct size, or shorter, then the discontinuity will be handled correctly and solution achieved.

Discontinuities of data are handled by internal routines within Flowmaster. This is best illustrated with an explanation of the handling routine for zero flows in a junction. In some cases the iterative process may predict a small positive flow at one iteration, and a small negative flow at the next, then oscillate between the two during future iterations. This results in the loss coefficient being obtained from two characteristics at alternate iterations. This discontinuous state is handled by fixing the flow at zero when below a tolerance, thereby forcing the loss coefficient onto the appropriate characteristic as the solution is approached.

Any error in loss coefficient prediction from this approach is negligible when the experimental and empirical nature of the loss coefficients is taken into account.

3.4.2.3 Method of Characteristics

A facility for the study of water hammer (17,18) within the pipe models of Flowmaster using the method of characteristics is provided. This can be run within any transient analysis with an appropriate time step.

Water hammer may occur in a closed pipe with full flow when the flow is either rapidly decelerated or accelerated, as in the case of rapid valve operation. If the changes are gradual, a surge method such as the Euler Solid Column Method [19], may be appropriate. Such methods consider the fluid incompressible and the pipe rigid. With rapid changes of pressure and flow rate the compressibility of the fluid and elasticity of the pipe must be considered.

To explain the effects of water hammer we shall take the network of Figure 3.2 as an example and ignore the effects of friction and assume the valve closes instantly so creating sharp pressure waves. If the pipe is flowing full at velocity vo and the valve closed instantaneously at time $t=0$ the fluid at the valve face will be compressed, the pressure will increase to h, due to the momentum of the flow, and the fluid be brought to rest stretching the pipe wall. When the upstream flow meets this stationary flow it will also be compressed and brought to rest at pressure h, stretching the pipe wall. This high pressure travels upstream as a wave at the sonic velocity of the fluid a, with stationary flow at h downstream of it, and flow at velocity v_o and reservoir pressure upstream of it. When it reaches the reservoir at time $t=L/a$ all the fluid in the pipe will be at rest at pressure h and the reservoir will be at the original pressure, causing an imbalance. Flow will start into the reservoir at velocity $-v_o$ and the pressure wave will return towards the valve at velocity a with stationary flow at pressure h downstream, and flow at velocity $-v_o$ and reservoir pressure upstream. When the wave reaches the valve at time $t=2L/a$ the flow in the pipe cannot be maintained at velocity $-v_o$ due to the closed valve, a low pressure $-h$ develops bringing the fluid to rest. This low pressure wave travels back upstream at velocity a with stationary flow at pressure $-h$ downstream, and flow at velocity $-v_o$ and reservoir pressure upstream. It will reach the reservoir at time $t=3L/a$ where an unbalanced condition will be met. Fluid flows back into the pipe at reservoir pressure at velocity v_o and the pressure wave returns towards the valve at velocity a with stationary flow at pressure $-h$ downstream, and flow at velocity v_o and reservoir pressure upstream. The wave reaches the valve at time $t=4L/a$ returning to the original conditions at time $t=0$. The whole process is repeated every $4L/a$ seconds. This description does not take into account the effects of pipe friction which will damp out the pressure waves eventually bringing the fluid to rest.

To determine water hammer transients the differential equations of transient flow of motion and continuity are required with the pressure and the average velocity at the cross section

being the dependent variables. Many derivations of these equations have been put forward in text books [17 to 19], the one used below is taken from Wylie and Streeter [17].

Equation of Motion

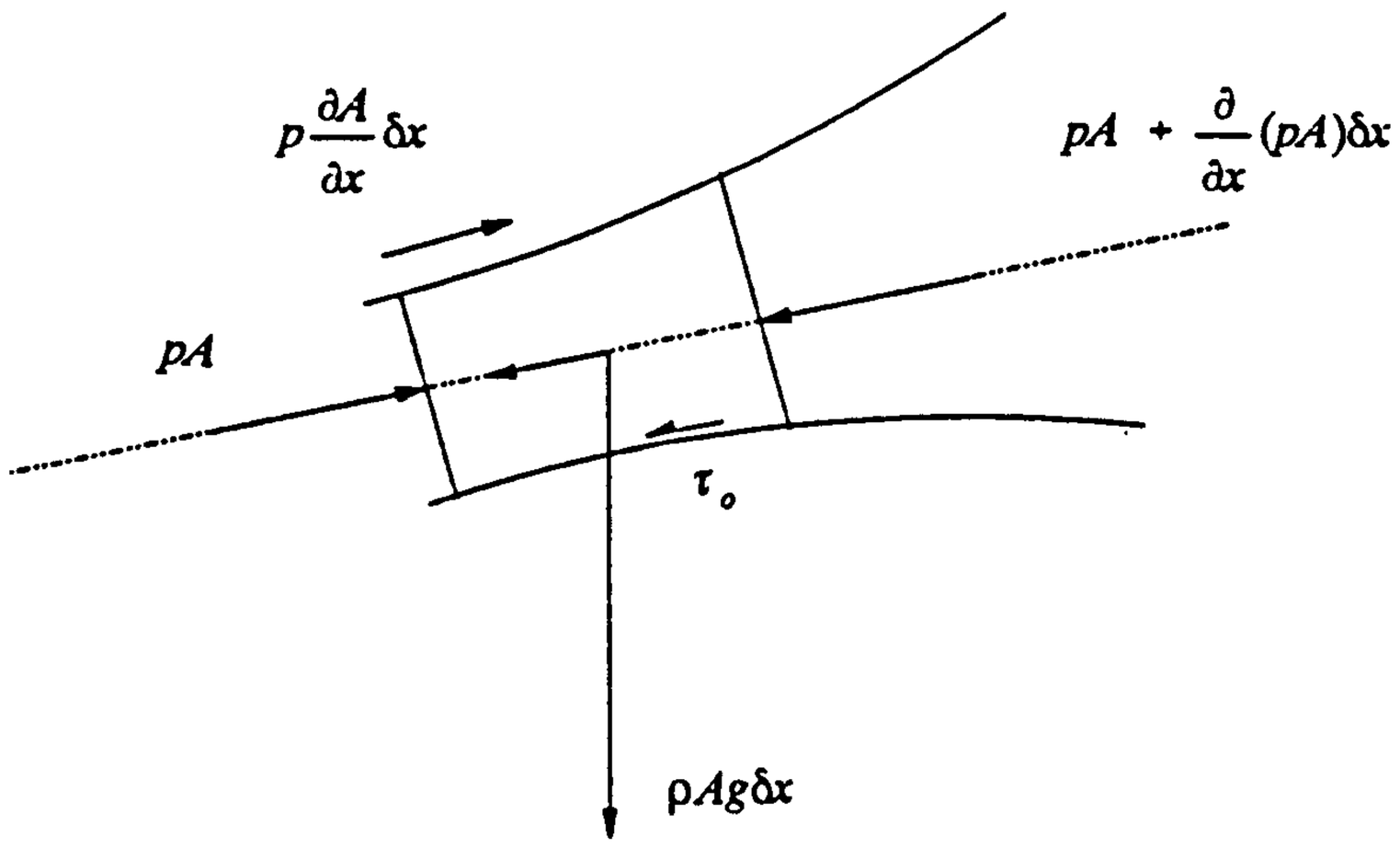

Taking a fluid element between two parallel planes δx apart and normal to the pipe axis as shown above and applying Newtons second law of motion.

$$pA - \left[pA + \frac{\partial}{\partial x}(pA)\delta x \right] + p\frac{\partial A}{\partial x}\delta x - \rho Ag\delta x \sin\theta - \tau_o \pi D\delta x = \rho A\delta x \frac{dv}{dt} \qquad 3.9$$

Dividing through by the mass of the element $\rho A\delta x$ and simplifying

$$-\frac{1}{\rho}\frac{\partial p}{\partial x} - g\sin\theta - \frac{4\tau_o}{\rho D} = \frac{dv}{dt} \qquad 3.10$$

For steady turbulent flows the Colebrook equation [17] gives

$$\tau_o = \frac{\rho f v^2}{8} \qquad 3.11$$

Assuming this is correct for unsteady flows and substituting

$$\frac{dv}{dt} + \frac{1}{\rho}\frac{\partial p}{\partial x} + g\sin\theta + f\frac{v\,|\,v\,|}{2D} = 0 \qquad 3.12$$

the total derivative of the acceleration term with respect to the axial motion of the pipe is

$$\frac{dv}{dt} = v\frac{\partial v}{\partial x} + \frac{\partial v}{\partial t} \qquad 3.13$$

In applications of water hammer the term $v\partial v/\partial x$ is much smaller than $\partial v/\partial t$ and usually omitted [17].

The equation is identified by L_1 to distinguish it from the continuity equation L_2.

$$L_1 = \frac{\partial v}{\partial t} + \frac{1}{\rho}\frac{\partial p}{\partial x} + g\sin\theta + f\frac{v\,|\,v\,|}{2D} = 0 \qquad 3.14$$

Equation of Continuity

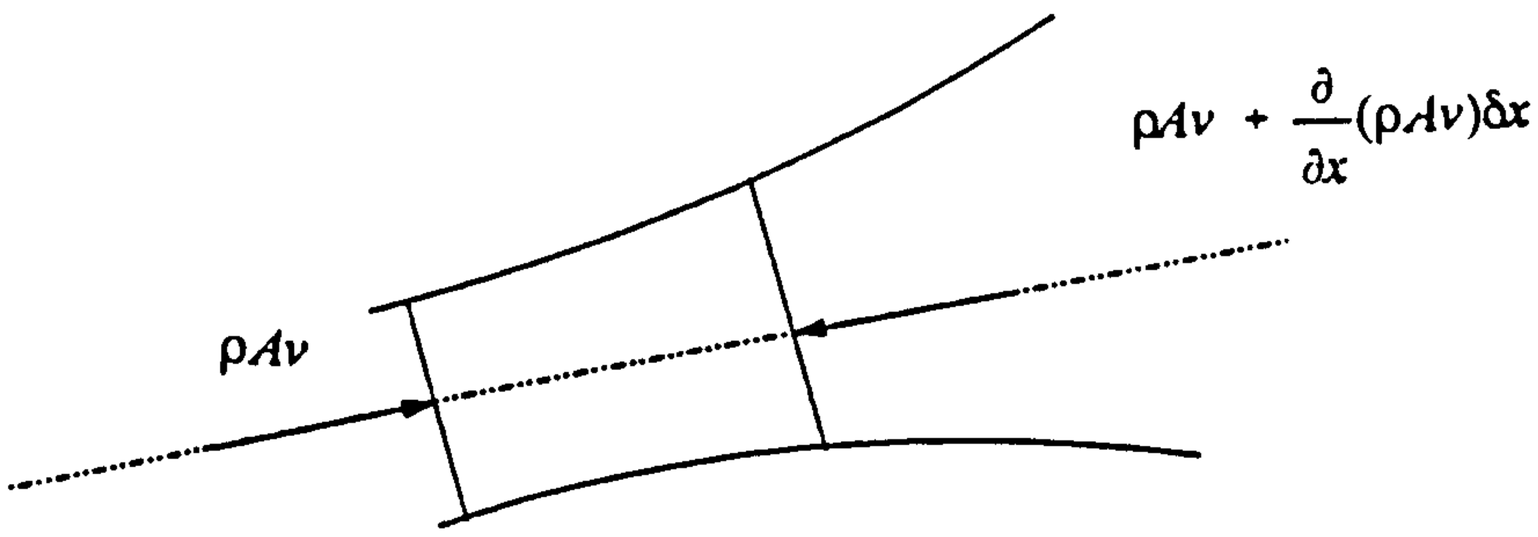

Taking a control volume as shown above and applying the unsteady continuity equation.

$$\rho Av - \left[\rho Av + \frac{\partial}{\partial x}(\rho Av)\delta x \right] = \frac{\partial}{\partial t}(\rho A\delta x) \qquad 3.15$$

δx is not a function of time, though the mass ($\rho A \delta x$) is. Expanding

$$\rho \delta x \frac{\partial A}{\partial t} + A \delta x \frac{\partial \rho}{\partial t} + v \rho \delta x \frac{\partial A}{\partial x} + v A \delta x \frac{\partial \rho}{\partial x} + \rho A \delta x \frac{\partial v}{\partial x} = 0$$

dividing through by the mass $\rho A \delta x$ and rearranging

$$\left[\frac{v}{A} \frac{\partial A}{\partial x} + \frac{1}{A} \frac{\partial A}{\partial t} \right] + \left[\frac{v}{\rho} \frac{\partial \rho}{\partial x} + \frac{1}{\rho} \frac{\partial \rho}{\partial t} \right] + \frac{\partial v}{\partial x} = 0 \qquad 3.16$$

The total derivative with respect to the axial motion in the pipe

$$\frac{d}{dt} = \frac{dx}{dt} \frac{\partial}{\partial x} + \frac{\partial}{\partial t}$$

can be applied to the terms in the parentheses and their total derivatives determined. Substituting into 3.15

$$\frac{1}{A} \frac{dA}{dt} + \frac{1}{\rho} \frac{d\rho}{dt} + \frac{\partial v}{\partial x} = 0 \qquad 3.17$$

The first term of equation 3.17 takes into account the elasticity of the pipe wall and its rate of deformation with pressure, the second term takes into account the compressibility of the liquid. The first term can be expanded from the definition of the rate of strain in a circular pipe and the second term can be expanded from the definition of the bulk modulus of the fluid.

The rate of increase of unit strain for a circular pipe [17] is

$$\left[\frac{d\varepsilon}{dt} = \right] \frac{D}{2eE} \frac{dp}{dt}$$

If this is multiplied by the radius, the rate of radial increase is obtained. If this is multiplied by the perimeter, the rate of increase of the area will be obtained hence the rate of deformation of the pipe with pressure

$$\frac{dA}{dt} = \frac{\pi D^3}{4eE} \frac{dp}{dt} \qquad 3.18$$

Therefore

$$\frac{1}{A}\frac{dA}{dt} = \frac{D}{eE}\frac{dp}{dt} \qquad 3.19$$

The bulk modulus of the liquid is defined as

$$K = -\frac{dp}{dV/V} = \frac{dp}{d\rho/\rho} \qquad 3.20$$

rearranging

$$\frac{1}{\rho}d\rho = \frac{1}{K}dp$$

Applying as a rate of change

$$\frac{1}{\rho}\frac{d\rho}{dt} = \frac{1}{K}\frac{dp}{dt} \qquad 3.21$$

Substituting equations 3.19 and 3.21, equation 3.17 becomes

$$\frac{1}{K}\frac{dp}{dt}\left[1 + \frac{K}{E}\frac{D}{e}\right] + \frac{\partial v}{\partial x} = 0 \qquad 3.22$$

Dividing equation 3.22 by $1+(K/E)(D/e)$ gives:

$$\frac{1}{K}\frac{dp}{dt} + \frac{\partial v}{\partial x}\left[\frac{1}{1 + (K/E)(D/e)}\right] = 0 \qquad 3.23$$

Multiplying through by K/ρ gives:

$$\frac{1}{\rho}\frac{dp}{dt} + \frac{\partial v}{\partial x}\left[\frac{k/\rho}{1 + (K/E)(D/e)}\right] = 0 \qquad 3.24$$

The constants of equation 3.24

$$\frac{K/\rho}{1 + (K/E)(D/e)}$$

are a common way of correcting the acoustic velocity of the fluid within the pipe for the effects of pipe expansion [17,19,20]. The numerator is the square of the acoustic velocity of

the liquid in the pipe, and the denominator is the correction. Therefore, the constants can be expressed as the corrected square of acoustic velocity (a^2), and equation 3.22 simplified.

$$\frac{1}{\rho}\frac{dp}{dt} + a^2\frac{\partial v}{\partial x} = 0 \qquad 3.25$$

Expanding the total derivative of pressure

$$\frac{dp}{dt} = v\frac{\partial p}{\partial x} + \frac{\partial p}{\partial t}$$

For water hammer applications $v\partial p/\partial x$ is usually much smaller than $\partial p/\partial t$ and can be neglected [17]

$$L_2 = \frac{\partial p}{\partial t} + \rho a^2\frac{\partial v}{\partial x} = 0 \qquad 3.26$$

This is the continuity equation for a compressible liquid in a pipe.

Method of Characteristics Equations

L_1 and L_2 are the differential equations of unsteady flow in v and p for Newton's second law of motion and continuity for a compressible liquid in an elastic pipe in terms of x and t. No general solution to these equations is known, but they can be solved with the method of characteristics. L_1 and L_2 can be related by a multiplier

$$L = L_1 + \lambda L_2 \qquad 3.27$$

Any two real values of λ will give two equations in v and p which can replace L_1 and L_2.

Substituting equations 3.14 and 3.26 into 3.27 and arranging in terms of v and p.

$$L = \left[\frac{\partial v}{\partial x}\lambda\rho a^2 + \frac{\partial v}{\partial t}\right] + \lambda\left[\frac{\partial p}{\partial x}\frac{1}{\rho\lambda} + \frac{\partial p}{\partial t}\right] + g\sin\theta + f\frac{v\,|v|}{2D} = 0 \qquad 3.28$$

Comparing the terms in parenthesis to the expansion of the total derivative in relation to the axial motion in the pipe

$$\frac{d}{dt} = \frac{dx}{dt}\frac{\partial}{\partial x} + \frac{\partial}{\partial t}$$

Then if

$$\lambda\rho a^2 = \frac{dx}{dt} \qquad \textit{and} \qquad \frac{1}{\rho\lambda} = \frac{dx}{dt}$$

$$\lambda\rho a^2 = \frac{1}{\rho\lambda}$$

$$\lambda = \pm \frac{1}{\rho a} \tag{3.29}$$

$$\frac{dx}{dt} = \pm a \tag{3.30}$$

Substituting into 3.28

$$L = \frac{dv}{dt} \pm \frac{1}{\rho a}\frac{dp}{dt} + g\sin\theta + f\frac{v\,|\,v\,|}{2D} = 0 \tag{3.31}$$

This solution can be visualised on an x, t plot of the characteristics

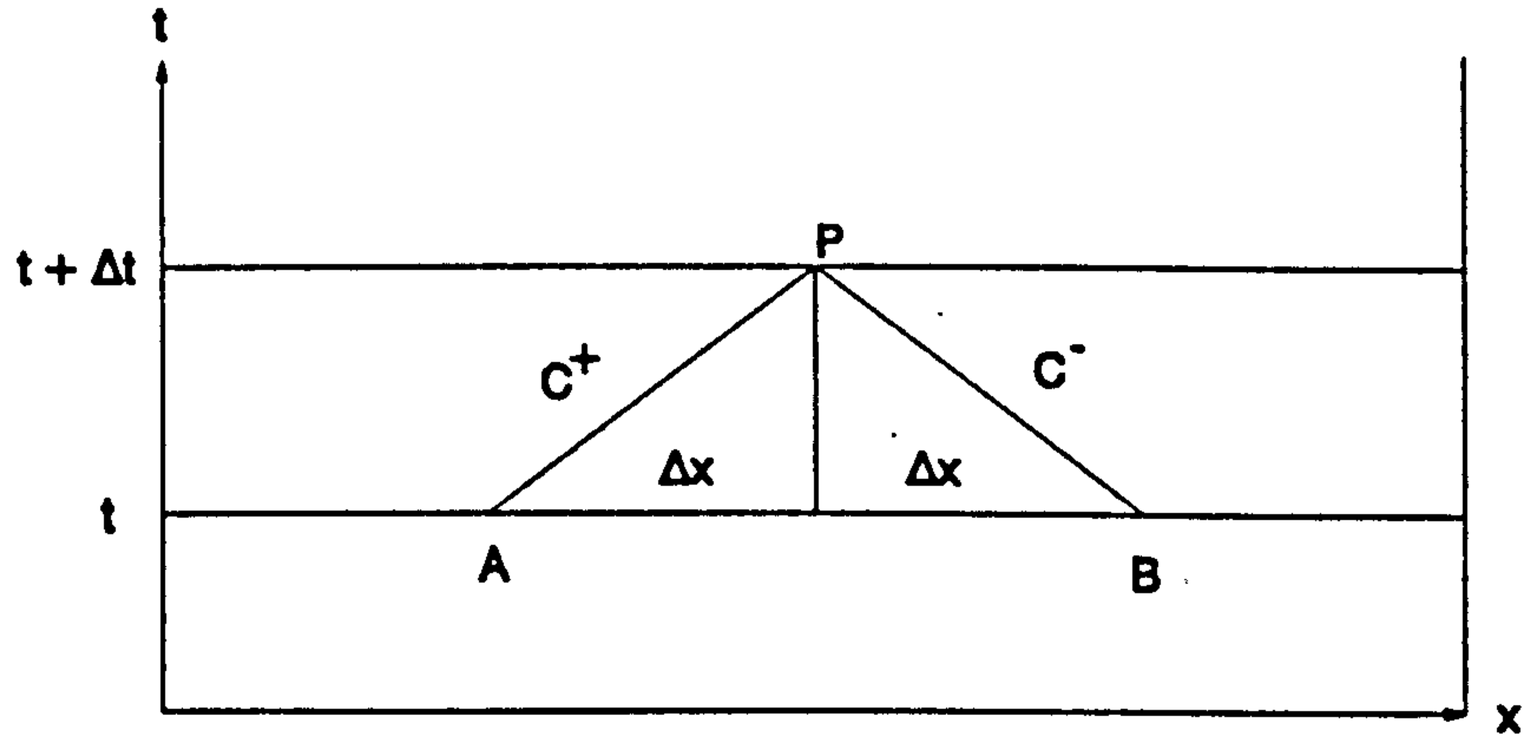

The pipe can be considered to extend from *0*, the upstream origin, to *L* its downstream end. *x* and *t* locate a position at a fixed time in the pipe where *v* and *p* are to be determined. Assume the conditions at *A* are known, then equation 3.31 with the positive term of λ, termed the C^+ equation, is valid along *AP*. Multiplying 3.31 by ρ*adt* and integrating from *A* to *P*.

$$\rho a\int_A^P dv + \int_A^P dp + \int_A^P \rho a g\sin\theta\, dt + \int_A^P \rho a dt f\frac{v\,|\,v\,|}{2D} = 0 \tag{3.32}$$

With similar assumptions the C^- equation along BP is

$$\rho a\int_B^P dv - \int_B^P dp + \int_B^P \rho ag\sin\theta\, dt + \int_B^P \rho a dt f\frac{v\,|\,v\,|}{2D} = 0 \qquad 3.33$$

The physical length these equations are analysed over is commonly called the reach length [66]. The integration method used within Flowmaster to solve these equations requires the pipe to be divided into a whole number of reach lengths. The application of this within an analysis places a restriction on the time steps that are appropriate because,

$$\Delta x = a\Delta t$$

Therefore for a pipe of length L, the number of characteristic lengths analysed within the pipe is,

$$N = \frac{L}{a\Delta t}$$

Where N must be a whole number.

Guide lines on the application of the method of characteristics, including the restrictions, within a Flowmaster analysis are given in Chapter 7.

3.4.3 Bath*fp*

3.4.3.1 Dynamic Analysis

In contrast to Flowmaster, Bath*fp* is a dynamic simulator with time response output. The steady state solution is obtained via a dynamic analysis, which can be achieved by defining steady pressures and flow rates on the boundaries of the system, which result in a steady state output. There are a variety of methods available for this type of simulation in order to solve the set of differential and algebraic equations describing the system. Bath*fp* uses an adaptive integrator based on the routine LSODA due to Petzold [21,22]. This is a type-insensitive integrator which uses Adam's methods of order 1 to 12 as a non-stiff integration algorithm and Gear's method with backward differentiation formula of orders 1 to 5 as the stiff integration algorithm.

Bath*fp* applies the integration method by describing the components with dynamic or algebraic models termed 'instantaneous', dependent on the action they have on the network and the output required.

Bath*fp* describes the dynamic operation of the system using first order differential equations of the form of equation 3.5. The instantaneous models are described by the general loss equation, equation 3.4.

In the majority of cases, the components within a fuel system are appropriately defined as dynamic models, all having associated complaint volumes. In many cases though, instantaneous models are used to describe the component because the dynamic effect is negligible. Typically a simulation of a fuel system network will comprise dynamic models of pipes interlinking, in the main, instantaneous models of components.

For the numerical integration technique, the models are required to be explicit. Therefore a method of control of variable transfer is required to ensure a solution. The method employed requires components to output flow rate and receive pressure, and pipes to output pressure and receive flow rate. The pipes are modelled in two subroutines. The first describes the dynamics of the pipe volume, and the second describes the pressure losses associated with the pipe. To facilitate connection of the pipes to both components and other pipes, a series of pipe models are available which differ only in the point within the pipe where the pressure loss is assumed to occur, as shown in Figure 3.3.

3.4.3.2 Discontinuity Handling

Numerical integrators assume that functions being integrated are continuous. If discontinuities are present in a function, it is important that these are taken into account. If this is not so and the integrator is allowed to pass through discontinuities without an appropriate checking procedure, inaccuracies, long run times and integrator failure may result.

Bath*fp* deals with discontinuities in three stages.

1. Integrating along a continuous function to detect when a discontinuity has been passed over.

2. Interpolate backwards in time to locate the discontinuity to within a prescribed tolerance.

3. Restart the integrator using the next continuous function.

The models are required to determine when a discontinuity has been 'passed over', inform the integrator, and when the discontinuity has been located sufficiently accurately, provide the relevant data for the model to restart with the new function.

Messages are sent between the integrator and the models on the current status of discontinuities using an integer variable limit, which is used as a subroutine argument. The allowed values of limit are given below.

limit = 0 Set by the integrator. The integrator has just started or restarted. Any initialisation of the model must be performed.

limit = 1 Set by the integrator. An intermediate step is in progress. Models must not check for discontinuities.

limit = 2 Set by the integrator. The integrator has satisfied its accuracy checks on the current time step, and will continue unless a model indicates otherwise by resetting limit.

limit = 3 Set by the models. A discontinuity has been 'passed over', and is not located sufficiently accurately. This is a request for the integrator to interpolate backwards in time.

limit = 4 Set by the models. A discontinuity has been stepped over, and is located sufficiently accurately. This is a request for the integrator to restart.

A discontinuity handling routine, *dishan*, is supplied with Bath*fp*, which when given the location of the discontinuity and the error tolerance required to locate it, determines if limit should be reset to 3 or 4.

3.5 Flowmaster

This description and all of the applications discussed throughout the thesis refer to Flowmaster version 3.2.

3.5.1 Structure of Flowmaster

The user interface of Flowmaster is via an icon oriented graphical system. The mouse is the main mode of communication. Networks are created with icons representing components, connected by nodes to form circuits. The components consist of an icon, a FORTRAN coded component model and appropriate characteristic curves or surfaces. Only one component can be associated with an icon.

Flowmaster is split into two parts, the actual analysis code Flowmaster [23], and a database of components and component development utilities Datamanager [24].

3.5.2 Flowmaster – The Analysis Code

The Flowmaster analysis code Figure 3.4 is split into three sections, Network Update, Network Analysis, and Results Display.

3.5.2.1 Network Update

The network update area, Figure 3.4, performs three functions; the selection and storage within the palette, Figure 3.5, of the components to be used to describe the network, the schematic creation and later updates of the network, and the input of data to describe the components. The layout of the network can be altered using utilities accessed via icons.

The palette is the interface with the database of components. It consists of icons representing the components which will be used in the network. Components can be added to or deleted from the palette at any time during network update.

The network is built using icons selected from the palette, to create a schematic diagram of the network. The components, which include pipes, are connected by nodes, which are loss less schematic connections. A simple network is shown in Figure 3.5.

Data to describe the components functionality is input into the components data sheet as shown in Figure 3.6.

3.5.2.2 Analysis Mode

Here the analysis type is selected, set-up and run. Data required to describe the analysis is input into a data sheet. The data required is dependent on the analysis type. For a steady state analysis, only the fluid type, atmospheric temperature and pressure are required. For a transient analysis, data on the start and end times, and time step are also required. The following analysis types are available in the British Aerospace installation.

Steady State	This solves for the steady state conditions of the network using the methods described in Section 3.4.2.1.
Transient (Dynamic)	This uses a series of steady state analyses at a user defined time step to solve for a defined transient condition as described in Section 3.4.2.1. Pipes may be described with the standard pipe model or with a method of characteristics model, as described in Section 3.4.2.3.
Flow balancing	This is a specialised application of the steady state solution method which when supplied with the volumetric flow rate through a component, determines the size of the component to achieve this flow rate. Components which can be sized are restrictors, pipes, valves, bends and discrete losses.

3.5.2.3 Results Mode

Flowmaster saves the results from all analyses carried out on the network, and it is in this mode that results are retrieved. If results for an old version of the network are accessed, a warning is given. Access is allowed, but the data for new and deleted components is not available. The results display is split into three main windows, one containing the network, one for the pressure results, and the other for the flow rate results and any additional results such as reservoir level, Figure 3.7. Results are displayed in the two windows by selection of the appropriate component or node on the network display, or the logfile can be displayed which contains all of the results in tabular form.

The presentation of the results is dependent on the analysis type. For steady state or flow balancing, the flow rates into and out of a component are displayed on an enlarged icon in the flow rate results window. For flow balancing, additional information on the size of the component is also displayed Figure 3.8. The pressures are displayed with their appropriate node number in either list form, or on a pressure gradient plot in the pressure display results window, as shown in Figure 3.9. Transient analysis results are displayed on time history plots in their associated window, with up to five plots of the same variable, Figure 3.10. Results for any of the analyses can be deleted.

3.5.3 Datamanager

Datamanager [24] contains the actual models of the components, their loss coefficient data in the form of curves and surfaces, and utilities for the input of liquids, gases, curves, component icons, and development of new component models. These are all shown in Figure 3.11.

3.5.3.1 Component Library

The components are split into groups, termed families. These contain similar components, Eg. the valve family, pump family, reservoir family etc.. The loss coefficient data for the components is taken primarily from reference [16].

3.5.3.2 Adding New Curves

Characteristic curves can be input either as tabular data, a curve digitised on screen, or as a formula. The tabular and digitised data are handled by one utility and the formula by a second utility. The on screen digitisation is achieved by using the mouse to define the axes and the curve from a transparency attached to the screen. The utility contains an algorithm which detects out of square of the axes drawn on the screen and adjusts them and the data accordingly. Accuracy is claimed to be 2–3%. Characteristic curves are restricted to two dimensional curves only.

3.5.3.3 Adding New Component Icons

Component icons are created with a simple icon editor with basic drawing capabilities, Figure 3.12. Both fluid and control connections are added using the editor.

3.5.3.4 Adding New Component Models

The component models used within a Flowmaster simulation are all resident within Flowmaster and only calls to these or copies of these models can be made. Therefore the only means by which a new component model may be introduced into Flowmaster is in the form of a characteristic curve associated with a copy of one of these models. The resulting model can only be defined within the confines of the data sheet copied from the standard Flowmaster model. Any component whose operation cannot be described by the above modifications to any of the supplied models cannot be modelled, unless included by Flowmaster UK Ltd. The models that are not available but required to enable Flowmaster to completely model aircraft fuel systems are:

- A fuel tank capable of adjustment of head due to rotation, and with multiple inlet/outlets at differing heights.
- A jet pump. Since there are no appropriate models which can accept a jet pump characteristic.
- An extension to the pump model to enable characteristics to be switched during analysis. This will enable degradation of pump performance during climb etc. to be included.

These models will be discussed in more detail in Chapter 6.

3.5.3.5 Adding New Liquids and Gases

New liquids and gases are created with two different utilities though their operation is identical. They are only separate because the liquid is the working fluid and the gas the fluid contained in accumulators etc. They are created by filling in a data sheet, Figure 3.13, describing the properties of the liquid or gas. Some of the data such as density, viscosity, and vapour pressure can be input as a function of temperature in the form of a curve from which the property is read using the atmospheric temperature set in the analysis data sheet. This temperature is then fixed throughout the analysis.

3.6 Bath*fp*

This description and all of the applications discussed throughout the thesis refer to Bath*fp* version 1.

3.6.1 Structure of Bath*fp*

The user interface of Bath*fp* is via an icon oriented graphical system. The mouse is the main mode of communication. Networks are created with icons representing components, connected with pipes to form a circuit. The components consist of an icon and a FORTRAN or C coded component model. Any characteristic data is tabulated within this model. In addition to the models included in the standard release of Bath*fp*, user models can also be included. Any number of models can be associated with an icon allowing different cases and levels of complexity to be modelled.

Bath*fp* is divided into four parts. The analysis code known as Bath, an icon editor known as Bath ICON, a model adding utility known as BathMAT (Bath model adding tool), and a modelling utility for input of simple components described from pressure flow curves known as BathME (Bath modelling environment).

3.6.2 Bath

The analysis code [25] is split into four areas; Circuit Drawing, Model Selection, Parameter Definition, and Run as illustrated in Figure 3.14.

3.6.2.1 Circuit Drawing

A schematic representation of the network using icons representing the components, as shown in Figure 3.14, is created with the components connected directly to each other or with pipes. The icons are selected from sets of generic icons as shown in Figure 3.15 and the pipes from the connections menu, Figure 3.16. The layout of the network can be adjusted by utilities accessed via icons or mouse operation.

3.6.2.2 Model Selection

Appropriate models are selected from those associated with the components and pipes, see Figure 3.16. The selection for pipes is dictated by the type of connection to be made and the application.

3.6.2.3 Parameter Definition

On entry into this area, a code generator incorporates the component models defined in Section 3.6.2.2 into a source code, which is compiled and linked to create an executable program. Data describing the functionality of the component is input in pop up windows Figure 3.17. The working fluid is selected from a list of available fluids or if not available it may be defined by its properties, Figure 3.18.

3.6.2.4 Run

Run mode performs two functions, the actual analysis and the display of results.

Before the analysis is run, parameters of the run can be changed. While the analysis is running the results can be examined.

Only the last set of results are saved. Earlier results are deleted to ensure results relate to the current state of the network, and to save on disk space. The results are displayed by selecting a component from the main network diagram and selecting the parameters to plot from a pop up window. This displays all the available parameters to plot and the values at that current time step. If the results at this time are steady, these current values give the steady state results. The plotted variables may be in the form of a time history, Figure 3.19, or against another variable. Up to five or six plots can be made on the same set of axes for both types of plot. Results plotted on the same axes are not restricted to the same variable, for example, flow rate and pressure may be displayed on the same plot.

3.6.3 BathICON

BathICON [26] creates component icons with a simple icon editor based on the UNIX bitmap editor, Figure 3.20. All connections are described within the editor, and a bitmap file is generated containing the pictorial and connection details.

3.6.4 BathMAT

User models developed in FORTRAN or C are added to Bath*fp* using BathMAT [27]. The information required by BathMAT are the component icon to associate the model with, the number and type of external variables to enable the code generator to link the model, and the descriptions of variables to appear in the parameter definition pop up window and results display.

3.6.5 BathME

BathME [26] is used to create instantaneous models which for this particular application are described by one or a series of pressure versus flow curves. It generates and compiles the actual source code to be used, so the user does not require programming capabilities. The models still require adding to Bath*fp* using BathMAT. This facility is only intended as a "black box" modeller for inclusion of data from test rigs or similar sources, and creation of simple instantaneous rotary type pump models.

3.7 Closing Remarks

The two software packages Flowmaster and Bath*fp* were selected in order to compare their capabilities in analysing aircraft fuel system behaviour. The two packages have been written with different solution methods and differing biases; Flowmaster originally the water and general utilities market and Bath*fp* the hydraulics market, and from different backgrounds; Flowmaster from HIPSMART an early commercial code developed by BHRA and Bath*fp* from HASP effectively an in-house code for hydraulic systems study at Bath University. These factors have bestowed each with quite different strengths and weaknesses and yet very similar user interfaces are both useful for aircraft fuel system analysis.

The major strength of both packages is their simple yet comprehensive interfaces which is a very important aspect for this type of work. Flowmaster's individual strengths are its direct steady state solution which also enables flow balancing analysis, its ability to model water hammer and hence pressure surge, and a very good component library lacking only a few models. Bath*fp*'s individual strengths lie in its open architecture enabling literally any component model to be included and the package to advance with the introduction of new components, and its dynamic analysis capabilities which enable flight profiles to be studied.

The current major limitations of both are:

- The analysis platform or direction of the gravity vector cannot be rotated in any plane, this is examined further in Section 6.3.2
- Only single fluid networks can be modelled. Therefore a vent and fuel network cannot be modelled in the same analysis with the associated coupling effects.

The major limitations of Flowmaster are:

- Its dynamic analysis capabilities. These are restricted by the quasi steady state approach and the requirement for the fixed user defined time step, these are explained further in Section 7.1.1.2.

- If multiple solutions are present in a network, problems can be encountered in achieving the correct solution. This is discussed in detail in the first case study of Chapter 8.

- Its component modelling capabilities are limited, even though there are a large number of components a true fuel tank and jet pump cannot be included by the user.

- The properties of the fuel cannot be altered either by the code or manually during an analysis to simulate altitude and temperature changes.

The major limitations of Bath*fp* are:

- Its component library, listed in Table 3.1, does not contain all of the component models required to simulate a fuel system, though this can easily be expanded.

- Water hammer cannot be currently modelled though a 'method of lines' [28] pipe model is soon to be released.

Flowmaster and Bath*fp* have completely different philosophies for results storage, Flowmaster storing all results and Bath*fp* saving only the latest. Both methods have their advantages and disadvantages. Stored results mean analyses do not need rerunning, but results become out of date with changes to networks and require disk space. Saving only the latest results, saves on disk space and means the results are always up to date with the current network. Both methods can be an advantage or disadvantage dependent on the situation and network being analysed.

Table 3.1 lists the components required for fuel system simulation, their availability in the standard release of Flowmaster and Bath*fp* and if they can, and have been, modelled in either. From the table, Flowmaster contains nearly all of the models required for fuel system analysis, but the models of the fuel tank and jet pump can only be supplied by Flowmaster UK Ltd. Bath*fp*'s supplied models are obviously lacking quite a few to enable full fuel system simulation, but all can be included, and many already have. Apart from the fuel tank and jet pump, simple instantaneous models requiring a loss coefficient to flow rate relationship are all that is required, allowing them to be based around a single model template.

Flowmaster is a very good steady state analysis tool which can model most networks competently. The flow balancing analysis module is a very useful feature for determining sizes of restrictors in branched networks. Flowmaster's drawbacks are its dynamic analysis capabilities, excepting water hammer, and its component modelling capabilities which only allow a component to be described by a pressure flow characteristic within the framework of

an existing model. Bath*fp* is a very good dynamic analysis tool which can be expanded by the inclusion of new components in user model libraries.

The strengths and limitations of each package compliment each other very well. As a result of this, plus the cross validation of the two different solution methods, they work together successfully.

CHAPTER 4

COMPONENT MODELLING AND COMPUTATIONAL FLUID DYNAMICS

This Chapter outlines component modelling with respect to an aircraft fuel system. It describes the methods of component modelling and the application of Computational Fluid Dynamics (CFD). The bulk of the Chapter covers the theory and operation of Star-CD, the CFD package used throughout this research.

4.1 Modelling Approaches

Chapter three introduced a component as a mathematical relationship of pressure to flow rate when considered within the context of network simulation. The methods and approaches described within this Chapter cover both the development of this mathematical relationship and the gathering of data either for inclusion within the model, or as a means of model validation.

The types of model developed can be broken down into two broad categories. Firstly those that completely model the component, generally in the form of a computer program or subroutine. These may be used in one of the network analysis methods or as a stand alone model. Secondly those that describe the model simply by an appropriate characteristic, either a constant factor or curve. This characteristic is commonly a loss coefficient either constant or varying with Reynolds number. It may, however, be a pressure versus flow rate relationship. These types of model are only used within a network analysis method.

A wide range of methods are available for the development of these models. At the simplest end of the scale is the use of loss coefficient data from sources such as references [16,29,30]. If required these may be further adapted for a particular application, though this will require experience of similar cases. Classical theory and empirical or experimental data is also a useful source of model development. Test rigs are an ideal source of data for model development, though generally this requires the data being collected to be critical or be of a large enough quantity to justify the cost. Recently CFD has became available to the engineer to aid in the development of component models, although this is only one of its many applications as reported by Marvin and Holst [31]. This creates new opportunities to obtain results similar to those from test rigs, but much more numerous and with no restriction on the number of measurement points. The cost is also significantly less.

4.2 Computational Fluid Dynamics

Computational Fluid Dynamics has only recently been available for general engineering applications. Traditionally it has always been a very complex solution technique with models usually being specific to one task and requiring the user to have an in depth knowledge of CFD methods. It introduces a new dimension to component modelling with the fluid flow through the component being modelled rather than the actions of the component on the fluid flow. This enables the pressure, flow characteristics of a component to be determined based solely on its inlet and outlet conditions, geometry and any associated movement of the geometry. From the results of these analyses, descriptions of the actions of the component on the fluid flow can be developed and included in component models for network analysis, but the CFD models themselves are not appropriate for direct inclusion. This is demonstrated later in the 'Y' junction studies of Chapter 5.

The model is developed by dividing the internal geometry into smaller regular volumes over which the attributes are assumed to vary linearly. The fluid flow and related phenomena of mass and heat transfer, and chemical reaction are calculated for these small volumes, although generally the application of this particular work does not require the chemical reaction and heat transfer to be modelled.

The CFD package used throughout this work is Star—CD from Computational Dynamics Ltd., [34 to 36]. It is one of the leading packages available, using up to date solution techniques and methods. It was chosen in preference to other packages for its user friendliness and simple, yet comprehensive, mesh generation utilities, this being a weakness in the other packages considered [32,33].

4.3 Star-CD

4.3.1 Theory

It is not the aim of this research to analyse in great detail the application of CFD, rather CFD is used solely as an analysis tool in the same manner as a systems design engineer would use it. A limited description of the theory is given solely to aid in the understanding of the application of these methods. A more detailed description of the application of the theory to Star-CD is given in references [34] and [35], and on the application to CFD in general in references [36] through to [47].

The following theory is taken directly from the Star-CD manuals [34,35] and is developed for a cartesian co-ordinate system, with the cartesian co-ordinates represented by x_i, x_j, x_k. The solution is appropriate also for cylindrical, spherical and torodial co-ordinate systems.

4.3.1.1 General Equations

A continuous dynamic fluid medium can be described by the Navier Stokes equations, these are fundamental laws governing continuity, force, and momentum in a fluid. Star-CD solves the inviscid Navier Stokes equations, with viscosity and turbulence accounted for by empirical approximations. The mass and momentum conservation equations are:

Conservation of Mass Equation

$$\frac{\partial}{\partial x_i}(\rho u_i) + \frac{\partial}{\partial x_j}(\rho u_j) + \frac{\partial}{\partial x_k}(\rho u_k) = 0 \qquad 4.1$$

Conservation of Momentum Equation for the x_i co-ordinate

$$\left[\frac{\partial}{\partial x_i}(\rho u_i u_i) + \frac{\partial}{\partial x_j}(\rho u_j u_i) + \frac{\partial}{\partial x_k}(\rho u_k u_i) \right] + \frac{\partial}{\partial x_i}\tau_{ij} = \frac{\partial p}{\partial x_i} + s_i \qquad 4.2$$

With similar expressions for the x_j and x_k co-ordinates.

Where

x_i = cartesian co-ordinate

u_i = absolute fluid velocity components along xi co-ordinate

q = density

p = piezometric pressure $p_s+\rho gh$ where p_s = static pressure

s_i = momentum source components along x_i co-ordinate

For the conservation of momentum equation (equation 4.2) the first term on the left hand side represents the rate of change of momentum, and the second term the stresses due to viscous effects. The first term on the right hand side of the equation represents the pressure forces and the second term the 'external' forces, for example boundaries, sources or sinks.

The relation connecting the viscous stresses to the main dependent variables for Newtonian laminar flow is:

$$\tau_{ij} = -\mu \left[s_{ij} + \frac{2}{3}\frac{\partial u_i}{\partial x_j}\delta_{ij} \right] \qquad 4.3$$

Where

μ = fluid viscosity

δ_{ij} = "Kronecker delta" has the value of unity if $i=j$ else zero

s_{ij} = rate of strain $= \dfrac{\partial u_i}{\partial x_j} + \dfrac{\partial u_j}{\partial x_i}$

For turbulent flows u, p, τ_{ij} and other dependent variables assume their ensemble average value. The relation connecting the viscous stresses to the main dependent variables for Newtonian turbulent flow is:

$$\tau_{ij} = -\mu \left[s_{ij} + \frac{2}{3} \frac{\partial u_i}{\partial x_i} \delta_{ij} \right] + \overline{\rho u'_i u'_j} \qquad 4.4$$

Where the u' are fluctuations about the ensemble average values. The rightmost term represents the additional Reynolds stress due to turbulent motion. These are linked to the mean velocities via turbulence models.

4.3.1.2 Turbulence Modelling

Due to the random nature of turbulence all current models of it are approximate representations of turbulence. The proximity of the CFD analysis to the exact solution is dependent on the nature of the flow and the turbulence model employed. Only experience can enable the 'best' model to be chosen.

Star-CD contains three mathematical models of turbulence the k-ε, k-l, and prescribed eddy viscosity models. The first two comprise differential and algebraic equations which relate the Reynolds stresses and turbulent scalar fluxes to selected ensemble averaged properties, and a solution framework to calculate these properties.

Turbulence Model Equations

The turbulent Reynolds stresses are in the same form as prescribed in equation 4.4:

$$\overline{\rho u'_i u'_j} = -\mu_t s_{ij} + \frac{2}{3} \left[\mu_t \frac{du_i}{dx_j} + \rho k \right] \delta_{ij} \qquad 4.5$$

Where

μ_t = turbulent viscosity

k = $\frac{\overline{u'_i u'_i}}{2}$ = turbulence intensity

and the viscous stress is:

$\tau_{ij} = \rho k \delta_{ij}$

The k–ε Model Equations

The k–ε model [37,38,39,42] is a widely used general model of turbulence [34], and is the preferred choice for Star–CD due to its economies of accuracy and CPU time. Other more accurate models are available but they require excessive CPU time to achieve solution. The model comprises differential equations for the ensemble averaged turbulence kinetic energy k and the rate of dissipation of kinetic energy ε. The form of these equations are:

Turbulence Energy

$$\frac{\partial}{\partial x_i}\left(\rho \tilde{u}_j k - \frac{\mu_t}{\sigma_k}\frac{\partial k}{\partial x_j}\right) = \mu_t(P + P_B) - \rho\varepsilon - \frac{2}{3}\left[\mu_t \frac{\partial u_i}{\partial x_j} + \rho k\right]\frac{\partial u_i}{\partial x_j} \qquad 4.6$$

Turbulence Dissipation Energy

$$\frac{\partial}{\partial x_j}\left(\rho \tilde{u}_j \varepsilon - \frac{\mu_t}{\sigma_\varepsilon}\frac{\partial \varepsilon}{\partial x_j}\right) = C_{\varepsilon 1}\frac{\varepsilon}{k}\left[\mu_t(P + C_{\varepsilon 3}P_B) - \frac{2}{3}\left(\mu_t \frac{\partial u_i}{\partial x_j} + \rho k\right)\frac{\partial u_i}{\partial x_j}\right] - C_{\varepsilon 2}\rho\frac{\varepsilon^2}{k} - C_{\varepsilon 4}\rho\frac{\partial u_i}{\partial x_i} \qquad 4.7$$

Where

$P = s_{ij}\frac{\partial u_i}{\partial x_i}$

$P_B = \frac{g_i}{\sigma_{ht}}\frac{1}{\rho}\frac{\partial \rho}{\partial x_i}$

$\mu_t = \frac{C_\mu \rho k^2}{\varepsilon}$

and σ_k , σ_ε , σ_{ht} , C_μ , $C_{\varepsilon 1}$, $C_{\varepsilon 2}$, $C_{\varepsilon 3}$ and $C_{\varepsilon 4}$ are empirical constants. The first term on the right–hand side of both equations represents turbulent generation by shear and normal stresses

and buoyancy forces, the second term viscous dissipation, and the third term amplification or attenuation due to compressibility effects.

The k–*l* Model Equations

The k–*l* model [40] is another well known model, but not so widely used as the k–ε model due to the economies of the latter and the requirement of the length scale distribution *l* to be prescribed. It dispenses with the dissipation equations and instead requires a user supplied length scale of the dissipation *l*.

The equation for *k* is the same as for the k–ε model, equation 4.6, and the following equation relating *k*, ε and *l* is used to eliminate ε.

$$l = C_{\mu}^{3/4} \frac{k^{3/2}}{\varepsilon} \qquad 4.8$$

where the turbulent viscosity is:

$$\mu_t = C_{\mu}^{1/4} \rho k l^{1/2}$$

The length scale *l* is supplied directly.

Prescribed Eddy Viscosity Model

The eddy viscosity model [41] has no differential or algebraic equations, instead the eddy viscosity μ_t is simply supplied directly by the user.

Near Wall Turbulence

None of the turbulence models are relevant at the low Reynolds number in the viscous sublayer very near walls. To overcome this, standard wall functions [37 and 42] which relate the velocities to the wall shear stress by a logarithmic 'law of the wall' are used.

4.3.1.3 Discretisation of Conservation Equations

The differential equations of conservation are solved over the whole of the solution domain using numerical techniques. The technique adopted in Star–CD is discretisation of the equations using the finite volume procedure [48].

Discussion of the application of the finite volume procedure employed within Star–CD is beyond the scope of this work as explained earlier. Details are available from reference [35].

The algebraic finite volume equations are solved by one of two implicit methods, a variant of the SIMPLE method [43] adapted for the nonorthogonal unstructured meshes of Star–CD, and the more recent PISO method [44 to 46] also adapted for nonorthogonal unstructured meshes.

PISO is the preferred method due to its more efficient and generalised application, requiring fewer parameters to be defined. It can be used for transient or steady state, the steady state being solved using either a time marching or iterative mode with the time derivatives deleted from the equations.

SIMPLE is used solely for steady state analyses in an iterative mode. For transient applications an additional iterative level is required making it more expensive than PISO. SIMPLE is primarily retained for use in cases with severe mesh distortion, which reduces numerical stability. The additional parameters of SIMPLE can aid in stabilising the solution for these circumstances.

The general solution approach for PISO and SIMPLE is very similar. Both use an iterative predictor and corrector stage, with the predictor providing a velocity field derived from the momentum equations and a provisional pressure distribution. The provisional fields are then refined in the corrector stages. SIMPLE employs only one corrector stage, while the number for PISO is determined internally dependent on the problem type. Continuity is ensured with an equation set derived from a combination of the momentum and mass conservation equations. Under–relaxation of the solution is employed for SIMPLE and the steady state iterative mode of PISO to stabilise the solution.

Convergence of the solution is determined for steady state when the normalised summation of the residuals for each of the dependent variables has fallen below a user prescribed value, typically 10^{-3}. For transient solution this method is not appropriate because the solution, by design, is only a close approximation to the finite volume equations. Instead the global rate of change of the dependent variables is used, in a similar test to that described above for steady state.

4.3.2 Solution Mesh

Star–CD subdivides the volume of the computational domain into cells using an unstructured mesh system. An unstructured mesh is one which does not require a constant number of cells throughout the solution domain. This can be illustrated if we consider a 'T' junction as shown in Figure 4.1, the mesh of 'a' being structured and the mesh of 'b' being unstructured. The major advantage of an unstructured mesh is in local mesh refinement for areas of interest, as illustrated in Figure 4.2 [35]. The application of an unstructured mesh saves on the number of cells required to define a problem, but additional information is required to define the cell's position relative to other cells.

The cells defined in the solution mesh are used in the numerical solution of the thermofluids conservation equations, equations 4.1 through to 4.8.

The cells are all straight edged and are either hexahedra, tetrahedra, triangular prism, or pyramids, Figure 4.3. The faces and vertices of adjacent cells must be coincident. The mesh may be constructed using any of these cell shapes, but for efficiency of solution hexahedra are preferred. The other cells are intended to enable difficult physical shapes to be modelled effectively and efficiently when hexahedra are inappropriate to model the geometry or would be excessively distorted. Distortion is measured by two criteria, the angle between cell faces, which should be greater than 45°, and the aspect ratio of the cell, which should be less than ten. In simple flows, for example a uniform velocity 'free' stream, these limits can be exceeded without affecting solution time or accuracy. If the use of a hexahedra cells causes distortion beyond these limits then a tetrahedra prism and pyramid cells should be considered.

The velocities, pressures, temperatures and any other dependent variables are solved at computational nodes at the physical cell centres.

4.3.3 Problem Description

Problem description can be broken down into four areas.

Mesh generation

Properties Description

Boundary Description

Solution Control Parameters

4.3.3.1 Mesh Generation

The generation of the mesh can be either a small or large part of the problem specification and analysis, dependent on the complexity of the geometry required. The co-ordinates of the mesh are defined in one of twenty co-ordinate systems, three global systems, cartesian, cylindrical and spherical with their origins at 0, 0, 0, and seventeen local co-ordinate systems whose type and origin are user defined.

The cells of the mesh are defined by their eight corner vertices following the right hand rule as shown in Figure 4.3. Tetrahedra, triangular prism, and pyramid cells can be regarded as degenerate hexahedra cells with a face collapsed to either a line or point.

The vertices of the whole or part of the mesh are first created. The most basic method of creating the vertices is input of the co-ordinates of each vertex individually. This method is rarely used because vertices can be generated from a single vertex or set of vertices, or filled

between a pair of vertices or sets of pairs of vertices, and sets of vertices can be reflected symmetrically about a co-ordinate axis. The path of vertex generation and fill is along the active co-ordinate system or a pre-defined spline. The numbering of the vertices is user defined, and it is important that they are numbered with thought of the cell generation strategy, as described below.

The cells are created on the vertex pattern. The most basic method available is to define the eight corner vertices of each cell individually. This method is only used for the first cell of similar cell sets, or individual cells, the rest being generated from either a single cell or cell set. Generation is along the direction of vertices with constant vertex number increment. It is for this reason thought must be given to vertex numbering to aid cell generation. Simple geometries can have cells generated in four steps, Figure 4.4, creation of the first cell, which is generated into a line of cells, which can then be generated into a surface of cells, which can subsequently be generated into a volume of cells. The cell numbers are automatically assigned. Utilities which generate a set of vertices and cells automatically for common basic shapes are also available.

4.3.3.2 Properties Description

The following fluid properties are available for description of the fluid:

Density
Viscosity
Prandtl Number
Specific Heat (Cp)
Conductivity
Schmidt Number
Heat of Reaction for chemical species

Only the properties required for solution need setting. Therefore the specific heat, conductivity, Schmidt number, and heat of reaction are not generally required for the types of analysis considered within this work. The density can be set to a constant value, or evaluated from the isobaric equation, or the ideal gas law as a function of pressure and temperature or temperature only. The viscosity, specific heat and conductivity can be set to a constant or evaluated based on user-defined criteria in a coded FORTRAN subroutine.

The turbulence model is selected if required, and the appropriate parameters supplied. For prescribed flow and pressure boundaries it is important the turbulence model is selected before the boundaries are defined because inlet turbulence parameters are dependent on the turbulence model selected.

4.3.3.3 Boundary Definition

Boundaries are shell type cells which are defined by four vertices describing a face, Figure 4.5. Boundary numbers, like cell numbers, are automatically assigned. Boundary cells can be defined by their vertices following the conventions of Figure 4.5 using techniques similar to those for cell generation, but are generally defined using the mouse. Each boundary cell is assigned to a region which is associated by the user to a boundary type. The types of boundary available are:

Prescribed Flow	Defines the inlet velocity and any turbulence parameters if appropriate. Prescribed flow boundaries generally provide the most appropriate inlet boundary types. They can also be used for outlets if the outlet velocity and turbulence are known.
Pressure	Defines the pressure and any turbulence parameters if appropriate. They may be used for either inlets or outlets. Generally pressure boundaries will require a greater number of iterations to solve than prescribed flow or outlet boundaries.
Outlet	Defines an outlet region. If there is more than one outlet boundary region the ratio of flow for each must be defined. These provide the most appropriate outlet boundaries, particularly in conjunction with prescribed flow inlets.
Wall	Defines a zero slip wall with provision for wall roughness. If required the wall can be prescribed as moving in its own plane with a known velocity.
Symmetry Plane	Defines a boundary at which the normal velocity and normal gradient of all other variables are identically zero. They are used with two-dimensional models to define the faces in the third dimension An example of this is given in Chapter 5.
Symmetry Axis	As for the symmetry plane except applied to an axis.
Cyclic	Defines a pair of boundary regions at which the flow repeats itself.

All outer cell faces not designated as a boundary cell are set to a wall region with zero slip velocity.

4.3.3.4 Solution Control Parameters

All solution control parameters have default settings and the following can be either set or adjusted:

- The solution method, either PISO or SIMPLE. The preferred choice is PISO, SIMPLE being used for steady state cases were its additional parameters may aid solution, particularly in cases of severe mesh distortion.

- The maximum number of iterations. The default is twenty, although any number up to one thousand or more may be required for complex solutions. Generally, the solution should be achieved in one hundred iterations.

- Relaxations of dependent variables. Generally these are best left at their default settings. If solution cannot be achieved, guide-lines on their adjustment is given in Reference [35].

- Residual tolerance to determine solution convergence. The default setting of 0.001 is appropriate for most cases. If solution cannot be achieved within this tolerance after adjustment of the solution control parameters, it may be appropriate to reduce the tolerance if the residuals of solution (printed to the screen during analysis) are found to be levelling out at a value near the default tolerance. It must be remembered though that even if solution had been achieved at the default residual tolerance, it would still not be an exact solution.

- The analysis type either steady state iterative, steady state time marching, or transient. If the solution is anticipated to be steady the steady state iterative solution of PISO or SIMPLE is the most appropriate. If this does not realise a solution PISO may be used in a 'steady state time marching' mode. In this case the time step is set to a large value to accelerate the approach to the steady state. The intervening time steps will not be time accurate. Guide-lines on the choice of time step are given in Reference [35]. Unsteady or 'transient' analyses can only be carried out with PISO. The choice of time step is very much dependent on the problem being analysed and can only be determined by experience and trail and error.

- The initial data used to start solution. For new analyses an initial constant data field of velocity or pressure may be set to aid initialisation of the solution. This is particularly useful for cases with pressure boundaries. For continuation or restart analyses the last saved solution should be used.

- Cell for monitoring solution progress. The values of the variables being solved are printed to the screen during solution for the monitoring cell. Ideally it should be in an area of interest and/or where approach to solution will be the slowest.

- Type of post processing data file stored, either restart with minimum post processing data or restart with all post processing data. A restart data file with minimum post processing data is only appropriate if it is anticipated solution will be not achieved, for example creating an initialisation field for a series of analyses.

4.3.4 Postprocessing Description

The types of plot available for postprocessing are vector plots of total velocity or component velocities, contour plots of scalar parameters and velocity magnitude, or combined plots of velocity vectors and any scalar property. The contour plots can be either line contours or filled raster type plots. The solution data is plotted at the cell centres or interpolated to vertices. The plots can be optimised by the following methods:

- Zoom and Pan
- Section Plots
- Presentation grid. Results are interpolated to a cartesian grid of even density. This is particularly useful where areas of high density of computational grid detract from solution in other areas
- Thinning of number of vectors by a constant factor
- Overlaying of plots, particularly useful for multiple section plots
- Display of multiple plots
- User prescribed scale of plotted parameters and number of colours
- Adjustment of the size of vectors to enable the results to be seen clearly
- Titles and labels.

4.4 Closing Remarks

Traditionally component modelling has been restricted to the use of theory, data from sources such as references [16,29,30] and test rigs. With the introduction of Star-CD to the analysis and assessment of a components performance a large range of data for development of component models now becomes available. The Star-CD models can be used to assess the

general flow patterns within a component to simply aid understanding, or may be used to develop empirical relationships describing the operation of the component.

In many cases the only restriction on the modelling of a component is the ability to produce the meshed geometry. This problem may be overcome with the use of a finite element stress modelling package such as PATRAN to develop the mesh, which can then be imported into Star-CD. Finite element stress modelling does not require such an ordered mesh as CFD. For this reason extensive automatic meshing utilities have been developed. Care has to observed with these meshes to ensure they do not have too great a degree of distortion due to the flexibility allowed in the finite element mesh. This method of mesh generation unfortunately has not been carried out within this research, because of limited access to PATRAN or any other suitable finite element package.

Star-CD enables a large range of components and their reactions to be investigated, with a view to the development of component models for Bath*fp* and Flowmaster. Care has to be exercised though because the computational methods employed are based on approximations in areas such as turbulence modelling, though experimental data as shown results to generally be good.

As part of this research, various components have been analysed using CFD to asses their flow patterns and/or loss coefficients. The data from these analyses has been used in general models in Bath*fp* and Flowmaster. An example of this is given in the second case study of Chapter 8. CFD data will also be used as the basis for the development of specific 'Y' junction models as described in Chapter 5.

CHAPTER 5

'Y' JUNCTION TEST WORK

The losses through junctions are a challenge to both the modeller and compiler of loss data. Unlike many other components where the loss coefficient is constant, for example bends, or a known function of flow rate, as in the case of pipes, the loss coefficient of a junction is a function of both the included angle of the junction and the flow ratio in the junction branches.

From current sources [16,30,49 to 52] there are large amounts of data describing the losses through 'T' junctions, but the data for 'Y' junctions is very limited. This has been highlighted in many of the analyses carried out during this programme particularly for cases of combining flows with included angles below 60°.

To address this problem the test programme described here was undertaken to determine loss coefficients for symmetrical combining 'Y' junctions down to 30° included angle. In addition to the testing of the junctions, Computational Fluid Dynamic (CFD) models of all the junctions tested have been developed with the intention of validating the application of CFD to the modelling of combined flows of this form. To help this validation, flow visualisation was included within the test rig in the form of dye injection into the inlet flows. This has been used for qualitative comparison to the CFD models.

'Y' junctions with included angles of 150°, 120°, 90°, 60°, and 30° have been tested. Validation of results for the 150° through to 60° junctions is provided from the work of D. S. Miller [16]. Reference [16] is a collection of loss coefficient data for the majority of 'standard components' from a wide range of test programmes and references thus providing one of the most appropriate sources for validation of the test results. Validation of the results for the 30° junction is based on both the CFD model of the 30° junction and the experience and confidence obtained with the test rig and procedures from the other junction tests.

5.1 Theory

5.1.1 Coefficient of Loss

Head losses for a component with fully developed turbulent flow are approximately proportional to (velocity)^2. Since velocity head is given by $u^2/2g$ a loss coefficient non-dimensionalised to this velocity head can be used to describe the total head loss.

The layout of a 'Y' junction showing the nomenclature applied to the legs is shown in Figure 5.1. Taking the general loss coefficient equation outlined in Chapter 3 and applying to a 'Y' junction,

$$k = \frac{\Delta H}{u^2/2g} \qquad 5.1$$

The total head loss is defined as:

$$H_{13} = \left(\frac{u_1^2}{2g} + h_1 \right) - \left(\frac{u_3^2}{2g} + h_3 \right) \qquad 5.2$$

From this the loss coefficient through a 'Y' junction based on the combined flow through the junction from leg 1 to 3 is:

$$k_{13} = \frac{\left(\frac{u_1^2}{2g} + h_1 \right) - \left(\frac{u_3^2}{2g} + h_3 \right)}{\frac{u_3^2}{2g}} \qquad 5.3$$

and the loss coefficient from leg 2 to 3:

$$k_{23} = \frac{\left(\frac{u_2^2}{2g} + h_2 \right) - \left(\frac{u_3^2}{2g} + h_3 \right)}{\frac{u_3^2}{2g}} \qquad 5.4$$

All loss coefficient data is described for zero length junction legs, so points 1, 2 and 3 in the above analysis are considered to be coincident. For descriptive and analysis purposes 1, 2 and 3 are taken to be the legs of the junction.

Application of this data will require the head loss due to friction of the junction inlet and outlet legs taking into account. There are a number of methods available to determine the head loss due to friction. One of the most common uses a friction factor (f), for which head loss is defined as:

$$\Delta h = \frac{fL}{d} \frac{u^2}{2g}$$

Where L is the length of the leg, d the diameter and u the velocity in the leg.

5.1.2 Measurement of Loss Coefficient

For constant flow rate, the rate of pressure loss with respect to distance along a pipe is constant. The inlet legs of a 'Y' junction will have a lower rate of loss than the outlet leg because their flow rates will be a percentage of the outlet flow rate. The mixing at the junction will create an additional loss due to shear and turbulent mixing losses. The resultant pressure profile along the inlet pipes, junction and the outlet pipe will have the form of Figure 5.2. The actual shape of the pressure profile due to the junction is unknown and lies within the shaded area of Figure 5.2.

The loss coefficients for the junction are based on experimental data and are calculated from equations 5.3 and 5.4. This requires the inlet and outlet static heads of the junction to be measured. These are taken from the pressure gradient of the inlet and outlet pipes, assuming the loss of the 'Y' junction is a discontinuity at the junction centre, of the form shown in Figure 5.3.

5.2. Test Rig

The test rig [53] was required to:

- Supply a constant head and flow rate to the 'Y' junction test specimen to ensure fully developed turbulent flow in the combined leg. This to be maintained for a minimum duration of two hours.
- Allow junctions with differing internal angles, both symmetrical and non-symmetrical to be tested (only symmetrical junctions were tested in this programme).
- Test combining and dividing flow cases (only combining junctions were tested in this programme).
- Provide a means to test the complete range of ratios of inlet to outlet flow rates.
- Provide flow visualisation

The test rig, shown in Figure 5.4, consists of the following major components:

Reservoir

Expense Tank

Test Section

Dump Tank

5.2.1 Reservoir

The 300 gallon reservoir is used as a buffer to ensure the expense tank always supplies a constant head.

5.2.2 Expense Tank and Delivery System

The expense tank is a 250 gallon tank supplying a constant head of 2440mm of water to the test section. This is achieved by the use of a 610mm long weir. From Bazin's formula for rectangular weirs [54] a 610mm long weir can be shown to maintain the head to within +3.2mm, with the weir spilling. This was verified as part of the test programme.

Delivery to the test section is through two pipes, each consisting of a gate valve at the tank outlet, a turbine flow meter in a straight 50mm internal diameter steel pipe of length five diameters upstream and ten diameters downstream of the meter, as prescribed by the manufacturer [55], and a length of 50mm internal diameter flexible pipe. This is shown in Figure 5.4.

5.2.3 Test Section and Settling Length

The 'Y' junctions under test were manufactured from clear perspex 44mm internal diameter pipe to permit flow visualisation for qualitative comparison to the CFD models of the 'Y' junctions, Figure 5.5. The 'Y' junctions were connected by bolted flanges to the inlet and outlet pipes. These are 50mm internal diameter steel pipe, each thirty five diameters in length. This is to ensure the characteristics of the 'Y' junction are not affected by other components. The difference in diameter of the 'Y' junctions and the settling lengths was due to the 'Y' junctions being manufactured from 50mm external diameter pipe. This error was not realised until well into the programme. The effect of this is allowed for in the calculation of the loss coefficient.

5.2.4 Dump Tank

The flow from the outlet settling length was fed to a submerged outlet in the dump tank which used a weir to maintain a constant back pressure to avoid cavitation in the outlet pipe. The water spilled over the weir was recirculated back to the reservoir with a variable capacity centrifugal pump.

5.2.5 Varying the Flow Ratio

The flow ratio was varied with specially designed clamping blocks (Figure 5.6) on the inlet flexible pipes (Figure 5.4). These were used in preference to the inlet valves, shown in

Figure 5.4, because the valves were found to cause a significant flow disturbance which resulted in large oscillations on the manometers. The clamping blocks gave a smooth variation of the cross-sectional area ensuring the minimum flow disturbance, hence minimum pressure oscillations.

5.2.6 Pressure Readings

Six sets of pressure tappings, at a spacing of 3 inch at the upstream end of the inlet lengths and the downstream end of the outlet length, measured the pressure gradient for the inlet and outlet lines. Four tappings were arranged around the circumference at each of these 3 inch spacings (Figure 5.7). Only one of the four tappings was used for determining the pressure gradient. The selection of these is explained in Section 5.3.1.

The pressure readings were taken with simple water manometers inclined at 15° on two manometer boards, one for the inlets and one for the outlet. These boards were adjustable for height to allow for changes in static pressure. The height of the boards above the test line was determined using a 'master' manometer fixed to the test rig and connected to the first line of each board. To enable all of the readings to be compared simultaneously rubber 'O' ring markers were used on the manomcter tubes.

5.2.6.1 Pressure Oscillations

A major problem encountered during commissioning of the rig was pressure oscillations registering on the manometers. The oscillations were small in size and due to small disturbances in the flow paths in the inlet and outlet settling lengths. They were found to be exacerbated if the inlet ball valves (Figure 5.4) were used to throttle the flow. It was for this reason the clamping blocks were developed to throttle the flow. Two additional methods were also introduced for reducing the frequency and size of the registered oscillations on the manometers; slugs in the manometer lines at the tappings and slave lines on each manometer, after the slug. This coupled the flow in the slave line and manometer, reducing the size and frequency of the registered pressure oscillations. Both methods are illustrated in Figure 5.8.

5.2.7 Flow Visualisation

Two dyes of different pigmentation were used for flow visualisation, one in each inlet leg. The dye was introduced into the flow with two injectors consisting of a dye reservoir pressurised slightly above test pressure feeding a 1.5mm diameter capillary tube which passed through the sealing gasket at the inlet settling length and 'Y' junction manifold facing downstream, Figure 5.9. The flow visualisation equipment was only attached to the rig during the flow visualisation tests.

5.3. Test Procedure

5.3.1 Commissioning Tests

The commissioning tests consisted of two major stages. Initially, it was necessary to evaluate and select an appropriate method to overcome the fluctuations of the pressure readings as described above. Secondly, the six tappings in each leg to measure the pressure gradient were selected. Only one of the four circumferential tappings at each axial position (Figure 5.7) could be used during the loss coefficient tests due to the availability of suitable manometers. In addition, only one tapping was selected at each station in preference to an average of all four tappings to eliminate any 'false' readings from 'bad' tappings. The levels on all four tappings were however observed to rise and fall in unison. For each line the selection was based on readings from all twenty four tappings, with the selected tapping being the one which approximated closest to the best fit pressure gradient through all twenty four. The inlet lines gave a very good set of data points, but the outlet line had a large scatter, and consequently two of the locations were ignored when plotting pressure gradients, Figure 5.10. The possibility of swirl induced by the mixing at the 'Y' junction causing the large scatter was investigated by carrying out the tests with the 'Y' junction removed. These gave very similar results to those with the 'Y' junction present. The large scatter is therefore due to incorrectly manufactured tappings, possibly due to the tappings being 'out of square' to the pipe wall. Burrs could also cause this scatter but a visual inspection of the pipe bore did not indicate this.

5.3.2 Loss Coefficient Tests

The aim of these tests was to record the pressure and flow rates at the inlets and outlet for all possible flow ratios for all junctions to enable the loss coefficients to be calculated.

Flow ratios from 0.2 to 0.8 in steps of 0.05 were tested. Ratios below 0.2 and above 0.8 gave unstable pressure readings. This is due to an instability in the flow paths caused by the largely differing flow ratios, this effect has been reported in previous tests by Idel'chik [30]. For each flow configuration four readings were taken during two separate runs, with approximately one to two hours allowed for the rig to settle between readings. This gives confidence in the results and the test rig, allowing repeatability of the rig to be investigated

The loss coefficients were calculated from equations 5.3 and 5.4. The inlet and outlet heads h_1, h_2, and h_3 were determined by extrapolation of the pressure gradients, obtained from the pressure tappings, to the junction centre.

5.3.2.1 Allowance for Dissimilar Diameters

When taking into account the effects of the dissimilar diameters of the settling lengths and the 'Y' junctions two factors must be considered.

- The contraction at the inlet and the expansion at the outlet of the 'Y' junction are small when compared to the diameter of the 'Y' junction.
- The head loss measured across the 'contraction – 'Y' junction – expansion' will be less than the sum of the individual losses taken in isolation due to component interaction effects. This is because in closely spaced components, the outlet flow from the upstream component is influenced by the presence of the downstream component, and the downstream component inlet flow is consequently affected by the upstream component. These interactions result in the flow being 'guided' from the upstream component into the downstream component with only a small flow disturbance, resulting in a reduced head loss across both components [16].

Applying this to the test rig for the three 'components' making up the measured head loss, it is clear that if the inlet head (h_1) were reduced by the head loss due to a contraction of the size of the dissimilar diameters, and the outlet head (h_3) increased by the head loss due to an expansion of the size of the dissimilar diameters, this would result in a lower head loss across the 'Y' junction than would be the case for a 'Y' junction in isolation. Likewise if the measured head loss were used with no allowance this would be greater than would occur across the 'Y' junction in isolation.

In considering the appropriate allowance to be made for the dissimilar diameters, we should consider the interaction between each of the 'components'.

- The inlet contraction will have a small measurable head loss.
- The interaction effects of the inlet contraction on the 'Y' junction will be negligible. This is because the inlet contraction will only create a small flow disturbance and therefore the static pressure and velocity profile will have recovered sufficiently at the 'Y' junction.
- The 'Y' junction will create a large flow disturbance due to the mixing of the two inlet flows. The static pressure and velocity profile will therefore require a significant length to recover due to this disturbance.
- The head loss due to the outlet expansion will be negligible as it occurs in the wake of the flow disturbance of the 'Y' junction.

Based on these considerations, the effects of the dissimilar diameters of the inlet settling lengths and the 'Y' junction are taken into account by reducing the head loss measured on the test rig by the loss through the inlet contraction only. The minimal loss of the outlet expansion is accounted for by not reducing the inlet contraction loss due to component interaction with the 'Y' junction. contraction loss.

To verify this assumption, we shall take a case for the 60° 'Y' junction at a flow ratio of 0.509 and calculate the loss coefficient based solely on the measured data, allowing for both the inlet contraction and outlet expansion, and allowing for the inlet contraction only. The results from these analyses shall be compared to data from Miller [16] for verification. The following heads and flow rates are available from the tests.

h_1 = 1.538m $\qquad$ u_1 = 1.497ms−1

h_3 = 1.170m $\qquad$ u_3 = 2.928ms−1

h_1 and h_3 are calculated from the pressure gradients of the pressure tappings. The loss factor k_{13} for a junction is described by equation 5.3.

$$k_{13} = \frac{\left(\frac{u_1^2}{2g} + h_1\right) - \left(\frac{u_3^2}{2g} + h_3\right)}{\frac{u_3^2}{2g}}$$

Reduction of h_1, allowing for inlet contraction, gives:

$$h_1 = 1.538 - \frac{k\mu_1^2}{2g}$$

From reference [16] a loss coefficient for an abrupt contraction with an area ratio of 0.7744 is given as 0.0993. The data of Figure 5.11 is for cases with a Reynolds Number greater than 10^5. In this case the velocity in the inlet leg is 1.497ms^{-1}, giving a Reynolds Number of 5.96×10^4. The loss coefficient is adjusted by a Reynolds Number correction factor. Miller [16] gives a Reynolds Number correction factor of 1.23.

$$k_1 = 0.0993 \times 1.23$$

$$= 0.122$$

Therefore

$$h_1 = 1.538 - \frac{0.122 \times 1.491^2}{2g}$$

$$= 1.524\text{m}$$

Increase of h_3 allowing for outlet expansion

$$h_3 = 1.170 + \frac{k_o u_3^2}{2g}$$

Miller [16] gives a loss coefficient for an abrupt contraction with an area ratio of 0.7744 as 0.112.

Therefore

$$h_3 = 1.170 + \frac{0.112 \times 2.928^2}{2g}$$

$$= 1.219\text{m}$$

The loss coefficient, not taking into account the dissimilar diameter, will be:

$$k_{13} = \frac{\left(\frac{1.497^2}{2g} + 1.538\right) - \left(\frac{2.928^2}{2g} + 1.170\right)}{\frac{2.928^2}{2g}}$$

$$= 0.0957$$

The loss coefficient allowing for both the inlet contraction and outlet expansion is:

$$k_{13} = \frac{\left(\frac{1.497^2}{2g} + 1.524\right) - \left(\frac{2.928^2}{2g} + 1.219\right)}{\frac{2.928^2}{2g}}$$

$$= -0.0326$$

The loss coefficient allowing for the inlet contraction only is:

$$k_{13} = \frac{\left(\frac{1.497^2}{2g} + 1.534\right) - \left(\frac{2.928^2}{2g} + 1.170\right)}{\frac{2.928^2}{2g}}$$

$$= 0.0693$$

For a 'Y' junction with a flow ratio of 0.509 Miller [16] gives a loss coefficient of 0.063, which supports the premise that the outlet expansion loss is negligible. Additionally when both the inlet contraction and outlet expansion are taken into account, a negative loss coefficient results. This is not possible at a flow ratio of what is effectively 0.5, because this would mean both k_{13} and k_{23} would be negative and therefore the 'Y' junction would be supplying energy to the system.

Adjusting all results shows similar effects. Therefore the inlet contraction only is accounted for in the processing of the results and all of the loss coefficients calculated from the measured data have been adjusted for the inlet contraction loss as above.

5.3.3 Flow Visualisation Tests

Recirculation was not used during the flow visualisation tests due to the intensity of the dyes discolouring the inlet flows. For all the 'Y' junctions and flow ratios four visualisation runs were carried out:

- Dye streams introduced into both inlet legs along the centre line.
- Dye streams introduced into each inlet leg individually, along the centre line.
- Dye streams introduced into both inlet legs at the inner wall.
- Dye streams introduced into each inlet leg individually, at the inner wall.

The streams introduced along the centre line give a general view of the flow pattern, those at the wall were to determine if any significant wall effects were present. The introduction of the streams both individually and together gives a clear picture of the mixing taking place.

5.3.4 Computational Fluid Dynamic Model of 'Y' Junction

The application of CFD within the test programme has been to satisfy two requirements. Initially data from Miller [16] and the test rig for junctions with an included angle of 150° through to 60° are used to assess the suitability of the CFD methods and in particular the turbulence models, to the modelling of combining flows in junctions. This assessment was

based on the prediction of the loss coefficients and the comparison of flow patterns to those obtained from the flow visualisation tests. If this assessment proved satisfactory the results from the CFD models could then be used as a validation aid for the loss coefficients obtained from the test rig for the 30° 'Y' junction, CFD providing the only direct validation. All of the models were analysed for flow ratios from 0.2 to 0.8 in steps of 0.1.

5.3.4.1 Geometry

The geometry of the 'Y' junction was identical to that used within the test as shown in Figure 5.5. The geometry of the 'Y' junctions creates a problem with determining if a two or three-dimensional model is appropriate. The actual shape is symmetrical in two planes so may be expected to be adequately modelled with a two-dimensional model, but the mixing action of the two flows may have three-dimensional effects to be considered. To assess the impact of any three-dimensional effects on the mixing both two and three-dimensional models were developed for the case of the 60° junction and the loss coefficients obtained from these models compared.

Settling lengths were not modelled on any of the junctions because the flow is assumed straight with no influence of other components for both the test rig and the data available from Miller [16]. The inlet and outlet legs of the junction were taken to be 200mm, the average length of all the junctions tested.

5.3.4.2 Calculation Mesh

Two-Dimensional

The calculation mesh for the two-dimensional model was constructed using the standard utilities embodied within PROSTAR. The mesh was constructed using standard hexahedra cells and is shown in Figure 5.11. The advantages of an unstructured grid were not exploited for this mesh because the number of cells involved was low and the time required to develop an unstructured mesh would not be justified. Additionally, using the structured grid shown aligns the cell pattern closely with the geometry and the expected flow path. This will aid solution both in terms of accuracy and time. The mesh consists of 870 fluid cells.

Three-Dimensional

The calculation mesh for the three-dimensional model was constructed using the standard utilities embodied within PROSTAR. The mesh was of an unstructured form with local mesh refinement and was constructed using hexahedra, tetrahedra, prism and pyramid cells, and is shown in Figure 5.12. A cartesian grid was used in preference to a polar grid because the polar grid was not appropriate for meshing the intersection of the inlet legs. The refinement

of the mesh on the inside of the inlet legs is to aid in the correct meshing of the intersection of the legs. The mesh consists of 4154 fluid cells.

5.3.4.3 Fluid Properties and Boundary Conditions

The fluid properties were those for water at 20°C and the k–ε turbulence model was used.

The boundary region indexing for the two-dimensional model is shown in Figure 5.13. Boundaries 1 and 2 are considered to be inlets with a fixed velocity, boundary 3 is considered to be an outlet, boundary 4 is considered to be a symmetry plane and boundary 5 is considered to be a zero slip wall.

The boundary region indexing for the three-dimensional model is shown in Figure 5.14. Boundaries 1 and 2 are considered to be inlets with a fixed velocity, boundary 3 is considered to be an outlet. All other external cell faces are considered to have a zero slip wall boundary condition.

The parameters of boundaries 1 and 2 are dependent on the flow ratios simulated. The parameters required are the velocity and turbulence parameters describing the inlet turbulent energy, k, and dissipation, ε. These are defined in Chapter 4 as:

$$k = \frac{u'u'}{2}$$

where typically $\frac{u'}{u} = 10^{-2}$

$$\varepsilon = \frac{C_\mu^{3/4} k^{3/2}}{l}$$

where $C_\mu = 0.09$

$$l = \frac{d}{10}$$

5.3.4.4 Determination of Loss Coefficient

The 'Y' junction loss coefficients of [16] do not include the effects of friction, and the loss coefficients determined from the test rig are calculated assuming zero length legs. The CFD models do include friction losses in the wall boundaries, and allowance was therefore made for this loss. The two-dimensional models are effectively 'laminates' with a single cell thickness and friction loss in the wall boundary is therefore insignificant. The pressure loss due to friction for the three-dimensional model must be taken into account when calculating the loss coefficient. CFD models of pipes of the same diameter and length as the inlet and

outlet legs were developed, and simulations performed for all the inlet and outlet flow rates. The pressure loss from these models gave the appropriate reduction of pressure for the inlet legs, and increase for the outlet leg to account for the pressure loss due to friction.

The loss coefficient for all the junctions and flow conditions were determined from equations 5.3 and 5.4.

5.3.4.5 Comparison of 60° Two-Dimensional and Three-Dimensional Model

The three-dimensional mesh of the 60° 'Y' junction required approximately twenty times longer to create and simulate than the two-dimensional mesh.

The loss coefficients determined from the analysis of the two and three-dimensional 'Y' junctions, and from the test rig are given in the following table.

Flow Ratio	Three-Dimensional Model	Two-Dimensional Model	Test Rig
0.2	-0.288	-0.295	-0.212
0.5	0.08	0.077	0.0619
0.8	0.237	0.201	0.167

It can be seen that both models show good agreement with those from the test rig, and the three-dimensional model gives no significant improvement over the two-dimensional model. The increased time required to mesh and analyse the three-dimensional model is not justified, with the increase in accuracy being insignificant. Two-dimensional CFD models only have been developed for all the other junctions.

5.4 Comparison of Data

Two forms of graph are used to present the results. The first shows loss coefficient as a function of flow ratio for each junction. The second shows junction angle as a function of flow ratio for a constant loss coefficient. This latter presentation is the form used by Miller [16].

The loss coefficients from Miller, the test rig and the two-dimensional CFD models are presented in graphical format in Figures 5.15 through to 5.21. Figures 5.15 to 5.19 present the data for the individual junctions. Each graph shows loss coefficients from Miller, those determined from the test rig and from the two-dimensional CFD models. A band representing the potential scatter of the test rig coefficients due to measurement inaccuracies is also

included. Figure 5.20 summarises Figures 5.15 to 5.19, presenting the loss coefficients of Miller and the test rig for all junctions tested and Figure 5.21 presents the loss coefficients of Miller and the two-dimensional CFD models. Figure 5.22 is the second form of graph and presents the loss coefficients of Miller and those determined from the test rig for all junctions.

5.4.1 Test Rig Results

The loss coefficients determined from the test rig data have been fitted with a third order least squares polynomial for Figures 5.15 to 5.20 and are given in Appendix A. These polynomials are only valid within the range of measured data, ie. between flow ratios of 0.2 and 0.8. The use of fourth order equations caused excessive divergence at the extremes of the ranges and no noticeable improvement of fit for the mid range. The correlation coefficient of the curves are given in the following Table for each junction.

Junction	Correlation Coefficient
30°	0.925
60°	0.942
90°	0.951
120°	0.957
150°	0.937

From these values it can be seen that the data is adequately fitted with these equations, all correlation coefficients being greater than 0.9.

Constant loss coefficient data for Figure 5.22 could not be obtained directly from the test rig results. Instead they have been determined from the equations representing the test rig data in Figures 5.15 to 5.19, at the loss coefficient values represented in [16].

The graphs of Figures 5.15 through to 5.20 show the loss coefficients determined from the test rig to be in very good agreement with that of Miller. Figure 5.22 does not show such a good comparison. This is attributed to the loss coefficients being derived from the equations representing the loss coefficients of Figures 5.15 to 5.19, and the limited number of observations that could be used. All analysis of the results has been carried out on the data of Figures 5.15 to 5.19, because these represent all the loss coefficient data obtained from the test rig rather than at discrete loss coefficients.

5.4.1.1 Repeatability of Results

A measure of the accuracy of the test rig is the ability to repeat results for the same test conditions. This can be examined for the rig by comparing the four sets of results obtained at each flow ratio for each junction. Inspection of the loss coefficients of Figures 5.15 to 5.19 show that loss coefficients at a particular flow ratio show a tendency to the same value.

The loss coefficients for the 60° and 90° junction, Figures 5.16 and 5.17, show a divergence to either side of their best fit line above a flow ratio of 0.5. The lower of these is for the flow ratios of 0.65 and 0.75, and the higher for the flow ratios of 0.7 and 0.8. This effect can be seen to a lesser extent through the total range of values. The testing for flow ratios of 0.2 through to 0.8 in steps of 0.1 were carried out at the start of the testing period and the flow ratios of 0.25 to 0.75 in steps of 0.1 were carried out at the end of the testing period. In the period between these tests the characteristics of the test rig will have changed due to the build up of rust in the steel piping. The pressure gradient will increase slightly for each line due to an increase in the friction loss. This will result in a reduced measured pressure drop across the 'Y' junction, and hence a lower loss coefficient, Figure 5.23.

The differences between these results are still within experimental error, and when the correlation coefficient of the loss coefficient curve is also considered the repeatability of the rig is found to be acceptable, with maximum error due to rig contamination.

5.4.1.2 Sources of Error

Overall errors were small as indicated by the correlation coefficients determined in Section 5.4.1. Much of the error can be attributed to problems with reading of the flow meters and manometers due to the oscillation of these readings. This is attributed to the sensitivity of the instrumentation to attain the accuracy required.

The effects the potential errors of reading due to the oscillations of the instrumentation on the loss coefficient can best be understood if the sensitivity of the loss coefficient to these oscillations is determined.

Sensitivity to Flow Rate

The fluctuation of the turbine flow meter output was due solely to the accuracy of the instrumentation, and was constant for all test conditions at $\pm 0.0163 ms^{-1}$.

The sensitivity of the loss coefficients to the potential error on flow rate measurement has been investigated for the loss coefficient curves of Figures 5.15 to 5.19. The analysis assumed a Reynolds Number of 105 in the outlet leg, and determined the loss coefficient for all combinations of maximum positive and negative reading errors on the inlet legs. The

maximum positive error on loss coefficient for all junctions was with a positive reading error applied to both inlet legs, and the maximum negative error on loss coefficient was with a negative reading error applied to both inlet legs. The potential maximum positive and negative errors for all junctions are given in Table 5.1.

Sensitivity to Head

The manometer oscillation was dependent on the degree of throttling applied. The minimum oscillations of ±20mm at an inclination of 15° (±5.2mm in the vertical) were for flow ratios of 0.5 where no throttling is required, and the maximum oscillations of ±60mm at an inclination of 15° (±15.5mm in the vertical) were for flow ratios of 0.2 and 0.8, where the maximum amount of throttling is required. It is not expected the maximum errors would be encountered reading the manometer boards because there was a definite mean value within the oscillation at which readings were taken, and the use of the 'O' ring markers gave an instantaneous reading of all the manometers. The most significant error in pressure measurement would be from the master manometers which did not benefit from the 'O' ring markers and were read separately to the inlet and outlet tapping manometers. However these manometers were read at the mean point of the oscillation.

The effects of errors in pressure measurement can be determined directly from equation 5.3. Rearranging gives:

$$k_{13} = \frac{\left(\frac{u_1^2}{2g} - \frac{u_3^2}{2g}\right) + \Delta h}{\frac{u_3^2}{2g}}$$

Therefore sensitivity of the loss coefficient to head is:

$$\frac{\Delta k}{\Delta h} = \frac{2g}{u_3^2}$$

For a Reynolds Number of 105 in the outlet leg, the sensitivity of the loss coefficient to head is found to be constant at 5.65×10^{-4} mm^{-1} when measured at an inclination of 15° (2.186×10^{-3} when measured vertically). Taking the maximum reading error on the manometers as ±60mm (±15.5mm vertical head) the maximum error of the loss coefficient, due to pressure reading, is 0.0678.

The maximum error due to reading is shown as the error band on Figures 5.15 to 5.19. From these plots it can be seen that all the data, both the measured and Miller's, lies within this band.

General Errors

Other possible causes of error are general items such as:

- Build up of rust as the test programme continued, though this would be symmetrical about the rig.
- The intrusion of the gaskets at the 'Y' junction to settling length manifolds, though this effect is minimised due to the effects of the dissimilar diameters.
- The welded joints on the 'Y' junctions showed slight signs of out-of-roundness and surface discrepancies.
- The geometry of the 'Y' junctions under test was defined to be a representation of those illustrated in [16]. There is no standard geometry for 'Y' junctions when determining their loss coefficients.

5.4.2 Computational Fluid Dynamic Results

The loss coefficients calculated from the CFD results are shown with those determined from the test rig and Miller's in Figures 5.15 through to 5.19. Figure 5.21 compares the loss coefficients determined from the CFD models to those of Miller for all junctions. A selection of flow visualisation results and relevant flow vector plots from the CFD analysis are shown in Figures 5.24 to 5.27. Unfortunately photographs of the 60° junction are not available.

Inspection of the graphs show the CFD determined loss coefficients to generally be in good agreement with those of Miller, and within the error band of the test rig loss coefficients. The following general conclusions can be made.

- The prediction of loss coefficient for flow ratios up to 0.5 is good, excepting 150° and 120° at a flow ratio of 0.5.
- For values over 0.5 the loss coefficient is over predicted for the 30° and 60° junctions, the effect being greater for the 30° junction, and is under predicted for the 90°, 120° and 150° junctions, the effect being greater for the 150° junction.

The loss of a combining 'Y' junction is due to the interaction of the two inlet flow paths and the associated turbulence generated. This loss is dependent on the included angle of the 'Y' junction and the flow ratio within the 'Y' junction.

For small included angles the turbulence will be lower because the interaction of the inlet flows will be low due to their straighter flow paths. This is illustrated in the flow visualisation photographs of the 30° junction, Figure 5.24. These show a smooth mixing of

the two flows. For large included angles the turbulence will be increased due to the increased interaction of the two inlet flows. This is again illustrated with the flow visualisation photographs, this time for the 120° and 150° junctions, Figures 5.26 and 5.27, these show substantial disturbance and mixing of the two dye streams even at the point of initial combination.

The magnitude of the turbulent mixing is also affected by the flow ratio in the junction. For high flow ratios the turbulence will be high due to the increased energy in the leg, but for lower flow ratios the turbulence will be lower. This effect is less pronounced than the effects of junction angle.

It is assumed the turbulence model does not completely model the turbulent mixing effects of the 'Y' junction, particularly at high flow ratios and large included junction angles, for these cases the turbulence will be above normally expected values. This would account for the over prediction of loss coefficients for the 60° and 90° 'Y' junction models and the under prediction of the loss coefficients for the 120° and 150° 'Y' junction models. The turbulence model is the weakest point of any CFD code [32] because it is an empirical estimation of a random occurrence. The model used here is a k–ε model, which although a very good general approximation to turbulence, does not completely model the turbulence associated with the interaction of inlet flows within a combining 'Y' junction. To achieve this a turbulence model specific to the characteristics of a 'Y' junction would be required. This has not been undertaken because this study is to assess the suitability of CFD to a general application to fuel system simulation without the need for further extensive programming.

A second means of validating the CFD analyses is in the use of the flow visualisation in comparison to the vector plots, Figures 5.24 to 5.27. All of the vector plots show a good agreement to the flow visualisation results. The most interesting aspect of these is the very good agreement on the position of the zero shear plane between the flow visualisation pictures and the vector plots.

The prediction of the loss coefficient is within the error band of the loss coefficients calculated from the test rig results, except high flow ratios for the 30° 'Y' junction and mid flow ratios for the 150° 'Y' junction. The loss coefficients of the 150° 'Y' junction seem to have a large error, but the shape of the curve is the same as the loss coefficients from Miller and those calculated from the test rig results, Figure 5.19 and 5.20, the only difference being that the low point occurs at a flow rate of 0.5 rather than 0.2.

5.4.3 30° 'Y' Junction Results

One of the major aims of this test programme has been to extend the loss coefficient data for combining 'Y' junctions down to included angles of 30°. Validation of this data determined

from the test rig for the 30° 'Y' junction cannot be carried out directly against known data as for the other junctions, the only validation available being:

- Confidence in the test rig based on the results for the other junctions.
- Comparison to the 30° CFD model.

The 30° loss coefficient curve of the test rig results, Figure 5.15, follows the trend of the other junctions. Comparison of the loss coefficients determined from the test rig results and CFD show very good agreement up to and including a flow ratio of 0.5, Figure 5.15. Above a flow ratio of 0.5 the two loss coefficients diverge and it is assumed both are in error. As explained above, CFD over predicts the loss coefficient for junctions with small included angles. If the loss coefficients calculated from the CFD model are compared to Miller's results, Figure 5.21, for flow ratios above 0.6 they are greater than Miller's 60° 'Y' junction loss coefficients. The test rig results predict a negative loss coefficient above a flow ratio of 0.5. If the negative loss coefficients below a flow ratio of 0.5 are taken to be correct, which would seem to be true when compared to the other junctions, then a negative loss coefficient for a flow ratio above 0.5 is not possible. If both loss coefficients were negative, then for a flow split at the junction of say 0.7 and 0.3, both flows, when combined, will have increased in pressure and so gained energy. Inspection of the loss coefficient data from the test rig at flow ratios above 0.5 shows the same trend reported for the 60° and 90° junctions in Section 5.4.1.1. Taking the reason for the divergence explained then the lower trend would be assumed to be in error.

5.4.3.1 Estimation of 30° 'Y' Junction End Conditions

To enable the 30° 'Y' junction results to be of any benefit, end conditions require determining. This was not possible from the test rig due to instability of readings at flow ratios above 0.8 and below 0.2, therefore the loss coefficients at flow ratios of 0 and 1 were estimated using known data from other sources.

For a flow ratio of 1, the optimum value the loss coefficient could achieve would be that of a 15° mitre bend. The difference between the junction and mitre bend loss coefficient can be determined by comparison of the loss coefficients from Miller for the other junctions and their equivalent mitre bends, Figure 5.28. This curve can be extrapolated to give the additional loss coefficient for the 30° degree junction when compared to its equivalent mitre bend as 0.0393. The loss coefficient, given by Miller [16], for a 15° mitre bend is 0.036. Therefore the loss coefficient for a 15° 'Y' junction at a flow ratio of 1.0 can be estimated to be 0.0753.

The loss coefficient at a flow ratio of 0.0 cannot be predicted in a similar manner. The best approximation can be obtained from extrapolation of the 30° junction loss curve, Figure 5.15, and the plot of constant loss coefficient, Figure 5.22 and comparing the two values. Linear

extrapolation of Figure 5.15 gives a loss coefficient of –0.82, and extrapolation of Figure 5.22 gives a value of –0.8, therefore a value of –0.81 shall be used.

These estimated loss coefficients at 0.0 and 1.0 are shown in Figure 5.29. The loss coefficients at flow ratios of 0.7 and 0.8 have been removed from this curve and the polynomial refitted. This data has been fitted with a second order polynomial equation given in Appendix A equation A.2. The use of third order polynomials, as for the other junctions, caused excessive divergence at flow ratios of 0 and 1.

5.5 Presentation of Data

Two methods of presenting the loss coefficients for the junctions have been used, the individual junction plots, Figures 5.15 to 5.21, and the plots of constant loss coefficient, Figure 5.22. The plots of constant loss coefficient have been used solely for direct visual comparison to Miller. The individual junction plots have been used for the analysis of the results and quantitative comparison of the data to Miller. The individual junction plots have been preferred to the plots of constant loss coefficient, because it is felt they give a better representation of the data both for analysis of these tests and interpretation for general use.

The constant loss coefficient contours are currently encoded in Flowmaster, and problems have been encountered with interpolation and extrapolation of the surfaces. If Flowmaster were modified to use the individual junction plots the problems should be overcome, or at least greatly reduced. The most robust solution would be to incorporate the curves as fixed included angle models, any error due to the use of a fixed angle model will be small.

Inclusion of this data in Bath*fp* will be for fixed included angle models using the curves of Figures 5.16 to 5.19 and Figure 5.29.

5.6 Closing Remarks

The loss coefficients determined from the test rig, when adjusted for the inlet contraction, show a very good agreement to that of Miller [16].

Generally CFD can model the characteristics of a 'Y' junction and hence predict the loss coefficient with approximately the same accuracy as the test rig. Care has to be taken with the results for included angles in excess of 120°, and to lesser extent with flow ratios above 0.6, unless a specialised turbulence model is available.

The test rig has provided substantial data to describe the loss characteristics of 'Y' junctions. The errors associated with the test rig are relatively small and within an acceptable range. The main source of error was the oscillation present on the manometers. For the accuracy of readings taken, this oscillation was of an acceptable size, and it would not be possible to

reduce it any further. With the introduction of the 'O' ring markers on the manometer tubes the impact of the oscillations was greatly reduced. The errors attributed to the test rig did not significantly affect the accuracy of the data obtained.

The test rig has been proved valuable for two purposes. Firstly it has been a source of validation for the application of CFD, in particular Star-CD, to the modelling of the pressure and flow characteristics of combining 'Y' junctions. Secondly, in conjunction with the CFD models it has provided loss coefficient data for combining 'Y' junctions down to included angles of 30°.

Based on the above conclusions, and experience, the loss coefficient curve obtained from the test rig for the 30° 'Y' junction, with the end conditions included, is a good representation of the loss in a combining 30° 'Y' junction. This data in conjunction with the other data obtained from the test rig provides a complimentary set of data to that collected in Miller.

As a consequence of this test programme a set of models describing the characteristics of combining 'Y' junctions in terms of their pressure and flow rate can be developed for use in Flowmaster and Bath*fp*. As stated in Section 5.5 these would use the curves developed within this work shown in Figures 5.16 to 5.19 and Figure 5.29 in preference to the constant loss coefficient contours of Figure 5.22.

CHAPTER 6

DEVELOPMENT OF BATH*fp* AND FLOWMASTER FOR THE MODELLING OF AIRCRAFT FUEL SYSTEMS

This Chapter considers how Flowmaster and Bath*fp* model the components and conditions which are specific to aircraft fuel systems, or have a specialised application for aircraft fuel systems. For the cases where these cannot be modelled with the components available within the component libraries of Flowmaster and Bath*fp*, models and procedures developed within this research are discussed. Initially the methods available with Flowmaster and Bath*fp* for the incorporation of these models shall be considered.

6.1 Inclusion of User Models

It is an important requirement to be able to include component models within Flowmaster and Bath*fp*, because of the specialised application of the aircraft fuel system described in Chapter 3.

6.1.1 Flowmaster

Flowmaster's method of including component models is limited by requiring a standard component model to describe the application of the new model, the only input allowed being a new characteristic curve. This is appropriate if a new component characteristic is to be incorporated, but does not allow the inclusion of completely new models. A FORTRAN interface is to be incorporated at some future date to allow user's own encoded models to be incorporated.

6.1.2 Bath*fp*

Bath*fp* has two methods of incorporating à component model, developing a FORTRAN or C subroutine describing the operation of the component, or use of the BathME utility.

6.1.2.1 FORTRAN and C Models

The component models are made up of two subroutines. An initialisation routine used to trap any user input errors, initialise state variables and calculate any constant factors. This routine is only called once at the start of the analysis. The second subroutine is the main analysis

subroutine. It contains the actual description of the component and is called at each integration time step.

In addition to the input and output variables, four arrays are passed between the subroutines and integrator. These are the *resp*, *iesp*, *con* and *icon* arrays. *resp* (real essential parameter) is a double precision array, containing the user inputs to the model, eg. length, diameter etc.. The *iesp* (integer essential parameter) array is an integer array containing user inputs to the model. These are generally indicators such as the material of a pipe. The *con* array is a double precision working space array and contains data such as constant factors calculated in the initialisation subroutine. The *icon* array is an integer working space array and generally contains flags eg. start of run indicators, locations of discontinuities etc.

All models have access to Bath*fp*'s sub–models and utilities such as curve fitting and discontinuity handling, etc.. The models are included in Bath*fp* through BathMAT as detailed in Section 3.6.4.

6.1.2.2 BathME

BathME provides a similar type of modelling environment to that of Flowmaster's, though more advanced. A series of pressure versus flow rate characteristics can be incorporated, all linked by a third variable. The relationship of the input pressure, and output flow rate to these characteristics is defined, giving a large degree of modelling capability. The major advantage of BathME is that quite complex instantaneous components can be incorporated with no programming knowledge, which may be important for an industrial design environment.

6.2 Modelling of Aircraft Components

The components which shall be considered in relation to their application to aircraft fuel systems are:

- Centrifugal fuel pumps
- Fuel tanks
- Aircraft diffusers
- Intakes
- Jet pumps
- Aircraft engines
- Non–standard components

Before considering the modelling of these components we shall examine a discrete loss. This is a general component which has been used in many applications throughout this research, and provides a good introduction to the other models.

6.2.1 Discrete Loss

The discrete loss is an instantaneous component which models the operation of a component based on the general loss equation given in Chapter 3, equation 3.4.

6.2.1.1 Flowmaster

The application of the discrete loss within Flowmaster requires the area of the inlet and outlet of the component, and either a constant forward and reverse loss coefficient, or a curve of forward and reverse loss coefficient against flow rate.

6.2.1.2 Bath*fp*

Bath*fp*'s standard release does not contain a discrete loss model, but a loss coefficient can be specified in the pipe models. To enable a reverse loss coefficient to be modelled, and give the model some autonomy from the pipe model, a discrete loss has been developed. The inputs to the model are the inlet and outlet pressure and the outputs are the inlet and outlet flow rate. The flow rate is modelled using the general loss equation given in Chapter 3, equation 3.2 and repeated below.

$$\Delta p = \frac{k\rho u^2}{2}$$

Expanding velocity in terms of flow rate gives

$$\Delta p = \frac{8k\rho q^2}{\pi^2 d^4} \qquad 6.1$$

Allowing for different loss coefficients in the forward and reverse directions, the forward and reverse flow rates can be written as,

Forward flow:

$$q_f = \sqrt{\frac{\pi^2 d^4 \Delta p}{8k_f \rho}} \qquad 6.2$$

Reverse flow:

$$q_r = \sqrt{\frac{\pi^2 d^4 \Delta p}{8k_r \rho}} \qquad 6.3$$

This is encoded in the model as shown below. The variables *con(1)* and *con(2)* are the constant factors of equations 6.2 and 6.3, all other variables are self explanatory.

```
      deltap=pin-pout
      deltap_si=1.0d5*deltap

c     The model

c     Check sign of deltap_si and calculate q

      if(deltap_si.lt.0.0d0)then

c           delta_p is -ve so reverse flow
c           convert to +ve and multiply q by -1

            deltap_si=deltap_si*-1.0d0
            q_si=-1.0d0*con(2)*sqrt(deltap_si)

      else

c           deltap is +ve so forward flow

            q_si=con(1)*sqrt(deltap_si)

      endif
c     Convert q to L/min

      qout=q_si*60000
c     calculate qin=-qout

      qin=-qout

      end
```

A curve of loss coefficient against flow rate has not been included in this model, because BathME provides a better graphical environment for incorporating data in this form.

6.2.2 Centrifugal Fuel Pump Modelling

Centrifugal fuel pumps used within aircraft fuel systems are, at present, constant speed pumps. For analysis purposes only their steady state operation need be considered. Therefore the pumps can be adequately described with a pressure flow characteristic. The modelling approaches used in Flowmaster and Bath*fp* use the same base data, but it is applied in different ways.

6.2.2.1 Flowmaster

In Flowmaster, pumps are modelled using modified Suter [16] parameters which convert the homologous pump laws:

$$\frac{N_1^\bullet}{N_2^\bullet} = \frac{Q_1^\bullet}{Q_2^\bullet} \qquad 6.4$$

$$\frac{H_1^\bullet}{H_2^\bullet} = \left[\frac{N_1^\bullet}{N_2^\bullet}\right]^2 = \frac{M_1^\bullet}{M_2^\bullet} \qquad 6.5$$

into a Suter head parameter and Suter Torque parameter,

$$W_H = \frac{H^\bullet}{N^{\bullet 2} + Q^{\bullet 2}} \qquad 6.6$$

$$W_M = \frac{M^\bullet}{N^{\bullet 2} + Q^{\bullet 2}} \qquad 6.7$$

which can be plotted against a Suter flow parameter,

$$\theta = \tan^{-1}\left[\frac{N^\bullet}{Q^\bullet}\right] \qquad 6.8$$

where

$N^\bullet$	=	Normalised pump speed.
$H^\bullet$	=	Normalised pump head.
$Q^\bullet$	=	Normalised pump flow rate.
$M^\bullet$	=	Normalised applied torque.
W_H	=	Suter head parameter
W_M	=	Suter torque parameter.

Typical curves are plotted in Figure 6.1. These relationships when used in preference to the head, torque and flow rate are reported [16] to eliminate difficulties which can arise within computational analysis when head, flow rate, torque or speed become zero. This is most marked for the iterative solution method of Flowmaster.

The Suter normalised characteristic enables similar pumps of different capacity and rotational speed to be modelled with the same curve. Unfortunately this generalisation cannot be utilised for aircraft fuel pumps because the pump characteristic changes with altitude and temperature. Thus curves for all conditions have to be determined creating a large volume of data. It has been found that the pump characteristic is dependent on the pressure at the pump inlet, sometimes referred to as the Net Positive Suction Pressure (NPSP) [18]. Creating a series of pump characteristics based on a constant NPSP greatly reduces the volume of characteristic curves required.

Flowmaster only allows one characteristic curve to be modelled. It requires the NPSP of the pump calculating before the analysis commences. For a direct entry pump this is simply calculated from the head of fuel above the inlet and tank pressure. For a remote inlet pump the pressure loss through the inlet pipe is ignored when calculating the NPSP.

6.2.2.2 Bath*fp*

There is no model of a centrifugal pump within Bath*fp*'s standard model library. Instead the BathME utility, described in Section 3.6.5, is used to develop a model based on pressure and flow rate data. The data is incorporated in BathME with the pressure as the independent variable (y) and the flow rate as the dependent variable (x). BathME models this data as $x = f(y)$ or $q = f(p)$. To define the x, y data in terms of a fuel pump characteristic the following equations are used:

$$x = p_{out} - p_{in}$$

$$q_{in} = -y$$

$$q_{out} = -q_{in}$$

BathME allows a set of characteristics to be incorporated within a single model, each characteristic being defined by a third variable (z) if required these can be interpolated. The pump characteristics can be incorporated as NPSP curves with z defined as the NPSP. The correct NPSP curve can then be automatically selected and altered during analysis, if a fourth equation is included.

$$z = p_{in}$$

This method enables NPSP curves to be used to describe the operation of both direct entry and remote inlet pumps. If z is interpolated, the number of curves required to describe the pump can be further reduced.

6.2.3 Aircraft Fuel Tanks

A tank is a specialised component that defines one of the boundaries of a simulation network, and as such requires either the flow rate or the pressure to be defined explicitly.

In the majority of disciplines a tank is considered and modelled solely as a pressure boundary condition. In a fuel system the tank is one of the most important components and is characterised by the following:

- The geometry is complex and varies due to both flexing of the wing, and pitch and roll of the aircraft
- The volume of fuel within the tank at any time is an important parameter
- Surface pressure varies due to altitude and atmospheric conditions
- There are multiple inlet/outlets at different heights, some having multiple applications, such as the refuel lines used also for the transfer of fuel.

A sectioned diagram of an aircraft wing tank is given in Figure 6.2 to give an indication of the typical complexity of a fuel tank.

6.2.3.1 Flowmaster

Aircraft fuel tanks can be modelled under normal operations in Flowmaster using the supplied constant head reservoir and finite area reservoir. For specialised applications the accumulator model or a representation of the tank with a pipe may be appropriate.

The constant head reservoir can only be used for cases where the pressure at the tank remains constant and the volume is not required to be modelled. This generally restricts this model to steady state conditions for aircraft applications.

The finite area reservoir seems quite an appropriate model but it suffers from two restrictions which make it difficult to apply. Aircraft fuel tanks are described by the manufacturers as a series of volume–height relationships, the finite area reservoir requires an area–height description. The second restriction is the interpretation of the area–height curve within the model. This has led to errors of geometry description up to 10%. The model integrates the area with respect to height to calculate the volume. The integration method used is fairly simplistic, only taking ten equal steps over the height range. This method is only suitable for relatively simple geometries, not for the complex geometries of aircraft fuel tanks. This is illustrated in Figure 6.3, which shows a typical area height curve for an aircraft fuel tank. When the spacing of the integration algorithm is superimposed on it, the errors can be clearly seen.

An accumulator can be used to model an aircraft fuel tank where the compression of the air in the tank is of interest. A restriction of this model is that venting of the air from the accumulator cannot be modelled. A good application of this model is for the prediction of the performance of the vent system during an emergency descent, see Section 7.3.3.1.

A pipe can be used to model an aircraft fuel tank though this is only appropriate if flow is passing through the tank. An application of this is to model an aircraft fuel tank during refuel overflow (Section 7.3.2.2) when the fuel leaves the tank through the vent system. Any shape of pipe is appropriate. The dimensions of the pipes are set so that its cross sectional area is the average cross sectional area of the tank, and its length is set to the height of the tank. The nodes at inlet and outlet are also set to represent the height of the tank. A discrete loss model will be required at inlet and outlet to model the inlet and outlet losses. The area of these will be set to the area of the inlet and outlet pipes.

All of the Flowmaster tank models have only one port, whereas aircraft fuel tanks have multiple inlets and outlets at different heights. To model these outlets a series of discrete loss models, representing the tanks outlets, are connected to the tank port as shown in Figure 6.4.

The height of the tank base above a pre-defined datum is set in the node at the tank outlet. The height of the tank outlets are set in the nodes at the outlet of the discrete losses representing them.

6.2.3.2 Bath*fp*

Bath*fp*'s standard release only contains models of constant pressure tanks. Generally these are restricted to steady state conditions for aircraft applications, similar to the constant pressure reservoirs of Flowmaster. To overcome this restriction, specific aircraft fuel tank models have been developed by the author during this research.

Development of Fuel Tank Model

The various applications require these models to be adaptive to the differing simulation requirements. For example, a complete model of the fuel system will require all of the outlets of the tank to be modelled, but when considering the engine feed system in isolation, only the relevant outlets need to be considered.

Three approaches to the modelling of aircraft fuel tanks in Bath*fp* were considered.

- A single complete model including all outlets.
- A series of models for the different applications.
- A set of modules from which a 'total' tank model can be built.

The first approach requires unused outlets to be 'blanked off'. This is both untidy and will create zero flows, which can lead to modelling problems. The second approach will lead to a very large number of models for each tank, leading to a large and cumbersome model library. The third approach has been selected as it gives flexibility to the models. Its only drawback being that the tank is constructed from more than one model, though this is of only minor concern.

The implementation of this approach uses two models to describe the tank. A model of the tank itself with a single port, and a series of outlet models with a differing numbers of ports.

Fuel Tank Model

The aircraft fuel tank is modelled as a pressure specifying component with a complete geometry description of the tank. The model has one input, the flow rate at the tank port, and one output, the pressure, which is defined as an external state variable. It has two internal variables, the volume of the fuel within the tank, which is an internal state variable, and the height of fuel within the tank.

The geometry description of the tank is in the form of a polynomial equation describing the tank volume as a function of the tank height. The polynomial is fitted from height–volume data, with a least squares method, the order being dependent on the complexity of the tank geometry. This is encoded in the model as a FORTRAN function.

The pressure on the tank port is defined as:

$$p = p_{sur} + \rho g h \qquad 6.9$$

Its time derivative is:

$$\frac{dp}{dt} = \frac{dp_{sur}}{dt} + \frac{d}{dt}(\rho g h) \qquad 6.10$$

$$\frac{dp}{dt} = \frac{dp_{sur}}{dt} + g\left[\rho \frac{dh}{dt} + h \frac{d\rho}{dt} \right] \qquad 6.11$$

Expanding dh/dt

$$\frac{dh}{dt} = \frac{dh}{dV}\frac{dV}{dt} \qquad 6.12$$

Dv/dt is the flow rate at the tank port.

dh/Dv is obtained from the geometry description of the tank. An equation describing the tank height as a function of volume is obtained from the tank geometry data, and differentiated with respect to volume. This is then encoded in the model in a similar manner to the volume height equation.

The rate of change of surface pressure dp_{sur}/dt is equal to the rate of change of atmospheric pressure. This is stored in the common block *atmos* which is created by the *environmental* component *EN01* described in Section 6.3.1.2.

The rate of change of density $d\rho/dt$ is due to changes in altitude and is defined by the *environmental* component *EN01*, and stored in the common block *flupro*.

$$\therefore \frac{dp}{dt} = \frac{dp_{sur}}{dt} + g\left[\rho q \frac{dh}{dV} + h \frac{d\rho}{dt} \right] \qquad 6.13$$

The volume of fuel in the tank is defined as:

$$V = V_i + \int_{t(n)}^{t(n+1)} q\,dt \qquad 6.14$$

Its time derivative is:

$$\frac{dV}{dt} = q \qquad 6.15$$

The tank volume has clearly defined upper and lower limits. The upper limit is the maximum volume of the tank, and the lower limit is the unusable volume of the tank. Within these limits the time derivatives of the tank pressure and the volume of fuel within the tank are set to the values of 6.13 and 6.15 respectively. Outside these limits the flow rate within the model is taken to be zero. Therefore the time derivative of volume is set to zero, and the time derivative of pressure is set to the rate of change of surface pressure. Although the flow rate is set to zero within the model, this is not enforced on the network because the tank's flow rate is an input.

A typical example of the coding of the model is shown below. *icon(1)* indicates the state of tank operation, *con(2)* is the unusable volume in litres, and *con(6)* the maximum volume of the tank. All other variables are self explanatory. The application of the subroutine *dishan* is explained in Section 3.4.3.2.

```
c       check if integrator has just started or restarted (limit=0)
        if(limit.eq.0)then
              if(vol.ge.con(2).and qin.ge.0.0d0)then
c             tank is full and attempting to fill further
                    icon(1)=1
              elseif(vol.le.con(6).and.qin.le.0.0d0)then
c             tank is empty and attempting to empty further
                    icon(1)=-1
              else
c             tank between full and empty or at limits
c             but flow in correct direction
                    icon(1)=0
              endif
        endif

        if(icon(1).eq.1)then
c       tank full and attempting to fill further
              voldot=0.0d0
              pdot=(dpsur_dt)/1.0d5
c             check if flow becomes negative.
              call dishan(limit,qin.lt.0.0d0,.false.)
        endif

        if(icon(1).eq-1)then
c       tank empty and attempting to empty further.
              voldot=0.0d0
```

```
                pdot=dpsur_dt/1.0d5

c               check if flow becomes positive.

                call dishan(limit,qin.gt.0.0d0,.false.)

        endif

        if(icon(1).eq.0)then
c       tank within operating range, or at limit but with flow
c       in correct direction

                voldot=qin/60
                dh_dv=dh_dv_tkct(vol)
                pdot=(dpsur_dt+(g*((h*drho_dt)+(rho*dh_dv*voldot))))/1.0d5

c       check if going out of range

                call dishan(limit,(vol.lt.con(6).and.qin.le.0.0d0)
     +                  .or.(vol.gt.con(2).and.qin.ge.0.0d0),
     +                  abs(con(6)-vol).lt.tol.or.abs(vol-con(2)).lt.tol)

        endif


c       Sort out static head from total

        pstat=(pout-resp(1))*1.0d5

c       Calc of head

        h=pstat/(rho*g)

        end
```

This model is restricted in application to cases where the volume remains within the unusable and maximum volume of the tank. This does not create too great a problem, because for the majority of applications it is required to model the tanks operating within these limits.

Fuel Tank Model with Control Port

For applications where it is desirable to analyse the network beyond the filling and/or emptying of a tank, a means of setting the input flow rate to the tank to zero when the volume of fuel in the tank exceeds the maximum volume, or becomes less than the unusable volume is required. This has been achieved by adding a signal port to the tank, which signals a tank inlet valve to close when the fuel volume is greater than the maximum volume or less then the unusable volume. At all other times it is signalled open. The port has one output which is a state variable. It is set to one if the tank volume is between unusable and full, and set to zero outside this range.

The use of a state variable for the signal may seem a strange choice as it is a discontinuous variable with only two possible values. The integrator requires the models to be explicit as explained in Section 3.4.3. For a component at the termination of a branch of the system this requires all of its outputs to be defined without reference to the inputs. Defining the signal as a state variable makes it available to the integrator and hence defined.

The model sets, or changes, the value of the signal at the start of the run, ie. when *limit=0*, or when the volume reaches the upper or lower limit and it as been located sufficiently accurately by *dishan* ie. when *limit=4*. A model is only allowed to change a state variable when the integrator is just starting or restarting, ie. *limit=0* or *4*. Attempts at changing state variables at any other time would fail the integrator, and this is prevented by the discontinuity handling routine.

The modification to the model is highlighted in the code below. This is only for the tank within its operational limits, but for the other two cases, the application is very similar.

```
      if(icon(1).eq.0)then
c     tank within operating range, or at limit but with flow
c     in correct direction

            voldot=qin/60
            dh_dv=dh_dv_tkct(vol)
            pdot=(dpsur_dt+(drho_dt*g*dh_dv*voldot))/1.0d5

c     check if going out of range

            call dishan(limit,(vol.lt.con(6).and.qin.le.0.0d0)
     +                .or.(vol.gt.con(2).and.qin.ge.0.0d0),
     +                abs(con(6)-vol).lt.tol.or.abs(vol-con(2)).lt.tol)

c     check if limit=4, if so require to reset sig

            if(limit.eq.4)then

                  sig=1.0d0

            endif
      endif
```

Tank Inlet/Outlet Model

The tank inlets are a series of instantaneous manifold type models with from two to six ports. In all cases there is a single outlet for connection to a tank model and between one and five inlet ports dependent on the model, for connection to the various parts of the fuel system, as indicated in Figure 6.5.

All ports have pressure as an input and flow rate as an output. For each inlet a forward and reverse loss coefficient, and the height above the base of the tank are modelled. These enable the model to be tailored to most circumstances.

The inlet flow rates are modelled using the general loss equation given in Chapter 3, equation 3.2, which can be expanded in terms of flow rate as in Section 6.2.1.2 equation 6.1, and repeated here:

$$\Delta p = \frac{8k\rho q^2}{\pi^2 d^4}$$

$$\Delta p = (p_i - p_o) - \rho g h \qquad 6.16$$

where

p_i = pressure at inlet.

p_o = pressure at outlet.

h = height of port above base.

Allowing for differing losses in the forward and reverse directions, the forward and reverse flow rates can be written as:

Forward flow:

$$q_f = \sqrt{\frac{\pi^2 d^4((p_i - p_o) - \rho g h)}{8k_f \rho}} \qquad 6.17$$

Reverse flow:

$$q_r = \sqrt{\frac{\pi^2 d^4((p_o - p_i) - \rho g h)}{8k_r \rho}} \qquad 6.18$$

An extract of coding for a two inlet model is given below. *resp(2)* is the height of port 1 above a pre defined datum and *resp(6)* is the height of port 2 above the pre defined datum. The four elements of the *con* array contain the constants of equations 6.17 and 6.18. All other variables are self explanatory.

```
c       Calculate pressure difference across manifold paths in N/m^2

        deltap1=((pout-pin1)*1.0d5-(rho*g*resp(2)))/rho
        deltap2=((pout-pin2)*1.0d5-(rho*g*resp(6)))/rho
c
c       The model

c       qin1

        if(deltap1.lt.0.0d0)then
c               flow out of tank
                deltap1=-deltap1
                qin1=-(con(2)*sqrt(deltap1))*6.0d4
        else
c               flow into tank
                qin1=(con(1)*sqrt(deltap1))*6.0d4
        endif

c       qin2

        if(deltap2.lt.0.0d0)then
c               flow out of tank
                deltap2=-deltap2
```

```
                qin2=-(con(4)*sqrt(deltap2))*6.0d4
        else
c               flow into tank
                qin2=(con(3)*sqrt(deltap2))*6.0d4
        endif

c       Calculate total outlet flow

        qout=-qin1-qin2

        end
```

Tank Inlet Valve Model

The valve for controlling the flow from the fuel tank is an instantaneous model which can be either open or closed. It has three ports, two fluid which have pressure as an input and flow rate as an output, the third port is the signal port which has an input only.

If the signal input to the model is zero, the inlet and outlet flow rates are set to zero. If the signal input to the model is one, then the flow rate is calculated from equation 3.2, the general loss equation. This can be expanded in terms of flow rate and rewritten as in Section 6.2.1.2, equation 6.2 and repeated here.

$$q = \sqrt{\frac{\pi^2 d^4 \Delta p}{8k\rho}}$$

This is encoded in the model as shown below. The variable *icon(1)* is set to the value of the signal (*sigin*) when a discontinuity has been located sufficiently accurately and a restart has been selected ie. when *limit = 0*. This enables the change in the valve signal to be detected by comparison to *icon(1)*. *con(1)* is the constant factors of the general loss equation, all other variables are self explanatory.

```
c       Find deltap

        deltap=pin-pout

        deltap_si=1.0d5*deltap

        if(icon(1).eq.0)then
c       valve closed

                qin=0.d0
                qout=0.d0
c               call dishan to check if sigin changed from last call

                call dishan(limit,sigin.eq.1.0d0,.false.)

                elseif(icon(1).eq.1)then

c                       valve open
                        q_si=sqrt(abs(deltap_si))*con(1)*sign(1.0d0,deltap_si)
```

```
                    qout=q_si*60000
                    qin=-qout
c                   call dishan to check if sigin changed from last call
                    call dishan(limit,sigin.eq.0.0d0,.false.)
      endif
```

6.2.4 Diffusers

The operation of aircraft diffusers is described in Section 2.3.2. Figure 2.6 shows a typical diffuser. Modelling of diffusers causes substantial problems due to a lack of data describing their performance in terms of pressure and flow rate. Testing has been carried out to assess their ability to diffuse the flow in the smooth manner required and with the minimum of spray, [56,57], but no testing to assess the pressure loss due to this diffusing action has been conducted. One of the recommendations for future work from this research is that an extensive test programme for aircraft refuel diffusers is undertaken.

Various methods are used by individuals to allow for the effects of diffusers in pressure flow rate analyses. These are usually a fixed loss coefficient, the magnitude being dependent on the individuals view. Two approaches to the modelling of diffusers are presented here. The first models the losses due to the diffusing action as a fixed loss coefficient of one and the friction losses of the diffuser are accounted for with a pipe the length of the diffuser. This results in the flow rate of the diffuser being equal to:

$$q = \sqrt{\frac{\pi^2 d^4 \Delta p}{8\rho\left(1 + \frac{fl}{d}\right)}} \qquad 6.19$$

Where l is the length of the diffuser pipe, d its diameter and f its friction factor. The second model is based on an orifice law with the diameter set to a value which represents the discharge area of the diffuser pipe outlet. This second method requires the orifice model to be based on a theory with the orifice diameter independent of the pipe diameter, because the area of the pipe discharge is always greater than the pipe area. A theory which is appropriate is one based on reference [56], where the pipe diameter and discharge characteristics are accounted for in a discharge coefficient(C_d).

$$q = C_d A\sqrt{2gh} \qquad 6.20$$

This method cannot be used with Flowmaster analyses because the restrictor model used is based around the general loss equation (equation 3.4), with the loss coefficient a function of the ratio of the orifice area to the pipe area, and is only valid for ratios between zero and one.

To illustrate the two methods a simplified refuel type network for a single tank is modelled with Bath*fp*, using both diffuser models, Figure 6.6. The tank is representative of an aircraft wing tank, the pressure at the refuel coupling was 3 bar. The discrete losses of Figure 6.6a are incorporated in the tank inlet model. Results for the analyses are given below for one of the diffusers.

	Flow Rate (L/min)	Pressure Drop (bar)
Discrete Loss Model	713	0.013
Restrictor Model	742	0.755

The above results show a large difference in the prediction of the pressure drop across the diffuser, but good agreement on the flow rate through the diffuser. Similar flow rates can be achieved in the two models even with the large difference in predicted pressure drop, because the flow rate is determined predominantly by the characteristics of the refuel restrictor (see Sections 2.3 and 7.3.2.1). The difference in pressure drops across the two models is not too significant because a refuel network is specified with an inlet and outlet pressure and determines the flow rates within the network. Which, if either, of the two models is predicting the correct pressure drop cannot be determined, due to the lack of data on the operation of diffusers. Until further data is available the application of either model to describe a diffuser is considered appropriate.

6.2.5 Intakes

In terms of a fuel system, intakes refer to those in the surge tanks which connect the vent system to the atmosphere, Figure 2.12. The intake is generally of the form of a flush fitting NACA intake, designed to resist ice build up during flight, and provide a small ram pressure (0.017 bar) to pressurise the tanks.

Modelling of intakes has similar problems to those associated with diffusers due to lack of loss data. In this case the problem is not so acute, because a characteristic of the inlet loss is known, a typical example is given in Figure 6.7, but the outlet loss characteristic is not available.

6.2.5.1 Flowmaster

Intakes are modelled with the discrete loss model with the outlet characteristic incorporated as a curve of loss coefficient against flow rate. The inlet loss is modelled with the outlet loss characteristic, as no better data is available.

6.2.5.2 Bath*fp*

The BathME utility, described in Section 3.6.5, is the most appropriate method for incorporating an intake. The pressure versus flow rate curve describing the inlet loss characteristic is incorporated in BathME with the pressure as the independent variable (y) and the flow rate as the dependent variable (x). BathME models this data as $y = f(x)$ or $q = f(p)$. To define the x, y data in terms of an intake loss characteristic the following equations are used:

$$\begin{aligned} x &= p_{in} - p_{out} \\ q_{in} &= -y \\ q_{out} &= -q_{in} \end{aligned}$$

The outlet loss will be accounted for with the inlet loss curve, in the light of no better data.

6.2.6 Jet Pumps

The operation of, and advantages and disadvantages of, jet pumps are presented in Section 2.5.2.2. Jet pumps have two applications within aircraft fuel systems, as a means of fuel transfer and as an engine feed boost pump. In the role of a transfer pump the motive flow of the jet pump is usually supplied from the centrifugal engine feed boost pumps. When the jet pump is the engine feed boost pump, the motive flow can be taken from engine mounted feed pumps if excess capacity is available, as reported by Klapprrot [59]. For commercial civil aircraft, the pressure and flow rate required by the engines would require a much larger motive flow than that reported in [59] and has been found to be non–economical [60 to 63]. The only application of jet pumps encountered within this research has been solely for transfer purposes. In this capacity a jet pump generates a small, almost negligible head, in preference to a high transfer rate. Modelling of this has been found to be adequate with a flow source.

Jet Pump Model

At present there is no model of a jet pump incorporated in either Flowmaster or Bath*fp*. The following is the form of model intended for Bathfp. At present there is no means of incorporating a jet pump into Flowmaster because a standard model with two inputs and one output is not available.

The approach that is to be adopted is to determine the operational characteristics of the jet pump from its geometry. The equations describing the operation are derived from continuity, and energy and momentum balances across the jet pump. This is one of the most common approaches to determining the operation of the jet pump and some of the notable works

published on this subject are those due to Kentfield and Barnes [65], Winchester et al [66], Sanger [67,68], Wilman [69], Reddy and Kar [70] and Reddy [71]. The algorithm proposed for this model is based on the theory of Sanger [67]. The equations developed by Winchester et al [66] also show a close similarity to those of Sanger. The determination of loss coefficients for the various components of the jet pump are taken from Wilman [69] and Reddy [71].

The model will have pressure as the input for the three ports and flow rate as the output. The input variables to the model will be:

- Motive flow nozzle outlet diameter
- Motive flow nozzle angle
- Motive flow nozzle length
- Suction flow nozzle angle
- Suction flow nozzle length
- Mixing tube diameter
- Mixing tube length
- Friction factor to apply to mixing tube
- Diffuser outlet diameter
- Diffuser efficiency
- Design mass flow ratio.

Four dimensionless parameters are commonly used to describe the performance of jet pumps, and are used in this model.

Jet nozzle to mixing tube area ratio

$$R = \frac{A_j}{A_m} \qquad 6.21$$

Suction to motive mass flow ratio

$$M = \frac{m_s}{m_j} \qquad 6.22$$

Pressure Ratio

$$N = \frac{P_d - P_s}{P_j - P_d} \qquad 6.23$$

Efficiency

$$\eta = MN \tag{6.24}$$

Sanger [67] developed an equation for the pressure ratio from continuity and momentum and energy balances across the jet pump. This analysis was based on one-dimensional incompressible equations, but the mixing process is three-dimensional. To account for these differences he supplemented the analysis with empirical information. The resultant relationship for pressure ratio taken from [67] is:

$$N = \frac{2R + \dfrac{2R^2M^2}{1-R} - (1 + k_m + k_d)(1 + M)^2R^2 - (1 + k_s)\dfrac{R^2M^2}{(1-R)^2}}{1 + k_j - 2R - \dfrac{2R^2M^2}{1-R} + (1 + k_m + k_d)(1 + M)^2R^2} \tag{6.25}$$

and the motive mass flow rate:

$$m_j = \frac{10.76\rho A_j g_c}{g} \frac{\sqrt{\dfrac{9.93(P_j - P_s)}{\rho/2g}}}{\sqrt{(1 + k_j) - (1 + k_s)\left(\dfrac{MR}{1-R}\right)^2}} \tag{6.26}$$

A complete development of these equations is given in reference [68].

For incompressible flow the density of the motive and suction flows is equal and therefore the volumetric flow ratio will be equal to the mass flow ratio of equation 6.22.

Solution Method

Solution of equations 6.22 to 6.26 requires the mass flow ratio to be known. This will only be known when the jet pump is operating 'on design' conditions. In general it will not be known if the jet pump is operating 'on design' conditions until a solution is obtained. Therefore a means of solving for the mass flow ratio for all conditions is required. The number of equations and data available do not permit an explicit solution for the mass flow ratio. The only means of obtaining it is through iterative solution of equation 6.25, with the pressure ratio N obtained from the input pressure at the three ports and equation 6.23. The iterative solution would be most appropriately started using the design mass flow ratio, this would be supplied as a user input to the model.

With the mass flow ratio known, the motive mass flow rate, and hence volumetric motive flow rate can be determined from equation 6.26. The suction volumetric flow rate can be obtained from the mass flow ratio, equation 6.22, and the delivery volumetric flow rate will be equal

to the sum of the motive and suction volumetric flow rates. Efficiency can be calculated from equation 6.24 if required.

Loss Coefficients of Individual Components

Motive Flow Nozzle Loss Coefficient k_j

Reddy [71] gives the loss coefficient through the driving nozzle as:

$$k_j = \frac{f}{8}\cot\theta_j\left(1 - \frac{1}{n_j^2}\right) \qquad 6.27$$

where θ_j is the semi–cone angle of the motive flow nozzle and n_j is the rate of contraction of the motive flow nozzle

Suction Flow Nozzle Loss Coefficient k_s

Reddy [71] proposes a modification of Equation 6.27 for the suction nozzle to reflect that it is an annular nozzle:

$$k_j = \frac{f}{8}\cot\theta_j\left(1 - \frac{1}{n_j^2}\right) + \frac{f}{8}\cot\theta_s\left(1 - \frac{1}{n_s^2}\right) \qquad 6.28$$

where θ_s is the semi–cone angle of the suction flow nozzle and n_s is the rate of contraction of the suction flow nozzle.

Mixing Section Friction Loss Coefficient k_m

For a given friction factor, this is calculated from [16]:

$$k_m = \frac{fl}{d} \qquad 6.29$$

Diffuser Loss Coefficient k_d

The loss coefficient for the diffuser, derived by Wilman [69] is given by:

$$k_d = (1 - \eta_d)\left(1 - \left(\frac{d_m}{d_d}\right)^4\right) \qquad 6.30$$

where η_d is the diffuser efficiency and d_m is the mixing tube diameter and d_d the diffuser outlet diameter.

6.2.7 Engines

The engine of a modern jet aircraft is a complex system with many control parameters to provide optimum performance. The engine manufacturers are concerned with controlling engine transient performance such as compressor surges, engine accelerations and decelerations, over fuelling control etc. To this end engine manufacturers have developed highly detailed models of the operation of the engines [72,73,74]. From the point of view of the airframe fuel system the engine can be considered simply as a flow demand, with an inlet pressure dependent on the characteristics of the engine feed system.

Both Flowmaster and Bath*fp* model the effects of an engine quite adequately with a flow source model [75,76]. In both packages this simply represents a flow source or demand on the network. Use of the flow source model ensures the pressure modelled at the engine inlet is determined by the characteristics of the network.

6.2.8 Non-Standard Components

This Section is concerned with components which are effectively 'one-offs' and can be adequately described with an instantaneous model. If the dynamic operation of the component is required to be modelled, then a specific component model would have to be developed.

These components can be split into two categories, both based around a model of their loss coefficient. The first are those for which the loss coefficient can be obtained from combinations of coefficients from sources such as [16,29,30]. The combination of the coefficients will usually require an educated engineering judgement to determine the appropriate combinations and weightings of the loss coefficients. A good example of this type of component is the gravity feed inlet of the engine feed system of the first case study, Section 8.1.4.

The second category are those for which the loss coefficient cannot be determined from modified standard component loss coefficients. The loss coefficient in these cases can be obtained from either test rigs or the use of CFD models of the component. As explained in Chapter 4, test rigs are usually not appropriate due to the cost of manufacture and test time. A good example of obtaining loss coefficients from both a test rig and CFD is given in Chapter 5, and an example of loss coefficients obtained solely from CFD is given in the second case study, Section 8.2.4.

6.3 Modelling of Aircraft Conditions

6.3.1 Altitude

To adequately model aircraft fuel systems the effects of altitude on the operation of the system must be taken into account. The atmospheric temperature and pressure are a function of the altitude, and the properties of the fuel are a function of the temperature. Therefore any change in altitude results in a change of atmospheric pressure and fuel properties.

To take account of the effects of altitude on the atmospheric conditions and fuel properties can range from simply setting the fluid properties and atmospheric conditions to those appropriate for a constant altitude, to modelling the variation of both the fluid properties and atmospheric conditions due to changes of altitude during analysis.

6.3.1.1 Flowmaster

Flowmaster can adequately model the fuel properties and atmospheric conditions for a constant altitude. It is restricted though in its application to the modelling of altitude changes, because the fluid properties remain fixed throughout the analysis. If it is required to model the effects of altitude change then the following guide-lines will be an aid to making the most of the analysis.

- When allowing for the changes it is important to always make pessimistic predications of the results. Therefore fluid properties at the lowest altitude should be used, giving the greatest loss.
- Tanks will be best modelled with pressure sources rather than reservoirs, a time history of pressure which reflects the atmospheric pressure can then be used.
- If a finite area reservoir must be used to model a fuel tank, the surface pressure will be constant throughout the analysis, so the pressure which will provide the most pessimistic solution should be used.
- An accumulator should only be used to model an un-vented fuel tank. The effects of compression or expansion of the air space are modelled, and reflected in the surface pressure. An example of this is given in Section 7.3.3.1 for the study of emergency descent.
- Inlet pressures to the system should be modelled with pressure sources, with the pressure reflecting the atmospheric pressure.

6.3.1.2 Bath*fp*

The standard release of Bath*fp*, like Flowmaster, is restricted to modelling constant atmospheric conditions and fuel properties. The effects of altitude changes on the atmospheric conditions and fuel properties have been included with the introduction of a specialised model. This adjusts the atmospheric conditions and fuel properties throughout the analysis, based on an altitude profile defined in the model. The model differs from other models as it has no ports. Any model of this type is interpreted by the code generator as an *environment* model, and is always the first model called by the integrator, ensuring any changes to the atmospheric conditions and fuel properties are made at the start of any time step.

Fluid properties are stored in a common block *flupro*. If any model or utility requires any fluid properties, they are read from this common block at each time step. Atmospheric conditions are not incorporated in Bath*fp* in its standard release. To allow for their effect a new common block *atmos* has been introduced into the code. This is used in an identical manner to *flupro*, and stores the atmospheric temperature, pressure and rate of change of pressure.

The Model

The altitude profile is defined in twenty stages which may be constant, stepped or ramped. The following atmospheric conditions and fuel properties are modelled:

Atmospheric conditions.

- Temperature.
- Pressure.
- Rate of change of pressure.

Fuel properties.

- Temperature.
- Density.
- Kinematic viscosity.
- Dynamic viscosity.
- Rate of change of density.

The atmospheric conditions are described with an International Standard Atmosphere (ISA) model [77] which is encoded within two 'C' functions [78]. An allowance for temperature variations from ISA is incorporated through a fixed temperature difference. The fuel temperature is given the same value as the atmospheric temperature but with a constant time delay to allow for the effects of structural heating. The description of the fuel properties

variation with time are taken from standard data sheets [79] and are encoded in a third 'C' function [78].

The atmospheric conditions and fuel properties are determined at each time step. The rate of change of the atmospheric pressure and density are calculated from their values at the start and end of the altitude profile stage and the time of the stage.

An extract from the code showing the modelling of the atmospheric conditions is given below. The *con* array contains the duty cycle of altitude against time, *icon(1)* is the current stage of the duty cycle and *resp(1)* is the variation from standard ISA temperature. *thetaatm patm* and *dpatm_dt* are the atmospheric temperature, pressure and rate of change of pressure respectively. *atmtemp_* and *atmpress_* are two 'C' functions which describe ISA for temperature and pressure respectively when passed the altitude as an argument. *iap1*, *iap2*, *iat1* and *iat2* are array pointers which define the position of the altitude and pressure in the con array at the start and end of the current duty cycle.

```
c       ATMOSPHERIC TEMPERATURE
        thetaatm=atmtemp_(alt)+resp(1)

c       ATMOSPHERIC PRESSURE
        patm=atmpress_(alt)

c       RATE OF CHANGE OF ATMOSPHERIC PRESSURE

c       set array pointers
        iap1=icon(1)+20
        iap2=icon(1)+21
        iat1=icon(1)
        iat2=icon(1)+1

c       determine rate of change of atmospheric pressure

        patm1=atmpress_(con(iap1))
        patm2=atmpress_(con(iap2))

        dpatm_dt=(patm2-patm1)/(con(iat2)-con(iat1))
```

If the analysis time is less than the time lag of the fuel temperature, the fuel properties are based on the temperature at the start of the first stage of the temperature profile.

6.3.2 Pitch and Roll

The effects of pitch and roll are required to be modelled to take account of the effects of the change in heights of the various points in the network. These changes in heights will only have an affect on the operation of the network at pressure specifying boundary conditions, where the change in head will either decrease or increase the pressure. It may also be required

to consider the effects of height on high points in the network where the pressure may drop to critical values.

6.3.2.1 Flowmaster

The network cannot be rotated through a defined angle in the pitch or roll axis. An application of this type is not appropriate to Flowmaster in its current form, because the network components are not defined spatially. The height of tanks and nodes can be defined, and it is by this means that pitch and roll are accounted. This requires the change of height of a node to be determined external to Flowmaster and incorporated within the analysis. These heights are fixed throughout the analysis so the effects of rotation during an analysis cannot be accounted.

6.3.2.2 Bath*fp*

As for Flowmaster the analysis platform cannot be rotated through a defined angle, nor is this appropriate, due to components spatial positions not being known. There is no provision within Bath*fp*'s standard release to allow for heights within the network. The height of the individual ports of the tank inlet models can be defined, Section 6.3.2, and the effects of pitch and roll accounted for similar to Flowmaster.

Inclusion of Rotation of Platform

It is possible to include the effects of rotation of the analysis platform within component models, with the rotation defined in an *environment* component similar to *ENV0*. This has not been developed due to the amount of data required to define the spatial coordinates of the components within the network. Before this is included, a link to the Computer Aided Design (CAD) package on which the fuel system is developed will be required. This link would automatically input the dimensions and position of the components.

A limited implementation could be incorporated which would be only allow rotation of the pressure specifying boundary conditions. This will require the position of the fuel tank outlets to be obtained from the CAD package. This has not been incorporated due to problems with obtaining this data. When this becomes more readily available it will be incorporated.

6.4 Closing Remarks

The development of the models and methods described above has enabled Flowmaster and Bath*fp* to model aircraft fuel systems adequately.

The restrictive method of including component models within Flowmaster has limited the component models that can included. Those not fully implemented at present are a jet pump,

fuel tank with a complete geometry description and the variation of fuel properties during an analysis. Both of these are only required when the dynamics of the system require considering, and for dynamic cases Flowmaster is not usually used. With the inclusion of the FORTRAN interface these restrictions should be lifted.

With the inclusion of the models described in this Chapter, Bath*fp* is able to simulate the majority of the operations of aircraft fuel systems. Its only restriction is the ability to automatically rotate the network through defined pitch and roll angles updating the relevant heights within the network. This has not been included due to the amount of data required from the CAD system for its implementation, which would make it impractical to use.

CHAPTER 7

APPLICATION OF THE COMPUTATIONAL METHODS TO AIRCRAFT FUEL SYSTEM MODELLING

This Chapter brings together the experience and knowledge that has been gained and developed during this research, and presents it in two forms. The first takes the software described in Chapters 3 and 4, and the models developed by the author during this research described in Chapter 6, and considers their application to the general analysis types. This section is intended to give general guidance as to the appropriate method to use in a particular instance and from this provide the basis for the development of new procedures and methods for new applications. The second part of the Chapter takes the same software and models and presents them in a design procedure for aircraft fuel systems that has been developed by the author as part of this research.

All of the methods and examples contained in this Chapter have been developed and undertaken during this research.

7.1 Analysis Types

7.1.1 Network Simulation

Chapter 3 introduced and explained the operation of the two network simulation packages used throughout this research. It explained the reason for the selection and use of two packages because a single commercial package cannot totally model an aircraft fuel system due to the unique operation and operating conditions. This Section details the advantages and disadvantages of each of the packages to typical analysis types.

7.1.1.1 Steady State

Both Flowmaster and Bath*fp* adequately model the steady state actions of a network. On the surface Flowmaster may seem the most appropriate method because it actually solves the steady state equations describing the network. On the other hand, if Bath*fp* is used for a steady state analysis, the input will be either a constant pressure or constant flow rate with constant boundary conditions, and will therefore solve directly for the steady state. Flowmaster does have a slight advantage with its specific steady state results display. Steady state results in Bath*fp* are displayed on the component's result selection pop up window.

Either Flowmaster or Bath*fp* are appropriate to the analysis of steady state networks. The choice of which to use will invariably come down to personnel preference, or whether the network to be analysed already exists in one of the packages.

7.1.1.2 Dynamic Analysis

Both Flowmaster and Bath*fp* analyse dynamic operation of a network, though the method employed by each is quite different. Bath*fp* uses a time series integration method, incorporating an adaptive time step with discontinuity handling, see Section 3.4.3.2. Little set-up is required for a run, with only the start and end times required. Flowmaster carries out a series of steady state analyses at fixed user defined time steps, as explained in Section 3.4.2.1. This results in effectively a quasi-steady state analysis. The major part of setting up the run is in the selection of the time step. Application of the fixed user defined time step requires additional set-up for the analysis and can result in excessively long run times. It requires the point of maximum dynamic activity to be determined, and a time step appropriate to this selected. This will usually require a series of runs to be carried out over this period to determine the optimum time step. If the time step is too large, failures to converge to solution will be encountered during the run, but if the time step is too small, excessively long runs will be encountered. The optimum number of iterations per time step is between five and eight.

To illustrate the application of the two methods we shall consider a four hour fuel transfer, with a valve closing, over a two second period, after one hour. If we consider the analysis both before and after the valve closure, flow rates and pressures will be fairly constant so a time step of the order of five minutes will be appropriate. To model the effects of the valve closure a time step of the order of 0.2 seconds will be required.

To run this analysis using Flowmaster an appropriate time step must be selected to model the valve closure. This will involve running a series of analyses over the period of valve closure to select the optimum time step. In this case it will be one which uses the majority of the twenty iterations available at each time step (Section 3.4.2.1). This time step will then be used for the total analysis. If the time step appropriate to the majority of the analysis were used, failures to converge to solution both during and after the valve closure would be encountered resulting in an incorrect solution.

If we now consider the same analysis run in Bath*fp*. The run will simply be set up by setting the start and end times of the run. During the analysis the integrator will automatically choose the appropriate time step. For the periods of constant flow this will be of the order of five to ten minutes, and during the valve closure will be reduced to around 0.2 seconds

The above analysis was carried out using both Flowmaster and Bath*fp* on a simple network. The run time for Bath*fp* was 9 seconds during which 290 time steps were carried out. The run time for Flowmaster was 2700 seconds during which 28,800 time steps were carried out. Therefore the analysis using Bath*fp*'s adaptive time step is 300 times quicker than Flowmaster's fixed time step.

7.1.1.3 Pressure Surge

Pressure surge is a particular type of transient analysis. It is concerned with predicting the overshoot of pressure due to a valve closure, pump shut-down, etc.. With respect to the aircraft fuel system, we are only concerned with pressure surge after valve closure. There are two methods appropriate to the modelling of pressure surge. A surge method, such as a solid column method [19], and methods which also take into account the elasticity of the pipe and any resultant pressure waves within the pipes, such as the method of characteristics [17].

Flowmaster contains two methods of modelling pressure surges, a solid column method and the method of characteristics. Version 1 of Bath*fp* does not contain a pressure surge model, but a method of lines pipe model is to be incorporated. This uses a finite element model of the pipe with an optimised non-uniform spaced interlacing grid with pressure and flow rates solved at alternate grid points [28]. This is used in preference to the method of characteristics because it readily lends itself to variable time step numerical techniques.

It is difficult to make reliable predictions of surge pressures using any method, other than in straight pipe lines. Bends, junctions and other components produce reflection waves which add to the fundamental wave. This can be illustrated using the method of characteristics model in an appropriate Flowmaster dynamic analysis. Consider a single pipe with a valve at the outlet and reservoir at the inlet, pipe diameter 200mm and 1000m long, fluid wave velocity 1000m/s, Figure 7.1a. If the valve is closed in 1 second, the pressure wave will not have returned from the reservoir interface before the valve closes. The resultant pressure surge is shown in Figure 7.1b for a 15 second analysis.

Consider now the same pipe, split into two equal parts, with a branch at the centre of length 500m, Figure 7.2a. If the valve is again closed in 1 second, the resultant surge at the valve face, as determined by Flowmaster, is shown in Figure 7.2b. This shows the smaller reflection waves from the junction interacting with the main pressure wave. The actual surge will be of this form and magnitude, but little is known of the reflection waves and how accurate the prediction is, therefore these results can only be used as guidance.

Although these methods do not give truly accurate predictions of the surges for cases other than straight pipes, their use in the analysis of surges give a very good indication of surge pressures that can be encountered.

Flowmaster Standard Pipe Model

The Flowmaster standard pipe model suffers from similar problems to those outlined in Section 7.1.1.2. These problems are not so acute because the period of analysis is generally around five seconds and requires a constant small time step during the full five seconds. It can however still require several attempts to determine the correct time step.

Method of Characteristics

Surprisingly for the method of characteristics, the time step is easier to chose because it is restricted to ones which will pick up whole reach lengths within all the pipes (Section 3.4.2.2). This can cause a restriction if there are different length pipes within the network, creating problems selecting a suitable time step. In these cases it may be necessary to adjust the length of the pipes to aid the time step selection. As explained above, the application of any numerical method to surge modelling in systems consisting of more than one pipe results in approximations of the surge due to reflection waves whose effects cannot be confirmed. As a result small adjustments to pipe lengths to aid in time step selection will not have significant effects.

7.1.1.4 Determination of Component Sizes

Flowmaster's Flowbalancing module is the most appropriate method for this type of analysis. This is a particular type of steady state solution method which, when supplied with the volumetric flow rate through a component, determines the size of the component to achieve this flow rate. Components which can be sized are restrictors, pipes, valves, bends and discrete losses.

Application of Flowbalancing requires a component within each flow path of the network to be specified as the balancing component, ie. the one to be sized. This is illustrated with the network of Figure 7.3. The circuit has four flow paths *abf, abe*, *ac* and *ad*. The balancing component of each of the flow paths can be in any of the branches of that path, but if a branch makes up more than one flow path it can only contain a balancing component for one of the paths. For example, branch *b* may only contain a balancing component for either *abe* or *abf*. With the flow rates specified for each of the flow paths of the network, a direct steady state, rather than iterative, solution can be obtained as explained in Section 3.4.2.1. Output is similar to steady state with the addition of the loss coefficient data, and if appropriate, the size for the balancing components.

7.1.1.5 Summary of Applications

Sections 7.1.1.1 to 7.1.1.4 discussed the application and performance of Bath*fp* and Flowmaster to standard analysis types. This Section summarises these applications and incorporates the models developed in Chapter 6, giving examples of the most appropriate analysis method for commonly met modelling requirements within an aircraft fuel system.

- Steady state conditions. Either Bath*fp* or Flowmaster are appropriate for steady state analyses. The choice of method will depend on whether a model of the network already exists in one of the packages.
- Analyses involving the response of a network over time. Generally Bath*fp* will be the most appropriate. If the network is already modelled in Flowmaster, and the time step for the response is expected to be fairly constant, then Flowmaster may also be appropriate.
- Pressure surge. Flowmaster will be the most appropriate for these cases. The choice of using method of characteristic model or rigid pipe model for the pipes will be dependent on the valve closure time.
- Analysis requiring the operations and effects of fuel tanks to be modelled. Bath*fp* is the obvious choice here as Flowmaster has too many restrictions when modelling tanks.
- Analysis requiring the effects of changing altitude to be considered. To allow for changing fuel properties Bath*fp* and the *environment* model *ENV0* are required. If the effects can be adequately accounted for with constant fuel properties, and changing atmospheric conditions applied at the boundaries, then Flowmaster will also be appropriate.
- If additional models are required to be modelled. Generally Bath*fp* is the most appropriate. However, if the additional modelling can be described as a characteristic curve, Flowmaster may also be appropriate.

7.1.2 Application of Computational Fluid Dynamics

The range and number of applications of Computational Fluid Dynamics (CFD) to the modelling of the aircraft fuel system is very large. The breaking down of the fluid domain into small blocks over which properties can be assumed to be constant, means that many fluid flow problems can be modelled. Often the only restriction on the ability to model a problem is the time required to develop the geometry. With the application of PATRAN, or similar, as discussed in Section 4.4, and the advances to mesh generation techniques within the CFD codes, this restriction is considerably eased.

Examples of studies undertaken or considered are given below, but this list is by no means exhaustive.

- Determination of loss coefficients for components. This is particularly appropriate for complex or damaged components. An example of this is given for 'Y' junctions in Chapter 5, and in the second case study of Chapter 8.

- Check of detrimental effects on flow paths in complex or damaged components i.e. dead zones, recirculation etc. An example of this is given in the second case study of Chapter 8.

- Increase the understanding of the characteristics of a component.

- Force on ball valves failed part open, to determine if they may be forced open or closed.

- Modelling of jet pumps.

- Effects of blockage due to impurities on strainers, water drains etc.

- Modelling of temperatures in a tank. This would be useful to determine the effects of the returning Integral Drive Generator (IDG) recirculation flow.

7.2 Application of Computational Methods to Aircraft Fuel Systems

The first question to be asked is whether a computational approach is appropriate to the solution of a particular problem. For example, if a single steady state calculation is required in a non-branching system with the loss coefficient data readily available, the computational methods will generally not supply an answer any quicker than graphical methods. However if it is considered that further analysis may be required for this system, the computational methods will enable the later analyses to be carried out much quicker, particularly if changes to the system are required to be studied.

If the system is branched, then computational methods are by far the most appropriate. This is particularly true if the flows in all, or some, of the branches are unknown. For the computational methods the introduction of a branch to the system only requires the additional components specifying, unlike graphical methods where estimates are required for the flows in each branch.

7.3 Design Procedure

The designer is required to ensure that the design meets all of the system specifications, complies with all airworthiness requirements and other requirements laid down by disciplines such as structural, and is of the minimum weight possible for the design. In the past weight savings have not always been exploited to their full potential because of problems adequately modelling the system. This is due to a variety of reasons, such as the modelling is not possible or it is not economical, ie. the cost of modelling is greater than the cost of additional weight on the anticipated number of aircraft. This would be typically for cases requiring a dynamic model where the man hours involved for traditional methods can be prohibitive. The introduction of computational methods to the design procedure enables many more weight savings to be achieved by creating a much more efficient design.

Chapter 2 gives a general description of aircraft fuel systems and divides it into individual subsystems. This division is used for both clarity of understanding and design purposes. The design procedure has also been developed around these divisions, and includes a first stage which is the initial system description which is applicable to all sections.

The fulfilment of the requirements laid down by the Airworthiness Authorities, explained in Chapter 2, are generally satisfied by the layout of the system. The design areas discussed in Sections 7.3.2 to 7.3.5 are concerned with verifying the operation of these systems. If they are found to be unable to meet their operational requirements, changes would be made at an early stage.

7.3.1 Initial System Description

This is the first stage of the design for all of the areas of the fuel system. At the commencement of this stage only the requirements of the aircraft specification and those laid down by Airworthiness Authorities are known. The methods of achieving these requirements will generally be satisfied in the system layout. For example the choice of negative 'g' protection for the engine feed system and where and how this will be positioned within structural and system limitations will be made. At the conclusion of this stage, schematics of each of the systems and their interdependence will be developed. These will only contain 'general' pipe runs, the final detail and verification of operation will be determined in the design studies of the individual areas, as outlined in Sections 7.3.2 through to 7.3.5.

7.3.1.1 Initial Component Sizing

At this stage of the design very little detail is known of the system. Generally it will only consist of approximate lengths of the branches of the system as defined in the general layout.

Details on the number or size of bends, junction angles, etc. will not be available. The aim of the analysis is to determine appropriate diameters for the branches of the system.

Component sizing, using any method either computational or traditional will invariably require trade–offs and assumptions to be made. This can be illustrated by taking the branching system of Figure 7.4. The size of branches *B*, *C* and *D* will be dependent on the size selected for *A*. Alternatively if a size was selected for say *B*, then the size of *A*, *C* and *D* would be dependent on the size of *B*. An estimation is therefore required of the size of one of the branches, before a sizing analysis can be carried out.

The Flowbalancing analysis module of Flowmaster is the most appropriate analysis method for component sizing. The procedure adopted using the Flowbalancing analysis is very similar to that which would be used with traditional methods. The major difference being that for the example in Figure 7.4, branches *B*, *C* and *D* will be sized in a single analysis which will take into account their interactions. Traditional methods would only size one of *B*, *C* or *D* at a time.

The following steps are required to determine the appropriate diameters;

- Estimate additional component losses in all the branches
- Select an appropriate diameter for branch *A (B, C* or *D)*
- Set up network as in Figure 7.4. The discrete losses will contain the estimated additional loss data. The pipes will be the approximate total length of pipe in that branch.
- Carry out Flowbalancing analysis to size branches *B, C* and *D*.
- If required, the analysis can be re–run with a different diameter for branch *A* to enable a sensitivity analysis to branch *A* to be carried out, or a diameter selected for branch *B, C* or *D* and a Flowbalancing analysis carried out to size the remaining branches.

7.3.1.2 Initial Pipe Detail

The majority of an aircraft fuel system is situated in the wing of the aircraft, with some equipment in the centre section between the wings and aft through the fuselage if there is a trim tank fitted. All of these positions, particularly the wing, are restricted for space and have complex structures, Figure 6.2, [56]. Taking these into account, and achieving the requirements of the system, can lead to complex shaped components with very high losses.

It is important when defining the layout of the various systems that the resultant shapes of bends, junctions etc. do not result in high loss components. To this end CFD should be used

to model the components and determine the flow patterns and losses through them and if they are judged to be too great, the effects of different layouts assessed. These new layouts may move the emphasis of the requirements slightly. A good example of this, though unfortunately carried out a late stage of the design, is given in the second case study of Chapter 8.

7.3.1.3 Benefits of Computational Methods

Typically the application of computational methods to the design of the fuel system brings in greater confidence, the ability to analyse more situations/cases, and a saving of time. With respect to the initial sizing of branches, the direct benefits are not as tangible. There is a small saving of time with the majority of branches being sized in one analysis. A secondary benefit with the application of these methods is a 'base' networks for development to analyse the system, to be described in the following sections.

7.3.2 The Refuel System

The design objectives of the refuel system are:

- All tanks to be refuelled within a specified time.
- Pressures within tanks remain within structural limits.
- Surge pressures due to closure of refuel valves are maintained below the limits of the system.
- The static charge of the fuel is maintained within safe limits during refuel.
- The system weight is kept to a minimum.

These objectives are achieved with a variety of modelling techniques and practices. Typical refuel systems are shown in Figures 2.7 and 2.8.

7.3.2.1 Refuel Times

The refuel rates into the tanks are dependent on the pressure and flow available at the refuel coupling, and the system pressure losses between the coupling and the tanks. Individual tanks require different refuel rates, due to differing sizes and times required for refuel of these tanks. This is achieved with a restrictor in the refuel line of each tank.

The sizing of the restrictor has to take into account the flow rate required into the tank to achieve the refuel time, and ensure that the pressure within the tank remains within structural limits.

The Flowbalancing module of Flowmaster, Section 3.4.2, is the most suitable application for sizing of restrictors as it enables all restrictors to be sized simultaneously. A typical simulation network for a five tank system is shown in Figure 7.5. The required flow rate into each tank is set in the tank restrictors, the output of restrictor size will be of the form shown in Figure 3.7.

7.3.2.2 Refuel Overflow

In normal operation the refuel valve will close when either a pre-selected quantity of fuel has been delivered to the tank, or by the high level sensor. If a failure occurs and the refuel valve does not close, then fuel is required to leave the tank through the vent system without the tank pressure exceeding the structural limits. This condition is known as refuel overflow. The design is only required to account for a single tank overflow, the probability of multiple failures of high level sensors is considered low.

To analyse this case the vent system is added to the network of Figure 7.5. This is shown in Figure 7.6, modelling the right inner tank at refuel overflow. This tank is modelled with two discrete losses and a pipe, Figure 7.6. The discrete losses model the inflow and outflow losses of the tank and the pipe, the tank itself. The pipe is set up as a 'short fat vertical pipe', the diameter representing the cross sectional area of the tank, and the length the height of the tank. The node heights are similarly set. This description is appropriate because flow is simply passing through the tank. The other tanks will still be modelled with constant head reservoirs, with both the refuel system and vent system connecting to the single port. Flow from the refuel system is prevented from entering the vent system with a non-return valve. This is used in the same manner as the discrete loss model in Section 6.2.3.1, with the node heights set as described for that case.

Steady state analyses are carried out on this network with all combinations of refuel allowed and disallowed to the non-overflowing tanks. This will be repeated for each of the tanks at refuel overflow.

If the pressures in any of the tanks exceed structural limits the effects of reduced restrictor sizes and possible vent system modification can be analysed with minor changes to the networks of Figures 7.5 and 7.6 and its derivatives. This type of iteration is most effectively carried out by computational methods.

7.3.2.3 Surge Pressure

When the inlet valves to the individual tanks close, surge pressures will be produced in the refuel system. The magnitude of these will depend on the valve closure characteristic, the distance the wave travels before being reflected back and the velocity of the fuel flow.

Care has to be taken to ensure that the inlet valve does not close before the pressure wave returns. If it does the pressure generated at the valve face due to the conversion of the kinetic energy of the flow to potential energy will be the same as if there had been an instantaneous valve closure. Allievi or Joukowsky [19] have defined the following expression for the pressure produced under these circumstances:

$$p = \rho u a$$

The density of fuel is typically 800kg/m^3 and a typical refuel rate will be 9.6m/s [80]. The wave velocity (a) is a function of the fuel sonic velocity and the elasticity of the pipe. For aircraft pipes containing fuel a typical value is of the order of 1000m/s [80]. Therefore if the valve did close before the wave returned, a pressure of 76.8bar would be generated.

This pressure cannot realistically be designed for within the weight restrictions placed on the fuel system. The system is therefore designed so that the valve closes after a number of wave reflections have taken place. The time required for the pressure wave to return to the valve can be calculated for a typical refuel system consisting of 20m of 50mm diameter aluminium alloy pipe, and 30m of 50mm diameter refuel hose. The point of reflection of the pressure wave will usually be the refuel vehicle's pressure controller. This will be situated either at the aircraft refuel coupling or on the refuel vehicle, dependent on the system used. The wave velocity for the aluminium alloy pipe can be taken from the above example, a typical wave speed for fuel in a flexible hose is 300m/s [80]. For a pressure controller situated at the refuel coupling this will give a wave reflection time of 0.04 seconds, and for a pressure controller situated at the refuel vehicle the wave reflection time will be 0.24 seconds. Typically tank inlet valves are specified to close in 2 to 5 seconds.

Flowmaster is most appropriate to the modelling of pressure surge using either the method of characteristics or its standard pipe model. Experience has shown that generally at the valve closures encountered within refuel systems (2 to 5 seconds), a Flowmaster method of characteristics analysis is not always required. Instead the standard rigid pipe model is appropriate. If we take the refuel system of Figure 7.5 the effects of closing all tank valves over a two second period is shown in Figures 7.7 and 7.8. Figure 7.7 is a method of characteristics model of the pressure within the pipes, and Figure 7.8 uses the standard pipe model. The only difference between these results is the 1psi pressure ripple predicted by the method of characteristics model. This is due to small pressure wave reflections which will be quickly damped out due to friction. The use of the method of characteristics does not give any increase in accuracy, it only restricts the choice of time step (see Section 3.4.2.2) and requires up to five times longer to run.

7.3.2.4 Monitoring of Tank Volumes

The time history of fuel in a tank during refuel can be determined using Bath*fp* to analyse the system. This will generally not be required due to the constant refuel rate, but in cases such as the second case study, Section 8.2, where the heights of fuel in the tanks was of primary importance it is the only means of predicting the output.

7.3.2.5 Benefits of Computational Methods

The major benefit the computational methods bring to the design and analysis of the refuel system is the addition of pressure surge analysis. Although these analyses do not give a truly accurate prediction of the surges, they do give a very good indication of the pressures that will be encountered and do not require extensive set up time by the designer. There are graphical methods which can be used to predict pressure surges, which range from methods which actually solve the characteristic equations of Chapter 3, equations 3.28 and 3.29, to simpler methods which make appropriate approximations. Of the accurate graphical methods one of the most common [16] solves equations 3.28 and 3.29 using numerical techniques similar to the finite difference method. The solution is generally represented on an x,t plot as shown in Figure 7.9. As for the application of the characteristic equations in Flowmaster the pipe is required to be split into equally spaced lengths Δx as shown in Figure 7.9. Solution of Equations 3.28 and 3.29 progresses through the length of the pipe and time in the same manner as for their application within Flowmaster. The conditions at positions $n-1$ and $n+1$ at time t provide the initial conditions to solve for position n at time $t+\Delta t$ (Figure 7.9). Where $\Delta t=\Delta x a$, the time taken for a pressure wave to travel from n to $n+1$. The arrows on Figure 7.9 show the progression of solution through the x,t plot. The time history of pressure and flow rate at each point within the pipe can be obtained from the x,t plot. The major problem with these methods is that they are complex and require a very long analysis time.

There are also quicker, simpler graphical methods which are less accurate. One of the most common of these methods used in the aircraft industry [19,20,80] requires the valve closure to be considered to occur in increments equal to the time required for the pressure wave to reflect back to the valve face ($2L/a$ seconds). The pressure loss characteristic for each increment of valve position can be plotted along with the refuel characteristic against velocity as shown in Figure 7.10. The instantaneous surge pressure (ρua) can be represented on this graph with a straight line of slope $-\rho a$ starting at the initialisation of the valve closing action C. If the valve closed in less than the critical time ($2L/a$ seconds) this line would represent the surge wave, and provide the maximum surge pressure (ρua). For valve closures in excess of the critical time the line of slope $-\rho a$ is plotted from the point of initialisation of valve closing C until it meets the loss characteristic at time $2L/a$ curve OEF at E. This represents the wave returning to the valve at this time and provides the pressure and flow velocity at the

valve face at time *2L/a*. The reflection of the surge wave back from the valve is represented by a line with slope ρa which is drawn from *E* until it meets the refuel characteristic at *G*. This represents the wave arriving at the refuel coupling, or point of up stream reflection, and provides the pressure and flow velocity at the coupling at time *3L/a*. The reflection of the surge wave back from the refuel coupling is represented by a line with a slope of $-\rho a$ which is drawn until it meets the pressure loss characteristic at time *4L/a* at point *H*, this represents the wave returning to the valve at this time and provides pressure and flow velocity at the valve face at time *4L/a*. Plotting of the characteristic is continued in this manner until the flow velocity reduces to zero at point *K*. From the point *KHEC* a time plot of the pressure surge at the valve face can be obtained.

The first, more accurate, graphical method described above has not usually been attempted due to the time involved, and the simpler method because it only represents an approximation to the surge pressure. Instead reliance has been on testing of the actual aircraft which may result in late modifications. With computational methods the time required to analyse a surge is greatly reduced, so changes can be incorporated based on the results, or anticipated with preliminary work undertaken, before the tests take place.

7.3.3 Vent System

The vent system is one of the most difficult systems to model for the computational methods. This is because it usually requires the modelling of the fuel and vent system simultaneously. Both Flowmaster and Bath*fp*, in their present states, can only model one fluid. Therefore simplifications must be made to the actions of the fuel on the vent system.

The vent system fulfils two roles. It ensures through the venting of air, either into or out of the tank, that the pressure within the individual tanks remains within structural limits. Additionally it ensures fuel can safely leave the tank in the event of a refuel overflow as described in Section 7.3.2.2.

The critical cases for design consideration are refuel overflow and the performance of the vent system during emergency descent. Vent system performance during refuel overflow is included in the analysis of the refuel system and is described in detail in Section 7.3.2.2.

7.3.3.1 Emergency Descent

Emergency descent is defined by the authorities [1] as a descent from 40,000ft to sea level in 110 seconds. This is based on the scenario of a cabin depressurisation at this altitude.

The effect of this descent on the fuel system, and in particular the vent system, is that air passes into the tanks through the vent system. With the high rate of descent, the air reaching the tanks will be at a lower pressure than the external atmosphere, causing a pressure

differential across the skin. It is this pressure differential that is the critical design parameter. Additionally due to the high rate of descent the effects of changing density may be significant and need to be allowed for in the analysis.

Emergency descent can be modelled with either Flowmaster or Bath*fp*. The following example is for the study of emergency descent using Flowmaster carried out by the author.

A simplification of constant air properties is required because these cannot be altered during the analysis. Values at sea level or the bottom of the descent should be used to over predict losses. A typical simulation network is shown in Figure 7.11 with typical results in Figure 7.12. The tanks are modelled using an accumulator as described in Section 6.2.3.1. This enables the air within the accumulator to be compressed as described by the gas law. The accumulators are valid as tank models until the accumulator fills.

Bath*fp* has not been used at present for the analysis of emergency descent because of its late introduction. With the inclusion of *environment* component *ENV0*, described in Chapter 6 Section 6.3.1.2 enabling the fluid properties to be adjusted during an analysis, Bath*fp* is now the most appropriate method for the study of emergency descent and would be used in future analysis.

7.3.3.2 Benefits of Computational Methods

The inclusion of the emergency descent case enables the vent system to be sized to its optimum minimum size, if this is the critical design case. Without this analysis an allowance would be made which will result in an over sized system.

7.3.4 Fuel Transfer

The fuel transfer system is required to ensure that the fuel is distributed to the correct tanks so that,

- Engine feed tanks have sufficient fuel.
- Bending relief is supplied.

and if a trim tank is used,

- The aircraft has optimum trim at all times.

If we consider a typical six tank aircraft fuel system, the transfers required will be as shown in Figure 7.13. The aim of these transfers is to ensure that the fuel from all tanks is eventually transferred into the inner tanks to feed the engines. The ordering of transfer will

be dependent on the aircraft, its loading and the sector to be flown. A few general rules that can be applied to all aircraft and conditions are:

- Fuel in the centre tank is usually the first to be depleted, so centre to inner tank transfer will be one of the first transfers.
- Trim tank fuel will be transferred forward when the centre of gravity (cg) of the aircraft reaches its aft limit. This will usually be a transfer of part of the tank's contents until the cg as moved sufficiently forward.
- Outer to inner tank transfer will be the last to take place, to maintain wing bending relief for the maximum period of the flight.

The design analysis has to take into account all of these transfers and their rates for all combinations of aircraft altitude, attitude and all variations of fuel types and properties. These have to be considered for normal operation and operation in the event of failures.

The transfer system is a dynamic system, which for a complete analysis also requires models with accurate descriptions of fuel tanks. Bath*fp* is ideally suited to these analyses being a dynamic analysis method with excellent fuel tank modelling capabilities. The application of Bath*fp* not only allows the transfer rates to be analysed, but enables the volume of fuel within tanks to be monitored.

The fuel tank models enable the effects on transfer rates of depletion of fuel levels in the tanks due to engine feed or transfer to be considered. This is particularly important for cases of gravity transfer, commonly used for trim and outer to inner tank transfers where the head of fuel in the tank may be a significant part of the total head, and for transfers with degraded pump performance when pumping with hot JETB at altitude (see Section 2.1). This is illustrated with an actual aircraft study undertaken by the author to assess centre to inner tank transfer with the inner tank inlet valves failed open. The analysis network is shown in Figure 7.14 and shall be used to explain the operation of the system. Both inner tanks are modelled because the cross feed line is not symmetrical about the trim line connection, resulting in a slight non-symmetrical flow to the inner tanks. Under normal operation the fuel in the centre tank is transferred equally into the two inner tanks at a nominal flow rate of 70 L/min. The centre tank transfer pump is the same as the aircraft boost pumps, for commonality, even though the flow rate and pressure required is much less. A restrictor at the pump outlet ensures the pressure and flow rate are reduced to the required level. The refuel restrictors, explained in Section 7.3.2.1, are included in the simulation networks of Figure 7.14 because the aircraft being studied, like many others, uses the refuel system for transfer purposes. The case analysed is the transfer of JETB at 54°C and an altitude of 41,000ft. The characteristic of the centre tank transfer pump under these conditions is shown in Figure 7.15, along with the nominal characteristic for JETB at 20°C to give an indication

of the degradation of pump performance caused by the variation of fuel properties explained in Chapter 2, Section 2.1. Though the likelihood of JETB being at a temperature of 54°C, and at 41,000ft is highly remote, it is still a possibility and so constitutes an extreme design condition. The analysis was carried out for two cases, the centre tank full and the centre tank at low level. In both cases the inner tanks were full at the start of analysis.

For the centre and inner tanks full, plots of the tank volumes against time are given in Figure 7.16(a). A plot of the flow rate through one of the inner tank inlet valves is shown in Figure 7.16(b), the flow through the other being almost identical. From these plots it can be seen that the transfer takes place inner tank to centre tank for the first 120sec, and then transfers the centre tank to the inner tank as required. The reverse transfer, from inner tank to centre tank, is due to the centre tank transfer pump not being able to overcome the head of fuel in the inner tank for the first 120sec. After this time the centre tank pumps transfer as designed because the head of fuel of the inner tank is sufficiently reduced by depletion of the inner tank fuel volume through engine feed. The transfer from centre tank to inner tanks is at a greatly reduced average rate of 20 L/min. This results in the inner tanks being depleted of fuel before the centre tank. The airworthiness requirement for this situation is that the centre tank transfers all fuel to the inner tanks before they are depleted. In this analysis this was not met, but the analysis assumes the fuel temperature is +54°C throughout. In reality this will not be the case because the outside air temperature is –50°C, so the fuel temperature will rapidly cool to near this value where the pump performance will greatly improve, ensuring the transfer from the centre tanks takes place well before the inner tanks empty.

For the centre tank empty and the inner tanks full, plots of volumes against height and the flow rate through one inner tank valve are shown in Figure 7.17. In this case the transfer is inner to centre for the first 1250sec. As for the case with full centre tank, the centre tank transfer pumps are unable to overcome the head of the inner tanks. In this case the centre tank does not have a head of fuel to increase the output pressure of the centre tank pump and therefore a greater volume of fuel is required to be removed from the inner tanks through engine feed before the centre tank pumps can overcome their head. Again the inner tanks are depleted of fuel before the centre tank completes transferring, but as before this is a small amount, and the fuel will have cooled early in the flight and the transfer pump performance increased.

7.3.4.1 Flight Profile Modelling

This is a natural extension of the analysis of fuel transfers. It models the operation of the transfer system for a total flight and takes into account the burn rate of the engines and all transfers. Implementation of this type of analysis requires limited aspects of the operation of the fuel system computer to be included. This is in the form of controlling the position of

tank inlet valves dependent on the volume within the tank and the phase of the flight. Control of the inlet valves, based on the volume of fuel within the tank, is achieved using tank models which control the position of the inlet valves. Tank and valve models appropriate for this operation have been developed during this research and a detailed description is given in Chapter 6. Control of valve position due to flight phase, is limited to signalling the valve position at predefined times using a signal source. A signal source is a standard Bath*fp* model which describes an output signal as a series of ten stages which may be ramped, stepped or constant. A typical simulation network is shown in Figure 7.18 for a medium capacity civil aircraft. Fuel volumes within the tanks are given in Figure 7.19 for a case considering an engine failure 3.5 hours into the flight. In this case the engine failure is accompanied by a rise in the left inner tank volume, Figure 7.19. This is because the centre tank is still transferring to both inner tanks and the left inner tank's fuel volume is not being depleted by engine feed. When centre tank transfer ceases, at approximately 4.5 hours, the left inner tank commences to cross feed to the right inner tank. This is standard design on all aircraft, where on an engine failure the fuel that would supply that engine is made available to the other engine.

7.3.4.2 Benefits of Computational Methods

The introduction of the computational methods to the analysis and design of the transfer system has enabled the analysis to be extended to cover dynamic cases. With traditional methods the analyses are restricted to considering singular steady state occurrences. With the introduction of the dynamic analysis, fuel tank volumes can be monitored as in the example above. A major benefit is the inclusion of flight profile modelling enabling the analysis of multiple transfers to be considered.

7.3.5 Engine Feed

The engine feed system is required to ensure that fuel is supplied to the engines at the correct flow rate and pressure for all normal and failure cases, fuels, temperatures, altitude and pitch and roll combinations.

The design requirement is to ensure that the engine inlet pressures and flow rates are able to meet the engine manufacturers requirements for all cases. The flow rate is a function of the engine demand, which will be dependent on the flight phase (cruise, climb, take off etc.), altitude and temperature. The engine inlet pressure is set by the engine manufacturers to be either gauge pressure or 0.34 bar above the vapour pressure of the fuel which ever of these is the greater.

The analysis of the system can be carried out by either Flowmaster or Bath*fp*. Only Flowmaster has been used at present due to the late introduction of Bath*fp*. A typical analysis

network is shown in Figure 7.20. All combinations of altitude, temperature, fuel, pitch and roll will be analysed with this network for all normal and failure operations. Typical results for certification purposes compiled into an engine feed system performance curve are shown in Figure 7.21. This curve is a summary of all the analyses carried out at a particular pitch, roll, altitude and temperature and verifies that the engine feed system either equals or exceeds the minimum engine inlet pressure for the complete range of engine feed flow rates. From these it can be seen that the analysis was continued beyond the maximum flow demand. This allows the impact of growth engines to be considered without the need for further analysis. In general an allowance of 25% growth is allowed for new aircraft.

7.3.5.1 Benefits of Computational Methods

The engine feed system is one area where the computational methods have been extensively applied within the Fuel Systems Engineering Group at Filton so that their impact can be better appreciated. The effects this has had on the analysis of the design are that a greater number of analyses have been achieved in a greatly reduced time. It is estimated that the use of Flowmaster achieves results typically twenty times quicker than traditional methods. This means that many more calculations have been carried out resulting in much greater confidence in the design. The introduction of Bath*fp* would further increase this effectiveness by allowing all flow rate conditions at a particular altitude and temperature to be assessed in a single run.

7.4 Closing Remarks

With the introduction of the procedures developed by the author during this research, and reported in this Chapter, a competent engineer who is not necessarily an expert user of any of the software, can carry out all of the design analyses detailed in a reduced time scale. In the past the complex nature of the systems has required a specialist to carry out the majority of the analyses.

The application of computational modelling to the design and analysis of aircraft fuel systems has greatly extended the range of analyses available and enables many more analyses to be conducted in a reduced time scale and results in a greater confidence in the design and reduced costs.

CHAPTER 8

CASE STUDIES

Two case studies have been selected to illustrate the application of the three chosen software packages to the simulation of aircraft fuel systems. They highlight some of the relevant factors when carrying out simulations and when analysing results. These two cases obviously only show a small part of the application of computational methods. They have been chosen not only to illustrate many of the points made earlier, but also to highlight, by practical example, typical problems that may be encountered.

The first study is of a test rig for a medium capacity civil aircraft engine feed system. It covers the application of Flowmaster for steady state analysis of the system. This study was originally carried out to prove Flowmaster's application to the simulation of aircraft fuel systems.

The second case study covers the sizing of restrictors for a fuel tank on a large civil aircraft. It includes the application of the Bath*fp* dynamic solution to a relatively steady state system, and the application of Star-CD to the evaluation of flow paths and loss coefficients in complex components. This study is not typical of the types of analysis that would be generally carried out for a refuel system outlined in Section 7.3.2. It is a special case because of the fuel distribution to the tank and is more typical of a transfer system analysis. This study has been included in preference to a typical transfer system for two reasons. Firstly it is a good illustration of how CFD links in with network analysis. Secondly it is an actual aircraft case that could only be solved with the computational methods. If such methods were not available, modifications to the system would have had to be made on assumptions and could only have been verified when installed and tested on the aircraft. The analyses were carried out on an actual aircraft case and were subject to very tight time constraints. The total work, from determining the problem to installation on the aircraft, was less than two months. The description is as the work developed rather than reporting on the pertinent results. It therefore includes the errors. It is felt this approach gives a better understanding of the application of the methods to analyse actual fuel systems.

8.1 Engine Feed Study

8.1.1 Introduction

The aim of the Engine Feed Study is to validate the application of Flowmaster's steady state analysis for a medium capacity civil aircraft engine feed system. This is achieved by comparison of Flowmaster's results against those of a test rig.

8.1.2 Description of Engine Feed System

The fuel system consists of three tanks, one centre tank and two wing tanks, Figure 8.1. The engine feed from the centre tank consists of two feed lines each of which has a boost pump with a non-return valve and a bleed for jet pump motive flow. Both wing tanks have the same arrangement as the centre tank, with the addition of a sequence valve for each of the pumps. The sequence valves are pressure relief valves which are used to 'clip' the pump characteristic as shown in Figure 8.2. The reduced output pressure of the wing tank pumps ensures that fuel is supplied to the engines from the centre tank in preference to the wing tanks. When the centre tank is depleted of fuel the wing tanks will commence supplying fuel to the engines, although at a reduced pressure. This arrangement provides a passive hierarchical control of pump operation, and hence fuel usage.

8.1.3 Test Rig

Since the system is symmetric the test rig consists of the engine feed for one wing only and half of the centre tank, Figure 8.3. All test work was carried out at Plessey Aerospaces, Titchfield fuel test facility [70]. This facility enables tests to be carried out at simulated altitudes by control of pressure and temperature within the test specimen. The test data available from the rig is limited due to the small number of instruments available, though there were sufficient to carry out a full analysis of the results. The major instrumentation deficiency was a lack of flow measurements for the centre and wing tank pumps, the only flow measurement being the total flow rate. This was alleviated by considering the pressure across the fuel pump outlet non-return valves. If the pump side pressure was greater than the downstream pressure the pump was considered to be supplying fuel to the engine.

8.1.4 Simulation

The simulation is of the test rig, and not the actual aircraft. A structured approach was taken for the build up of the simulation. This consisted of three distinct phases:

- Simulation of the centre tank and associated systems.
- Simulation of the wing tanks and associated systems.
- Simulation of combined centre and wing tank.

All three stages were validated against test results.

All of the components except the remote pump inlet and the gravity feed inlet are modelled with standard Flowmaster components.

The remote pump inlet is shown in Figure 8.4. This can be broken down into three standard components, a filter, a re-entrant flared inlet and a 90° bend.

- The fuel filter is made up of a 76 micron mesh with an open area of 60%. This is modelled with a discrete loss, using a loss coefficient of 1.0 taken from Reference [16] as appropriate for this area.
- The re-entrant flared inlet is modelled as an inlet loss of 0.8 taken from Reference [16] in a standard Flowmaster reservoir.
- The 90° bend is modelled with a standard Flowmaster bend.

The gravity feed inlet, Figure 8.5, consists of a non-return valve and a bend with a rectangular cross section inlet transforming to a circular cross section outlet. The bend is simulated using a discrete loss model with a loss coefficient of 0.8, taken from Reference [16]. This takes into account the bend and varying cross section. The non-return valve is simulated using a standard Flowmaster model.

The fuel pump is simulated with a standard Flowmaster centrifugal pump model. The curve of pressure rise versus flow rate describing its operation [71] is given in Figure 8.6. The fuel pump outlet non-return valve and the sequence valve are simulated with standard Flowmaster models. Characteristic curves describing their operation [71] are given in Figures 8.7 and 8.8. The curves of Figures 8.6 to 8.8 are taken from the Flowmaster models. The points shown on these curves are those used to define them within Flowmaster.

8.1.4.1 Centre Tank Model

The network developed for the centre tank model is shown in Figure 8.9. Only half of the centre tank has been modelled due to symmetry, and the junction to the wing tank and the right wing have been included with blanks.

Tests were carried out to verify the results of this module of the simulation against data from the rig. Two cases were considered, one with a flow demand of 1003.2igph and the second with a flow demand of 1273.7igph. At these flows the centre tank pumps only will supply fuel to the engine. A summary of both the test rig results and simulation results is shown in Table 8.1.

The simulation predicts pressures 3 to 4psi below those recorded on the test rig, although this is not too significant an error it was investigated to determine the cause. The predicted pressure drops throughout the network are of the same value as those recorded on the test rig. This indicates that the low predicted pressures are due to either the tank pressures being specified too low, or the simulated pump characteristic having a lower pressure than that for the test rig. The tank pressures used in the simulation are taken from the test rig results, so are correct. The lower predicted pressures are therefore a result of the simulated pump characteristic. This will be due to the variation (tolerance) allowed on the pump characteristic through its specification. The specification of a fuel pump given to the supplier is based on a pump characteristic lying inside a series of pressures and flow rates. A typical specification is shown in Figure 8.10. From this it can be seen a range of potential characteristics are available which are acceptable to the specification. The pump characteristic used in the analysis is the nominal characteristic given in the suppliers data [71], which is generally in the middle of the range of the specification. To produce the greater pressures of the test rig, the characteristic of the test rig pump will be closer to the upper limit shown on Figure 8.10. To verify this, the pressure of the simulated pump characteristic was increased by 3.5 psi, Figure 8.11. The additional results are given in Table 8.1. Using the uprated pump characteristic gives a good agreement with the test rig, indicating the difference in the predicted pressures is due to pump characteristic tolerancing. This is substantiated by further test data which confirms that for the flow rate of the test, the test rig pump is generating a greater pressure than the initial simulation pump characteristic could. The initial differences in predicted pressures are therefore due to pump tolerancing.

Under normal circumstances an investigation of this type would not have been undertaken because the difference in the predicted and test rig pressures are not too significant. The investigation was undertaken and reported here to highlight that a components characteristic has a tolerance band. In some circumstances the solution for a network will be dependent on the position of components characteristic's within their tolerance bands.

8.1.4.2 Wing Tank Model

The network developed for the wing tank is shown in Figure 8.12. The flow source attached to the connection of the junction to the centre tank and right wing tank, is used to supply a very small flow to overcome solution problems with zero flow conditions in 'T' junctions.

Tests were carried out to verify the results of this module of the simulation against data from the rig. Two cases were considered, the first a flow demand of 782igph and the second a flow demand of 1785igph. In both cases the centre tank pumps were not operational on the test rig. A summary of both the test rig results and simulation results is shown in Table 8.2.

The total flow rate only is available from the test rig results and this restricts the verification of the simulation results. It can be determined which of the wing tank pumps are feeding the engine by inspection of the pressure across the non-return valve, and comparison with its characteristic curve, Figure 8.8.

For the test rig at 782igph the pressure drop across the inboard pump outlet non-return valve is not sufficient to operate it. Therefore the total flow will be from the outboard pump. This is also predicted by the simulation. The simulation pressures show good agreement with those of the test rig being within 1.7%.

For a flow demand of 1785igph the network shown in Figure 8.12 was unable to converge to a solution. Investigation of this is restricted because Flowmaster's information is limited to the final flow convergence error in components which failed to reach solution. From this information it was concluded that flow had not converged to solution in the outboard pump, sequence valve and jet pump branch. It is assumed at a flow rate of 1784.7igph that the pressure developed by the outboard pump is approaching the limit of being able to hold the inboard pumps outlet non-return valve closed. If the flow rate were increased, flow would then be from both pumps. With a steady state iterative type solution, when two solutions are in close proximity, the solver can oscillate between the two, and not solve for either, unless correct solution weighting is applied. For a Flowmaster type analysis solution weighting would be applied to the flow rate during the iteration process outlined in Chapter 3, Section 3.4.2.1. Without solution weighting the new values of the flow rates determined during the iteration process are used to provide new updated loss coefficients to calculate new estimates of pressure. When weighting is applied the flow rates are adjusted by the following formula to weight them towards the flow rate at the previous iteration.

$$q'_n = \gamma q_{n-1} + (1 - \gamma) q_n$$

Where q'_n is the weighted flow rate, q_n the new flow rate, q_{n-1} the previous flow rate and γ the weighting factor which has a value between 0 and 1. These weighted flow rates are then used to update the loss coefficients and new estimates of pressure determined. Application

of solution weighting has the effect of damping any solution oscillations and aiding approach to solution. Flowmaster has fixed weighting and damping which are optimised for the majority of cases. An attempt was made to increase the flow demand to investigate this, but solution could still not be attained. The use of a dynamic simulation was also investigated to attempt to 'approach' the required solution from the 'correct direction'. This was found to require excessive computation times due to the limitations outlined in Chapter 7, Section 7.1.1.2. To aid the solution, the network was simplified by incorporating the sequence valve characteristic into the pump valve characteristic to form a 'pseudo' pump characteristic, Figure 8.2. This was used in the network of Figure 8.13. This characteristic gives only an approximate model of the pump and sequence valve because it is made up of a pump pressure rise, and valve pressure drop, rather than outlet pressures. Additionally the line loss on pump inlet will be under-predicted because the flow will be reduced due to the omission of the sequence valve return flow. The network of Figure 8.13 does converge to solution. This is assumed to be due to the reduced number of branches required to balance and indicates the initial problem to be balancing of the flows at the pump outlet non-return valve and sequence valve. The solution of this network splits the flow approximately equally between the inboard and outboard pumps. The test rig results give flow totally from the outboard pump as for 782igph. The 782igph case was also analysed in the network of Figure 8.13, and the solution for this case was an almost equal split of flow rate from the inboard and outboard pumps. This difference is attributed to the approximation of the 'pseudo' pump model. A network of this type is quite sensitive to the delivery pressures of the pumps. If one pump delivers a greater pressure which is sufficient to keep the other pump's non-return valve closed, then that tank will supply all of the flow. If both pumps deliver the same pressure then the flow will be a 50/50 split. These alternative solutions can be attributed to pump tolerancing.

8.1.4.3 Combination of Two Models

Two networks were developed to model the test rig in its entirety based on the experience of the wing tank models. One including the sequence valves, Figure 8.14, and one without the sequence valves and using the 'pseudo' pump model, Figure 8.15.

Tests were carried out to verify the results of these two networks against data from the test rig. The data were taken from a case with all three pumps operating with a total flow demand of 2944igph, and the cases used for the centre tank model and the wing tank model verification. For the wing tank verification tests the centre tank pump was isolated by setting its rotational speed to zero. A summary of both the test rig results and the simulation results is given in Table 8.3.

At a flow rate of 2944igph the complete network of Figure 8.14 was unable to converge to solution. As in the case of the wing tank tests this was found to be due to balancing of flows

across the sequence valves. The network using the 'pseudo' pump model, Figure 8.15, was able to produce results, but again, as for the wing tank tests, it solved for the flow from the wing tank being split approximately equally between the inboard and outboard pumps. The test rig results showed the flow to be from the outboard wing tank only, since the pressure drop across the non-return valve is too low for it to operate. These differences of solution again can be attributed to the approximation of the 'pseudo' pump model, and sensitivity of solution to pump outlet pressure.

The centre tank simulation tests gave exactly the same results as for the centre tank only model, in both the network with, and without, the sequence valve.

The results of the wing tank simulation tests were nearly identical to those for the wing tank only models. This was with the exception of the test at 782igph with the sequence valves included, which gave total flow from the inboard pump only, rather than from the outboard pump as for the wing tank tests and the test rig. Investigation of various network configurations has shown this to be due to the inclusion of the centre tank line. In the network of Figure 8.14 with a flow demand of 782igph there is a very small flow back down the centre tank line. This flow is only 0.02% of the total flow and is therefore considered insignificant in comparison to the other flows. If this flow is included in the wing tank model with a flow source, instead of the blank at the junction to the centre tank, the results are unchanged. If we consider the wing tank only supplying the engines there are three possible combinations of flow, 100% from the inboard pump, 100% from the outboard pump and 50% from each. This is illustrated in Figure 8.16. This diagram is a combination of the two pump characteristics. The x axis from left to right is the flow rate of the inboard pump, and from right to left the flow rate of the outboard pump. Addition of the flow rates on these axes at any point will always give a constant value. The left hand y axis represents the outlet pressure of the inboard pump, and the right hand y axis the outlet pressure of the outboard pump. A solution can only be achieved when either both pump pressures are equal, solution 2, or when one of the pumps is at its stall point ie. $q = 0$, solutions 1 and 3. To explain the solution which will be achieved we require to consider the system curve and total pump characteristic for the total system. These will be very complex discontinuous curves, so for illustration purposes, a single system characteristic depicting the three solutions and a pump characteristic are shown in Figure 8.17. On the test rig the solution will be dependent upon which direction the solution is approached along the system curve ie. if the flow rate is increasing or decreasing. For the simulations the solution will be dependent on where the initial iterations predict an approximate solution. For the case without the centre tank the initial iterations are predicting an approximate solution near solution 1 and hence solve at solution 1. The inclusion of the centre tank causes the initial prediction to be moved near to solution 3 and

hence solving at solution 3. This cannot be completely verified as information on each iteration is not available from Flowmaster.

An attempt was made to run a transient analysis with the flow demand altered from 0 to 3000igph to run the network through its total operating cycle, but the run time was too excessive, and convergence errors could not be overcome with sensible time steps.

8.1.5 Conclusion

For the cases that Flowmaster achieved solution the results were well within experimental error of those from the test rig. There were two major problems encountered, the balancing of flows across the sequence valves at high flow rates, and handling of multi-stable solutions.

For the case of balancing of flows the problem may be due to the maximum number of iterations being reached before solution is achieved rather than an inability to find solution. This cannot be confirmed because solution data is not available. Even if this is the case it means the solver is not performing to its optimum in this area. The introduction of user control of convergence and solution weighting may overcome this problem, but non-expert users will not be able to apply this effectively.

For the case of multiple solutions, there are two options which may give control to which solution is achieved, and allow investigation into the possibility of different solutions. They are the setting of initial conditions in the branches of the network, or the use of transient analysis in a similar manner. The use of transient analysis was tried but resulted in excessively long run times due to the small time step required to account for the change of state of operation of the pump outlet non-return valves. Problems of this nature are highlighted and discussed in detail in Chapter 7, Section 7.1.1.2.

The effects of component tolerances are highlighted in this network due to the sensitivity of the wing tank solution to the outlet pressure of the pumps. The significance of the effects of component tolerance is very much dependent on the networks. In this case the incorrect solution was not significant because both pumps are supplied from the same tank. If these pumps were supplied from different tanks and the analysis was concerned with monitoring the volumes of these tanks, then the effects of an incorrect solution are considerable. In general the effects cannot be completely investigated due to the time required, only their effects borne in mind when analysing results. In the future, it is proposed to assess the effects of combinations of the extremes of tolerances on the key components in the network.

Overall the simulation showed close agreement with measured data and the problems encountered would lead to either no solution being available or another valid numerical solution rather than an incorrect solution being achieved. The fact it is a valid numerical

solution though does not mean it is necessarily a practical one, so results should always be assessed with experience rather than just accepted.

The major problems encountered were all solver-based and proved impossible to completely investigate due to lack of data on how the solution progresses. To enable truly complete analysis of aircraft fuel systems this information would have to be made available.

8.2 Modelling of Refuel in a Partitioned Tank

8.2.1 Introduction

This study was initiated to determine the size of the refuel restrictors in a partitioned tank. The tank is split into two cells as shown in Figure 8.18, which are treated for gauging purposes as a single tank. The two cells are linked by the refuel line which maintains a level fuel surface across the partition at all times, this being a design requirement. During refuel, the refuel line cannot adequately balance the levels in the two partitions. Therefore the refuel rates into each partition are required to be set to maintain a level fuel surface. The study was carried out in four stages:

- Initial sizing of the refuel restrictors (Section 8.2.3).
- Investigation of a problem with the refuel system highlighted during the initial sizing of the refuel restrictors (Section 8.2.4).
- Analysis and determination of modifications to the refuel system (Section 8.2.5).
- Sizing of the refuel restrictors with the modifications incorporated (Section 8.2.6).

This study describes the work as it developed rather than reporting on the pertinent results. It therefore includes the errors. It is felt this approach gives a better understanding of the application of the methods to analyse actual fuel systems.

Throughout this case study, the difference in height of the surface of fuel in the forward and aft cells is referred is as the 'fuel step across the partition', which is shown in Figure 8.19.

In parallel with the simulation, aircraft tests were conducted. The fuel step across the partition on the aircraft was measured with simple manometers connected to drains at the base of the cells.

8.2.2 Refuel System

The tank is split into two cells, forward and aft, linked by the two inch refuel line. The tank is refuelled via two restrictors as shown in Figure 8.18. The aft restrictor feeds the two outboard aft tank diffusers *A1* and *A2*, and the forward restrictor feeds the inboard aft tank diffuser *A3*, and the two forward tank diffusers *F1* and *F2*.

8.2.3 Initial Restrictor Sizing

The restrictors could not be sized in the manner described in Section 7.3.2.1 because the flow rate required through each was unknown. The criteria for sizing of the restrictors was to maintain as near as possible a zero step across the partition throughout refuel.

The restrictors and associated pipework were modelled with Bath*fp* standard components, bends and junctions being accounted for as additional losses in the pipe models. The forward and aft cells were modelled with tank models as described in Section 6.2.3.2, there volume–height descriptions being taken from Reference [2].

The diffusers, Figure 2.6, have 1½ inch diffusing pipe which is connected to a 2 inch refuel pipe. They are modelled using a discrete loss as described in Section 6.2.4. In addition to the loss coefficient of 1 for the diffuser, a loss coefficient of 0.35 is used to allow for the contraction from the 2 inch refuel pipe. The refuel supply is from a pressure versus flow rate characteristic, Figure 8.20, incorporated in a pump model using BathME. The simulation network is shown in Figure 8.21.

8.2.3.1 Initial Results

A series of analyses was carried out to determine the size of the restrictors. From these analyses it was found that a level surface across the partition could not be maintained throughout refuel. This is due to the shape of the cells, and because the base of the aft cell is below that of the forward cell. The optimum size of restrictors determined were a 35mm forward and 22mm aft restrictor. The predicted maximum fuel step across the partition for the simulation, and the measured maximum fuel step across the partition on the aircraft for these restrictors are given below.

Forward Restrictor	Aft Restrictor	Simulation	Aircraft
35mm	22mm	7.5cm aft high	35cm aft high

To reduce the size of the fuel step across the partition measured on the aircraft, and provide additional data to determine the difference between the simulation and aircraft tests the 35mm

forward restrictor was removed. The predicted maximum fuel step across the partition for the simulation, and the measured maximum fuel step across the partition on the aircraft for the 22mm aft restrictor only is given below.

Forward Restrictor	Aft Restrictor	Simulation	Aircraft
-	22mm	6.4cm fwd high	20cm aft high

In both these cases the simulation predicts the fuel step across the partition between 26cm and 27cm forward high of those measured on the aircraft for the same restrictors. Additionally the aircraft system cannot meet the design requirement of maintaining a level or near level fuel surface across the partition. Even with no forward restrictor an aft high fuel step is still measured.

An investigation was therefore undertaken to determine the reason for the difference in the predicted fuel steps across the partition and those measured on the aircraft, and why the aircraft can only achieve an aft high step.

8.2.4 Refuel System Design Investigation

The layout of the refuel system to the two cells has the aft cell supplied through both the forward and aft refuel lines. Increasing the flow down the forward refuel line will result in an increase in the flow to both the forward cell and the aft cell. In the present arrangement the proportion of flow through the aft diffuser *A3* is too great. Therefore, to achieve a zero or forward high fuel step across the partition, the loss downstream of the junction of the aft diffuser *A3* on the forward refuel line requires reducing. Only two of the components in this line could cause a loss great enough to give the measured aft high steps: the emergency isolation valve, if it was not fully closed, or the junction of the two forward diffusers which has a complex shape as shown in Figure 8.22. The latter possibility was assumed to be the most probable cause since the emergency isolation valve would be required to be two thirds open which was unlikely.

The shape of the junction, Figure 8.22, suggests a possibility of a high loss due to its complex shape. Unfortunately this cannot be fully appreciated from a drawing and it requires the actual junction to be seen. As explained in Section 7.3.1.2 it is important to consider the losses of such complex shaped components early in the design. This has not been undertaken for this junction because the design of the system and junction were carried out before the methods developed within this research were introduced. If this design were carried out now, the loss of this junction would have been considered. To investigate the losses of the junction a two-dimensional Computational Fluid Dynamic (CFD) model of the junction was developed. This

model also included a swan neck on the inlet and 100mm settling lengths on the inlet and outlets, Figure 8.23. A two-dimensional model was developed in preference to a three-dimensional model because an answer was required within a very short time scale, ie. one day. A three-dimensional model would not have been possible to develop in this time. It was felt the two-dimensional model represented the junction fairly accurately because although the junction was not co-planar it did not lay far out of plane. From this model the flow paths of the junction were determined. A velocity vector plot is shown in Figure 8.24 and 8.25. These show a large recirculation zone in the branch which supplies diffuser *F2*, in effect reducing its diameter by half.

The branch supplying diffuser *F2* is 1½ inch diameter. To assess the effects of the recirculation zone, an 18mm restrictor was added in this branch of the Bath*fp* network and simulations carried out for the previously tested restrictors. The predicted maximum fuel step across the partition for these simulations, and the previously measured maximum fuel step across the partition on the aircraft for these restrictors are given below.

Forward Restrictor	Aft Restrictor	Simulation	Aircraft
35mm	22mm	36.5cm fwd high	35cm aft high
-	22mm	17.5cm aft high	20cm aft high

Inclusion of the additional loss for the junction brings the simulation in line with the aircraft results. Based on these results it was decided to redesign the junction.

8.2.5 System Modification

The original design of the junction is intended to achieve the main balancing flow through diffusers *A3* and *F1*. Structural limitations on routing of pipes has resulted in the branch to diffuser *F2* being placed on the bend, and the diameter of the branch being reduced to aid the required balanced flow. These factors have led to the creation of this re-circulation zone. To reduce the size of the re-circulation and loss of the junction, the emphasis of achieving the main balancing flow through diffusers *A3* and *F1* was lifted. It was decided to straighten the branch to diffuser *F2* and increase its diameter to 2 inches. The modified design of the junction is shown in Figure 8.26. To enable the branch to be straightened, structural limitations required diffuser *F2* to be moved further forward as shown in Figure 8.27. To further aid in the reduction of loss, the size of diffuser F2 was increased from 1½ inches to 2 inches, but the outlet gap was proportionally reduced to give the same outlet area at the end of the pipe as a 1½ inch diffuser, Figure 8.28. With this new design it was anticipated that

the balancing flow from the forward cell would be evenly split between the two forward diffusers.

8.2.5.1 Junction Design and Modelling

To assess the performance of the redesigned junction, a three–dimensional CFD model of the junction was developed because more time was available than for the analysis of the original junction. The advantage of three–dimensional CFD models over two–dimensional models is that they will supply a more accurate prediction of the performance of the junction, particularly for three–dimensional effects such as re–circulation out of the two–dimensional plane. The problem with three–dimensional CFD models is the development of the geometry itself. This is particularly true for intersecting circular cross sections.

Complications were encountered during the development of the actual intersection of the junction due to a complex cell development. Inspection of the junction, Figure 8.26, shows that the intersection itself can be approximated to a straight–through pipe with a 60° branch. The intersection of the three–dimensional, 60° 'Y' junction developed for the 'Y' junction testing detailed in Chapter 5, was modified to allow for a straight–through branch as shown in Figure 8.29. The inlet and outlet to diffuser *F2* were extruded from this along splines describing their centre line, and the outlet to diffuser *F3* extruded as a straight pipe. The CFD model is shown in Figure 8.30. The additional cells on the outlet legs are included to aid in generation of the mesh at the intersection, as described in Section 5.3.4.2.

With the time limitations on this study it was decided to initially only obtain loss coefficient data for the two anticipated extremes of flow ratio and from these assess Bath*fp*'s sensitivity to them. It was anticipated that at best 50% of the flow would go down each branch and at worst, would split 65% through the through–pipe to diffuser *F2*, and 35% through the branch to diffuser *F1*.

The CFD model of the junction was run for these flow ratios using the inlet flow rate measured during the aircraft tests, and with turbulence modelled with a k–ε turbulence model described in detail in Sections 4.3.1.2 and 5.3.4.3. A small recirculation zone was found in the junction as shown in Figure 8.31. This is typical of this type of junction. The loss coefficients obtained are given below, along with loss coefficients for a standard 60° junction, obtained from Reference [16] for comparison.

65/35 Flow Ratio

Loss Coefficient	Junction	Standard 'T'
k_{tp}	0.454	0.100
k_b	0.689	0.680

50/50 Flow Ratio

Loss Coefficient	Junction	Standard 'T'
k_{tp}	0.353	0.040
k_b	0.652	0.600

As expected, the CFD model of the junction predicts a greater loss coefficient than the 'T' junction. The through flow loss coefficient, ktp is considerably greater for the refuel junction than the standard 'T' junction. This is due to the inclusion of the inlet 'swan neck' and the outlet bend, see Figure 8.30. The loss coefficient for the branch pipe kb is only slightly greater than for the standard 'T' junction, even though the inlet 'swan neck' is included. This is because the branch on the refuel junction has a radiused edge, whereas those of Reference [16] are sharp edged, the radiused edge reducing the loss coefficient [16].

8.2.5.2 Inclusion of Modified Components in Network Model

The original Bath*fp* analysis network requires the inclusion of the loss coefficient of the new junction, the modified diffuser and the extended pipework. The sensitivity of the network to the junction loss coefficient was assessed. As described in Section 6.2.4 diffusers are difficult to model due to a lack of data on the loss characteristic. In the original network the diffusers were simulated with a discrete loss model using a loss coefficient of 1.35 based on a 1½ inch diameter and frictional losses taken into account with a 1½ inch diameter 0.6m long pipe. If all the diffusers are identical and simulated with the same model, but the model is incorrect, then the predicted flow rate will also be incorrect. However the ratio of flows through each diffuser will be predicted correctly because the same error is applied to each flow. Therefore the maximum step across the partition will be predicted correctly although the time may not be because of the incorrectly predicted flow rates. To model the effects of the modified 2 inch diffuser, *F2*, relative to the other diffusers it was decided to use a similar model. The effects of the discharge through the reduced length discharge gap are accounted for with a discrete

loss with a loss coefficient of 1.0 based on a 1½ inch diameter and the frictional losses of the diffuser modelled with a 2 inch 0.6m long pipe.

The predicted losses for the new junction show little sensitivity of loss coefficient to flow ratio. Therefore the flow ratio through the junction will be dependent on the downstream losses of the two branches too diffusers *F1* and *F2*. When the loss coefficients for the junction were included in the network with a 35mm forward refuel restrictor and a 22mm aft refuel restrictor this was found to be true with the network showing very little sensitivity to the two sets of loss coefficients. For the loss coefficients based on a 50/50 flow split, a flow split of 62/38 was predicted and for the loss coefficients based on a 65/35 flow split, a flow split of 63/37 was predicted. Based on these results the loss coefficient for the 65/35 flow split were used.

8.2.6 Restrictor Sizing with Modifications Incorporated

With the loss coefficient of the new junction and the modified diffuser included in the network model, the refuel restrictors were again sized as outlined in Section 8.2.3. Aircraft testing was restricted to a single test. From this test and the simulations, a set of restrictors would be selected. With the selected restrictors fitted a second test would then be carried out to measure the size of the fuel step across the partition, but it would not be possible to carry out any further tests or change the size of the restrictors. It was therefore decided to size two sets of restrictors for installation in each wing of the aircraft for the initial test. One set was sized to give a small aft high fuel step across the partition during refuel. These were 20mm aft restrictor and 35mm forward restrictor. The second set were sized to give a small forward high fuel step across the partition during refuel. These were 17mm aft restrictor and 37mm forward restrictor.

The predicted maximum fuel step across the partition for the simulation, and the measured maximum fuel step across the partition on the aircraft for these restrictors are given below.

Forward Restrictor	Aft Restrictor	Simulation	Aircraft
35mm	20mm	9.5cm aft high	20cm aft high
37mm	17mm	2.0cm fwd high	20cm fwd high

From these results there are two factors to consider. First it is evident that the simulation still does not adequately model the aircraft system. Second, and the most significant factor, is the sensitivity of the measured fuel step across the partition on the aircraft to small changes in restrictor size. Based on the results for the simulation and the aircraft tests, a 36mm forward

restrictor and 19mm aft restrictor were selected as the final set of restrictors. The predicted maximum fuel step across the partition for the simulation, and the measured maximum fuel step across the partition on the aircraft for these restrictors are given below.

Forward Restrictor	Aft Restrictor	Simulation	Aircraft
36mm	19mm	6.0cm fwd high	14cm aft high

As an aid to the understanding of the results from both the simulation and the aircraft tests, the fuel step across the partition was plotted as a function of time, Figure 8.32. In all of the cases, the first few minutes of refuel can be disregarded because the simulations start from both cells empty (-5.3cm step) and the aircraft tests started from various near empty cells. No attempt was made to replicate the initial conditions of the aircraft precisely because the volume of fuel and hence height in each cell was not available, only the total volume for both cells. Experience from the testing and analysis also indicated that the surfaces in the two cells levelled out quickly during the initial stage of refuel.

There are a number of important facts that can be obtained from Figure 8.32.

- The simulation results for all the restrictors follow an expected trend, ie. increasing the size of the forward restrictor and decreasing the size of the aft restrictor, results in an aft high fuel step across the partition decreasing and a forward high step increasing.
- The aircraft results for the 35/20mm (Figure 8.32b) and 36/19mm (Figure 8.32c) restrictors follow a similar trend to the simulation results, with the error between the simulation and the aircraft measurements similar in both cases.
- The 37/17mm (Figure 8.32a) aircraft results are inconsistent with both the 35/20mm (Figure 8.32b) and 36/19mm (Figure 8.32c) aircraft results.
- The error between the simulation and the aircraft measurements for the 37/17mm restrictors (Figure 8.32a) is not consistent with this error for the other restrictors.

From the above observations it can be concluded that the aircraft results for the 35/20mm and 36/19mm restrictors are correct and the simulation is predicting a fuel step across the partition forward high of those measured on the aircraft. This conclusion is based on the following facts.

- The aircraft results for the 35/20mm and 36/19mm restrictors show the expected sensitivity of the fuel step across the partition to changes in restrictor size, and this sensitivity is in agreement with that predicted by the simulations for all three restrictor sets.

- The method of measuring the height of the fuel step across the partition on the aircraft, namely simple manometers, is not prone to error.

- The model of the new junction used in the simulation has not been verified against test data, and may have an error in the loss coefficients.

- The potential error of the modified diffuser model, particularly relative to the other diffuser models, is large.

- If either, or both, the new junction and modified diffuser model have too small a loss coefficient attributed the simulation will predict a greater flow rate into the forward cell, and hence the fuel step across the partition forward high of those measured on the aircraft.

Generally test results should not be taken as correct and the simulation adjusted to exactly reproduce them. In this case, the decision to modify the simulation to agree with the 35/20mm and 36/19mm restrictors was only taken due to the conclusive evidence detailed above. This conclusion could not have been fully justified if, for example, the height of the fuel step across the partition was measured with electronic probes rather than manometers. The potential error of the probes would place a doubt over all of the measured data.

A final conclusion that can be drawn from the observations of the results of Figure 8.32 is the aircraft results for the 37/17mm restrictors are incorrect, because they do not follow the trend of the other test results or simulation results. This could be due either to a reading or manufacturing error. A reading error of this magnitude is unlikely with simple manometers used to measure the fuel step across the partition. Air could have been trapped in one manometer, but the manometer lines were checked before the tests and an air bubble of this size going unnoticed is highly unlikely. The most probable cause is an incorrectly manufactured restrictor, either the incorrect size, off centre, out of round, or burred. These manufacturing faults are possible because test restrictors are simply drilled and filed, whereas actual production restrictors are cast in.

8.2.6.1 Simulation Error

As stated above the simulation predicts too great a flow rate into the forward cell. This will be due to too small a loss being simulated in either the new junction or the modified diffuser.

All other components are identical to those used for the simulation without the system modifications which provided good correlation.

The increased loss required for the forward line can be achieved in three logical combinations.

- Increasing the loss of the new junction.
- Increasing the loss of the modified diffuser *F2*.
- Increasing the loss of both the modified diffuser *F2* and the new junction.

Of the three options only the second two were used. The first option was not considered because, based on the experience of the 'Y' junction testing (Chapter 5) the error of the junction model will be small.

For the second option, the required increase of the modified diffuser loss coefficient to reduce the flow rate sufficiently into the forward cell to predict a fuel step across the partition similar to the test data was 1.25.

When considering the increase of the loss for both the modified diffuser and the junction, there are a number of combinations of through line loss coefficient and branch line loss coefficient increases which will achieve the required fuel step across the partition. The ones selected for this case are an increase of the through line loss coefficient of 1 (this accounts for both the increase in the loss coefficient of the through line of the junction and the modified diffuser) and an increase of the branch pipe loss coefficient of 0.2.

For both options, the predicted fuel step across the partition for all three sets of restrictors was found to be identical and is given in Figure 8.33.

From these simulations it is still not possible to determine if the error of the simulation is due to the modified diffuser model or the junction model. It can be concluded though that only a relatively small increase in loss coefficient (particularly when compared to the potential error of the diffuser models) brings the simulation results in line with the aircraft results.

Unfortunately, due to the cost and time involved, further aircraft tests were not possible to verify any of these findings. The system actually incorporated on the aircraft consisted of the new junction and modified diffuser with a 19mm aft restrictor and 36mm forward restrictor.

8.2.7 Conclusions

Two of the Bath*fp* simulations were undertaken with inappropriate models. In the first case the error of the simulation was because a different junction to that fitted on the aircraft was modelled. The difference in results did aid in locating the source of error on the aircraft to

be the junction of the forward diffusers. The resulting simple change to the network (inclusion of an 18mm restrictor) produced acceptable results compared to the aircraft.

In the second case the difference between the simulation and aircraft results was due to an error in the diffuser model and/or junction. As stated in the design procedure, loss coefficients obtained from CFD analysis will contain some inaccuracies, though usually fairly small. The major cause of this error is assumed to be modelling of the new 2 inch diffuser relative to the 1½ inch diffusers. This is a known weakness in the modelling techniques and at present there is no means of determining this error due to a lack of test data. One of the recommendations of this research is that a test programme be undertaken to determine the pressure, flow rate characteristics of diffusers.

Overall results from this study have been acceptable and have shown that these methods are capable of investigating aircraft systems and producing quite acceptable results and solutions. At the worst they gave some indication of the reason the original system would only achieve an aft high fuel step across the partition that focused the investigation on the junction in forward line. This gave a great deal more confidence to undertake the responsibility to re-design and manufacture with the new junction.

8.3 Lessons From Case Studies

8.3.1 First Case Study

This first case study has examples of typical modelling techniques and solution of problems within the simulation.

Different methods of incorporating components which are not included in standard component library are given. These range from the determination of loss coefficient for the remote pump inlet and gravity feed inlet from combinations of standard loss coefficients, to the incorporation of the sequence valve (pressure holding valve) characteristic in a standard non-return valve model.

This study is a good example of building a network from smaller networks and determining the operation of each to be correct before combination. In this case the network was quite small so may not have required this build up, but the complexity of its operation and solution was only fully appreciated through this build up.

An important point highlighted, is that a simulation model is idealised and pumps of the same type have exactly the same characteristic and loss laws. In reality all components have a tolerance band to which they are manufactured and the sensitivity to this tolerance may require investigating and characteristics adjusted as the pump was in the study.

A very important characteristic of an iterating flow balancing solution technique is highlighted with the results for the flow demand of 782igph, ie. more than one solution may be available and the choice is dependent on the direction of the iteration procedure. For cases where this can happen, it is important to appreciate the possibility of other solutions and investigate through dynamic analysis, if possible, how each solution would be achieved. For example a particular solution may only be achieved when 'approached' from one direction, and in practice this may not be possible.

8.3.2 Second Case Study

This case study highlights some important aspects of simulation and test results. The most important of these is that test results should not always be taken to be correct and the simulation adjusted to reproduce them. If we consider the final restrictor sizing then although the simulation was in error, the aircraft results for the 37/17mm restrictors were also incorrect. If the network could have been, and had been, adjusted to re-create aircraft results for the 37/17mm and 35/20mm restrictors, it would have been completely wrong.

This case study highlights the care which must be observed when modelling diffusers. This is particularly true when assessing diffusers with dissimilar sizes. For cases where the diffusers are of the same size, the errors are quite small. This is an accepted current deficiency in the modelling techniques and there is a real need for testing of diffusers to overcome this. This can similarly be applied to other components because it is vital to have reliable flow rate, pressure loss characteristics for all components for an accurate analysis.

The results from the CFD analyses highlight typical CFD modelling traits. For three-dimensional junctions, the complexity and time involved in developing the meshes is great and for co-planar junctions two-dimensional models will usually be adequate. If a three-dimensional model is required the use of a finite element code such as PATRAN should be considered. The CFD models provided very good predictions of the flow paths, particularly in locating the recirculation. The prediction of loss coefficients from CFD gave adequate results for this case, and also in the studies of Chapter 5. The use of CFD in this manner is a powerful tool.

8.4 Closing remarks

Both of these case studies illustrate well how the three software packages are applied to the analysis of fuel systems. For each of the studies, one of the most important aspects of computational modelling is highlighted; neither simulation predictions or experimental data should just be accepted without scrutiny. It is essential that the data is always assessed by somebody with experience. For the first case study, the simulation predicted the incorrect wing tank pump to be supplying the engine. In this case this was not significant, but if the

pumps were supplying from different tanks, incorrect fuel volumes would have been predicted. In the second case study, if the aircraft results had been accepted as correct for the final restrictor sizing, serious doubt would have been thrown on the simulation as it would have been impossible to adjust it to model both the 37/17mm and 35/20mm cases. The biggest sceptic of both the methods and experimental data should always be the engineer carrying out the analysis.

CHAPTER 9

CONCLUSIONS AND RECOMMENDATIONS FOR FURTHER WORK

9.1 Conclusions

Within this research the author has evaluated and proved the application of commercial software to the design and analysis of aircraft fuel systems. This has been achieved through:

- Extensive evaluation and testing of the commercial software packages, Flowmaster, Bath*fp* and Star-CD, through their application to practical simulations.

- The development of additional component models by the author to expand the model library of Bath*fp* to include the majority of components required to simulate aircraft fuel systems.

- Evaluation of the application of CFD for the development of operational characteristics for components models to be incorporated in Flowmaster and Bath*fp*.

- The development of guide-lines and a design procedure for the three packages to enable a competent engineer, who is not necessarily an expert user of the software, to confidently and efficiently use the software for both the design and analysis of aircraft fuel systems.

- The investigation and solution of problems that may be encountered with the application of Flowmaster, Bath*fp* and Star-CD.

It was decided at the outset of this research that commercial software would be used as the basis for the methods. Basing this research on commercial software has enabled the work to concentrate on the application of the software and the development of methods in preference to development of the software itself. The advantages of using commercial software are:

- They have simple, yet comprehensive user interfaces.

- Advantage can be taken of the investment and knowledge incorporated in user interfaces, and for Flowmaster and Bath*fp* their component libraries.

- They provide the flexibility required to model the diversity of operation and design of different aircraft types.

Two types of computational modelling of aircraft fuel systems have been investigated within this research; (i) network analysis with Flowmaster and Bath*fp*, and (ii) component modelling with CFD using Star-CD.

Flowmaster is a very good steady state analysis tool which can model most networks competently. The flow balancing analysis module is a very useful feature for determining sizes of restrictors in branched networks. It is capable of modelling pressure surge with either a rigid pipe model or the method of characteristics pipe model. Flowmaster's drawbacks are its poor dynamic analysis capability, excepting pressure surge, and its component modelling restrictions which only allow the user to describe a component with a pressure flow characteristic within the framework of an existing model. Bath*fp* is a very good dynamic analysis tool which can be expanded by the inclusion of new components. Its only drawback is the limited number of fuel system specific components in the standard release, although this has been overcome by the introduction of the fuel system model library developed by the author. The present version is also not able to model pressure surge, although this will be overcome with the inclusion of a method of lines pipe model in the next release.

Due to the background of Flowmaster and Bath*fp*, it was anticipated at the outset that component models would have to be developed. Flowmaster has a limited ability to accept user component models. For this reason it has not been possible to include an aircraft fuel tank and jet pump model, or a means of altering the atmospheric and fuel properties during an analysis. Bath*fp* accepts a wide range of models and the majority of the model development carried out by the author, detailed in Chapter 6, has been aimed at expanding Bath*fp*'s model library to include fuel system specific components. The only major model that has not yet been included is the ability to rotate the network through prescribed pitch and roll angles. This does not reflect a limitation of Bath*fp* but is due to the volume of data required from the CAD system being impractical to incorporate manually. The most significant of the models incorporated are the aircraft fuel tank models and the *environment* model *ENV0*. The latter allows adjustment of the atmospheric and fuel properties during an analysis. These two models are the basis around which any dynamic fuel system analysis must be built, and are the two which differentiate a network analysis package suitable for aircraft fuel systems from those which are not. Without the development of these, Bath*fp* would have limited application to the simulation of aircraft fuel systems. The inclusion of these models enables Bath*fp* to simulate the majority of operations of an aircraft fuel system.

The analysis capabilities of Flowmaster and Bath*fp* overlap to an extent, but in the majority of cases one provides the most appropriate solution. From the experience gained by the author, through practical analyses carried out, the following summary of the application of

Flowmaster and Bath*fp* to the various analysis types has been developed:

- Steady state conditions. Either Bath*fp* or Flowmaster are appropriate for steady state analyses. The choice of method will depend on whether the network already exists in one of the packages.

- Analyses involving the response of a network over time. Generally Bath*fp* will be preferred. If the network is already modelled in Flowmaster, and the time step for the response is expected to be fairly constant, then Flowmaster may also be appropriate.

- Pressure surge. Flowmaster will be the most appropriate for these cases. The choice of using the method of characteristics model or a rigid column model for pipes will be dependent on the valve closure time. In the experience of the author the typical valve closure times encountered within aircraft fuel systems are adequately modelled with the rigid pipe model.

- Analysis requiring the operation and effects of fuel tanks to be modelled. Bath*fp* is the obvious choice here as Flowmaster has too many restrictions when modelling tanks.

- Analysis requiring the effects of changing altitude to be considered. To allow for changing atmospheric and fuel properties Bath*fp* and the environment model *ENV0* are required. If the effects can be adequately accounted for with constant fuel properties and changing atmospheric conditions applied to the boundary pressures and flows of the network, then Flowmaster will also be appropriate.

- If additional components are required to be modelled. Generally Bath*fp* is preferred. However, if the additional modelling can be described as a characteristic curve, Flowmaster may also be appropriate.

CFD has been used within this research to develop operational characteristics of components for inclusion in the network analysis methods. Before the introduction of CFD the only means of assessing a component's performance was through costly rig testing which would only be undertaken where the performance of a component was critical and could not be obtained by any other means. CFD opens up a whole new range of possibilities for study of component operation. One of the most important of these is the determination of appropriate geometries during initial system description as detailed in Chapter 7. The consequence of not carrying out this form of analysis is illustrated in the second case study of Chapter 8, where the complex geometry of a junction created an unacceptably high loss which resulted in late modifications to the aircraft. A second important application of CFD that has been

demonstrated by the author is the determination of characteristics for component models which are then included in Flowmaster or Bath*fp*. These characteristics can be used in either general models, as illustrated by the junction example in the second case study of Chapter 8, or can be incorporated in dedicated models, as in the use of the 'Y' junction data described in Chapter 5. In addition to supplying these characteristics, the 'Y' junction testing and CFD modelling detailed in Chapter 5 has extended the data available for combining 'Y' junctions down to included angles of 30°. It has also provided a valuable source for the validation of the application of CFD to the development of component characteristics.

The major drawback of Star-CD, and any other CFD code, is the development of the meshed geometry. The use of meshes generated automatically from Finite Element stress modelling packages, as outlined in Chapter 4, may overcome this. Alternatively the latest release of Star-CD has greatly improved meshing capabilities which provide simple methods for the development of complex meshes.

The author's development of guide-lines and design procedures as a result of experience and knowledge obtained throughout this research, has greatly increased the number of, range and complexity of simulations, providing an increased understanding of the operation and performance of the system. The effects of the increased number of simulations is illustrated in Chapter 7, with the application of Flowmaster to the design and analysis of engine feed systems. It is estimated that the analysis time has been reduced by a factor of twenty in comparison to traditional methods. This has enabled additional analyses to be undertaken, giving a better understanding of the system, such that design engineers are now confident they can predict the performance of the system for growth engines on current aircraft with little additional work. The application of Bath*fp* will further reduce the analysis time for the modelling of the engine feed system, as all flow rates are undertaken in a single analysis for a particular combination of altitude, temperature and failure condition. The increased range and complexity of simulations is most evident with the inclusion of dynamic analysis and determination of component characteristics with CFD. With traditional methods, these types of analysis were rarely undertaken due to the excessive time required. There have been a number of cases throughout the research where these new capabilities have been the only means of analysis. The most significant of these have been:

- Analysis of emergency descent, detailed in Section 7.3.3.1.
- Analysis of refuel pressure surge, detailed in Section 7.3.2.3.
- Analysis of centre to inner tank transfer, detailed in Section 7.3.4.
- Analysis of refuel in a partitioned tank, detailed in Section 8.2.

- Development of loss coefficient characteristics for 'Y' junctions, detailed in Chapter 5.

- Determination of loss coefficients for the junction of the second case study, detailed in Section 8.2.

If the computational methods had not been available then either costly testing would have been required, or components would have been over sized to ensure the design was safe. The major application of dynamic analysis, in association with the fuel tank models developed within this research (Section 6.2.3.2), has made possible flight profile modelling as outlined in Section 7.2.6.

One of the most important aspects of computational simulation is highlighted in both case studies of Chapter 8; namely what can be expected of a simulation, particularly when comparing with measured data? When analysing simulation and measured data it must always be remembered that there will be an error associated with both. For the simulation this is due to the experimental and empirical data used to define the majority of component models. For measured data the error is due to the accuracy of the measuring equipment or that the system being measured may not be what was defined due to incorrectly fitted or manufactured components. A good example of this comparison of simulation and measured data is given in the final results of the second case study of Chapter 8.

Assuming all of these potential errors were overcome, then the simulation would still not predict exactly the same results as those measured. This is because the simulation models the 'ideal' system. In reality all of the components have a tolerance band on their operational characteristic and the output of each is dependent on the location of their characteristics within their tolerance bands. The simulation will generally be based on a nominal characteristic. An example of the effects of component tolerancing is given in the first case study of Chapter 8.

The second case study of Chapter 8 highlights problems with Flowmaster when multiple solutions are present in a network. In some cases Flowmaster is unable to achieve solution or achieves the wrong solution. Investigation determined the cause to be the iterative solution method employed by Flowmaster. When this solution technique is applied to networks with multiple solutions, the solution achieved is dependent on where the initial iterations predict an approximate solution. If the solutions are in 'close proximity' the iterative solution method can oscillate between the two solutions and not solve for either. A detailed description of this problem is given in the first case study of Chapter 8.

The need for a means of analysing the operation of aircraft fuel systems and their components is now being more generally accepted. At the commencement of this research (1987), very little simulation and modelling of aircraft fuel systems was being undertaken. Since then the methods developed in this thesis have been accepted as the standard implementation of

computational modelling of aircraft fuel systems within British Aerospace Sites and Divisions. With publication of information on this research [83], other aerospace manufacturers are considering the implementation of Flowmaster and Bath*fp* to the design and analysis of aircraft fuel systems, using methods developed by the author.

The computational methods developed by the author in this thesis give the aircraft fuel system design engineer a set of tools which enable detailed design and analysis prior to testing and flight. The application of these tools and associated methods achieves a greater understanding of the system and a reduced time from concept to first flight. This results in a safer design and reduced costs.

9.2 Recommendations for Future Work

Diffuser Test Programme

Aircraft diffusers are an important part of an aircraft fuel system. Unfortunately there is a distinct lack of data available describing their operation in terms of pressure and flow rate. It is widely accepted within the aerospace industry that this is a shortcoming in the data used to describe aircraft fuel systems. To overcome this, and extend modelling capabilities, it is recommended that a test programme be undertaken to determine the operational characteristics of aircraft diffusers. In conjunction with this, a CFD modelling exercise should be carried out to validate the application of CFD to the modelling of aircraft diffusers. This will then enable further investigations with CFD models to be undertaken without the need for further testing.

Modelling of the Fuel System Computer

Control of the operation of components in both Flowmaster and Bath*fp* is achieved through standard control components. These components are not appropriate for modelling the operation of the fuel system computer. As explained in Chapter 2, the fuel system computer controls the operation of all the components of the aircraft fuel system through logic in normal operation and all combinations of failures. Incorporation of this amount of logic in either Flowmaster or Bath*fp* in their current implementations is inappropriate. To completely emulate the operation of the aircraft fuel system, the logic contained within the fuel system computer must be incorporated, or linked to, the simulation of the fuel system. This may be through development of a logic modelling tool within either Flowmaster or Bath*fp*, similar in operation to BathME, or developing a link to a logic modelling package which would model the operation of the computer.

Development of Software for Modelling of Transition between Flight Phases

Currently the design of the aircraft fuel system is restricted to the assessment of its performance during the major flight phases. The performance of the fuel system during the transition between flight phases is not considered. It is anticipated, based on experience of the latest aircraft developments, that this will become an area of concern. To meet this requirement the performance of the methods developed within this thesis will require assessing in these transitional areas, and the fuel tank models described in Chapter 6 Section 6.2.3.2 will require development to allow for changes in the volume, height description due to pitch and roll during an analysis.

Link to CAD System

A fuel system is a complex network of components which including all pipes, bends etc. can consist of well over 700 components. At present Flowmaster and Bath*fp* require all dimensions describing each component to be manually incorporated into the component models. This is time consuming and prone to operator error, which is difficult to trace. Development of a link between the Computer Aided Design system, on which the fuel system is designed, and Flowmaster and Bath*fp* to enable the data describing the components to be automatically incorporated and possibly even 'draw' the network would substantially reduce network development times. In addition to the dimensions of the components, the spatial co-ordinates of each of the components could be incorporated. This would allow the inclusion of models to rotate the network in pitch and roll and appropriately update heights within the network, as described in Section 6.6.3.2.

Modelling of Air and Fuel in a Network

In the current versions of Flowmaster and Bath*fp* the fuel and vent systems are modelled in isolation. The effects of each system on the other are included as approximations in the components, at the interface of the two systems. This is usually in the form of surface pressure on a tank, or modelling of the fuel surface as an incompressible boundary. Development is required to allow the coupling of the fuel and vent systems to be modelled.

Assessment of Mesh Generating Methods

CFD provides a powerful tool in its component modelling capabilities. At present its application is limited only by the ability to produce the meshes describing the geometry of the component to be modelled. This has been found to be particularly true within this research, because the majority of components investigated are complex shaped junctions. These provide extensive meshing problems at the actual intersection of the junction as is illustrated in

Section 8.2.4.1. However, meshes can be automatically generated with Finite Element Stress Modelling Packages and incorporated within Star-CD as outlined in Chapter 4. Nevertheless finite element stress modelling allows greater mesh distortion than CFD so care has to be taken with these meshes. Additionally there is a considerable amount of investment now being made in the meshing capabilities of CFD codes. A release of Star-CD due out very shortly has greatly enhanced meshing capabilities. A study to assess all the possible methods of generating meshes is required. This should take into account the ease by which meshes can be generated and also the degree of distortion within these meshes as well as future development in CFD codes.

9.3 Closure

The amount and complexity of design calculations required for both performance and airworthiness requirements for an aircraft fuel system are now very demanding. Up to the present they have barely been achieved with traditional methods. On recent aircraft programmes limited application of computational methods has been required [2 to 5,84]. The author has shown through this thesis that it is now possible to design and analyse the operation of aircraft fuel systems with computational methods, and these methods are now being accepted within the U.K. aircraft manufacturing industry. To meet the design and analysis requirements of the next generation of aircraft fuel systems will require the application of the methods developed and outlined within this thesis.

APPENDIX A

POLYNOMIAL EQUATIONS DESCRIBING MEASURED 'Y' JUNCTION LOSS COEFFICIENTS

For interpretation, display and application of the test rig results the loss coefficient data when adjusted for the inlet contraction has been fitted with a polynomial equation using Lotus 123 regression analysis. This uses a least squares method. The equations and coefficients for each junction are given below.

30° 'Y' Junction

The data obtained directly from the test rig for flow ratios between 0.2 and 0.8 has been fitted with a third order polynomial.

$$k = A_{30} + B_{30}\left(\frac{q_1}{q_3}\right) + C_{30}\left(\frac{q_1}{q_3}\right)^2 + D_{30}\left(\frac{q_1}{q_3}\right)^3 \qquad \text{A.1}$$

Where:

A_{30} = −0.88917

B_{30} = 3.2267×10^{-2}

C_{30} = -3.7908×10^{-4}

D_{30} = 1.3940×10^{-6}

With the loss coefficient at flow ratios of 0.0 and 1.0 included a second order polynomial has been fitted to the loss coefficient data.

$$k = A_{30e} + B_{30e}\left(\frac{q_1}{q_3}\right) + C_{30e}\left(\frac{q_1}{q_3}\right)^2 \qquad \text{A.2}$$

Where:

A_{30e} = −0.7628

B_{30e} = 2.2678×10^{-2}

C_{30e} = -3.7908×10^{-4}

60° 'Y' Junction

The data obtained directly from the test rig for flow ratios between 0.2 and 0.8 has been fitted with a third order polynomial.

$$k = A_{60} + B_{60}\left(\frac{q_1}{q_3}\right) + C_{60}\left(\frac{q_1}{q_3}\right)^2 + D_{60}\left(\frac{q_1}{q_3}\right)^3 \qquad \text{A.3}$$

Where:

A_{60} = –0.5721

B_{60} = 2.2725×10^{-2}

C_{60} = -2.5969×10^{-4}

D_{60} = 1.1381×10^{-6}

90° 'Y' Junction

The data obtained directly from the test rig for flow ratios between 0.2 and 0.8 has been fitted with a third order polynomial.

$$k = A_{90} + B_{90}\left(\frac{q_1}{q_3}\right) + C_{90}\left(\frac{q_1}{q_3}\right)^2 + D_{90}\left(\frac{q_1}{q_3}\right)^3 \qquad \text{A.4}$$

Where:

A_{90} = –0.2413

B_{90} = 1.4597×10^{-2}

C_{90} = -1.9652×10^{-4}

D_{90} = 1.2191×10^{-6}

120° 'Y' Junction

The data obtained directly from the test rig for flow ratios between 0.2 and 0.8 has been fitted with a third order polynomial.

$$k = A_{120} + B_{120}\left(\frac{q_1}{q_3}\right) + C_{120}\left(\frac{q_1}{q_3}\right)^2 + D_{120}\left(\frac{q_1}{q_3}\right)^3 \qquad \text{A.5}$$

Where:

A_{120} = −0.2413

B_{120} = 1.4597×10^{-2}

C_{120} = -1.9652×10^{-4}

D_{120} = 1.2191×10^{-6}

150° 'Y' Junction

The data obtained directly from the test rig for flow ratios between 0.2 and 0.8 has been fitted with a third order polynomial.

$$k = A_{150} + B_{150}\left(\frac{q_1}{q_3}\right) + C_{150}\left(\frac{q_1}{q_3}\right)^2 + D_{150}\left(\frac{q_1}{q_3}\right)^3 \qquad \text{A.6}$$

Where:

A_{150} = −0.2413

B_{150} = 1.4597×10^{-2}

C_{150} = -1.9652×10^{-4}

D_{150} = 1.2191×10^{-6}

REFERENCES

1 Joint Aviation Requirements (1989). JAR-25 Large Aeroplanes, change 13, Joint Aviation Authorities.

2 Allen, D.J., (1992). "Fuel Tank Movements of Inertia and cg Program: INRTv1.01. Verification and Validation Report." British Aerospace Airbus Ltd. and Ricardo Aerospace, Report No SDF/B83-03/GEN61/1569.

3 Allen, D.J., (1992). "Aircraft Centre of Gravity in Flight Program: CG_Flite v1.1 user Guide." British Aerospace Airbus Limited and Ricardo Aerospace, Report No SDF/B83-03/GEN61/1574.

4 Davidson, N., (1987). "Software Report for Program Fuel-Temp which Performs Thermal Analysis of A320 IDG Cooling System", British Aerospace Commercial Aircraft Ltd., Report No SDF/B81/GEN/61/0889.

5 Harding-Jones, N.J., (1991). "Program Fuel-Temp Thermal Analysis of A320 IDG Cooling System", British Aerospace Commercial Aircraft Ltd., Report No SDF/B83-03/GEN/61/0839.

6 Roylance, A.J., (1987). "Simulation of Fuel Systems", British Aerospace PLC. Civil Aircraft Division, ref. B00/JAH/148

7 Stirling, R., Plastow, I., (1988). "The Development of an Automated Design Procedure for Aircraft Fuel Systems - Technical Proposal", University of Bristol and British Aerospace PLC. Civil Aircraft Division.

8 Engineering Outline Number 123, (1968). "Jet Pumps", Engineering.

9 ESDU 85032, (1985). "Ejectors and Jet Pumps. Design and Performance for Incompressible Liquid Flow".

10 Bowns, D.E., Tomlinson, S.P., Bull, S.R., (Undated). "The Development of an Automatic Structured Program for Hydraulic System Design", Fluid Power Centre, University of Bath.

11 Bowns, D.E., Tomlinson, S.P., Dugdale, S.K., (Undated). "Progress Towards a General Purpose Hydraulic System Simulation Language", Fluid Power Centre, University of Bath.

12 Dorey, R.E., Chapple, P.J., (1987). "Hydraulic CAD with Minimal Maths", CME, pp 42-45.

13 Bowns, D.E., Tomlinson, S.P., (Undated). "Prediction of Thermal Transient Effects Using the Hydraulic Automatic Simulation Package" Fluid Power Centre, University of Bath.

14 Plastow, I., (1988). "Simulation of Fuel Systems, Evaluation of Commercial Software Packages", University of Bristol.

15 Plastow, I., (1991). "Notes on Bathfp Beta Testing," British Aerospace (Commercial Aircraft) Ltd., Report No SDF/B83/A/108/1560.

16 Miller, D.S (1978). Internal Flow Systems, 1st Edition, BHRA Fluid Engineering.

17 Streeter, V.L., Wylie, E.B., (1987). Fluid Transients, McGraw-Hill.

18 Massey, B. S., (1983). Mechanics of Fluids, 5th Edition, Von Nostrand Reinhold (UK).

19 Fox, J. A., (1977). Hydraulics Analysis of Unsteady Flow in Pipe Networks, The MacMillian Press (Ltd.).

20 Lockhead Power Plant Laboratory Course E2260, Course Notes.

21 Petzold, L., (1983). "Automatic Selection of Methods for Solving Stiff and Non-Stiff Systems of ODE's", SIAM J. Sci. Comput., Vol 4, pp. 136-148.

22 Richards, C.W., Tilley, D.G., Tomlinson, S.P., and Burrows, C.R., "Type-Insensitive Integration Codes for the Simulation of Fluid Power Systems", ASME, Report No. 90-WA/FPST-6.

23 Flowmaster User Manual (1993). Flowmaster International Ltd., UM_3.4.

24 User Manual For Flowmaster Datamanager (1990). Revison 3.1, Release 6, Amstral.

25 Richards, C.W., Fung, K.C.J., The Bathfp User Guide, The Fluid Power Centre, University of Bath.

26 Richards, C.W., Fung, K.C.J., The BathME and BathICON User Guide, The Fluid Power Centre, University of Bath.

27 Richards, C.W., Fung, K.C.J., The Bathfp Model Writer's Guide, The Fluid Power Centre, University of Bath.

28 Sanada, K., Richards, C. W., Longmore, D. K., and Johnstone, D. N., (1993). "A Finite Element Model of Hydraulic Pipelines using an Optimised Interlacing Grid System", Proc. Instn. Mech. Engrs. Vol 207, pp213-222.

29 SAE Aerospace Applied Thermodynamics Manual, Thermodynamics of Incompressible Flow, (1990), AIR1168/1.

30 Idel'chik, I.E., (1966). "Stream Junctions and Divisions–Resistance Coefficients of Wyes, Tees and Crosses.", Handbook of Hydraulic Resistance: Coefficients of Local Resistance and of Friction. Translated from Russian and published for U.S. AEC & National Science Foundation, Washington by Israel Program for Scientific Translations. AEC–tr–6630.

31 Marvin, J.G., Holst, T.L., (1990). "CFD Validation for Aerodynamic Flows – Challenge For The 90's", A1AA–90–2995–CP

32 Plastow, I., (1990). "Evaluation of Computational Fluid Dynamic Software Packages", British Aerospace (Commercial Aircraft) Ltd., Report No. SDF/B83/A/108/1185.

33 Sutton, A.J., (1989). "Air Systems Computational Fluid Dynamics Applications and Review.", British Aerospace (Commercial Aircraft) Ltd., Report No. SDF/B83/GEN/61/1158.

34 Star–CD Methodology, Part 1 Mathematical Modelling, SCD2.1/2.

35 Star–CD Methodology, Part 2 Numerical Solution Techniques, SCD2.1/3.

36 Star–CD User Guide, SCD2.1/4

37 Launder, B.E., and Spalding, D.B., (1974). "The Numerical Computation of Turbulent Flow", Comp. Meth. In Appl. Mech. Eng., 3 P269.

38 Rodi, W., (1979). "Influence of Boundary and Rotation on Equations for Turbulent Length Scale", Proc. 2nd Symp. On Turbulent Shear Flows.

39 El Talry, S.H., (1983). "k–ε Equation for Compressible Reciprocating Engine Flows", AIAA Journal of Energy, 7, No.4, pp345–353.

40 Reynolds, W.C., (1976). "Computation of Turbulent Flows", Ann. Rev. Fluid Mech., 8, pp183–203.

41 Schlichting, H., (1968). Boundary Layer Theory, 6th Edition, McGraw–Hill.

42 Launder, B.E., Reynolds, W.C., Rodi, W., (1984). Turbulence Models and their Applications, Volume 2, Eyrolles.

43 Patanker, S.V., Spalding, D.B., (1972). "A Calculation Procedure for Heat, Mass, and Momentum in Three–dimensional Parabolic Flows.", Int. J. Heat Mass Transfer, 15.

44 Issa, R.I., (1986). "Solution of the Implicitly Discretised Fluid Flow Equations by Operating–splitting", J. Comp. Phys., 62, pp40–65.

45 Issa, R. I., Gosman, A.D., and Watkins, A.P., (1986). "The Computation of Compressible and Incompressible Recirculating Flows by a Non-iterative Implicit Scheme", J. Comp. Phys., 62, pp. 62-82.

46 Issa, R. I., Ahmadi Befrui, B., Beshay, K., and Gosman, A.D., (1990). "Solution of the Implicitly Descretised Reacting Flow Equations by Operator-splitting", J. Comp. Phys., in the press.

47 Cranfield College of Aerodynamics (1990). "Introduction to Computational Fluid Dynamics - A Three-day Course", Course Notes.

48 Patanker, S.V., (1980). "Numerical Heat Transfer and Fluid Flow", Hemisphere.

49 Boldy, A. P., (1970). "Performance of Dividing and Combing Tees", The British Hydromechanics Research Association, ref. RR1061.

50 Blaisdell, F.W., Manson, P.W., (1963). "Loss of Energy at Sharp-Edged Pipe Junctions in Water Conveyance Systems", Agricultural Research Service U.S. Dept of Agriculture, Technical Bulletin No 1283.

51 Miller, W., Stratmann, H., (1971). "Pressure Losses in Branch Pipes and Distributors", Subyer Technical Review 4/1971.

52 Ito, H., Imai, K., (1973). "Energy Losses at 90° Pipe Junctions", Proc. Amer. Soc. Civil Engs, Vol. 99, No. HY9,pp1353-1368.

53 Shufflebotham, N., (1989). "Proposed Hydraulic Test Rig (Amazon Flowmaster) Specification", British Aerospace PLC. Civil Aircraft Division, Specification No TS/MECH/26/2020.

54 Lewitt, E.,H., (1959). Hydraulics and Fluid Mechanics, 10th Edition, Pittman.

55 ITT Barton, Series 7100 Liquid Turbine Meters, Product Bulletin 7100.

56 Flight International, 2nd-8th September 1992, No 4334 Vol. 142, Reed Business Publishing.

57 Hawker Siddeley Aviation Ltd. (1970). Technical Note, DHI/N/1361.

58 Hawker Siddeley Aviation Ltd. (1978). Technical Note, HPP-M-460-280199.

59 Douglas, J.F., Gasiovels, J.M., Swaffield, J.A., (1985). Fluid Mechanics, 2nd Edition, Longman Scientific and Technical.

60 Klapprott, R.L., and Smith, L.D., (1966). "The Jet Pump as a Fuel Pump for Todays Aircraft", Lear Jet Corp., report No. 660223, SAE Business Aircraft Conference, Kansas.

61 Boucher, H.T.C., (1973). "The NVE (Airframe/LP) Fuel System", British Aircraft Corporation Ltd.. Commercial Aircraft Division, ref. FUEL/GEN/LBR/15.

62 Richards, L.B., (1975). "A NVE (Airframe/LP) Fuel System", British Aircraft Corporation Ltd.. Commercial Aircraft Division, ref FUEL/GEN/LBR/19.

63 Richards, L.B., (1976). "A NVE Fuel System for Sub-Sonic Aircraft-Preliminary Comparison with a Conventional System", British Aircraft Corporation Ltd.. Commercial Aircraft Division, ref. FUEL/GEN/LBR/23.

64 Richards, L.B., (1978). "Outline Proposal for a Test Programme to Demonstrate the Practicality of an Aircraft Fuel System Having no Electrical Power and no Moving Parts in its (airframe) Pumping System," British Aerospace Aircraft Group. Weybridge - Bristol Division. Ref FUEL/GEN/HTCB/57.

65 Kentfield, J. A. C., and Barnes, R. W., (1972). "The Prediction of the Optimum Performance of Ejectors", Proc. Instn. Mech. Engrs., Vol 186 54/72, pp 671-681.

66 Winchester, H.F., Van Dyke, R.H., Moinat, C.J., (1967). "Development of an Ejector Pump Engine Fuel Feed System", Douglas Aircraft Company Aircraft Division.

67 Sanger, N. L., (1971). "FORTRAN Programs for the Design of Liquid-to-Liquid Jet Pumps.", NASA Technical Note NASA TN D-6453.

68 Sanger, N. L., (1968). "Non-cavitating Performance of Two Low-Area-Ratio Water Jet Pumps having Throat Lengths of 7.25 Diameters.", NASA Technical Note, NASA TN D-4445.

69 Wilman, J. T., (1966). "Jet Pumps", European Atomic Energy Community, EUR 3253.e.

70 Reddy, Y. R. and Kar, Subir, (1968). "Theory and Performance of Water Jet Pump", Journal of the Hydraulic Division, Proceedings of the American Society of Civil Engineers, HY5, pp 1261-1281.

71 Reddy, Y. R., (1966). "Theory of Jet Pump", M.Tech. Thesis, Indian Institute of Technology, Bombay.

72 Howden, J. W. and Lewis, A. M., (1977). "Power Complex - A Suitable Case for Treatment", RAeS/IEEE Symposium on "The Application of Electrical Control to Aircraft Propulsion Systems".

73 Wood, R. K., (1977). "Improved Control by Application of Advanced Control Techniques", ISA/77, Spring Conference, Anaheim, pp 31-39.

74 Northcott, A. J., (1989). "VSTOL Power Plant Control Lessons From Harrier Experience", ISABE, Athens.

75 Flowmaster Single Phase Technical Guide (1993). Flowmaster International Ltd., SS_T3.4.

76 Richards, C.W., Fung, K.C.J., The Bathfp Model Directory, The Fluid Power Centre, University of Bath.

77 Normalair-Garret Ltd., (1969). "ISA Standard Atmosphere Tables", 4th issue, publication No. 159.

78 Ward, I.P. (1993). "Software Report on 'Props' Controlled Software Task Register Number 0272", British Aerospace Airbus Ltd., Report No SDF/B81-01/GEN/61/1839.

79 Rolls Royce,(Undated). "Fuel Property Tables", ref. 20361.

80 Richards, L.B., (1992) "Fuel System Notes", British Aerospace Airbus Ltd., B81-01/GEN/3155.

81 Plastow, I., (1993). "A320 Fuel System Test Rig Data Analysis Program, Software Tasks Register No 237", British Aerospace Airbus Ltd. Report No. SDF/B81-01/GEN/61/1864.

82 Plessy Equipment Specification No BA280100, ref. 16/85/2045.

83 Plastow, I., (1992). "Aircraft Fuel System Modelling", Computer Modelling in Aerospace Seminar, I.Mech.E.

84 Reed, M. A., (1993). "A340 Engine Feed System Certification Analysis", British Aerospace Airbus Ltd., Report No SDF/B81-01/P/17/2006.

Component	Flowmaster		Bath*fp*	
	Released	Modelled	Released	Modelled
Pipe	✓		✓	
Bend	✓			✓
'T' Junction	✓			✓
'Y' Junction	✓			✓
Ball valve etc.	✓			✓✓
NRV	✓		✓	
Transitions	✓			✓
Restrictor	✓		✓	
Simple tank	✓		✓	
A/C fuel tank		N		✓✓
Centrifugal pump	✓			✓✓a
Jet pump		N		✓
Diffuser		✓		✓
Intakes eg. NACA		✓		✓

✓ Component released or can be modelled.
✓✓ Component Model incorporated.
N Component cannot be modelled.
a Modelled using BathME.

Table 3.1 Component Availability in Flowmaster and Bath*fp*.

30° Junction		
Flow Ratio	Maximum Positive Error	Maximum Negative Error
0.2	0.0115	–0.0119
0.3	0.0139	–0.0144
0.4	0.0153	–0.0159
0.5	0.0158	–0.0163
0.6	0.0155	–0.0160
0.7	0.0147	–0.0151
0.8	0.0134	–0.0138
60° Junction		
Flow Ratio	Maximum Positive Error	Maximum Negative Error
0.2	0.0150	–0.0156
0.3	0.0166	–0.0171
0.4	0.0174	–0.0180
0.5	0.0176	–0.0183
0.6	0.0176	–0.0182
0.7	0.0172	–0.0178
0.8	0.0168	–0.0173
90° Junction		
Flow Ratio	Maximum Positive Error	Maximum Negative Error
0.2	0.0193	–0.0200
0.3	0.0198	–0.0205
0.4	0.0198	–0.0205
0.5	0.0197	–0.0203
0.6	0.0195	–0.0202
0.7	0.0194	–0.0200
0.8	0.0196	–0.0202

Table 5.1 Maximum Errors of Loss Coefficient due to Flow Measurement.

120° Junction

Flow Ratio	Maximum Positive Error	Maximum Negative Error
0.2	0.0240	–0.0248
0.3	0.0240	–0.0248
0.4	0.0237	–0.0245
0.5	0.0234	–0.0242
0.6	0.0230	–0.0238
0.7	0.0227	–0.0235
0.8	0.0226	–0.0233

150° Junction

Flow Ratio	Maximum Positive Error	Maximum Negative Error
0.2	0.0300	–0.0311
0.3	0.0288	–0.0298
0.4	0.0278	–0.0288
0.5	0.0271	–0.0279
0.6	0.0265	–0.0274
0.7	0.0263	–0.0272
0.8	0.0264	–0.0273

Table 5.1 (contd) Maximum Errors of Loss Coefficient due to Flow Measurement.

	Flow Rate (igph)	Centre Tank Pump Outlet Pressure (psi)	Delivery Pressure (psi)
Test Rig	1273.2	48.4	48.1
Simulation	1273.2	45.8	45.3
Simulation with Uprated Pump	1273.2	48.8	48.3
Test Rig	1003.2	52.7	52.5
Simulation	1003.7	49.1	48.7
Simulation with Uprated Pump	1003.7	52.4	52.0

Table 8.1 Centre Tank Verifcation Tests.

	Flow Rate (igph)			Pressure (psi)				
				Inboard		Outboard		Delivery
	Total	Inboard	Outboard	Pump Outlet	NRV Outlet	Pump Outlet	NRV Outlet	
Test Rig	782.3	–	–	39.7	39.2	40.9	39.5	39.1
Simulation with Sequence Valve	782.3	0.0	782.3	38.4	40.2	41.6	40.2	39.5
Simulation without Sequence Valve	782.3	391.7	391.5	42.2	41.2	42.1	41.1	40.6
Test Rig	1784.7	–	–	39.5	40.6	43.3	40.6	39.8
Simulation without Sequence Valve	1784.7	892.9	892.6	40.1	38.6	40.0	38.5	37.8

Table 8.2 Wing Tank Verifcation Tests.

	Flow Rate (igph)				Pressure (psi)					
					Centre	Inboard		Outboard		
	Total	Centre	Inboard	Outboard	Pump Outlet	Pump Outlet	NRV Outlet	Pump Outlet	NRV Outlet	Delivery
Test Rig	2944.1	–	–	–	39.5	39.6	39.4	41.0	39.5	38.3
Simulation without Sequence Valve	2944.1	1714.5	603.4	626.2	40.4	41.3	40.2	41.3	40.1	39.3
Test Rig	1273.7	1273.1	–	–	48.4	–	–	–	–	48.1
Simulation with Sequence Valve	1273.1	1273.1	–	–	45.4	–	–	–	–	15.3
Simulation without Sequence Valve	1273.1	1273.1	–	–	45.8	–	–	–	–	45.3
Test Rig	1003.2	1003.2	–	–	52.7	–	–	–	–	52.5
Simulation with Sequence Valve	1003.2	1003.2	–	–	49.1	–	–	–	–	48.7
Simulation without Sequence Valve	1003.2	1003.2	–	–	49.1	–	–	–	–	48.7

Table 8.3 Combined Centre and Wing Tank Verifcation Tests.

	Flow Rate (igph)				Pressure (psi)					
					Centre	Inboard		Outboard		
	Total	Centre	Inboard	Outboard	Pump Outlet	Pump Outlet	NRV Outlet	Pump Outlet	NRV Outlet	Delivery
Test Rig	782.3	–	–	–	–	39.7	39.2	40.9	39.5	39.1
Simulation with Sequence Valve	782.3	0.0	782.3	0.0	–	42.0	40.6	38.8	40.5	39.9
Simulation without Sequence Valve	782.3	0.0	379.0	403.4	–	42.3	41.3	42.2	41.2	40.6
Test Rig	1784.7	–	–	–	–	39.5	40.6	43.3	40.6	39.8
Simulation without Sequence Valve	1784.7	0.0	907.3	877.5	–	40.2	38.7	40.1	38.6	37.5

Table 8.3 (Cont'd) Combined Centre and Wing Tank Verifcation Tests.

	Flow Rate (igph)				Pressure (psi)					
					Centre	Inboard		Outboard		
	Total	Centre	Inboard	Outboard	Pump Outlet	Pump Outlet	NRV Outlet	Pump Outlet	NRV Outlet	Delivery
Test Rig	782.3	–	–	–	–	39.7	39.2	40.9	39.5	39.1
Simulation with Sequence Valve	782.3	0.0	782.3	0.0	–	42.0	40.6	38.8	40.5	39.9
Simulation without Sequence Valve	782.3	0.0	379.0	403.4	–	42.3	41.3	42.2	41.2	40.6
Test Rig	1784.7	–	–	–	–	39.5	40.6	43.3	40.6	39.8
Simulation without Sequence Valve	1784.7	0.0	907.3	877.5	–	40.2	38.7	40.1	38.6	37.5

Table 8.3 (Cont'd) Combined Centre and Wing Tank Verifcation Tests.

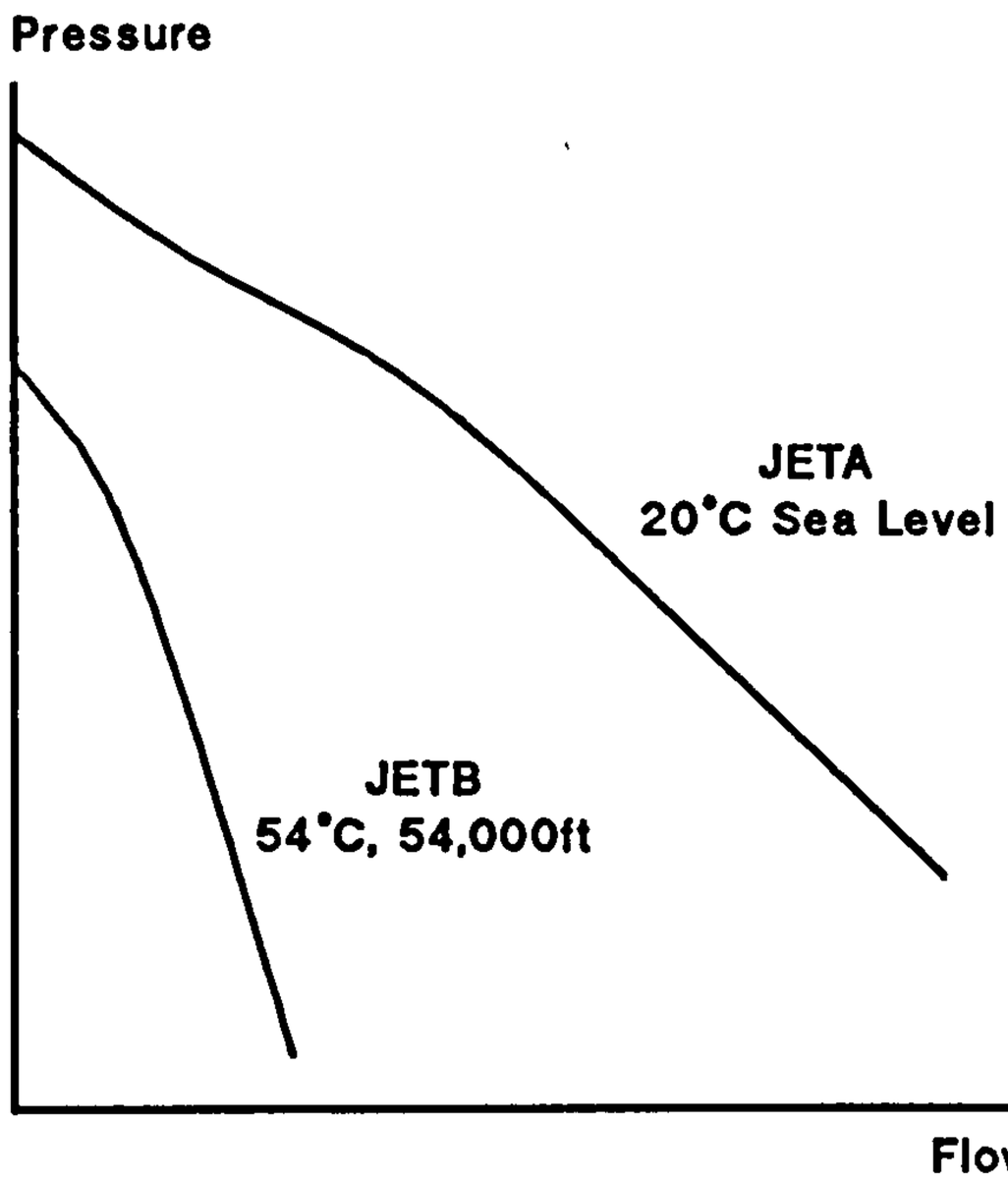

Figure 2.1 Illustration of the Effects of Fuel Type and Temperature on Pump Performance

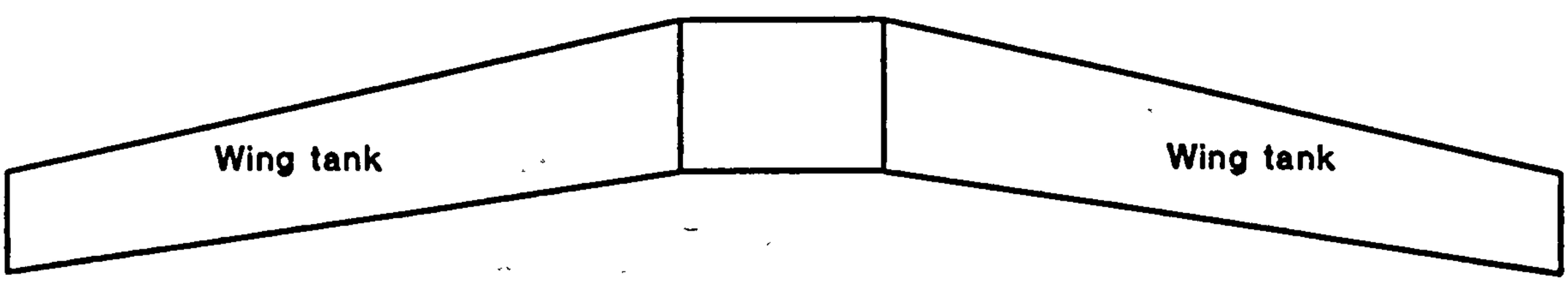

Figure 2.2 Two Tank Fuel System

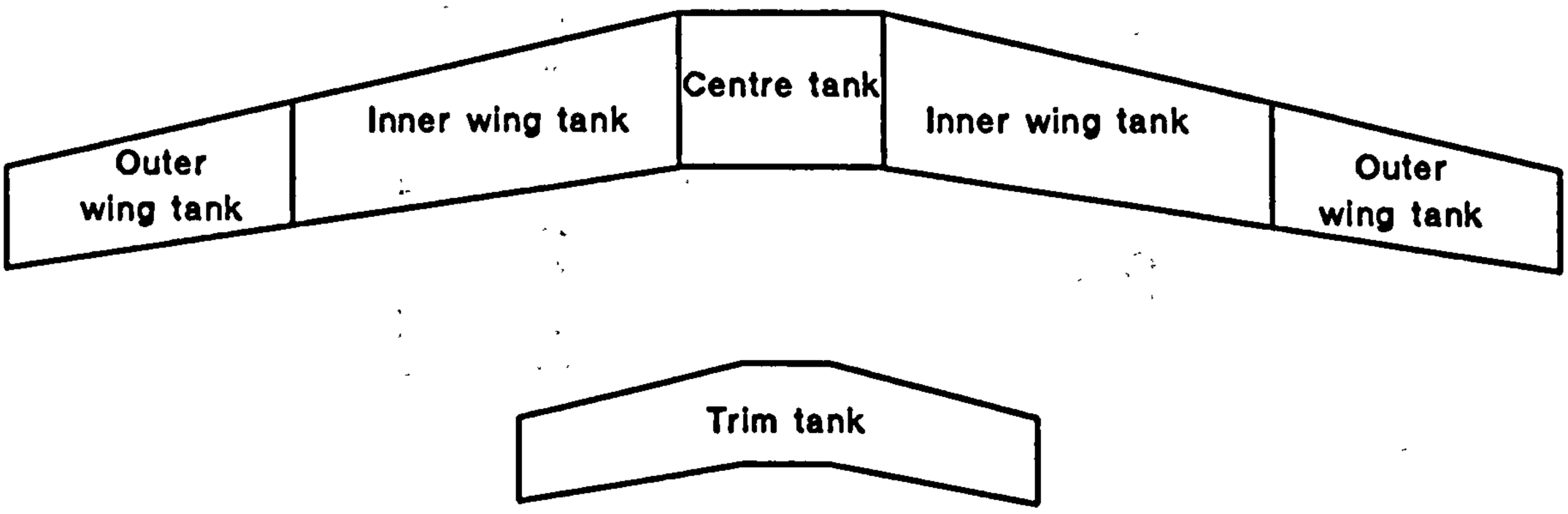

Figure 2.3 Six Tank Fuel System

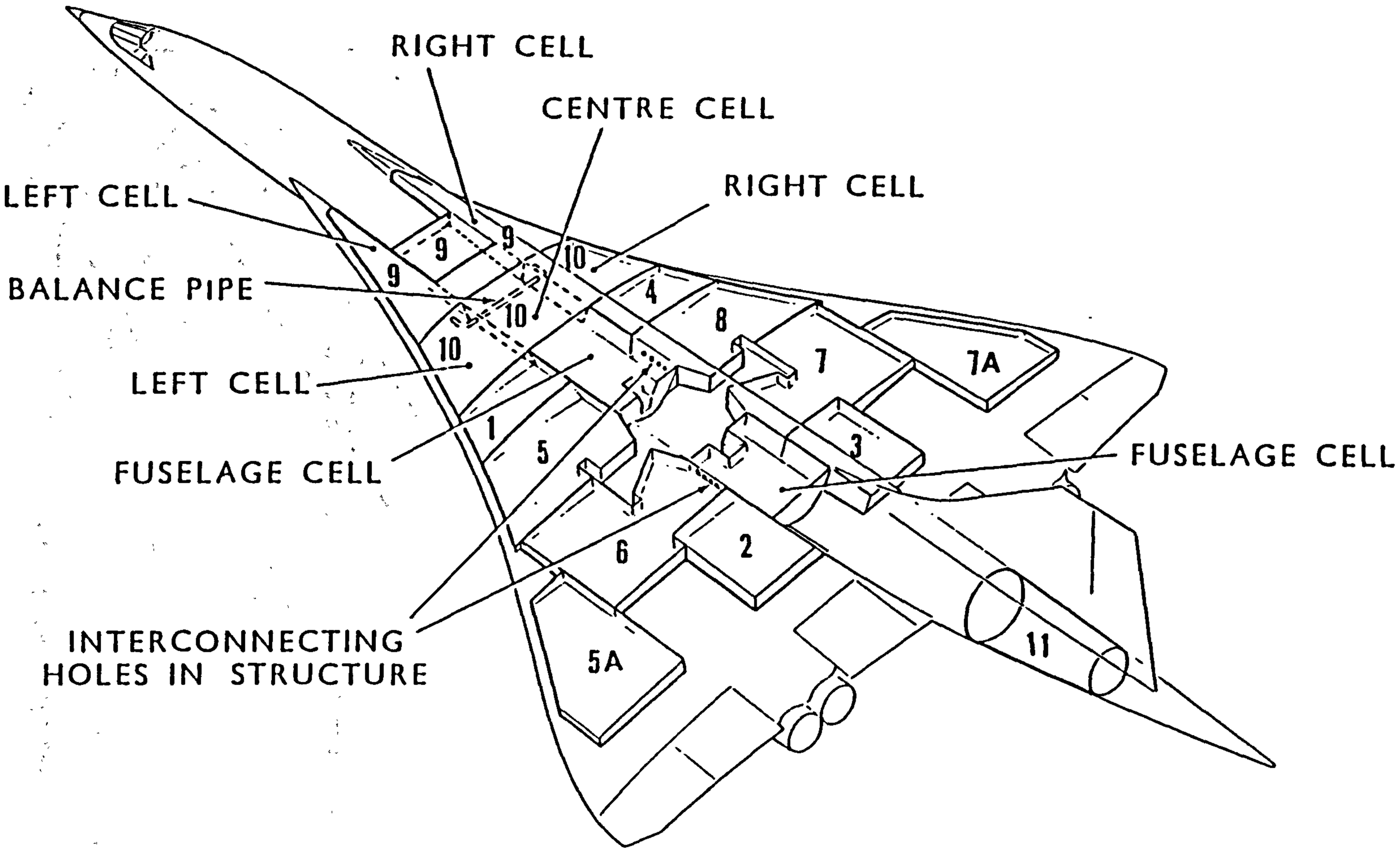

Figure 2.4 Layout of Concorde Fuel Tanks

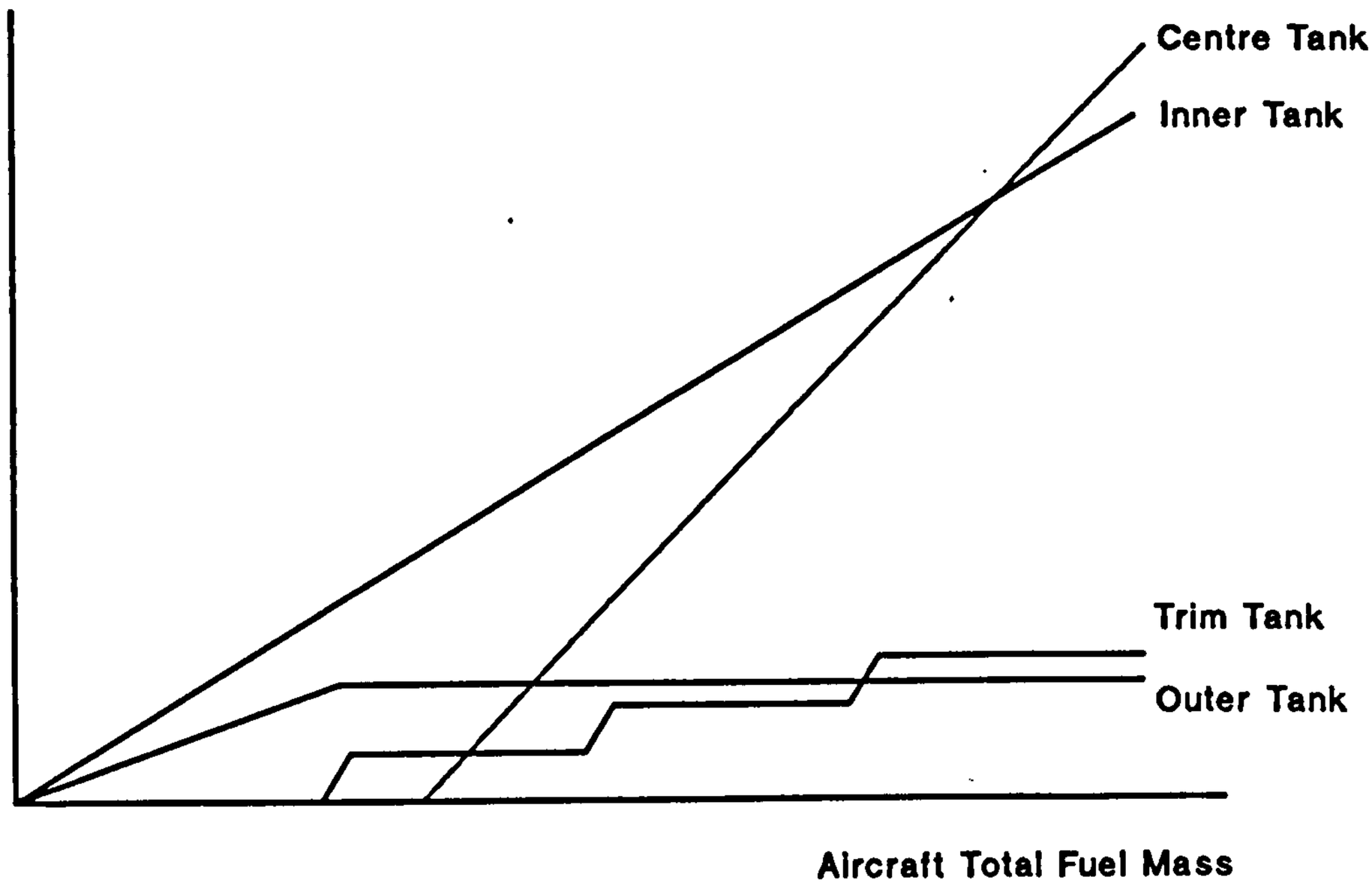

Figure 2.5 Fuel Distribution Graph

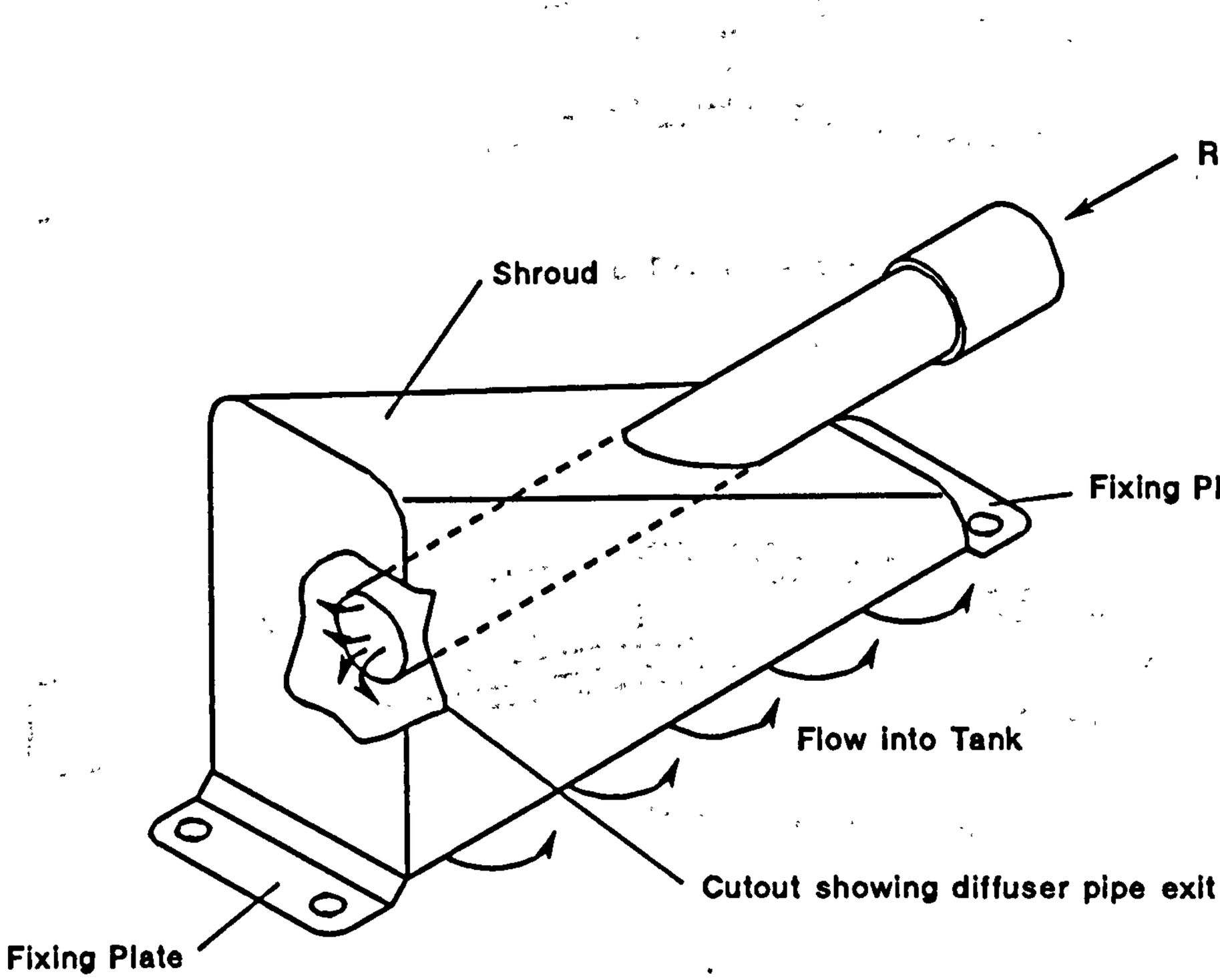

Figure 2.6 Aircraft Refuel Diffuser

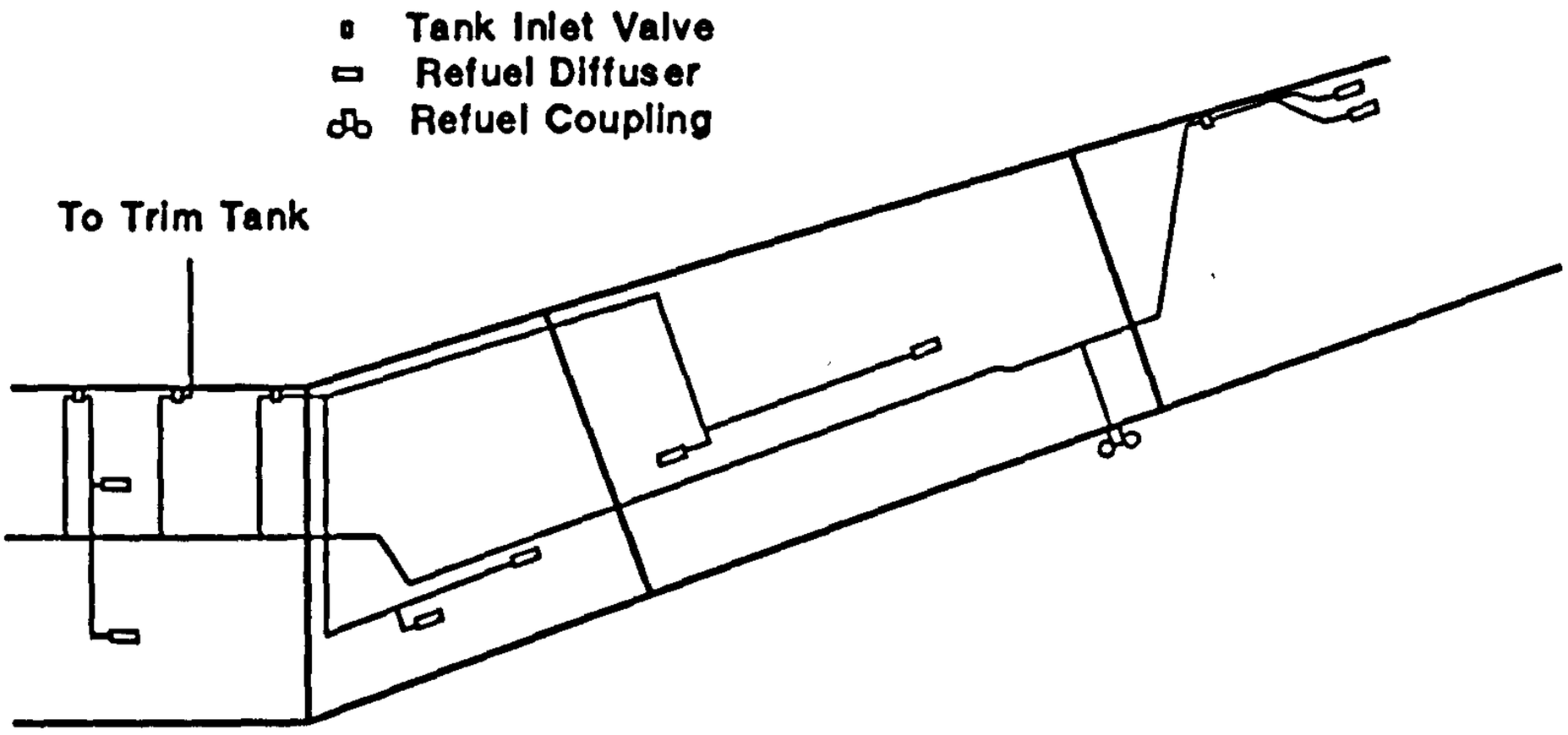

Figure 2.7 Typical Large Aircraft Refuel System

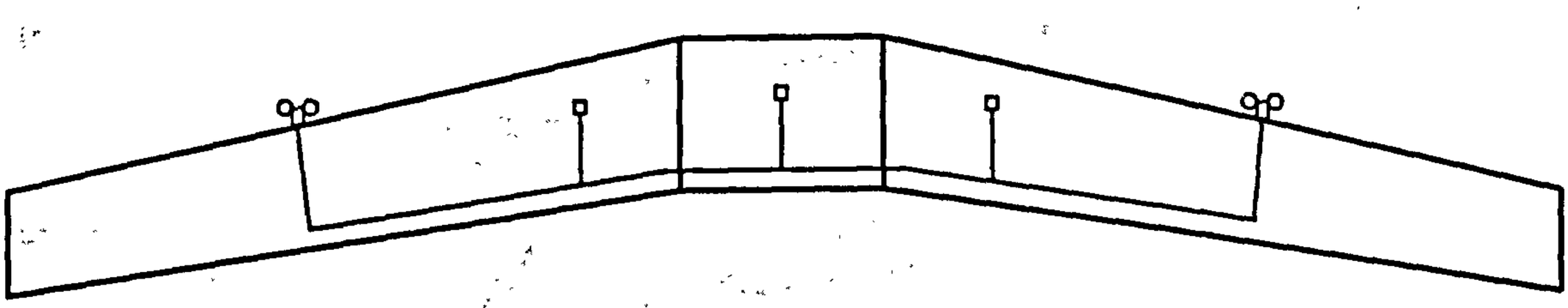

a. Refuel Gallery

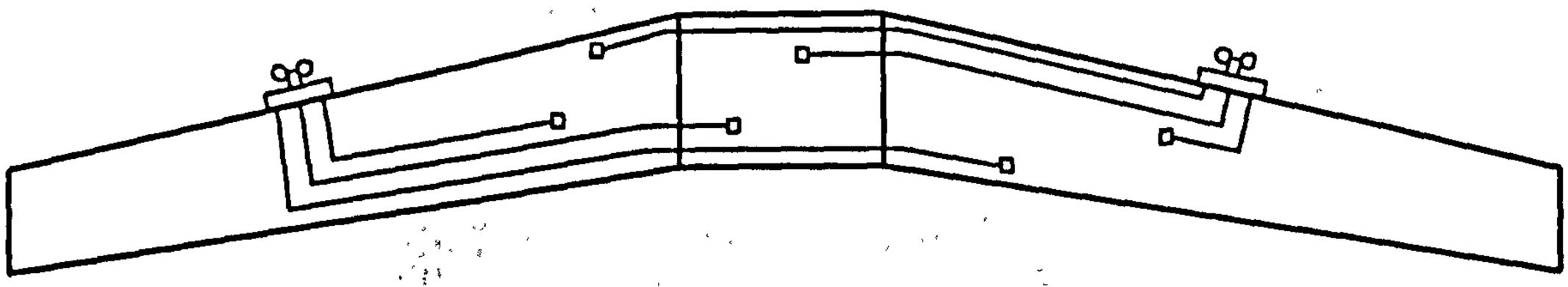

b. Manifold Type

Figure 2.8 Two Types of Refuel System

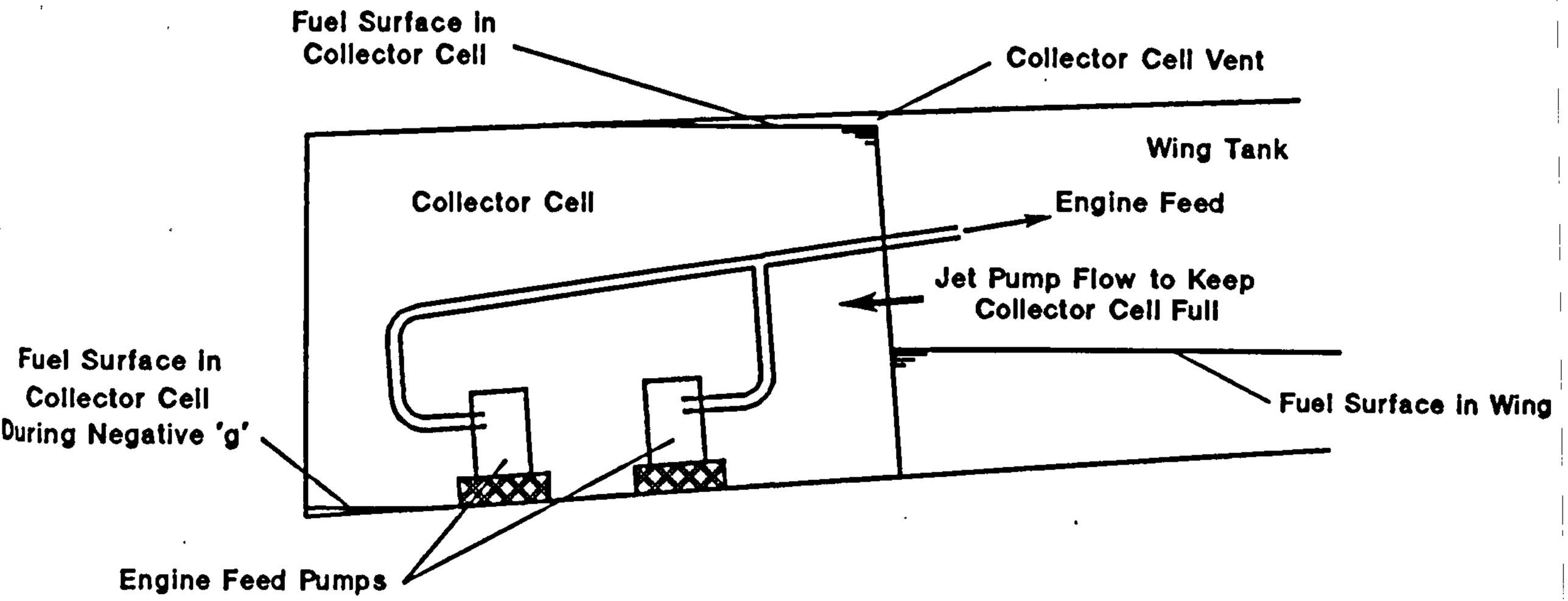

Figure 2.9 Negative 'g' Protection Using Collector Cells (Viewed From the Front)

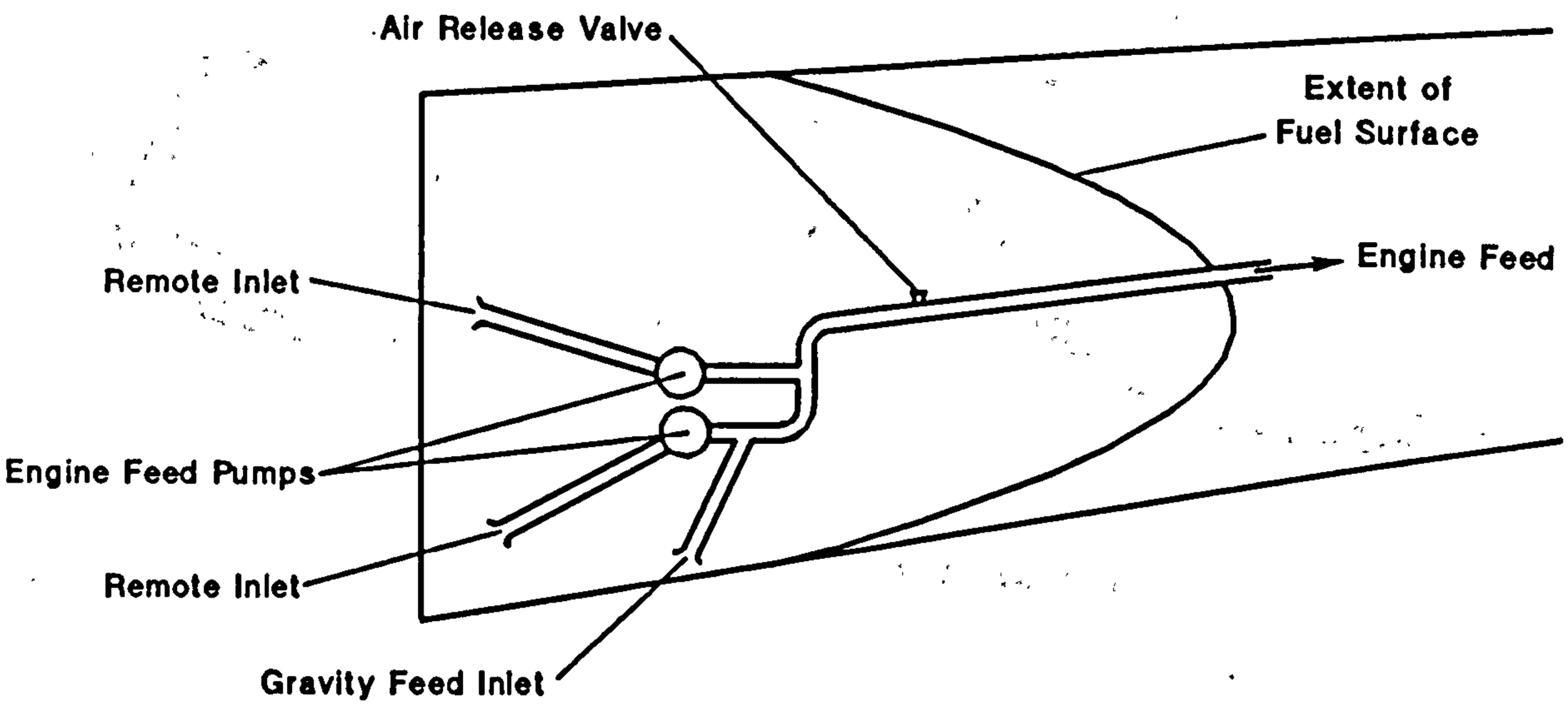

Figure 2.10 Negative 'g' Protection Using Remote Pump Inlet (Viewed From Above)

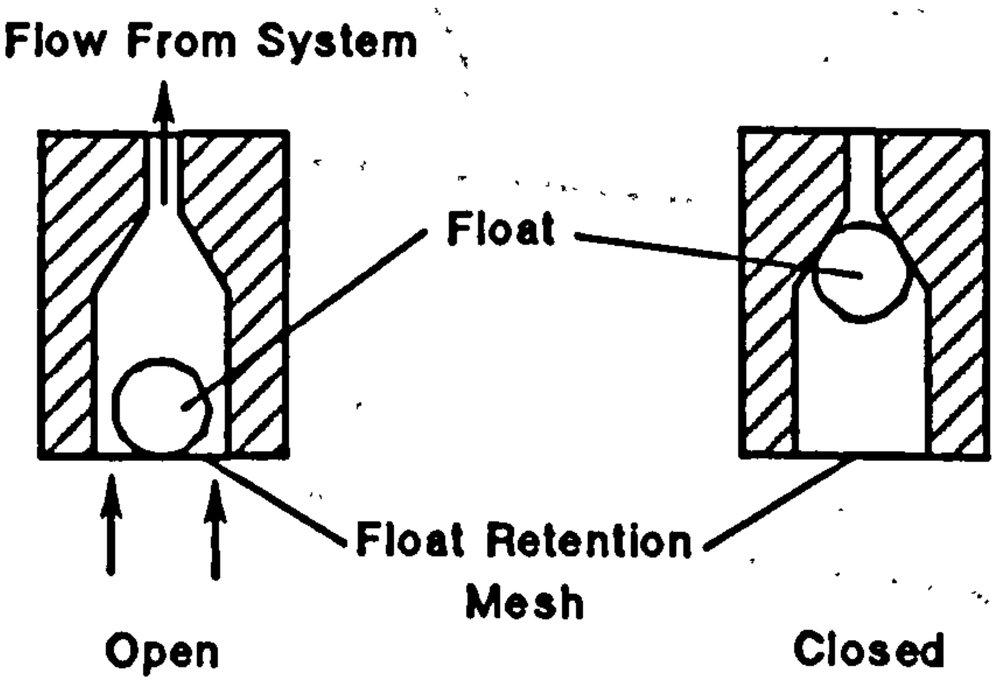

Figure 2.11 Air Release Valve

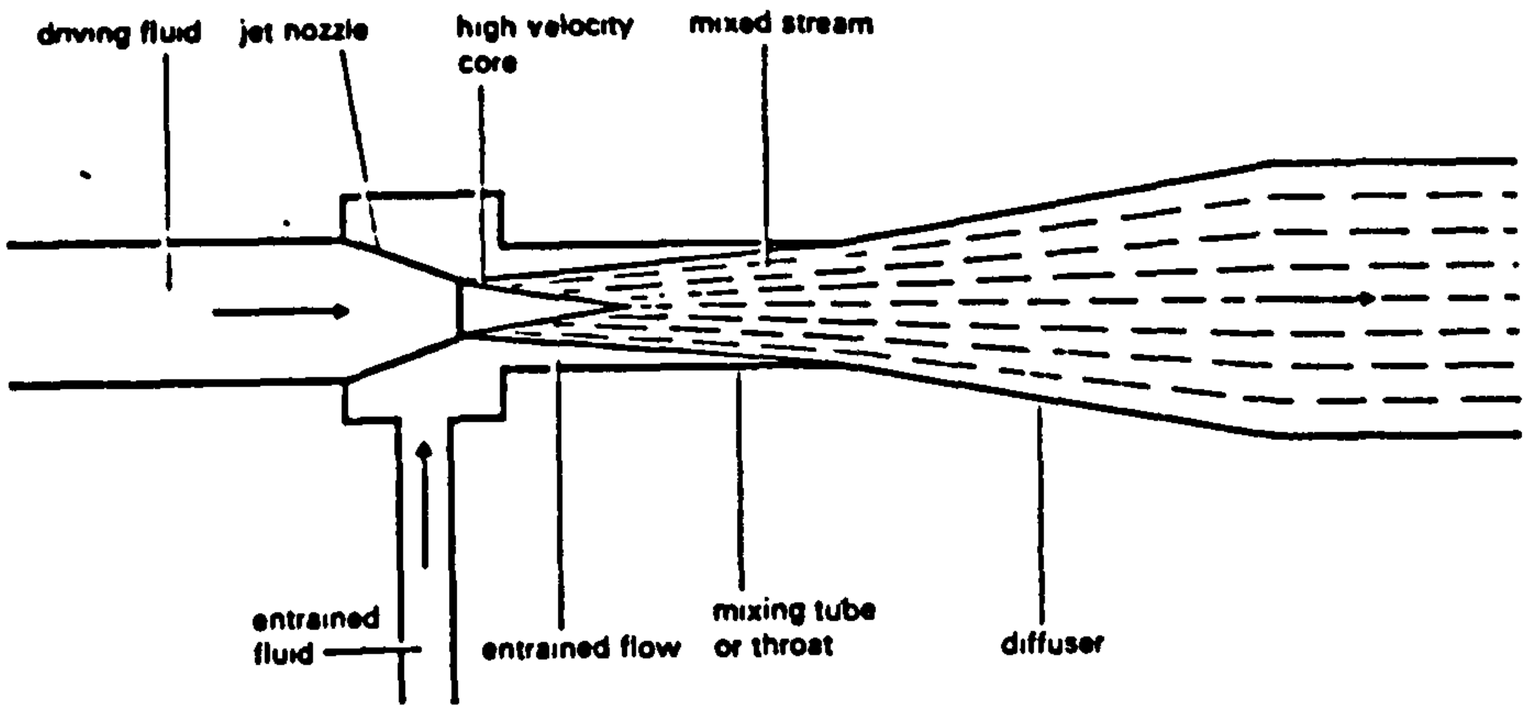

Figure 2.12 Arrangement of a Jet Pump.

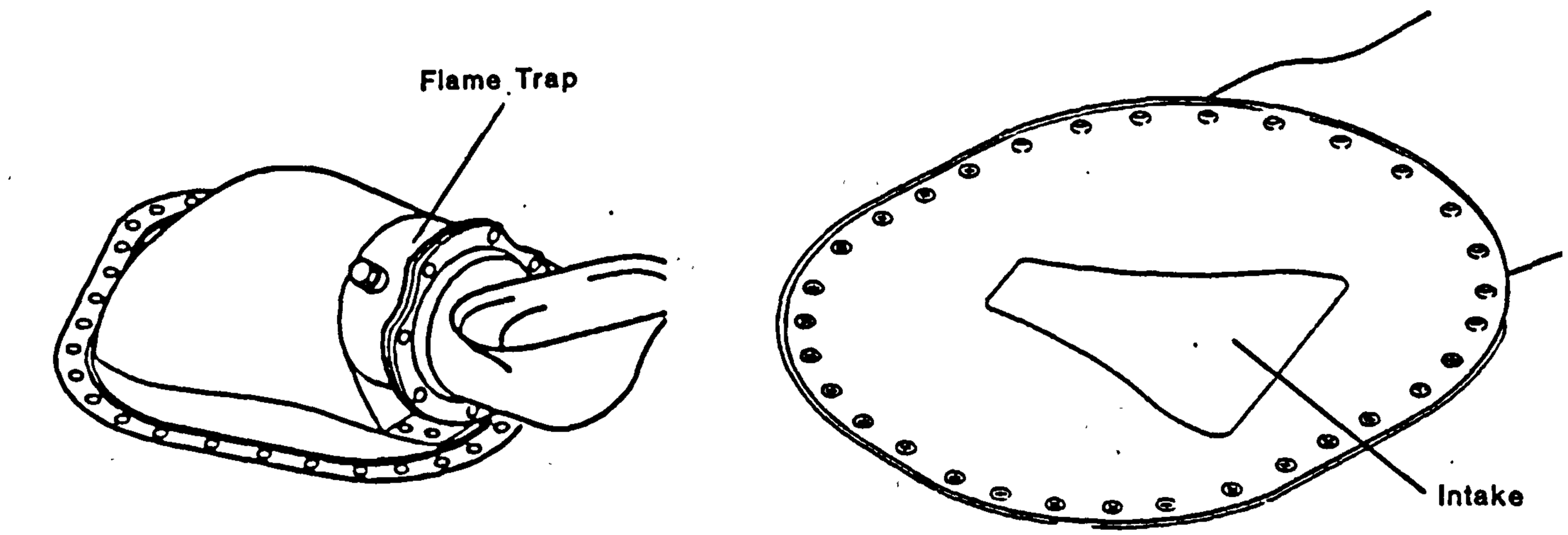

Figure 2.13 NACA Intake.

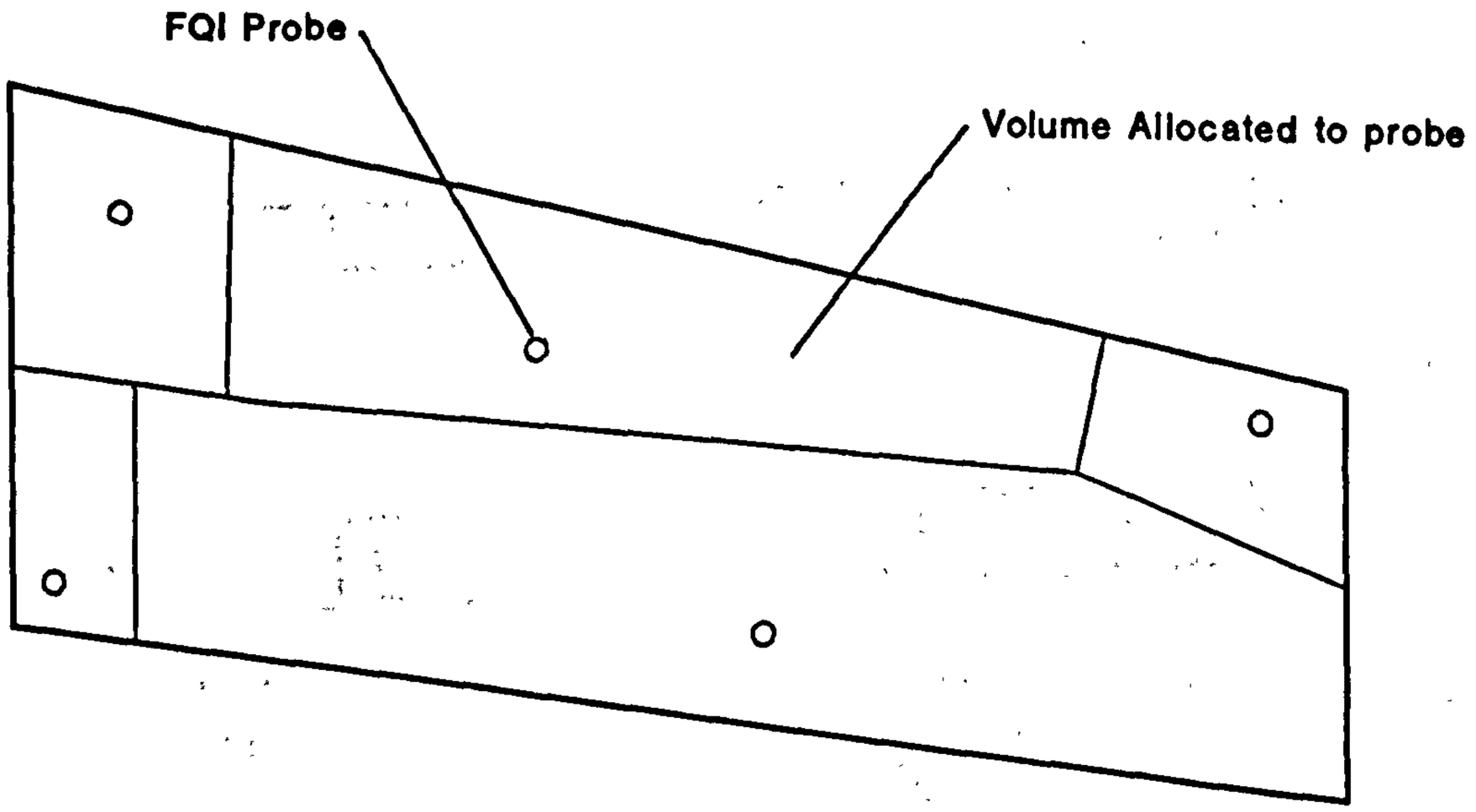

Figure 2.14 FQI Probe Volume Allocation.

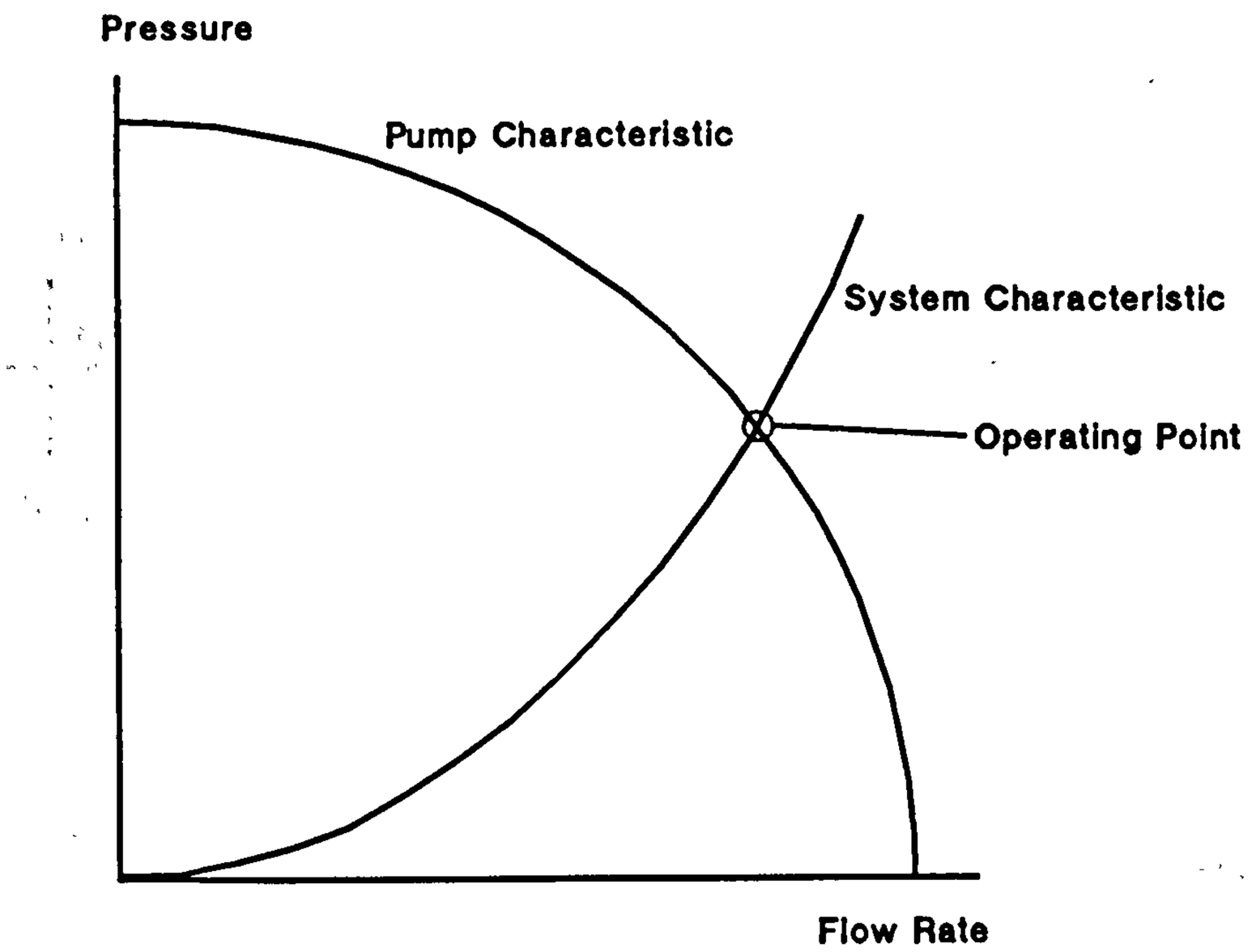

Figure 3.1 System and Pump Characteristic

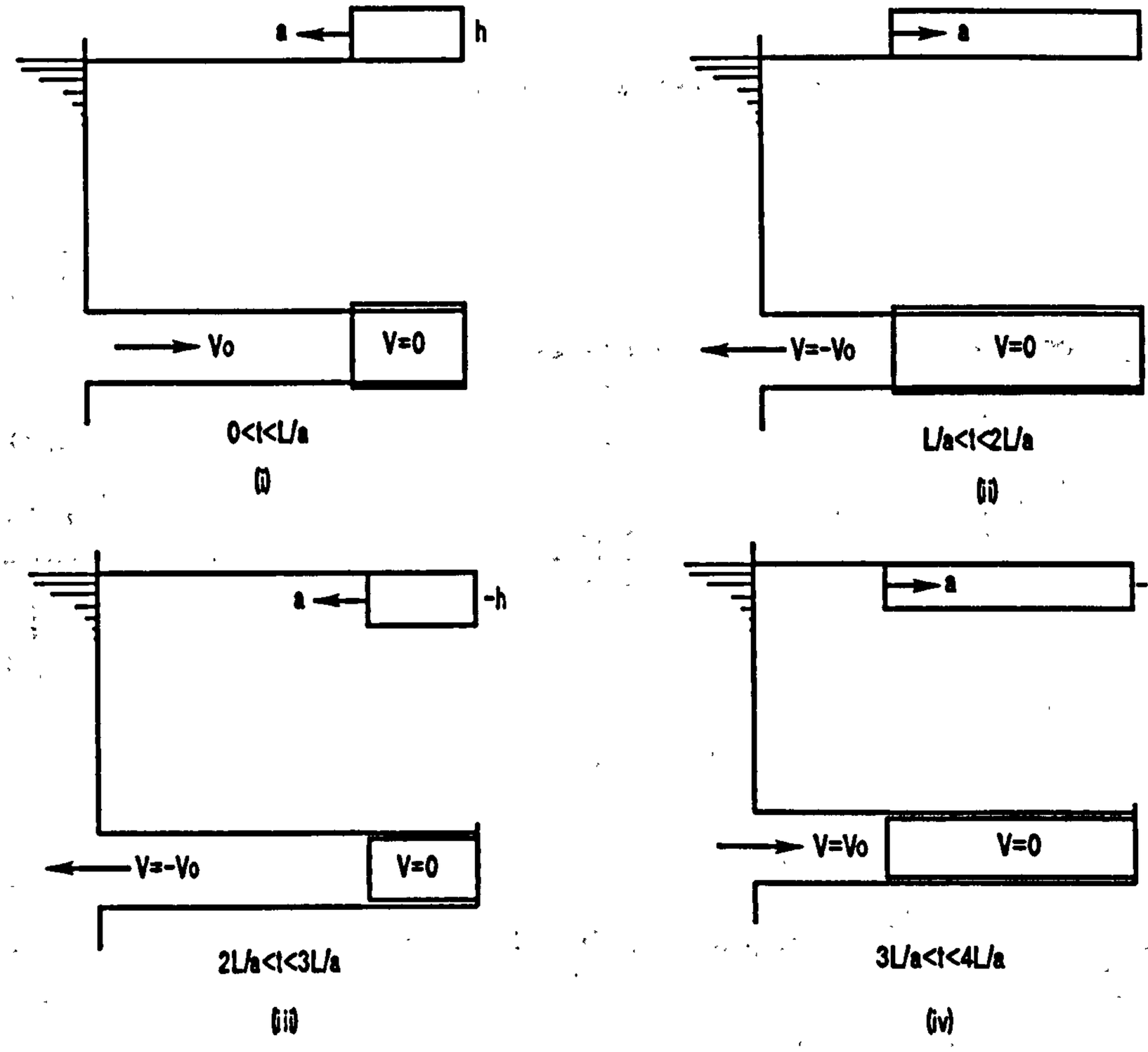

Figure 3.2 Sequence Of Events For One Cycle Of Sudden Valve Closure

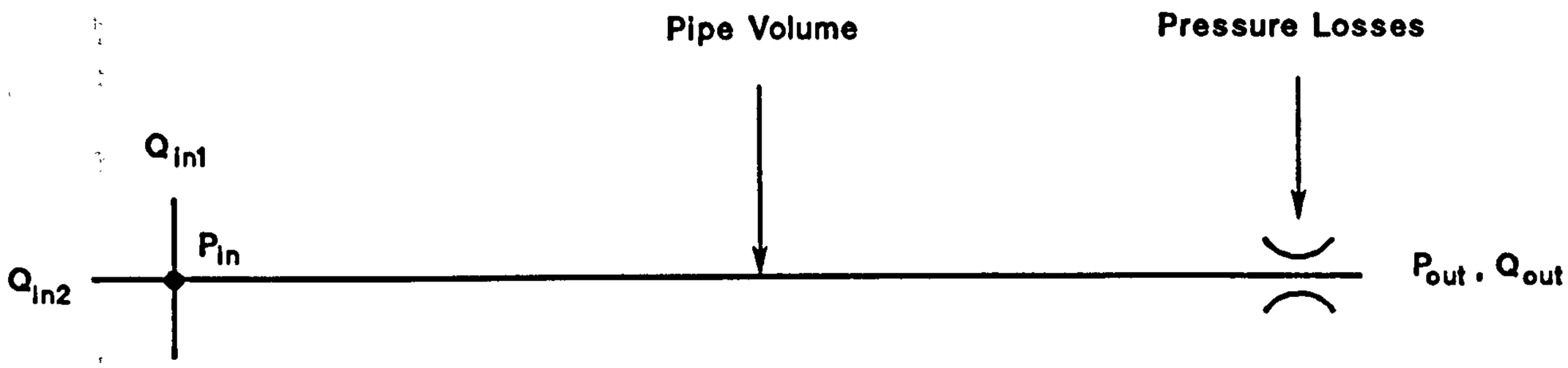

Pipe Model HP01

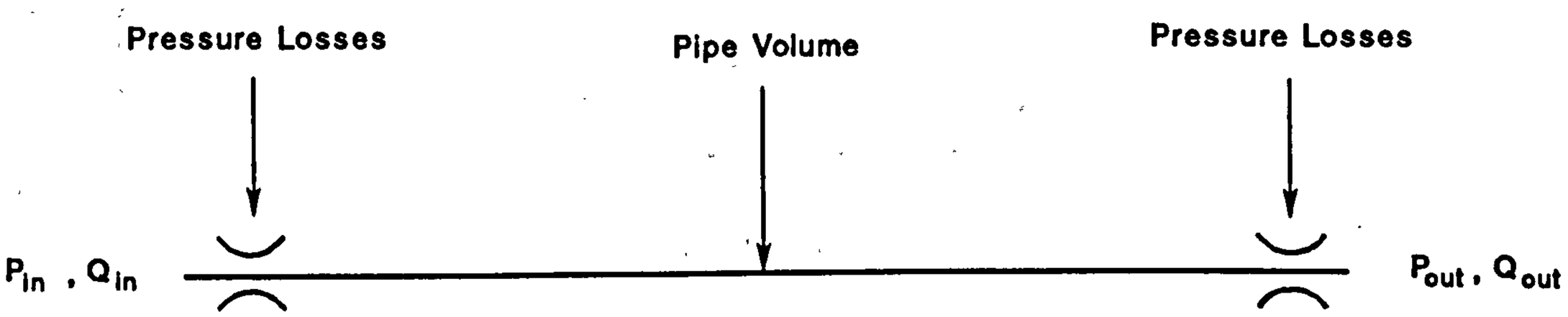

Pipe Model HP02

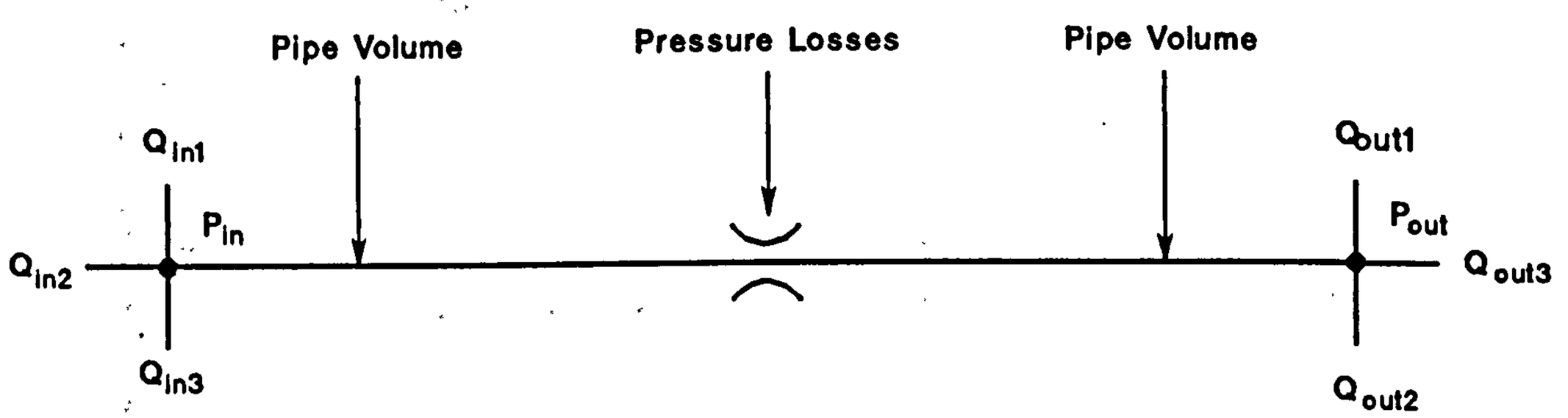

Pipe Model HP03

Figure 3.3 Bath*v*p Pipe Models

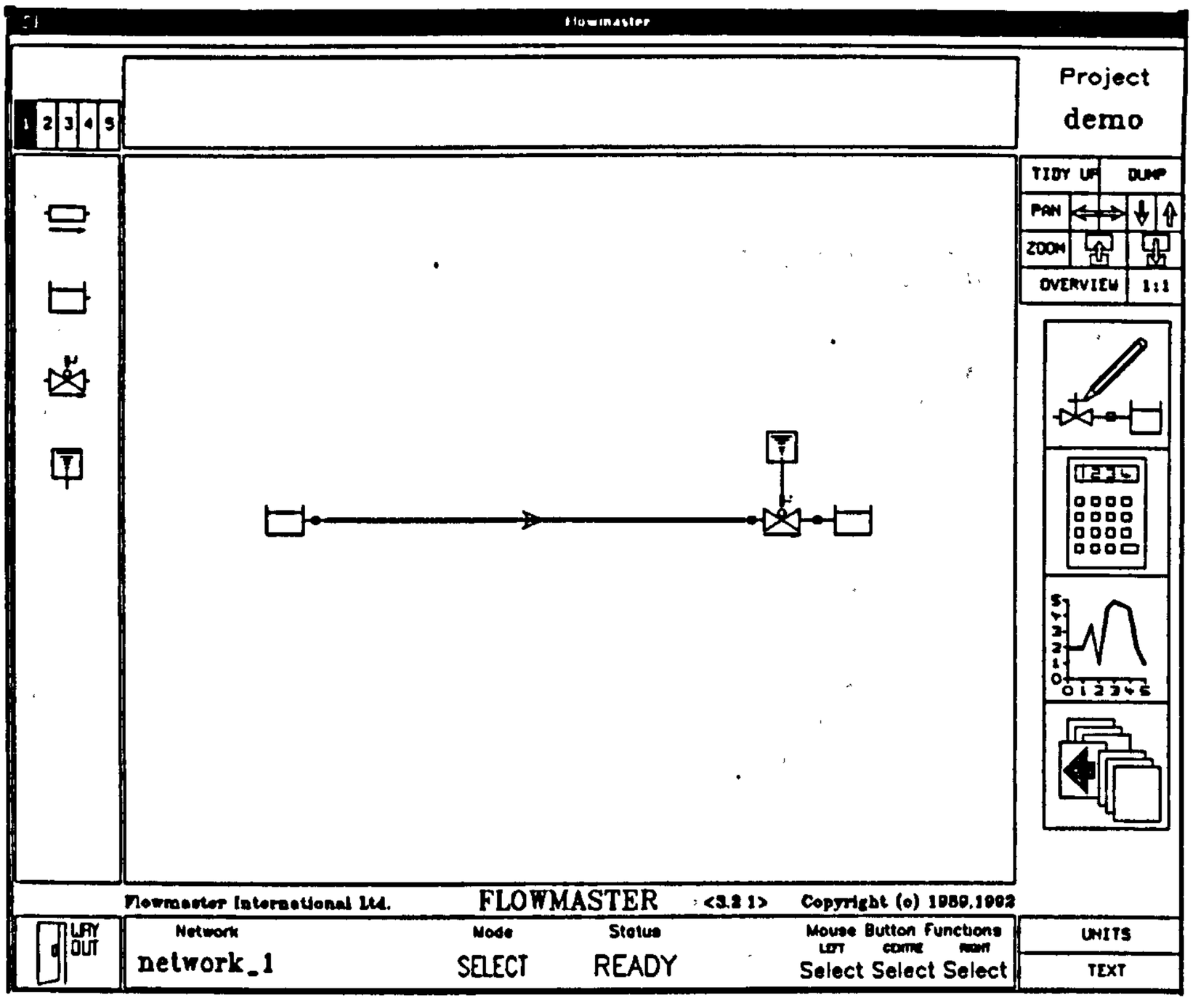

Network Update

Network Analysis

Results Display

Figure 3.4 Flowmaster.

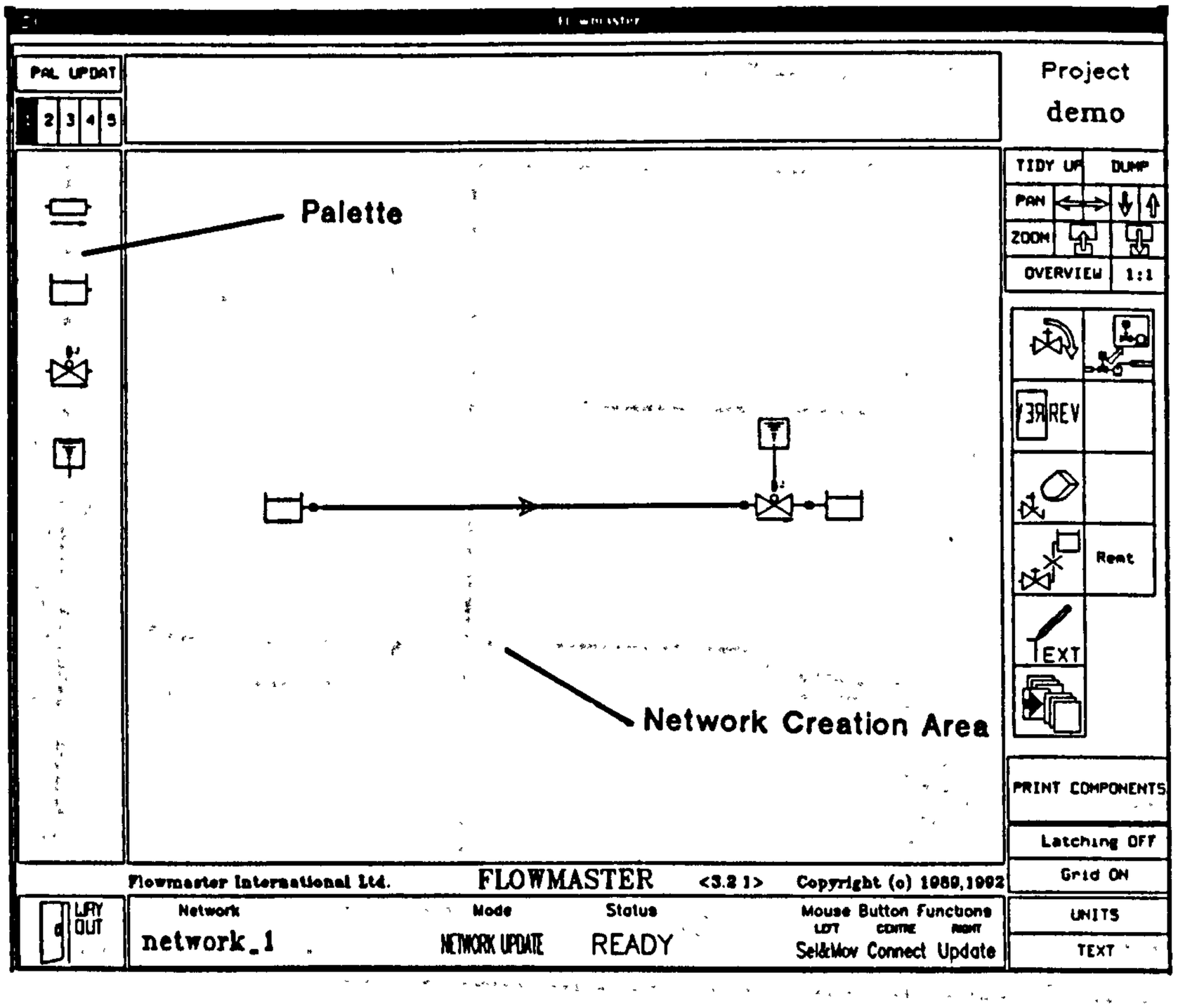

Component Manipulation Icons

Figure 3.5 Network Update, Flowmaster.

Component Number : 0004	PIPE:CYLINDRICAL
Last Modified : 17/3/93 15:05	
Family Reference : 002001	
Page 1 of 1	

DESCRIPTION	VALUE	UNITS	USAGE
Length	10	(m)	SPSS.SPFB. SPT.SPPSPS1SPS2SPNMPBMPSWMPWFPSS
Friction Option	3		SPSS.SPFB. SPT.SPPSPS1SPS2MPBMPSWMPWFPSSFPT
Friction Data	See Sub-Frm		SPSS.SPFB. SPT.SPPSPS1SPS2MPBMPSWMPWFPSSFPT
Diameter	0.0488	(m)	SPSS.SPFB. SPT.SPPsps1sps2SPNMPBMPSWMPWFPSS
Vapour Pressure	0.02062	(bar)	spt. spp. fpt. cft
Compliant Model	2		SPT. SPP. FPT. CFT
Bulk Modulus of pipe	** NOTSET **	(GN/m2)	spt. spp. fpt. cft
Elastic Model	1		SPT. SPP. FPT. CFT
Wave Speed	** NOTSET **	(m/s)	spt. spp. fpt. cft
Variable Wave Speed Data	See Sub-Frm		spt. spp. cft
Muliphase Pressure Increment	** NOTSET **	(bar)	MPB
Multiphase Fric Calc. Option	2		MPSW.MPW
Sizing Criteria option	See Sub-Frm		SPS1.SPS2
Heat Transfer option	See Sub-Frm		spss.spfb. spt. spp.sps1.sps2fpssfptcfsscft
Flow Process	4		CFSS. CFT
Compressible Flow Option	See Sub-Frm		CFSS. CFT
Noise Data	See Sub-Frm		SPN
Volumetric Flow Rate	** NOTSET **	(m3/s)	spfb.sps1.sps2

Analysis Usage

Figure 3.6 Component Data Sheet, Flowmaster.

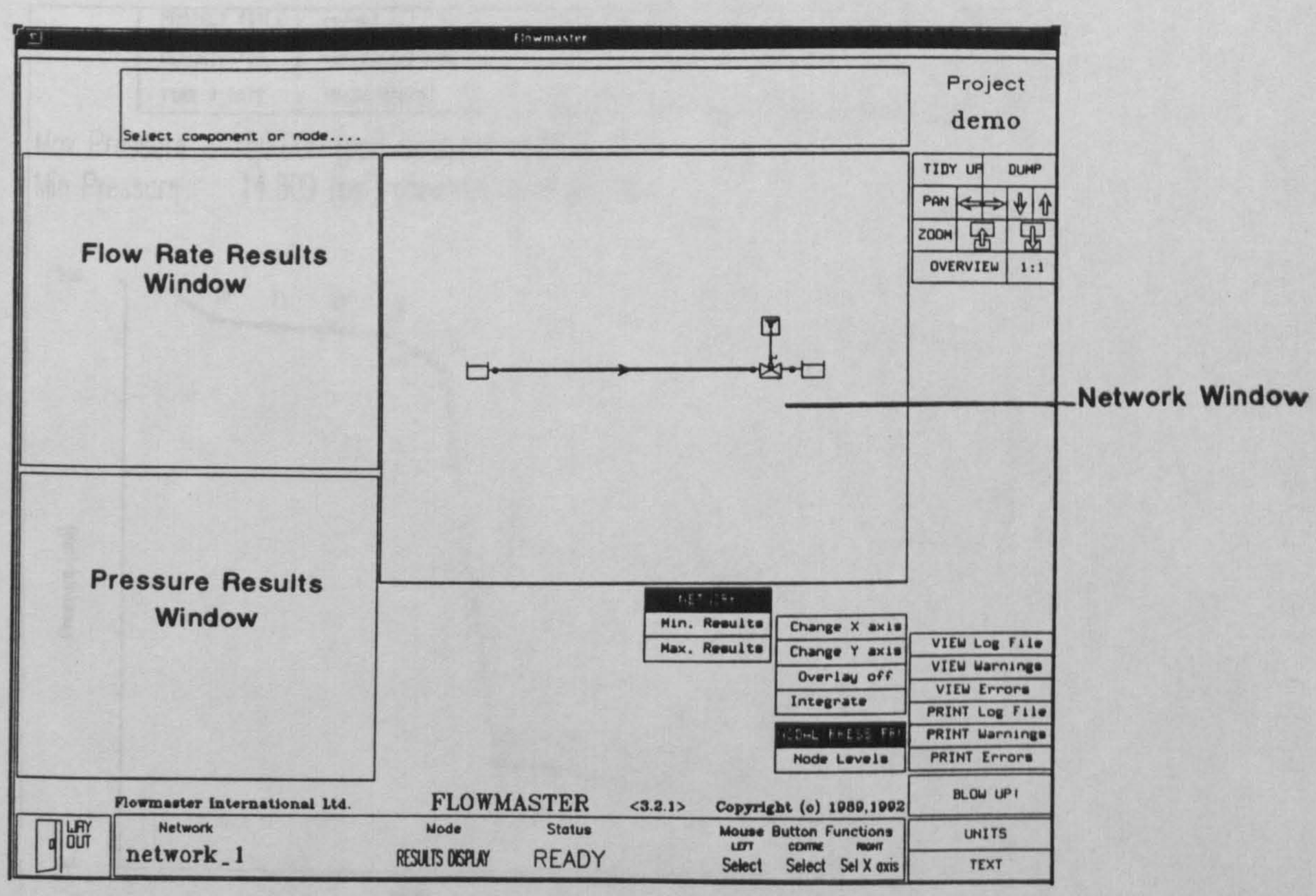

Figure 3.7 Results Screen, Flowmaster.

PROJECT TITLE : test1
NETWORK NAME : flow_balnce_two
DESCRIPTION :

TIME / DATE : 15:13 4/8/93 PAGE : 1

Component Number 11

ORIFICE:SHARP-EDGED

STD. ORIFICE PLATE

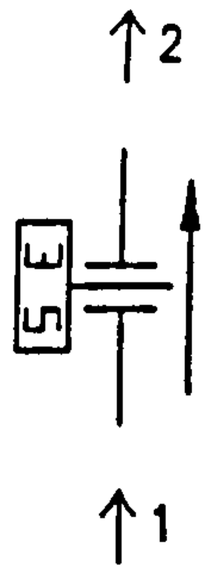

Flow Rate	into conn.	1	=	15.000 (l/s)
Flow Rate	from conn.	2	=	15.000 (l/s)
Specified Flow			=	15.000 (l/s)
Required Pressure Loss			=	3.314 (bar)
Actual Pressure Loss			=	23.193 (bar)
Loss Coefficient			=	11.378
Selected Diameter			=	29.472 (mm)

Figure 3.8 Flowbalancing Results, Flowmaster.

PROJECT TITLE : refuel
NETWORK NAME : refuel
DESCRIPTION : refuel network

TIME / DATE : 15:34 5/8/93 PAGE : 2

Max Pressure 50.000 (psi) occurred at NODE 9
Min Pressure 14.809 (psi) occurred at NODE 16

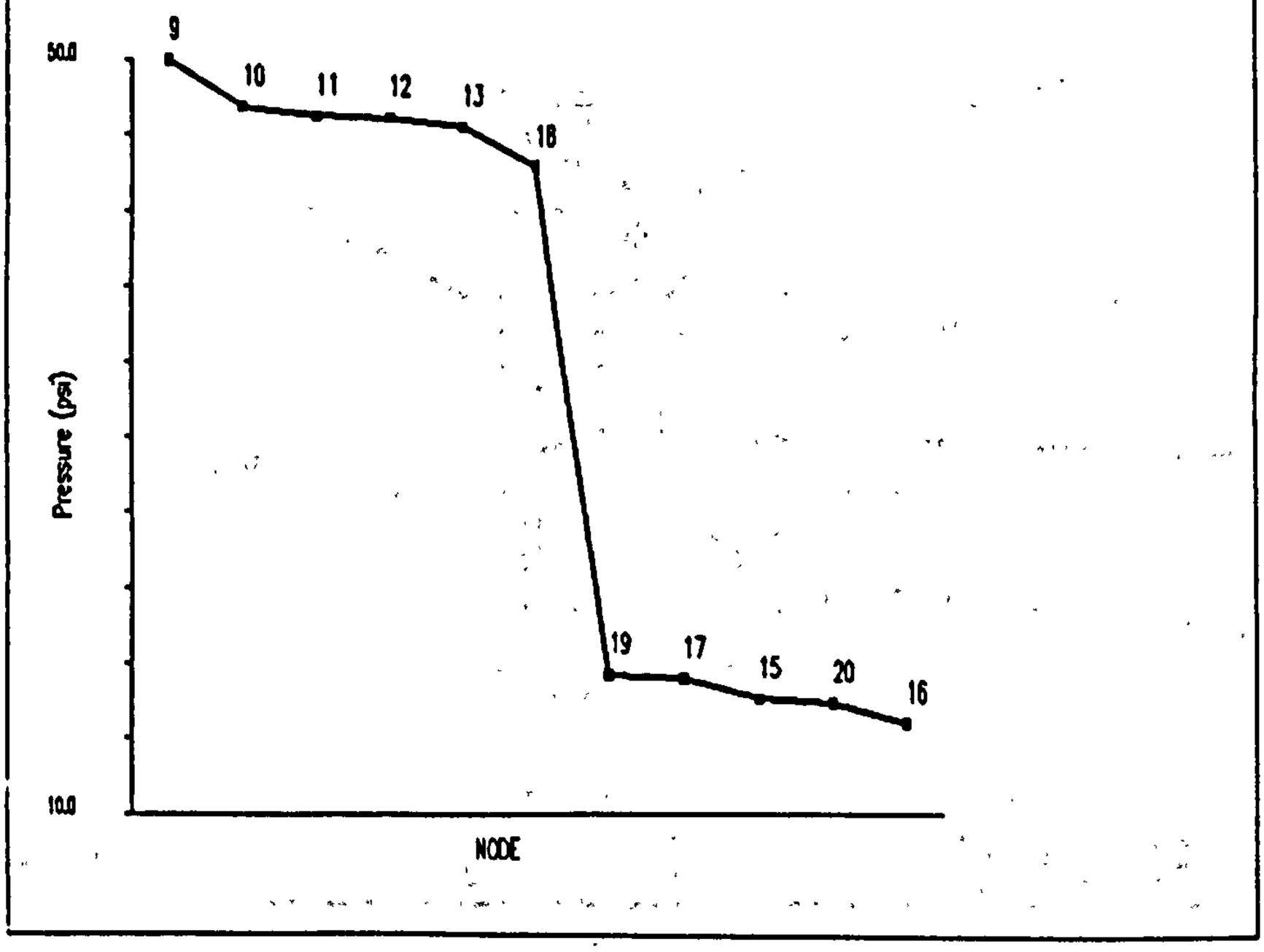

Figure 3.9 Pressure Gradient Plot, Flowmaster.

PROJECT TITLE : demo NETWORK NAME : network_1
DESCRIPTION : network for figures

TIME / DATE : 16:56 17/3/93 PAGE : 1

Maximum value was 4.65E+00 (bar) at 5.690 (s)
Minimum value was 1.13E+00 (bar) at 0.000 (s)

Pressure (bar) at node 2 ——— v0003

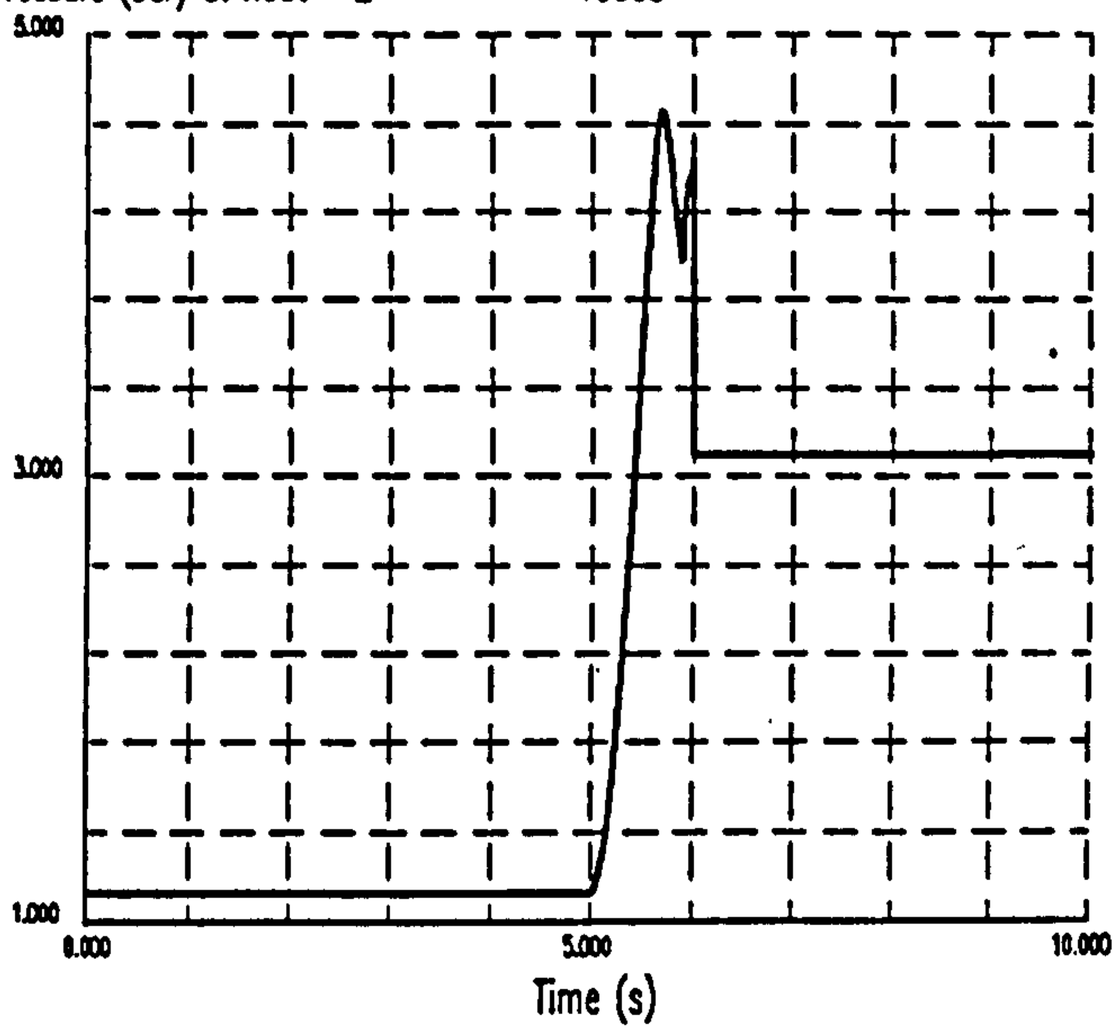

FIGURE :

Figure 3.10 Transient Result, Flowmaster.

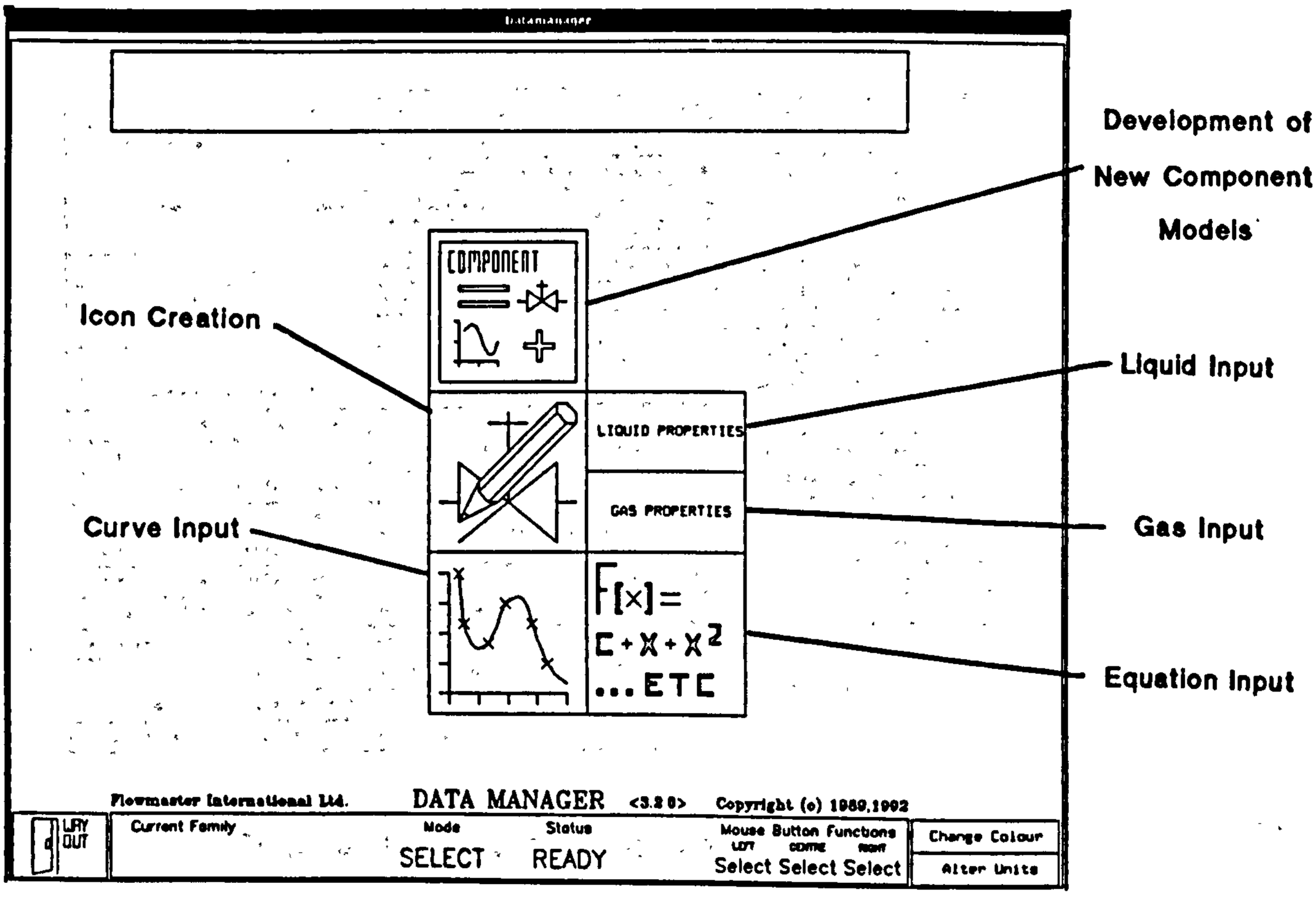

Figure 3.11 Datamanager.

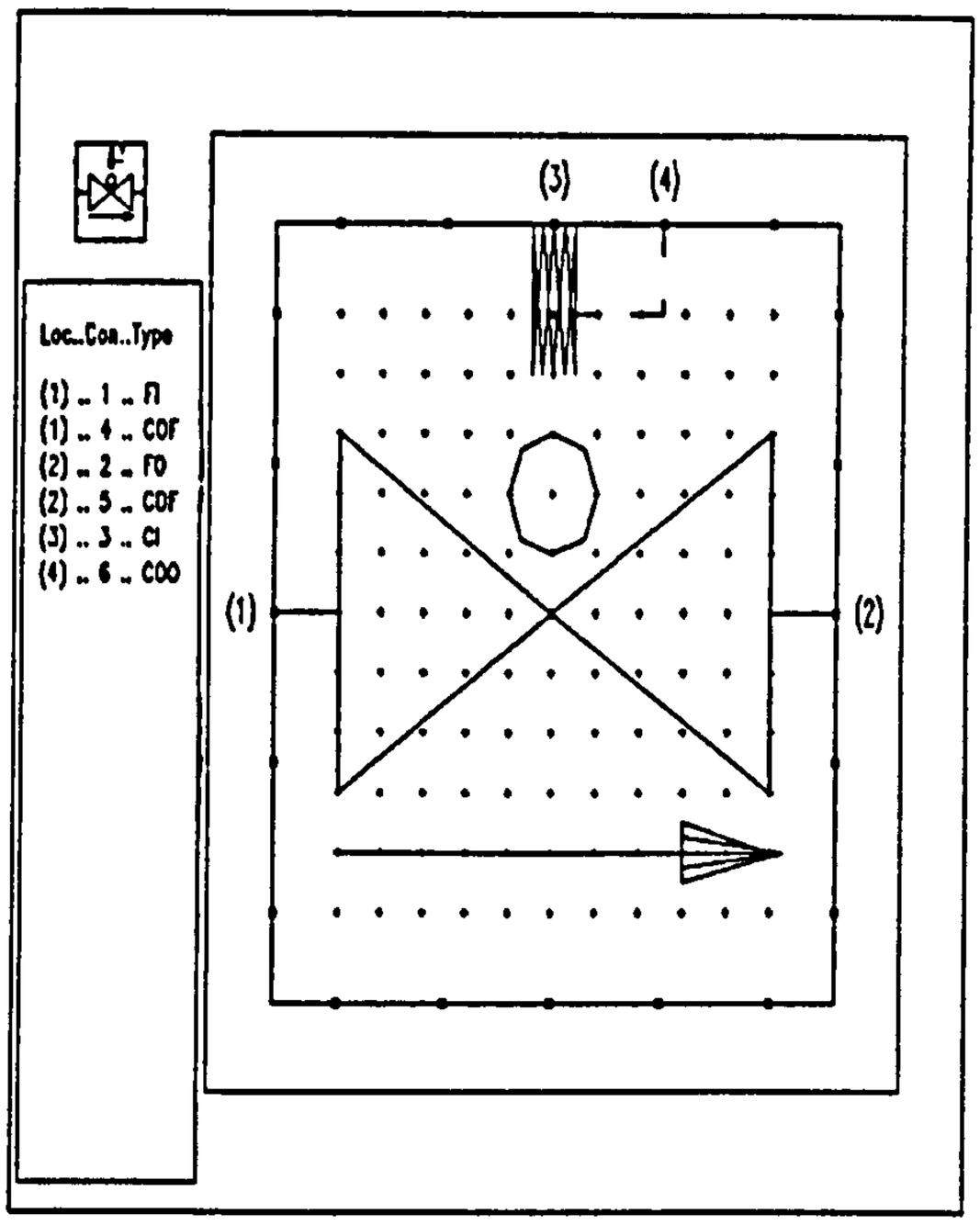

Figure 3.12 Icon Editor, Flowmaster.

Last Modified : 26/1/93 15:58	Avtur [alex]
	Nominal Properties
Page 1 of 2	

DESCRIPTION	VALUE	UNITS	USAGE
Reference temperature	** NOTSET **	(deg C)	spss.spfb. spt. spp.spsl.sps2.fpss. fpt
Reference density	** NOTSET **	(kg/m3)	spss.spfb. spt. spp.spsl.sps2.fpss. fpt
Thermal Expansion Coefficient	** NOTSET **		spss.spfb. spt. spp.spsl.sps2.fpss. fpt
Bulk Modulus	1.32	(GN/m2)	FPSS. FPT
Vapour Pressure	** NOTSET **	(bar)	spss.spfb. spt. spp.spsl.sps2.fpss. fpt
Reference Dynamic Viscosity	** NOTSET **	(N s/m2)	spss.spfb. spt. spp.spsl.sps2.fpss. fpt
Walther Equation Z	0.7		spss.spfb. spt. spp.spsl.sps2.fpss. fpt
Walther Equation A	9.9897		spss.spfb. spt. spp.spsl.sps2.fpss. fpt
Walther Equation B	4.1951		spss.spfb. spt. spp.spsl.sps2.fpss. fpt
Specific Heat Coefficient A	0.67267		spss.spfb. spt. spp.spsl.sps2.fpss. fpt
Specific Heat Coefficient B	0.00435		spss.spfb. spt. spp.spsl.sps2.fpss. fpt
Specific Heat Coefficient C	0		spss.spfb. spt. spp.spsl.sps2.fpss. fpt
Specific Heat Coefficient D	0		spss.spfb. spt. spp.spsl.sps2.fpss. fpt
Specific Heat Coefficient E	0		spss.spfb. spt. spp.spsl.sps2.fpss. fpt
Specific Heat Coefficient F	0		spss.spfb. spt. spp.spsl.sps2.fpss. fpt
Eagle Ref for Component 1	** NOTSET **		CFSS. CFT
Mole Fraction for Component 1	** NOTSET **		CFSS. CFT
Eagle Ref for Component 2	** NOTSET **		cfss. cft
Mole Fraction for Component 2	** NOTSET **		cfss. cft
Eagle Ref for Component 3	** NOTSET **		cfss. cft

Figure 3.13 Fluid Data Sheet, Flowmaster

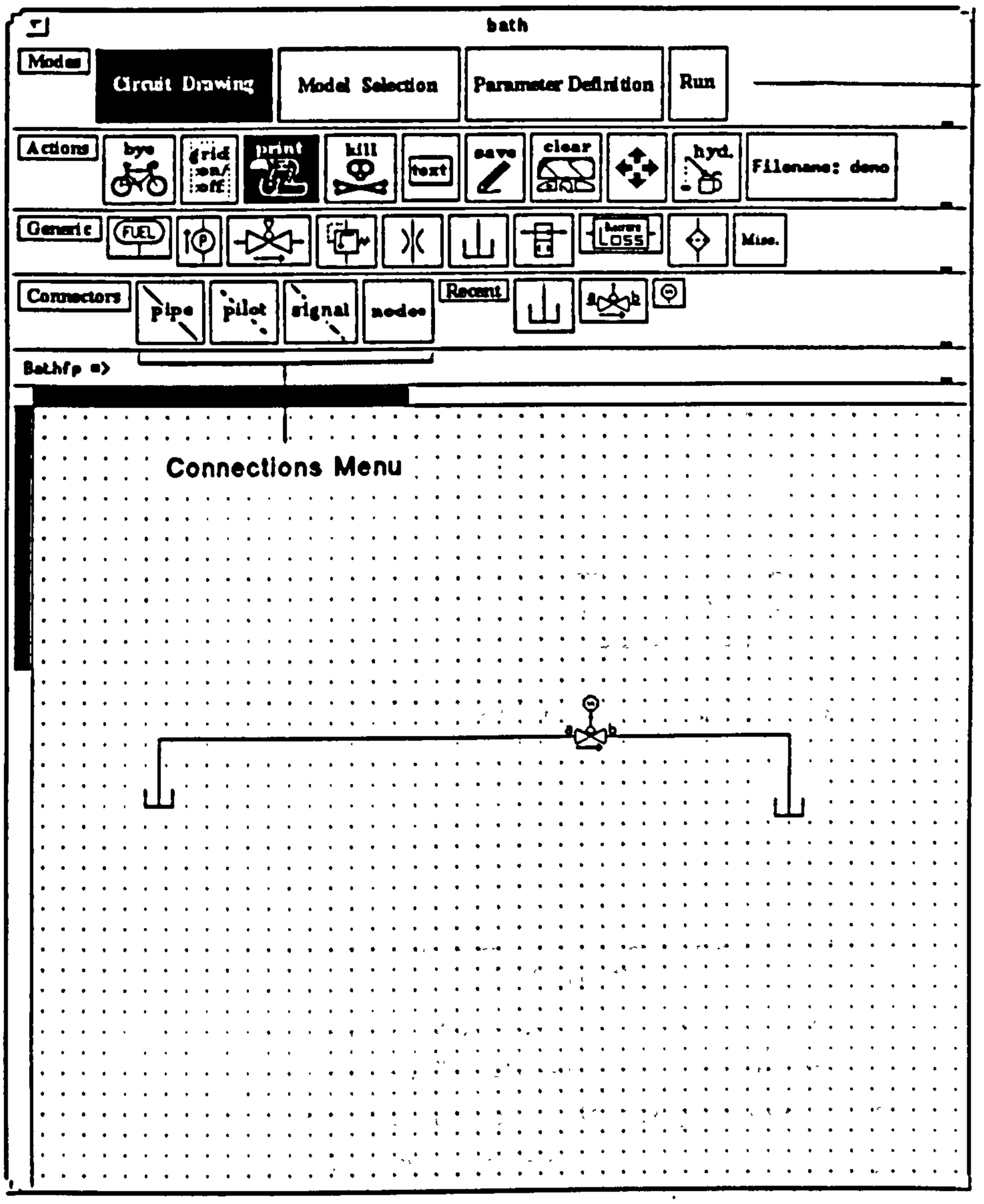

Figure 3.14 Network Draw, Bath*fp*

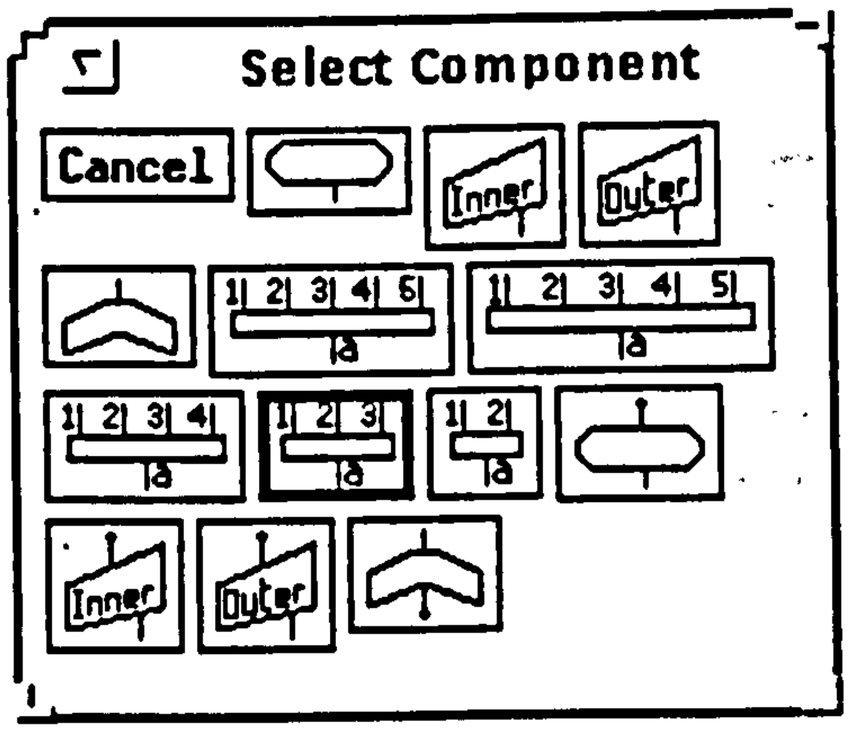

Figure 3.15 Generic Component Pop Up, Bath*fp*

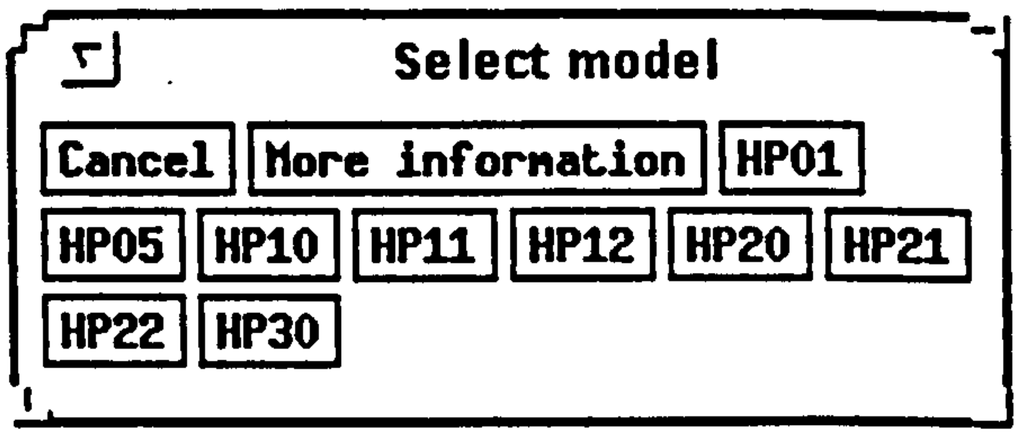

Figure 3.16 Model List, Bath*fp*

Change Parameter

Model *TKCT (1)

*Centre tank pressure 0 bar
Surface pressure in tank 1 bar
Total volume 41545 L
Unusable volume 524 L
Initial volume in tank 30000 L
Initial level 0 m
Indicator of inital state (1=volume,2=level) 1

Continue * = initial value of state variable

Figure 3.17 Parameter definition Pop Up, Bath*fp*

Oil properties

Operational parameters are given in the box below. To change any parameter select with cursor. Exit oil properties by selecting Continue

Oil type : Default
Volumetric fractional air content: 0.1
Saturation pressure : 0 [bar]
Operating temperature : 40 [C]

Continue

Corresponding oil properties are:

Density : 860 [Kg/m3]
Bulk modulus : 17000 [bar]
Kinematic viscosity : 50 [cSt]
Absolute viscosity : 43 [cP]

Figure 3.18 Fluid Set up, Bath*fp*

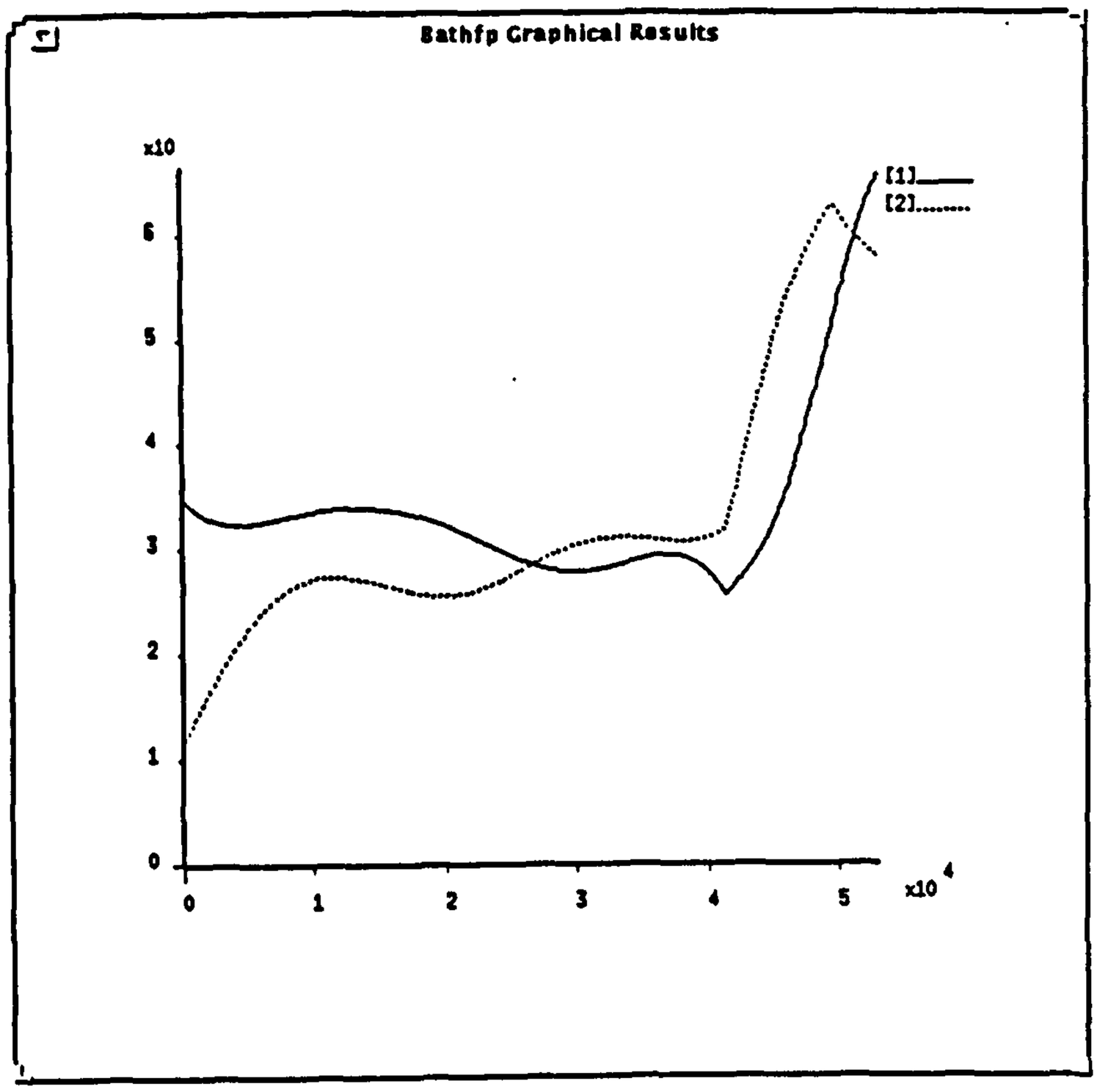

Figure 3.19 Typical Time History, Bath*fp*

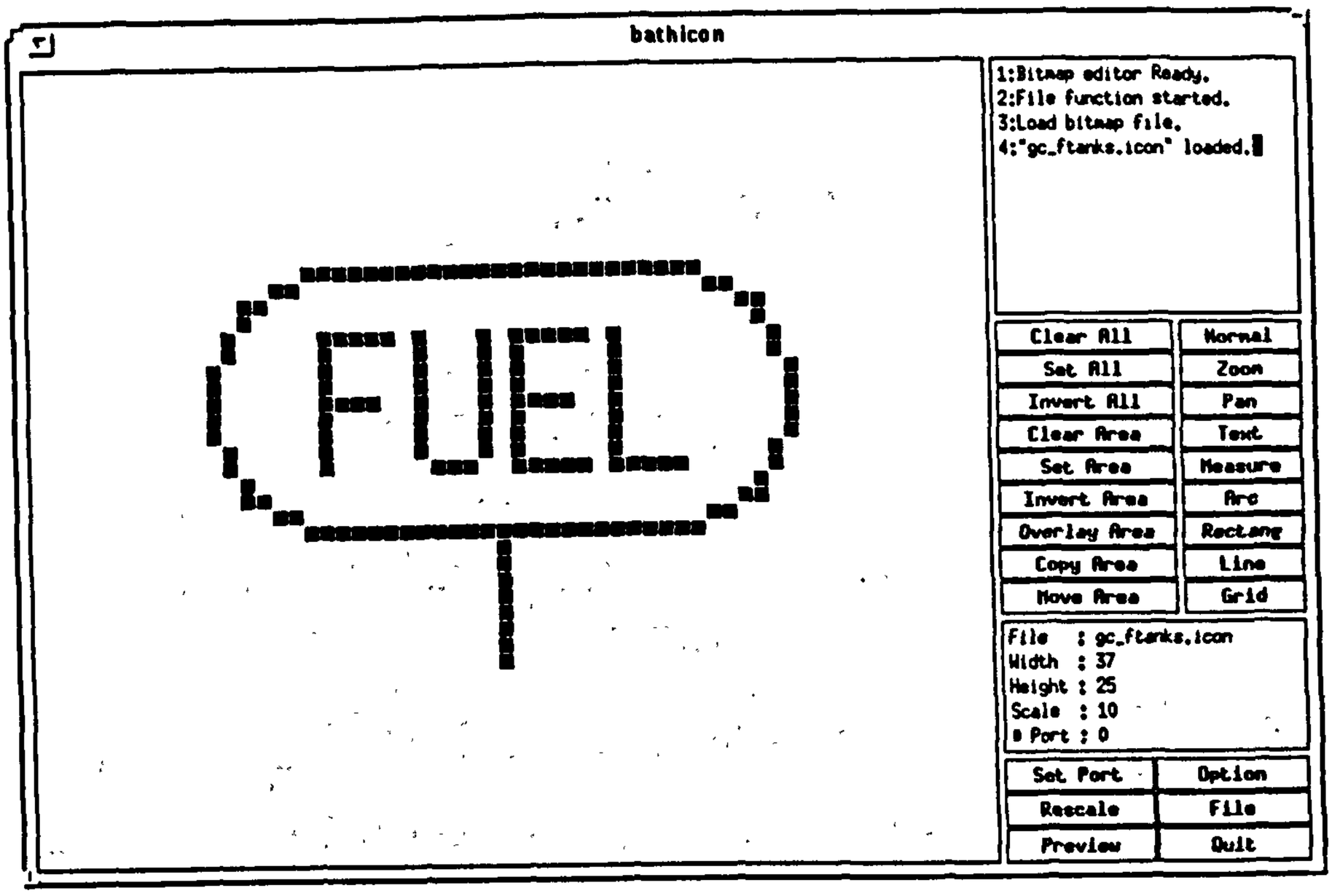

Editor Functions

Figure 3.20 BathICON

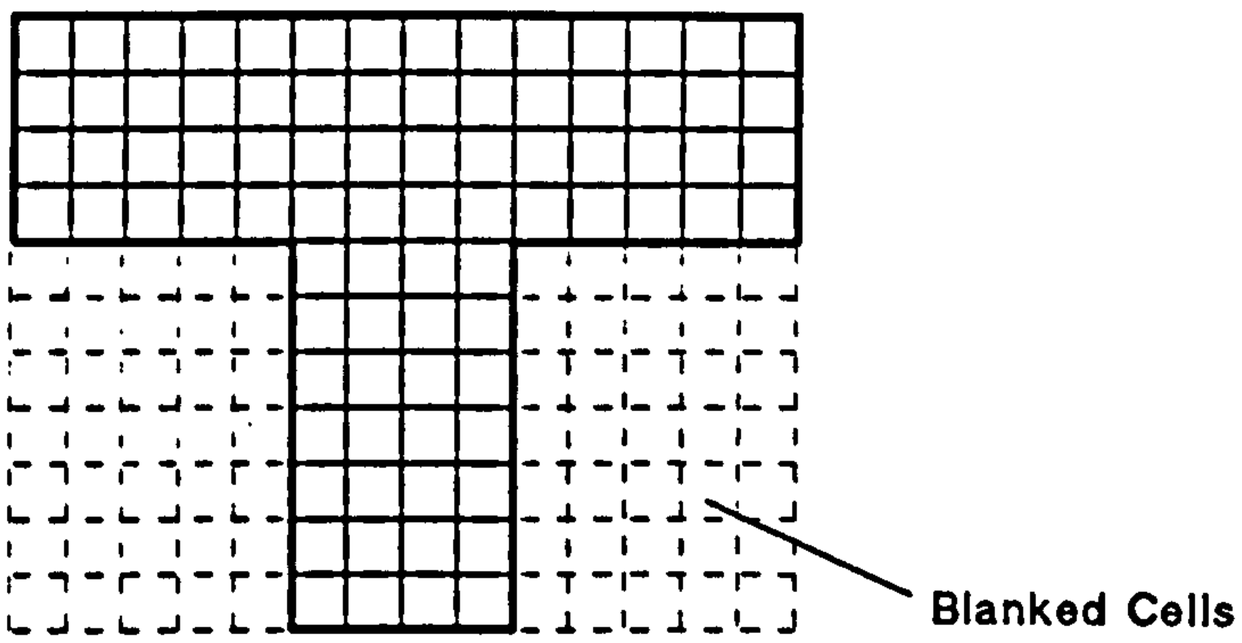

a. Structured Mesh

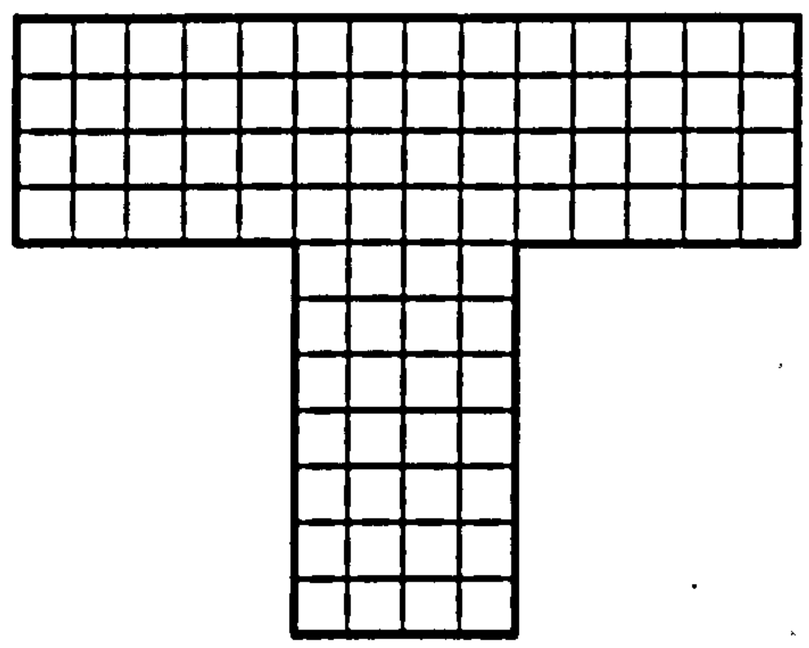

b. Unstructured Meshes

Figure 4.1 Structured and Unstructured Meshes

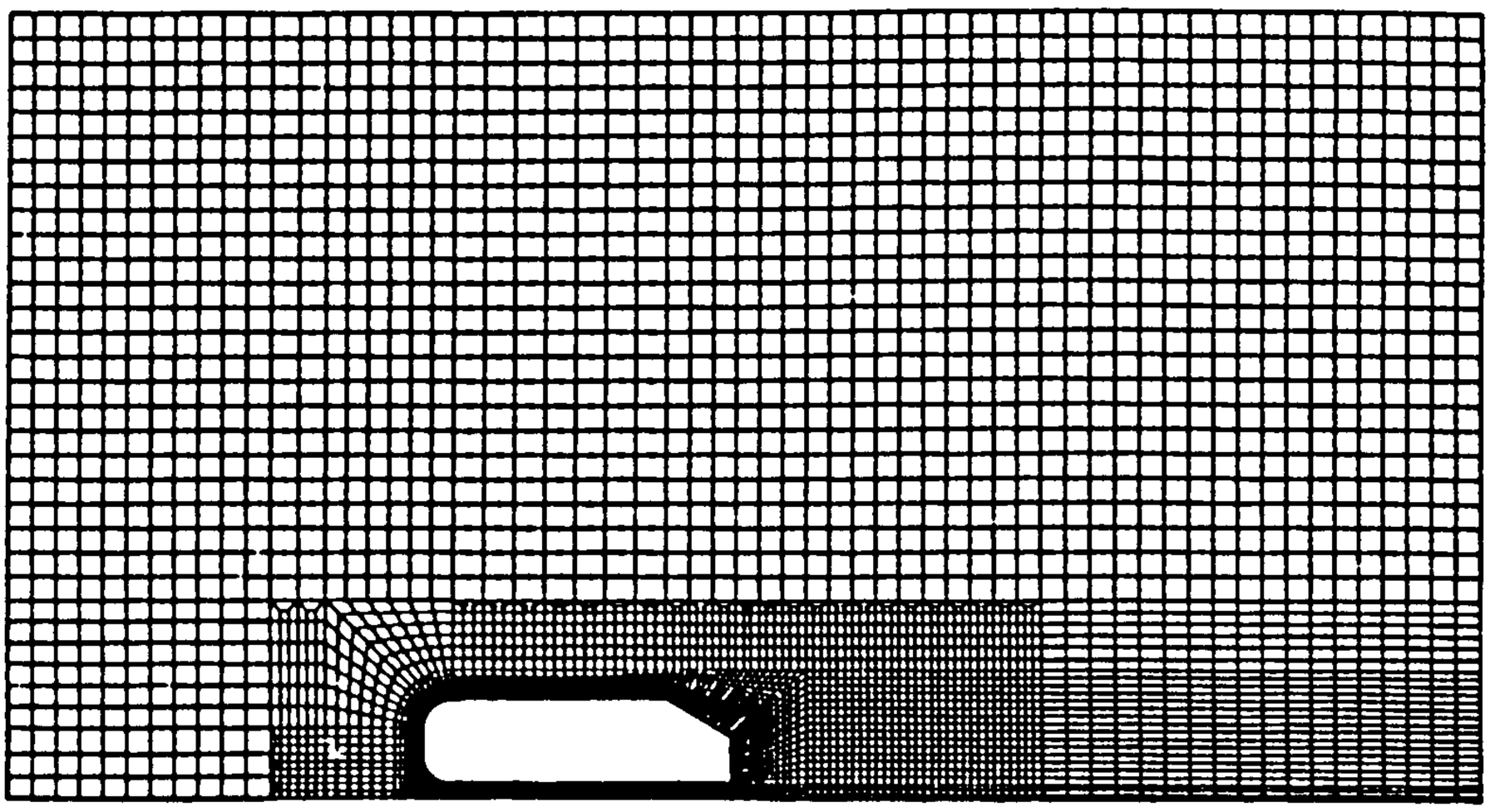

Figure 4.2 Example of Local mesh Refinement.

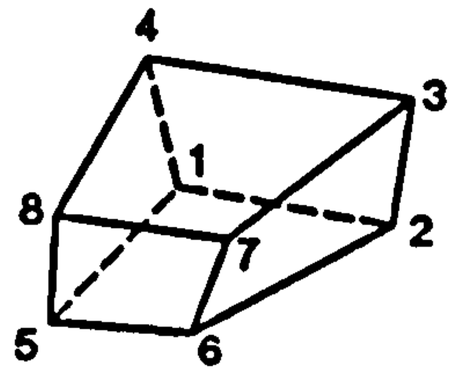

Hexahedron

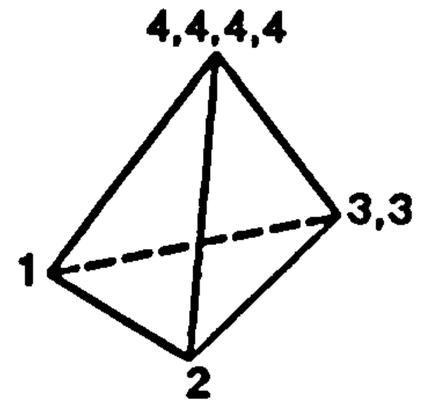

Tetrahedron

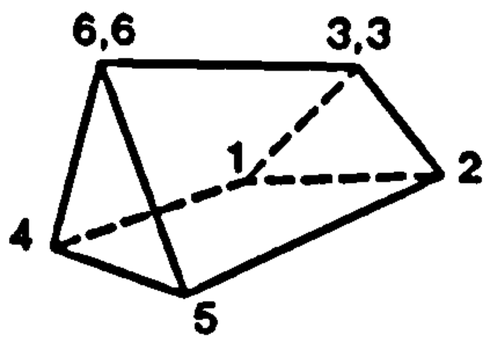

Triangular Prism

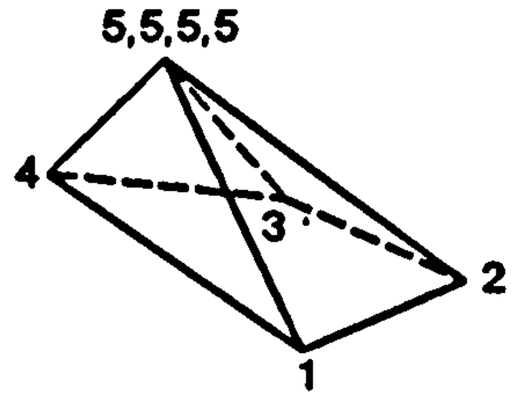

Pyramid

Figure 4.3 Star-CD Cell Types

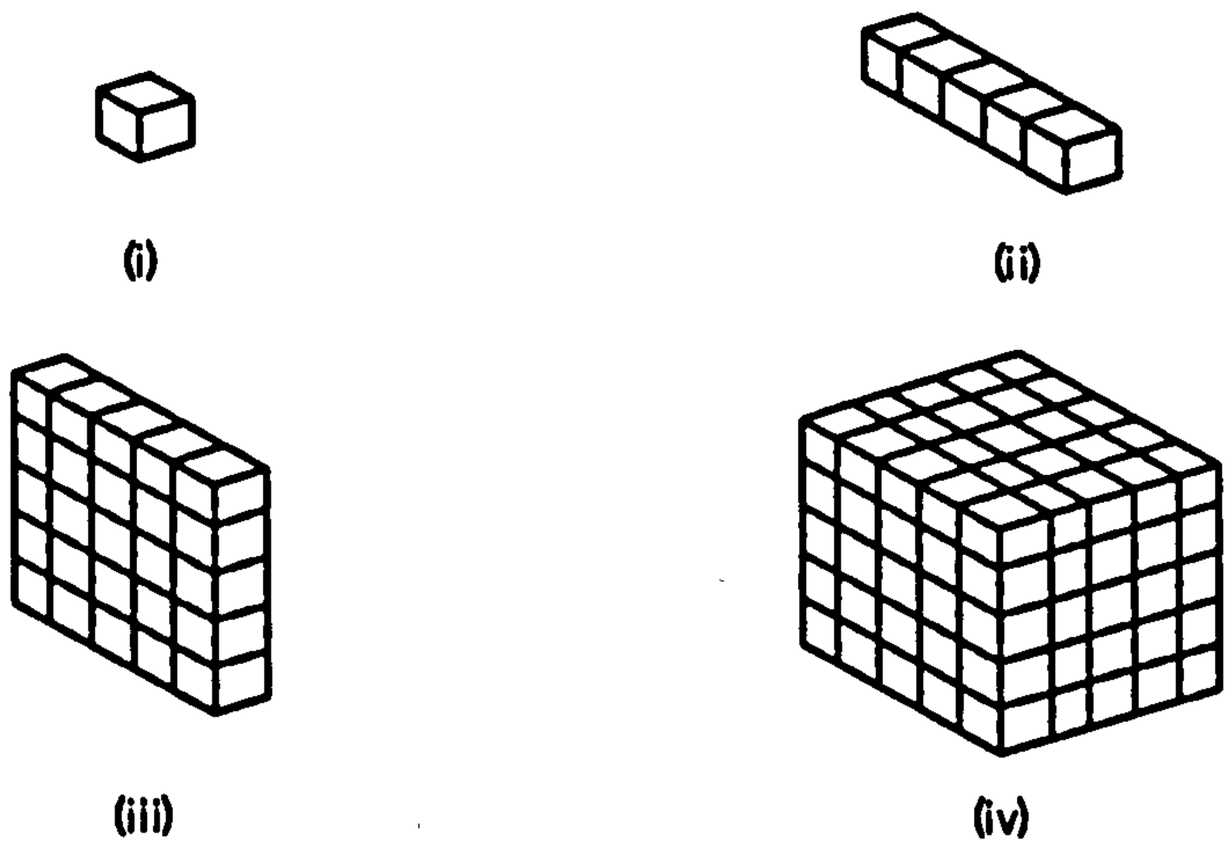

Figure 4.4 Generation of Simple Mesh

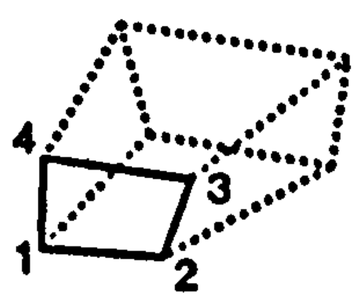

Hexahedron

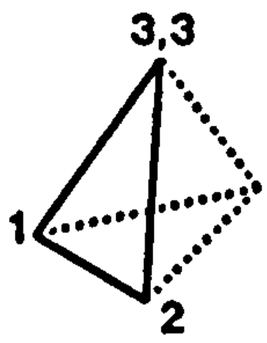

Tetrahedron

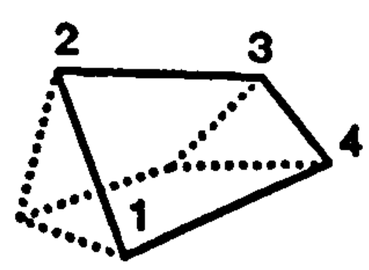

Triangular Prism

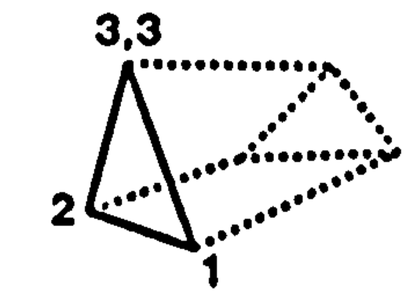

Triangular Prism

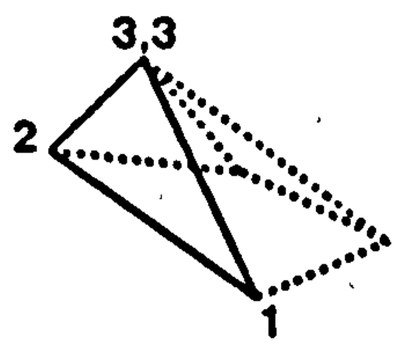

Pyramid

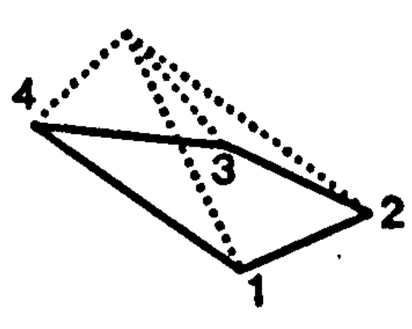

Pyramid

Figure 4.5 Star-CD Boundary Cells.

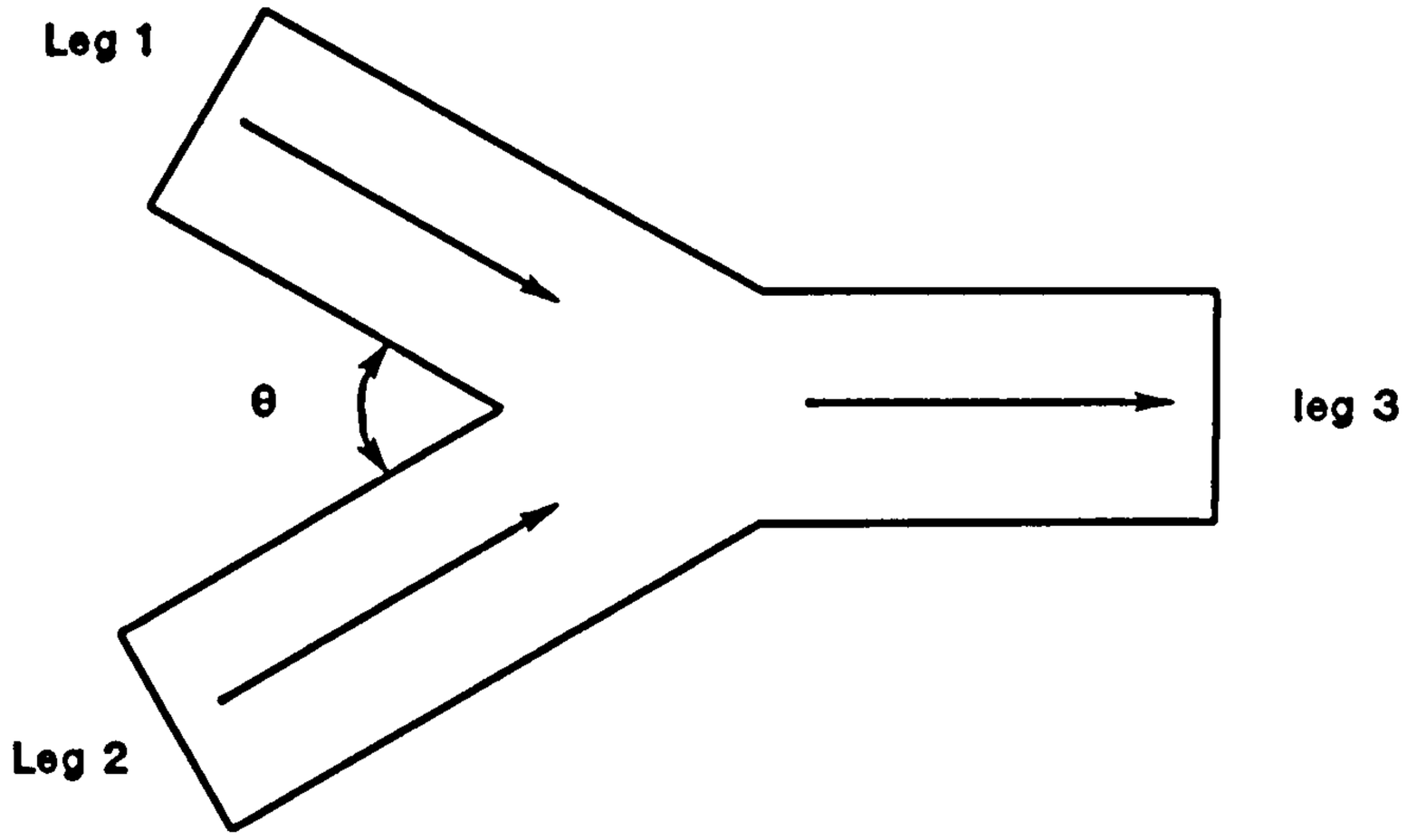

Figure 5.1 Layout and Numbering Convention Applied to 'Y' Junction

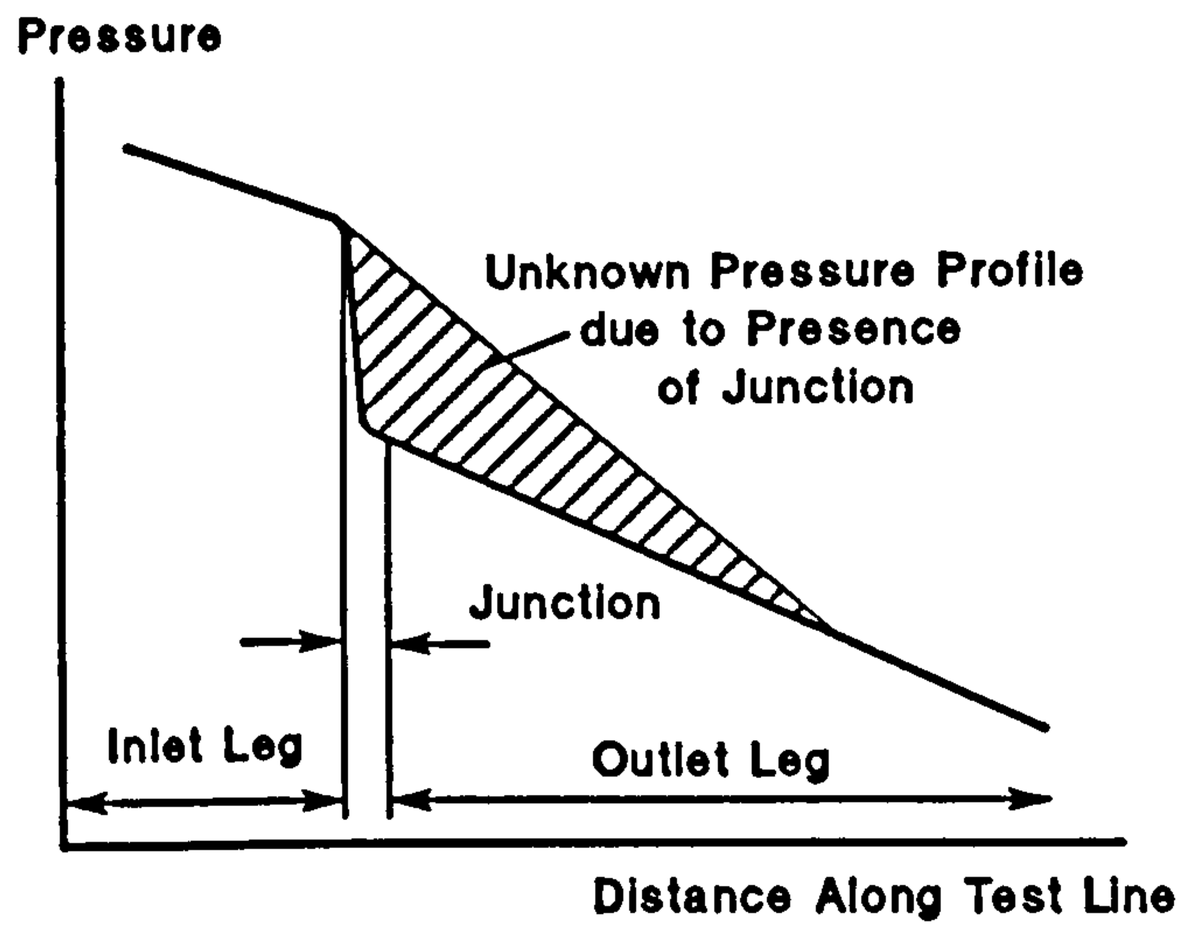

Figure 5.2 Pressure Profile due to Presence of 'Y' Junction

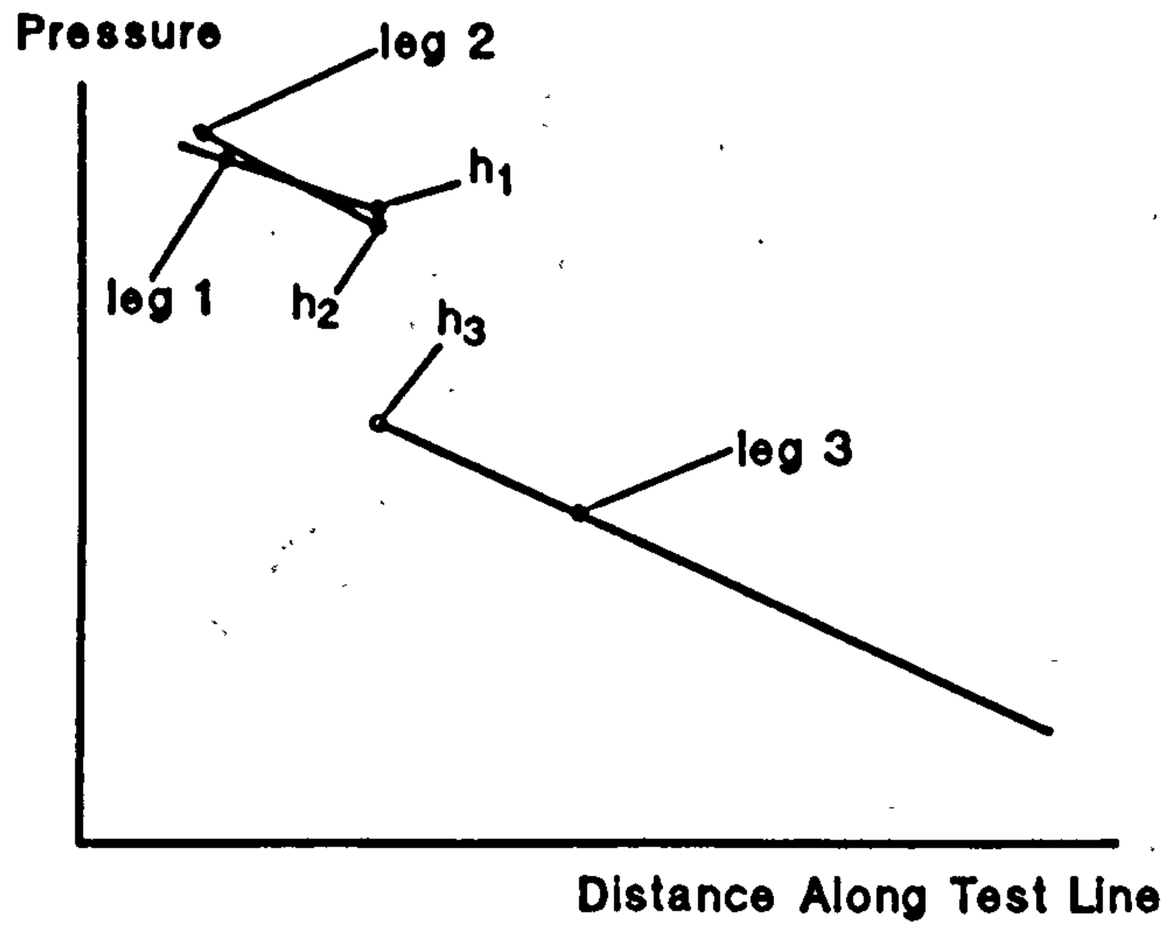

Figure 5.3 Assumed Pressure Profile due to Presence of 'Y' Junction

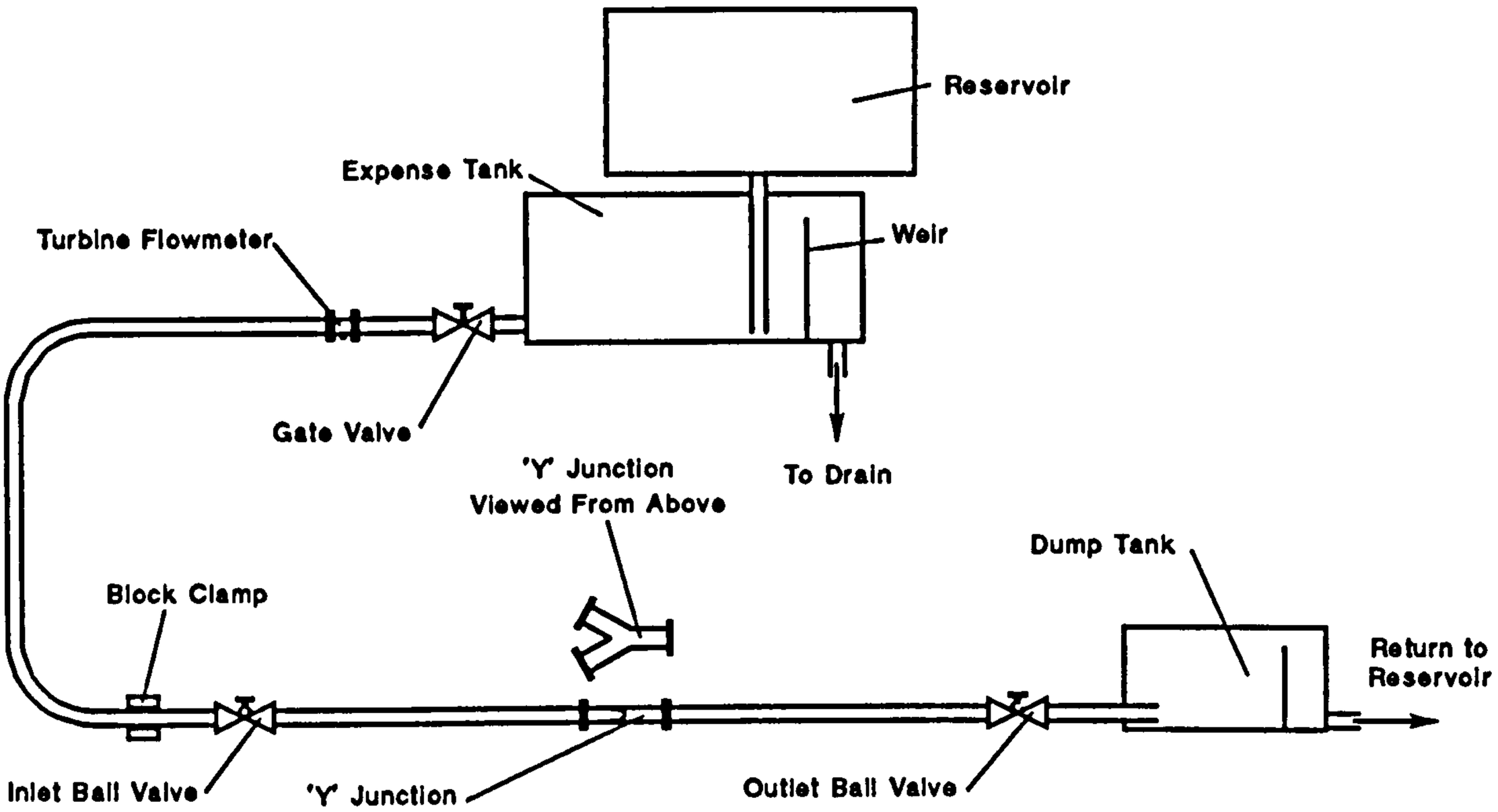

Figure 5.4 Schematic Diagram of 'Y' Junction Test Rig

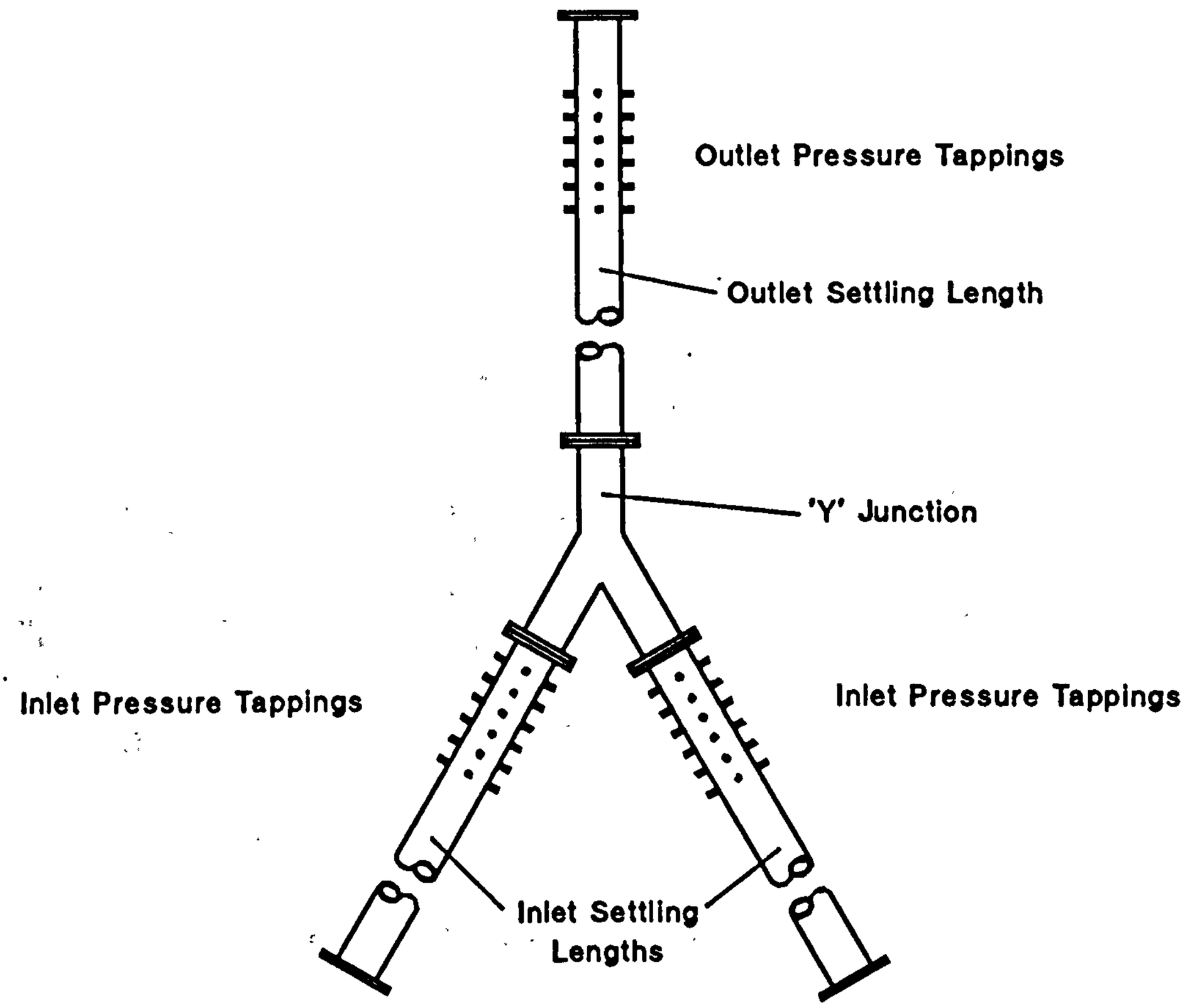

Figure 5.5 Test Section and Settling Lengths

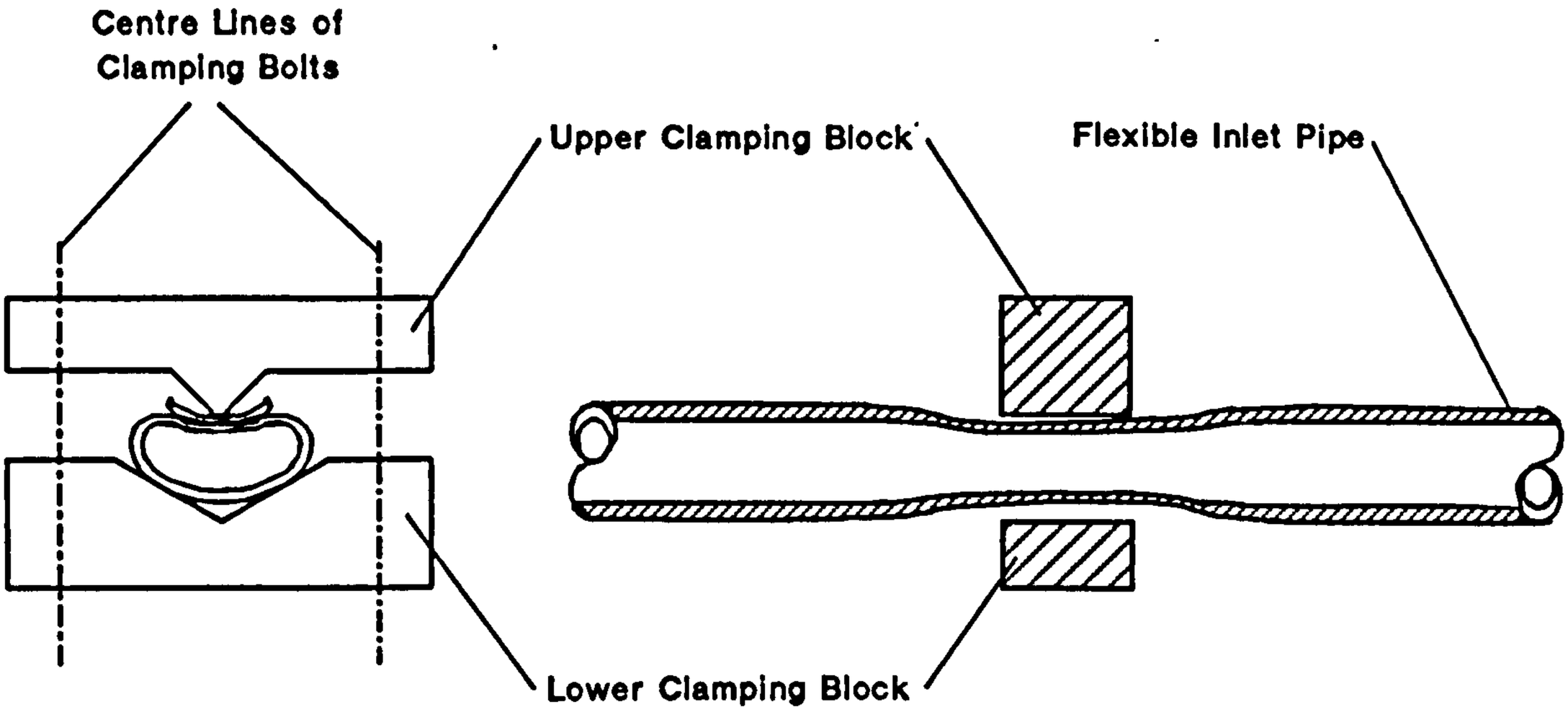

Figure 5.6 Flow Rate Throttling Clamp

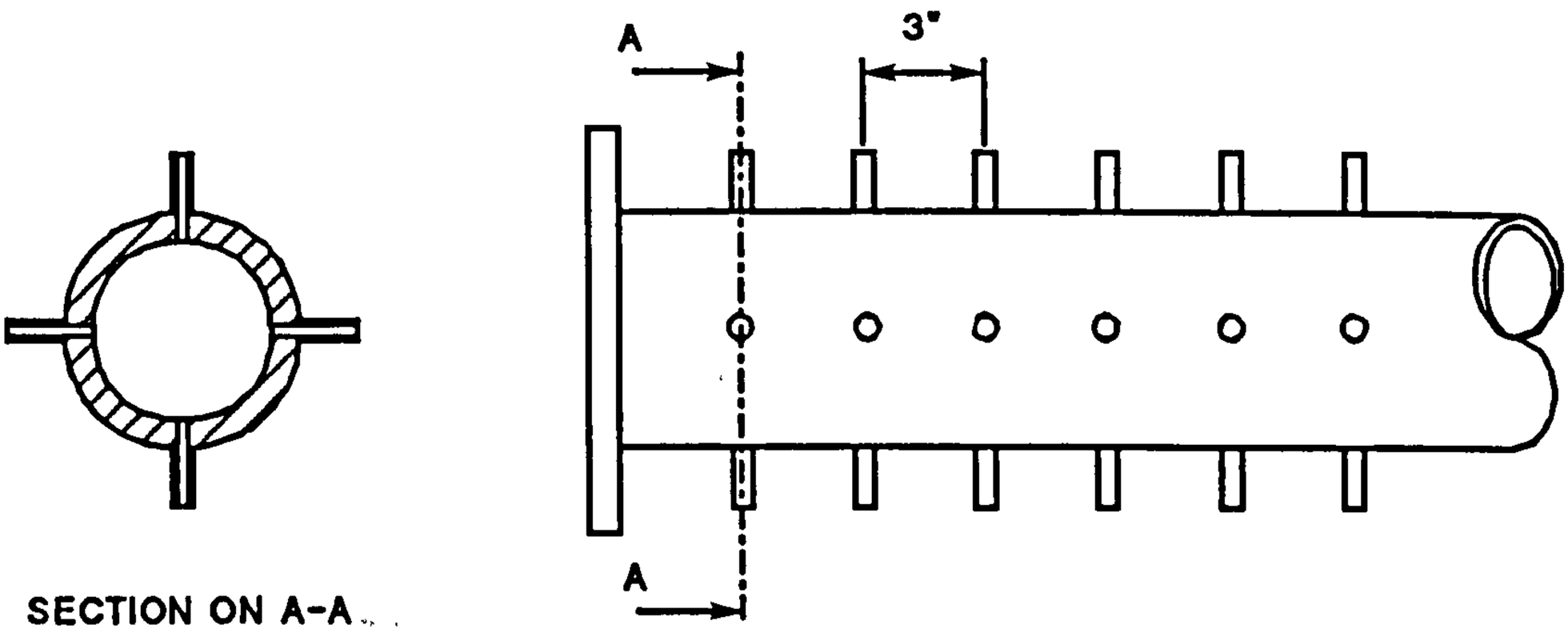

Figure 5.7 Layout of Pressure Tappings

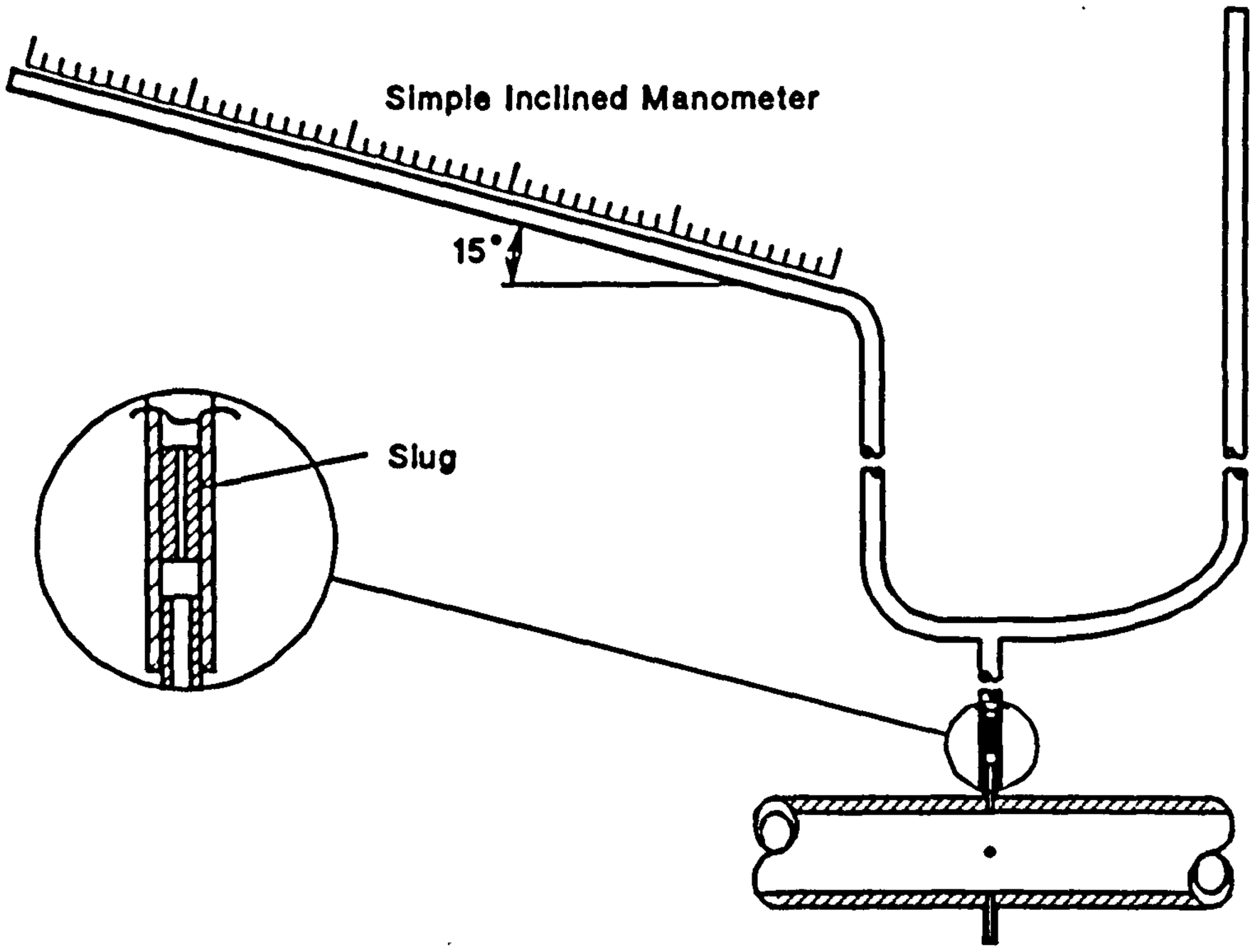

Figure 5.8 Pressure Oscillation Reduction Methods

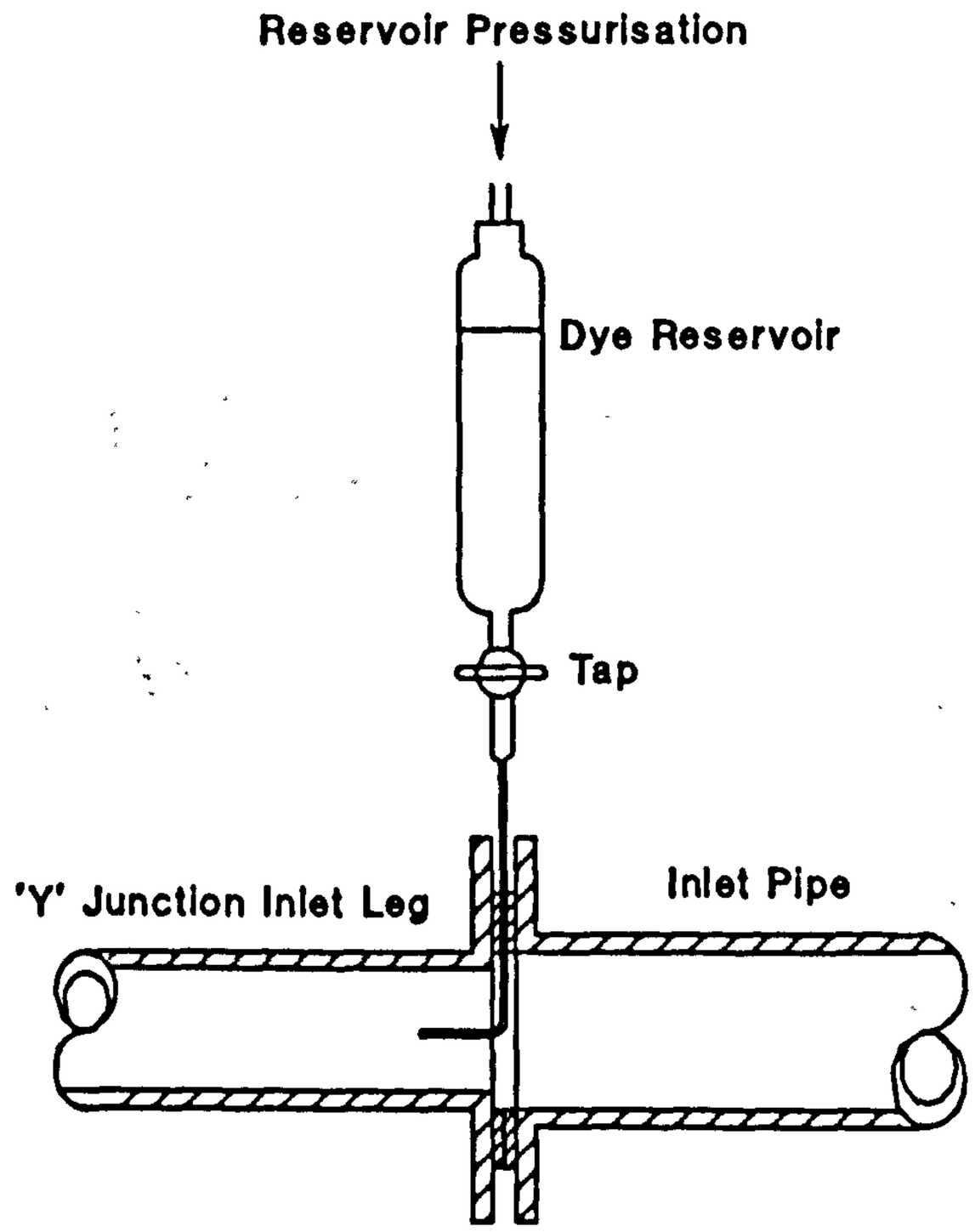

Figure 5.9 Flow Visualisation Equipment

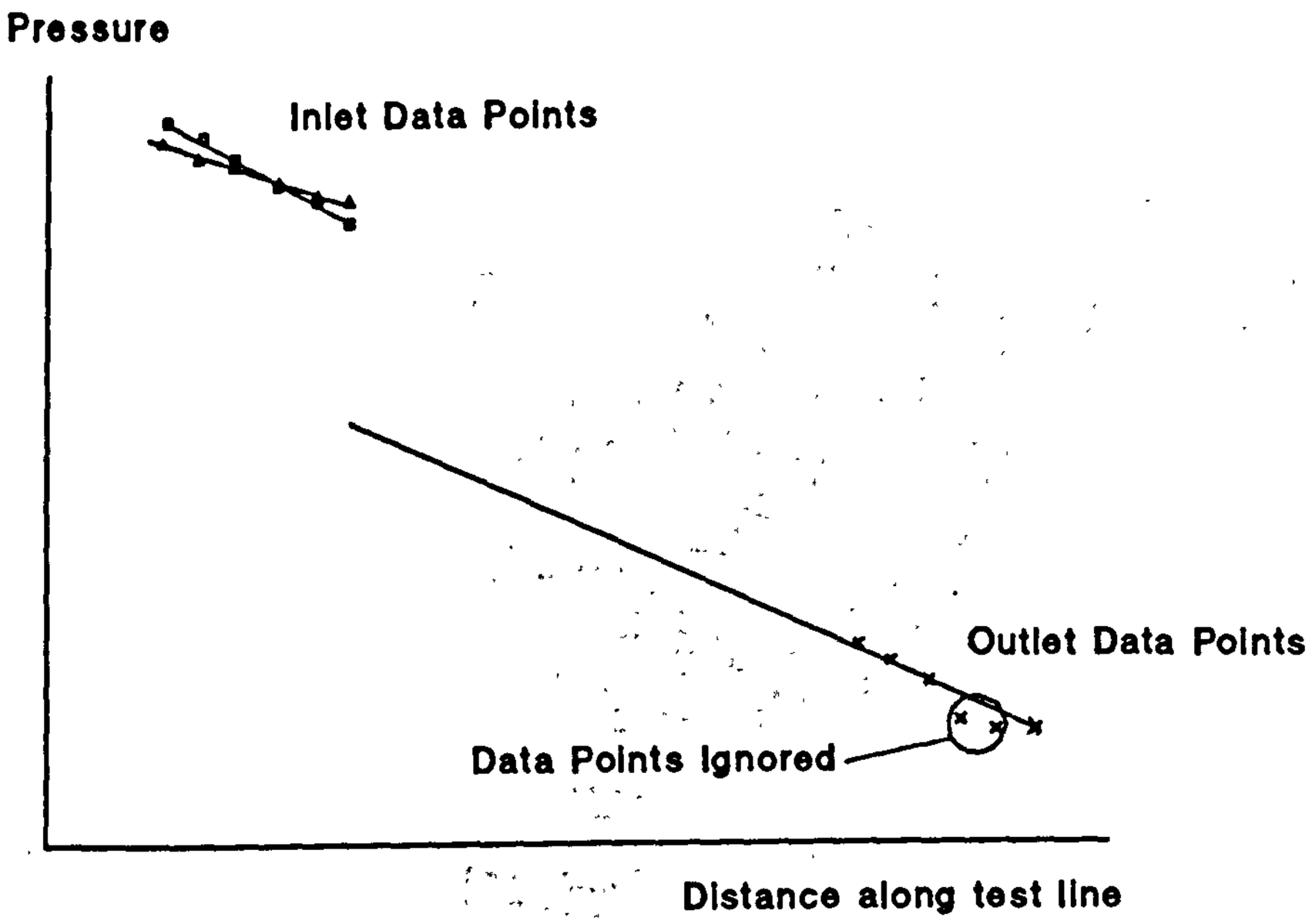

Figure 5.10 Illustrative Pressure Gradient

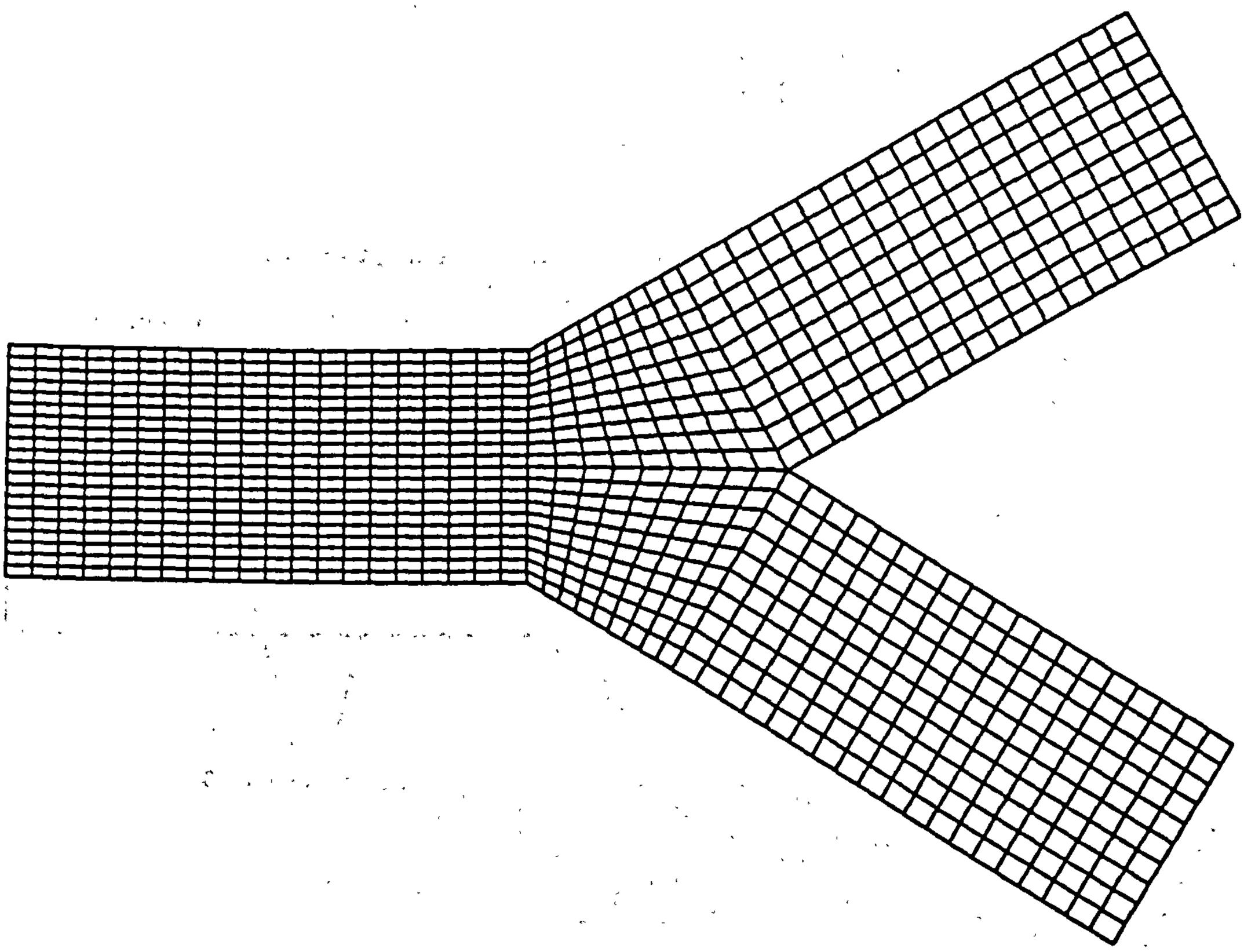

Figure 5.11 Two-Dimensional CFD 'Y' Junction Model.

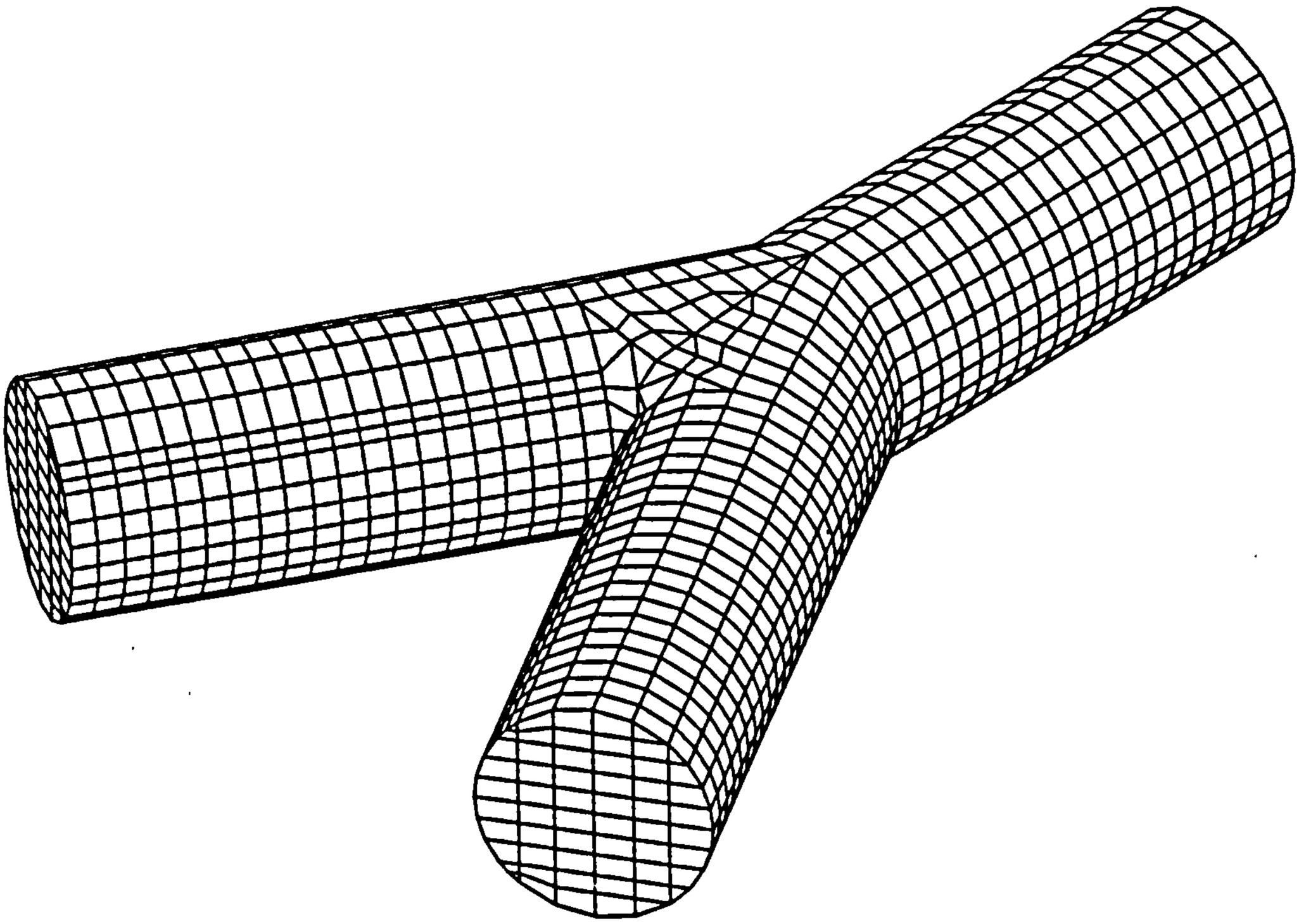

Figure 5.12 Three-Dimensional CFD 'Y' Junction Model.

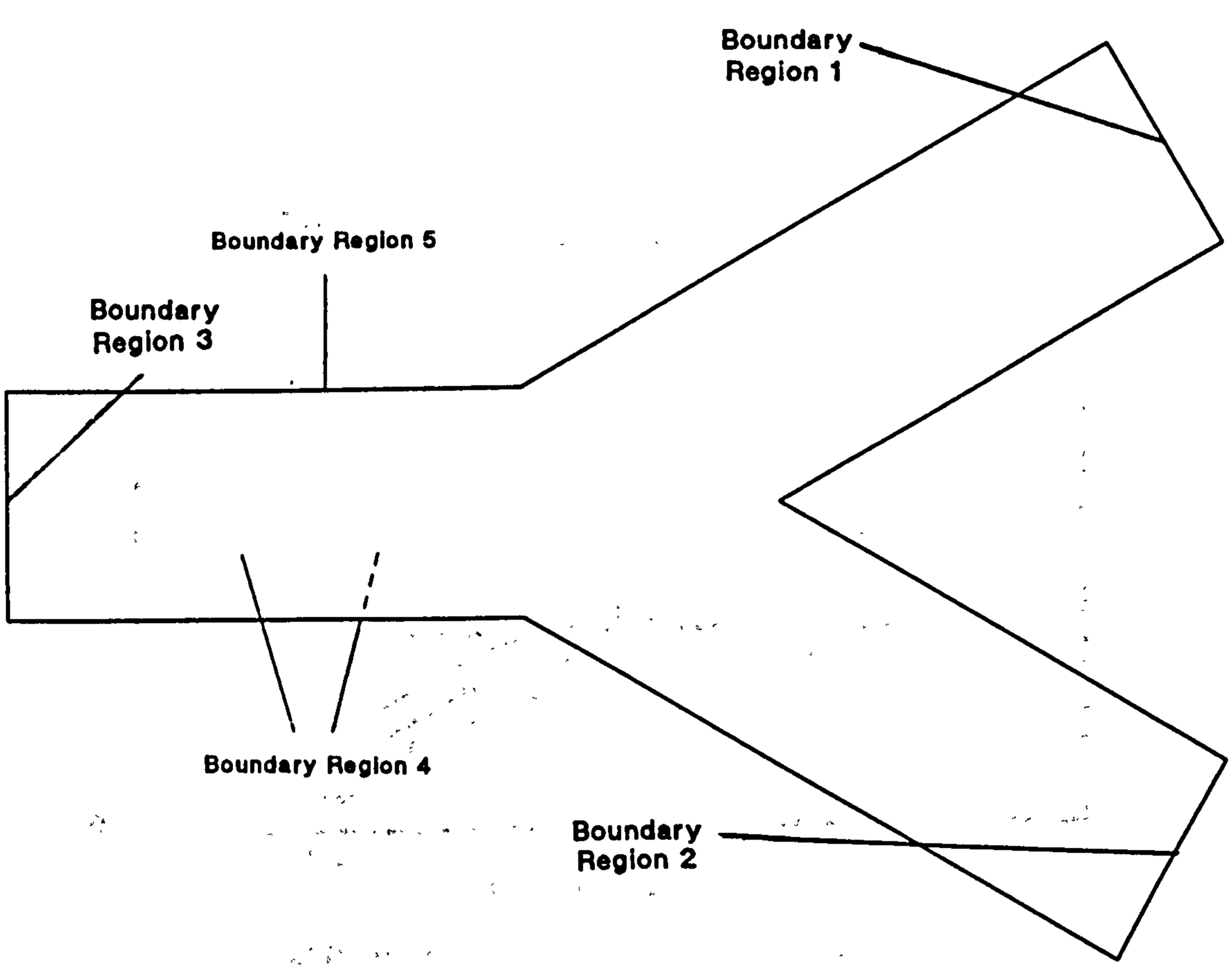

Figure 5.13 Boundary Regions for Two-Dimensional 'Y' Junction.

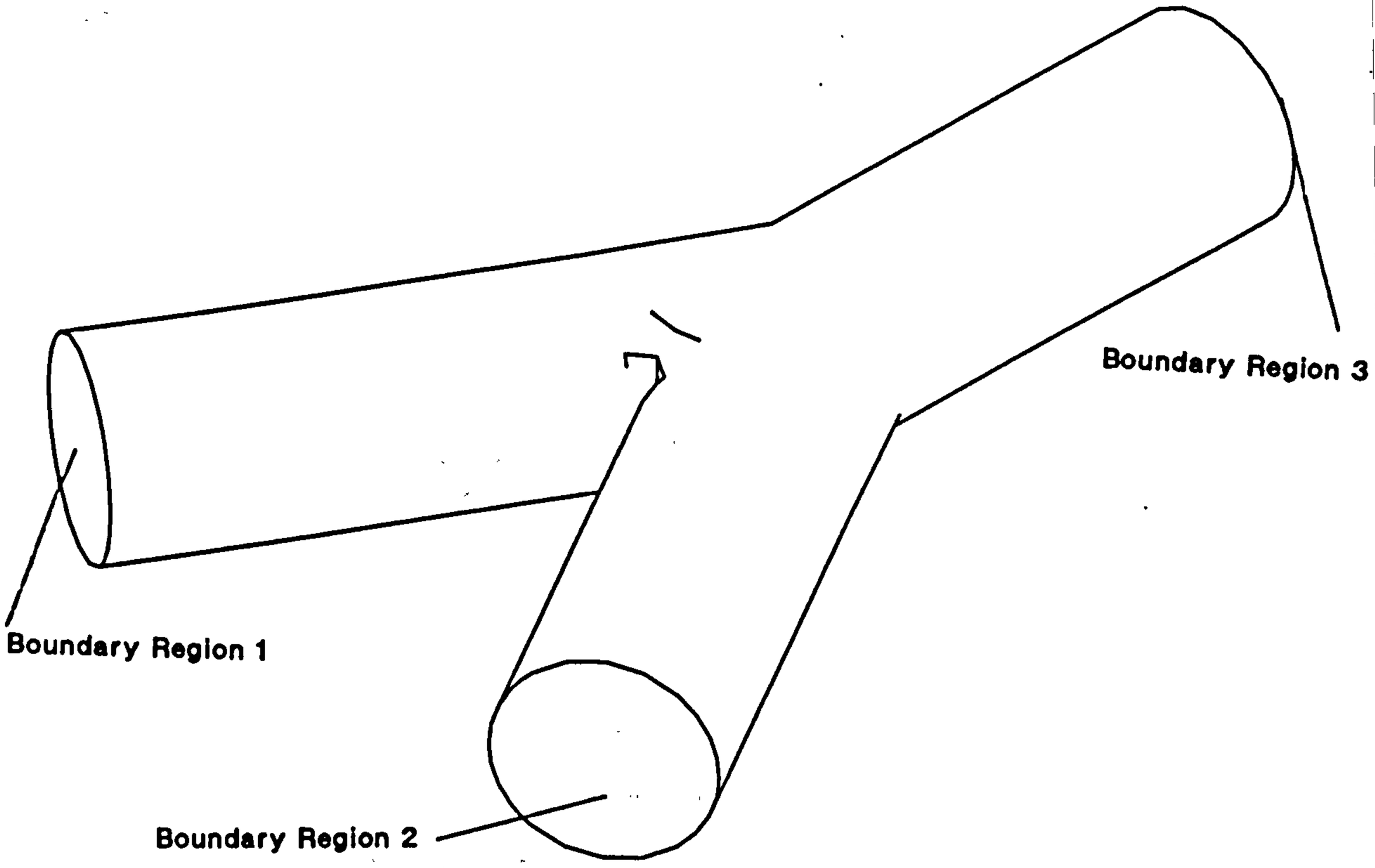

Figure 5.14 Boundary Regions for Three-Dimensional 'Y' Junction.

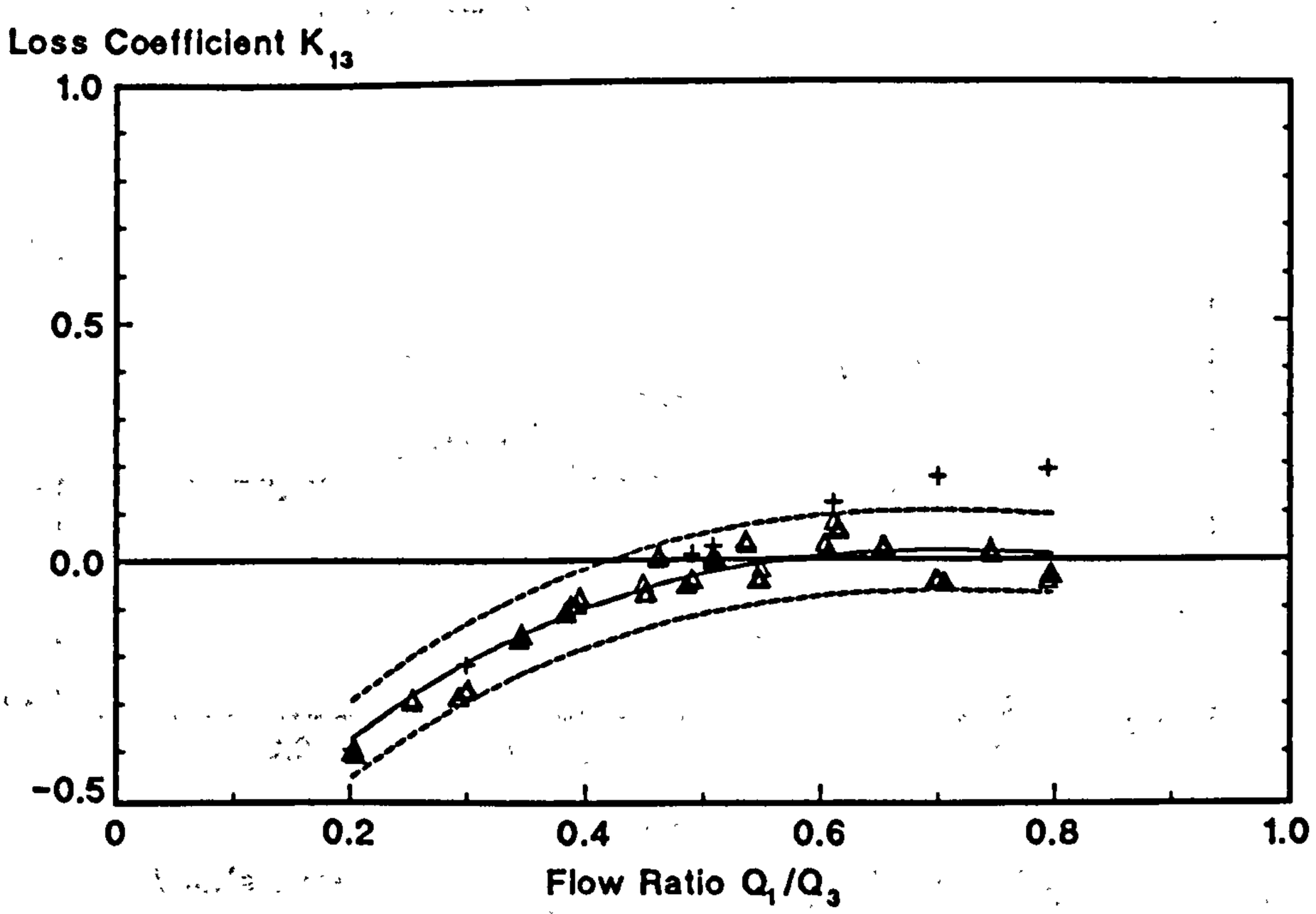

Figure 5.15 Loss Coefficient Data for 30° 'Y' Junction

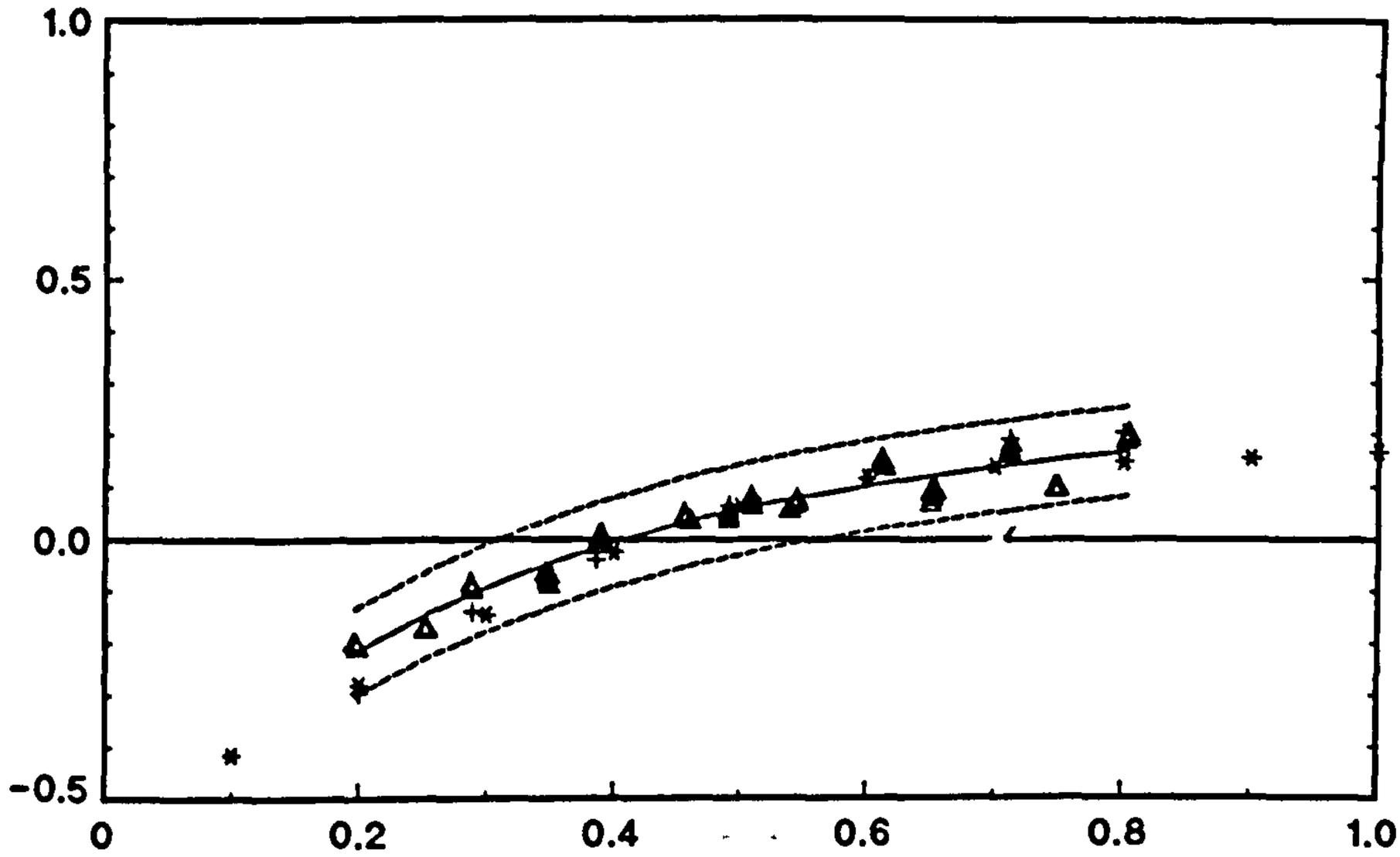

Figure 5.16 Loss Coefficient Data for 60° 'Y' Junction

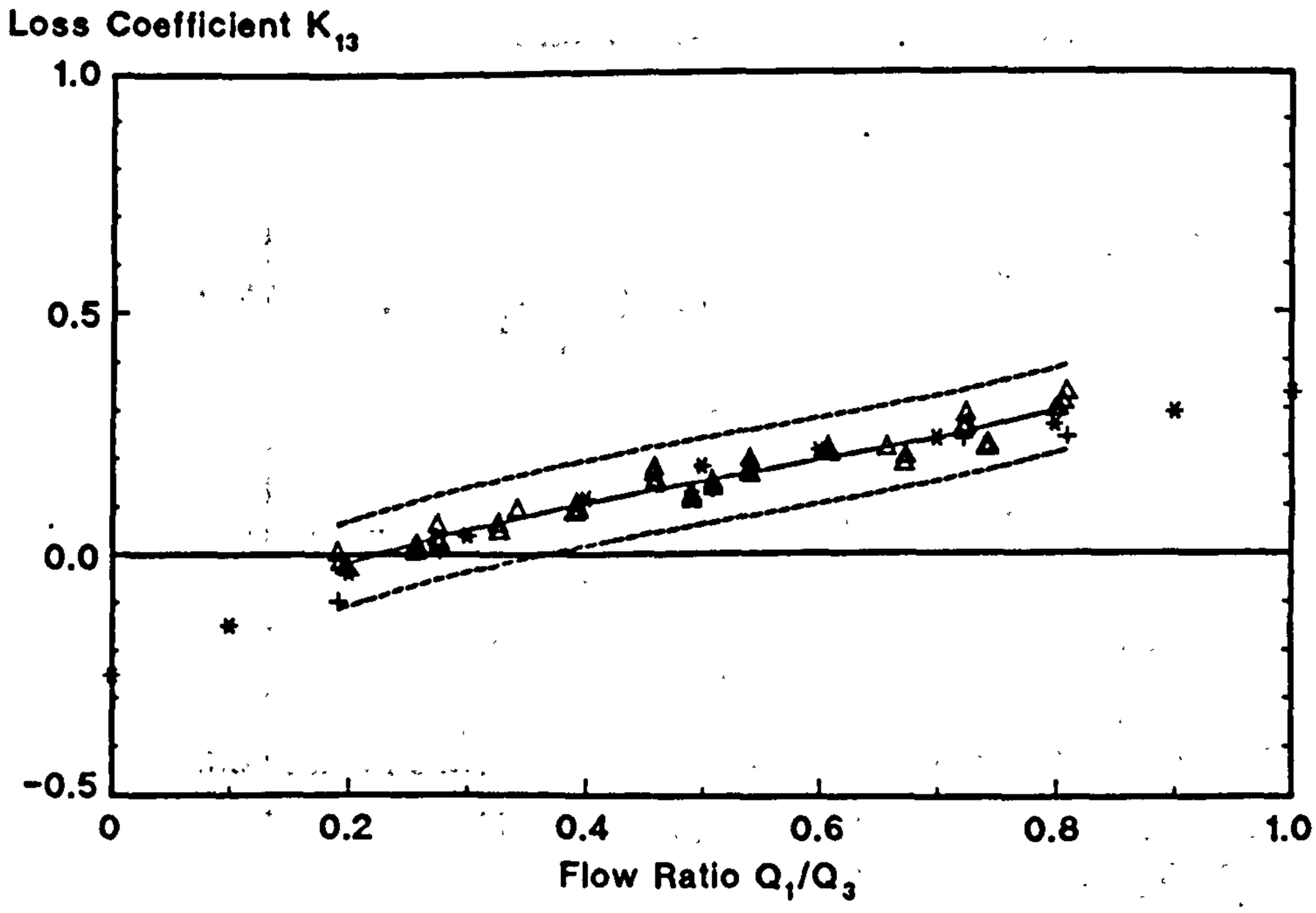

Figure 5.17 Loss Coefficient Data for 90° 'Y' Junction

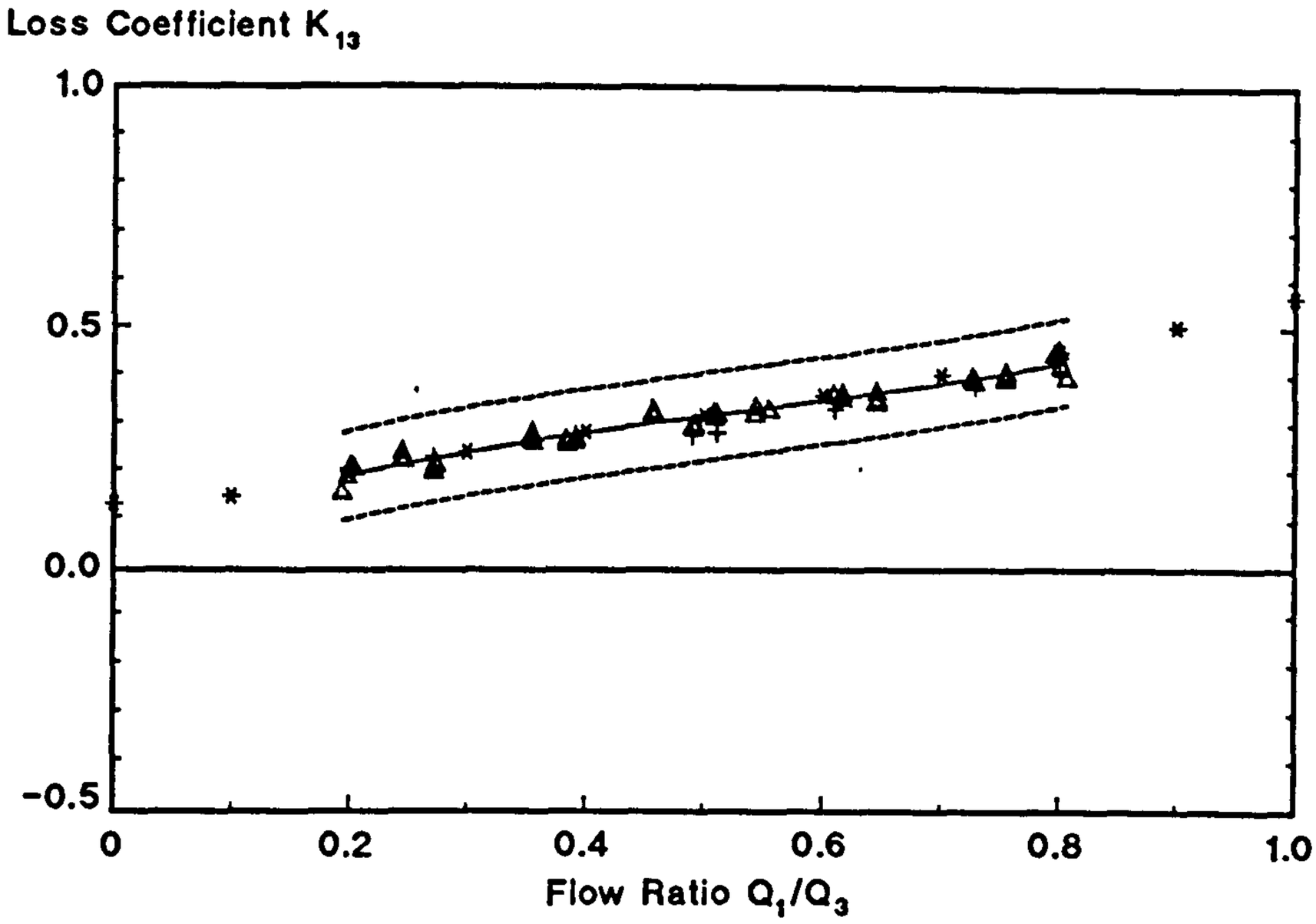

Figure 5.18 Loss Coefficient Data for 120° 'Y' Junction

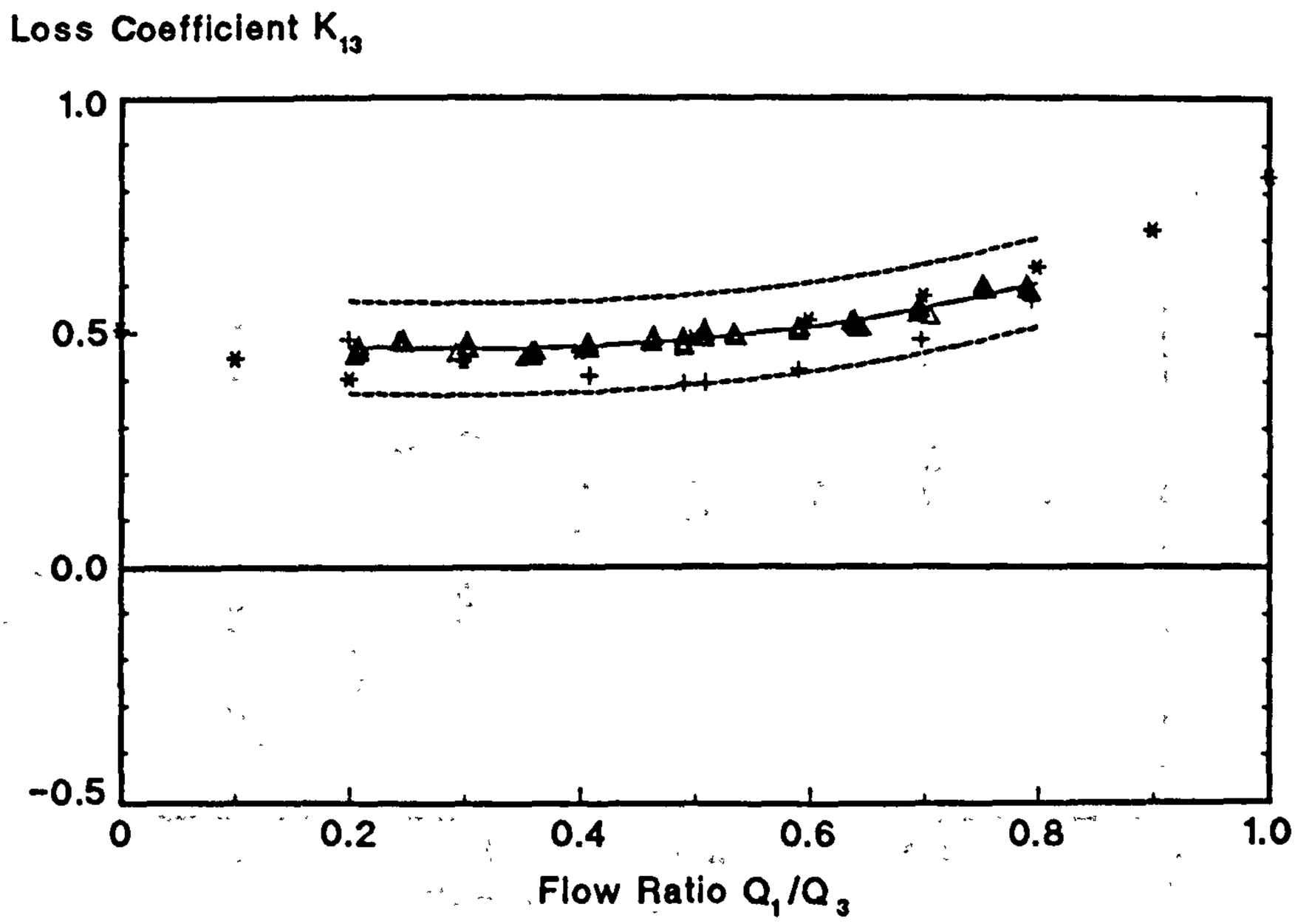

Figure 5.19 Loss Coefficient Data for 150° 'Y' Junction

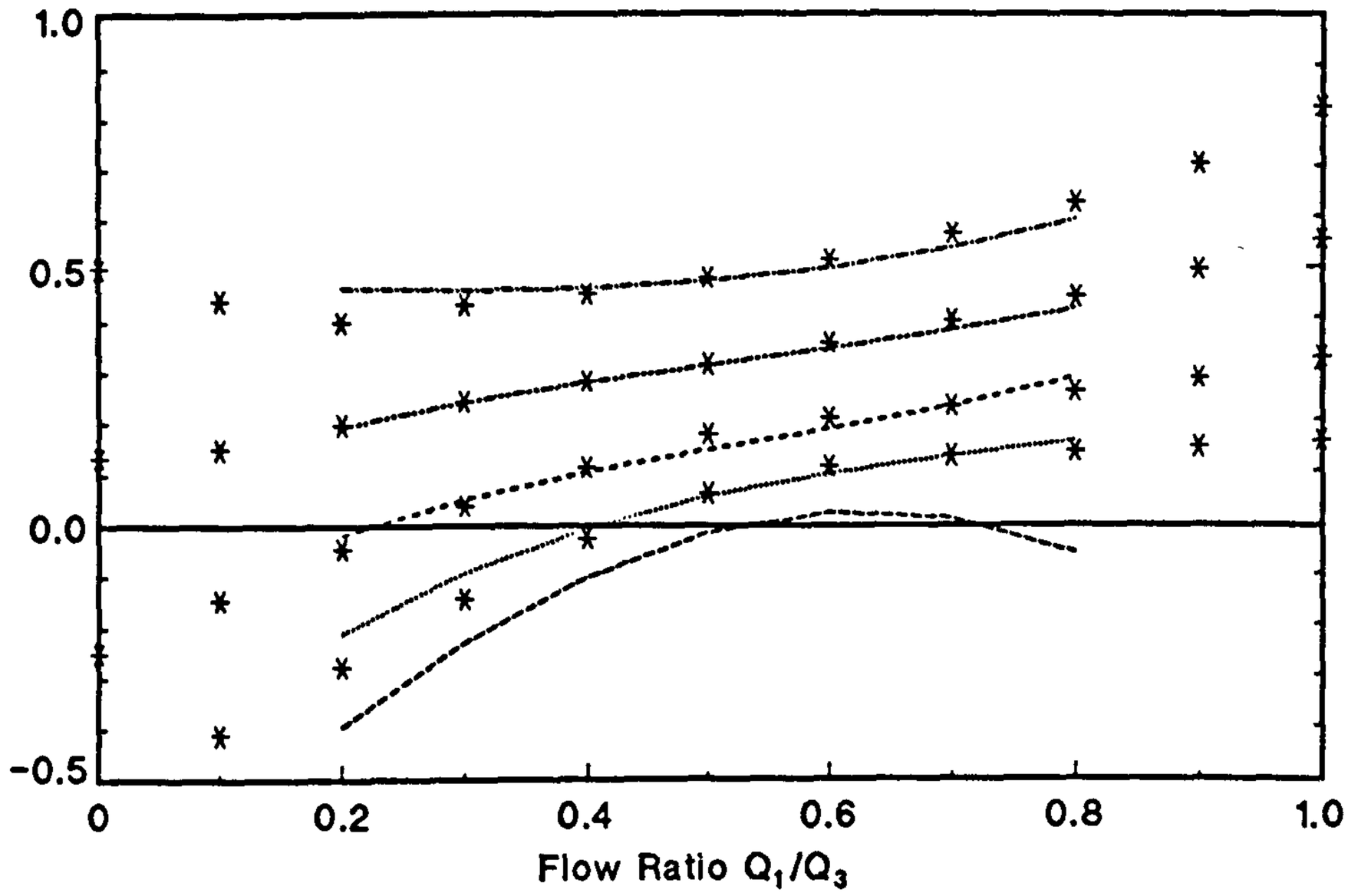

Figure 5.20 Summary of Loss Coefficient Data for all 'Y' Junctions
Miller's Data and Test Rig

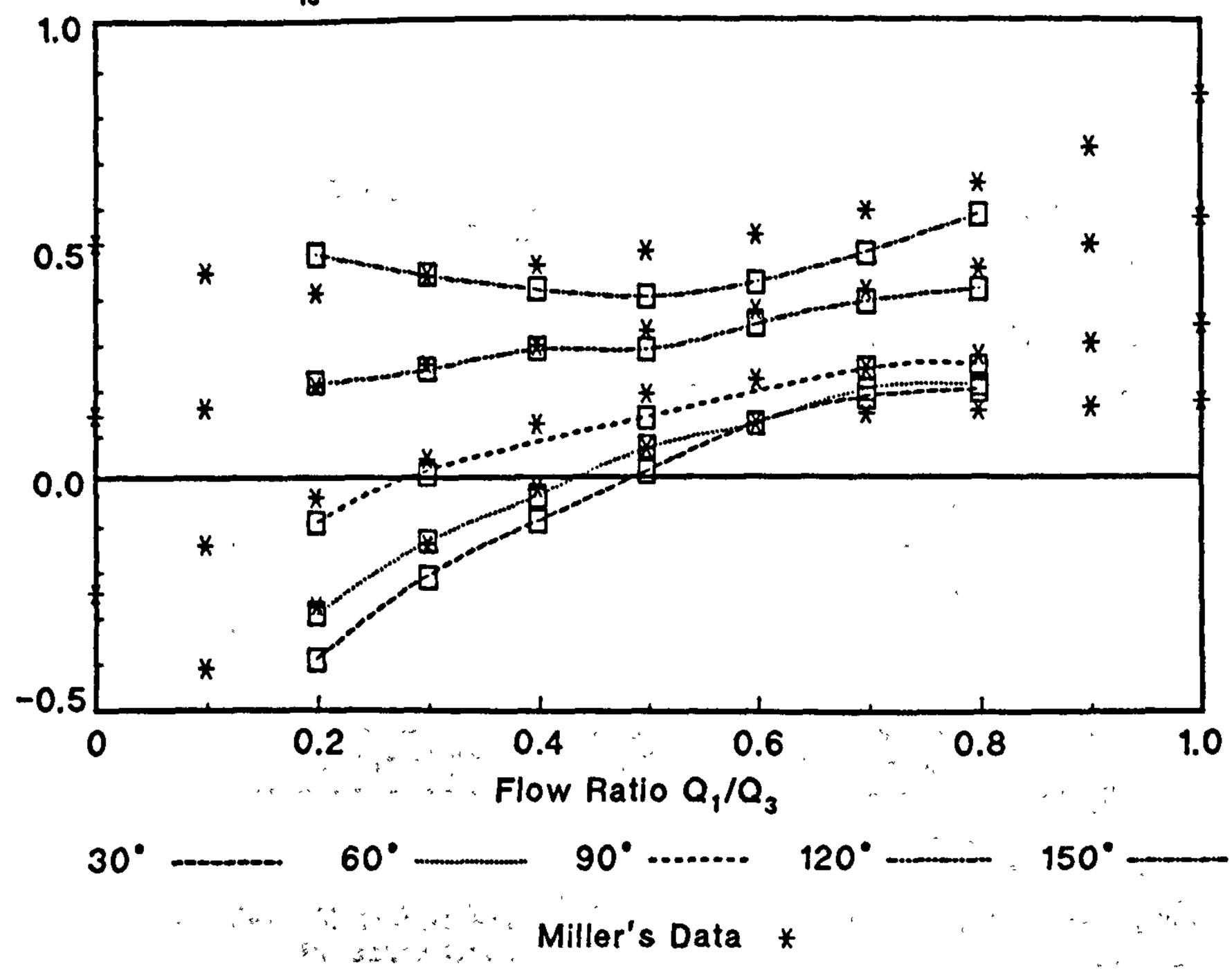

Figure 5.21 Summary of Loss Coefficient Data for all 'Y' Junctions
Miller's Data and CFD

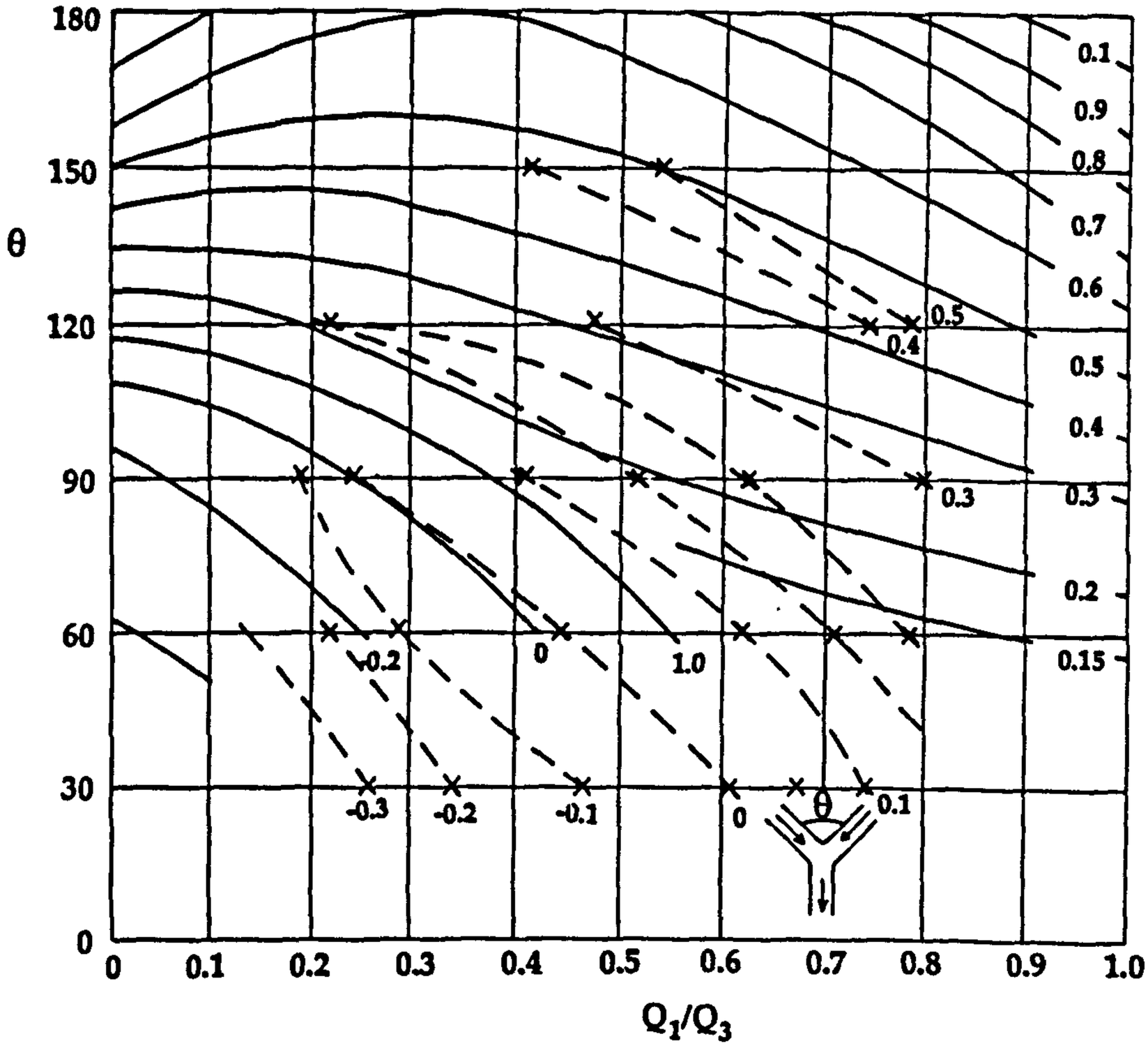

Figure 5.22 Constant Loss Coefficient Plot for all 'Y' Junctions.

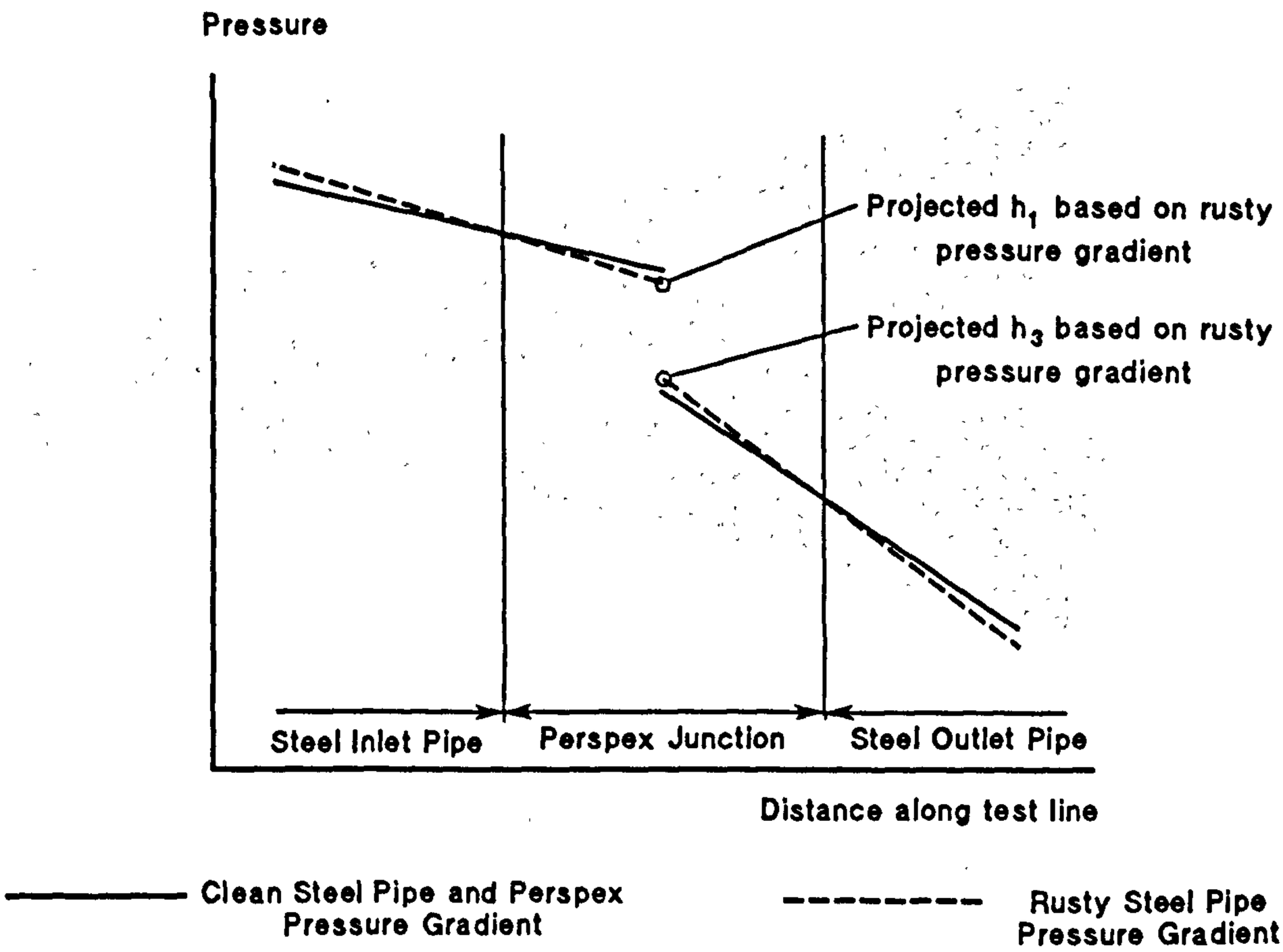

Figure 5.23 Effects of Contamination of Test Rig on Predicted Pressure Drop.

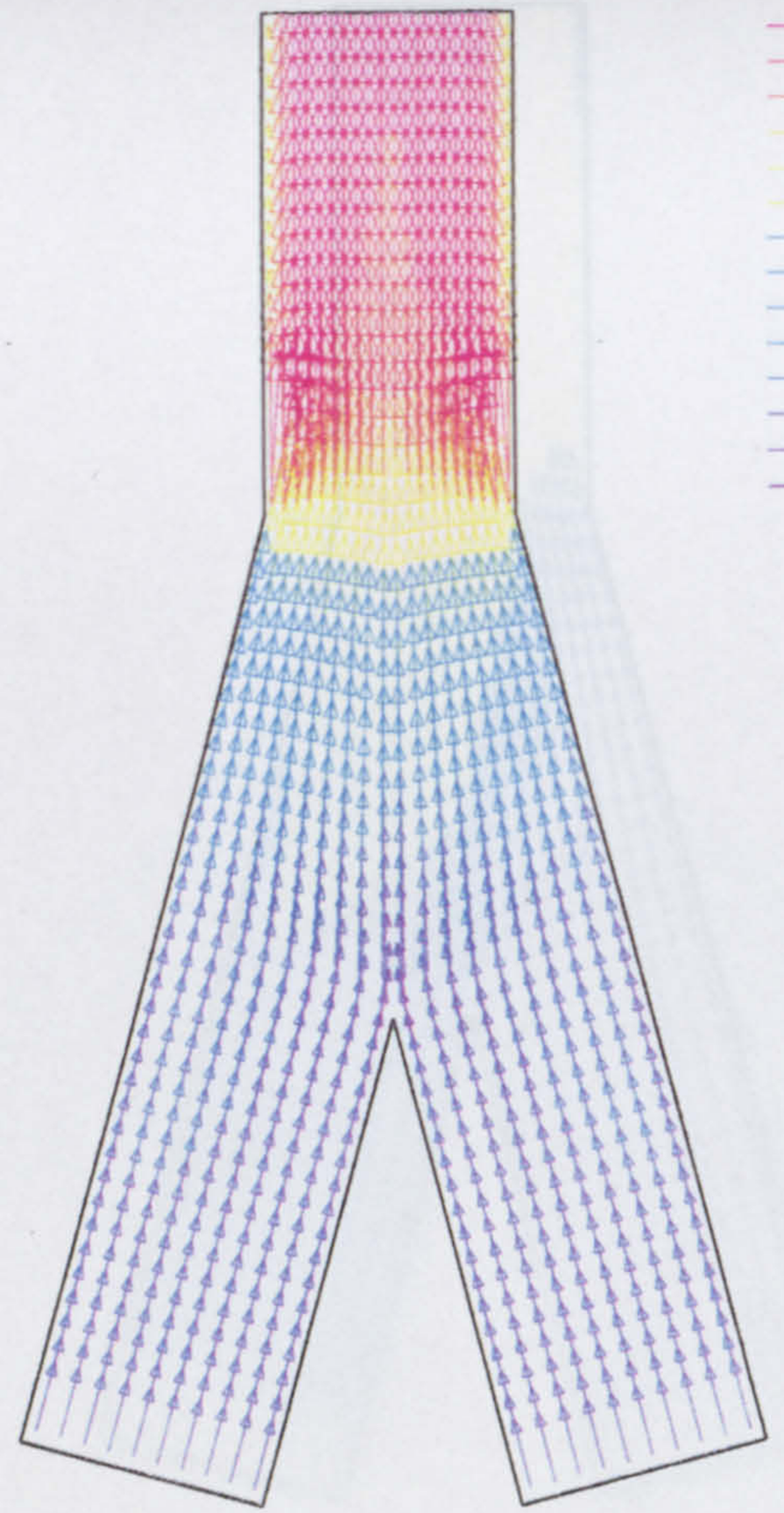

Figure 5.24a Flow Visualisation and CFD Vector Plots for 30° 'Y' Junction Flow Ratio 0.5/0.5.

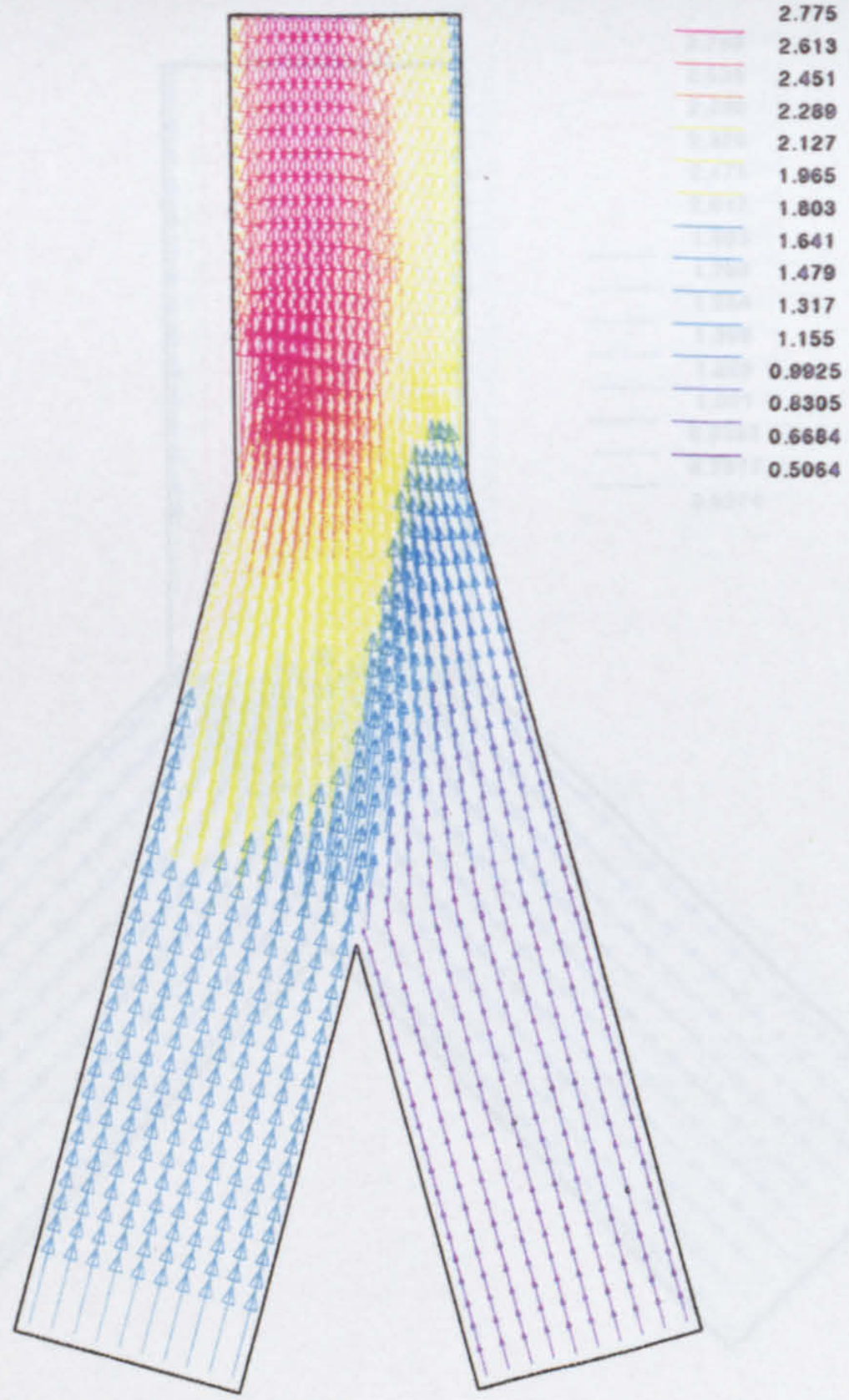

Figure 5.24b Flow Visualisation and CFD Vector Plots for 30° 'Y' Junction Flow Ratio 0.75/0.25.

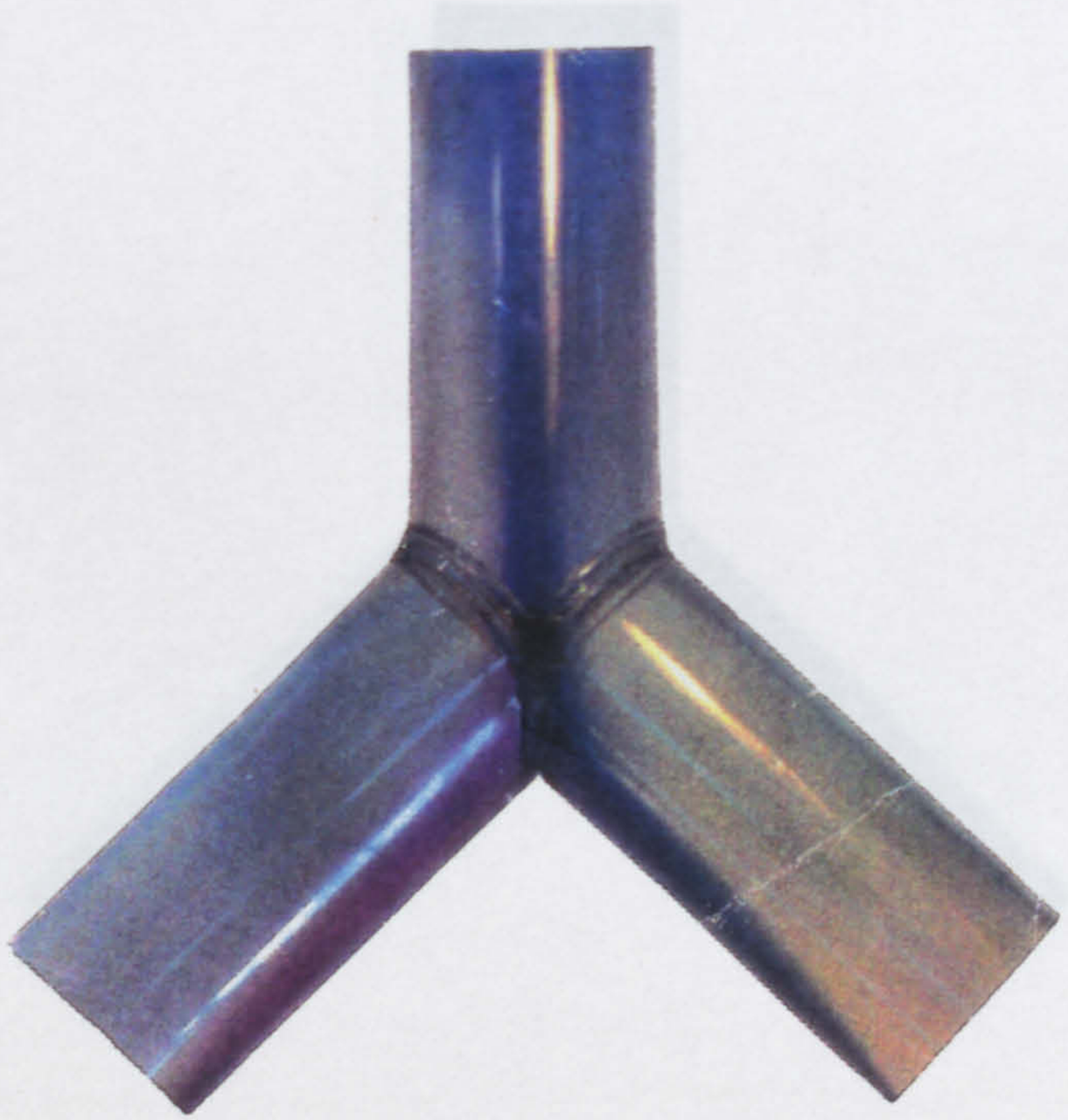

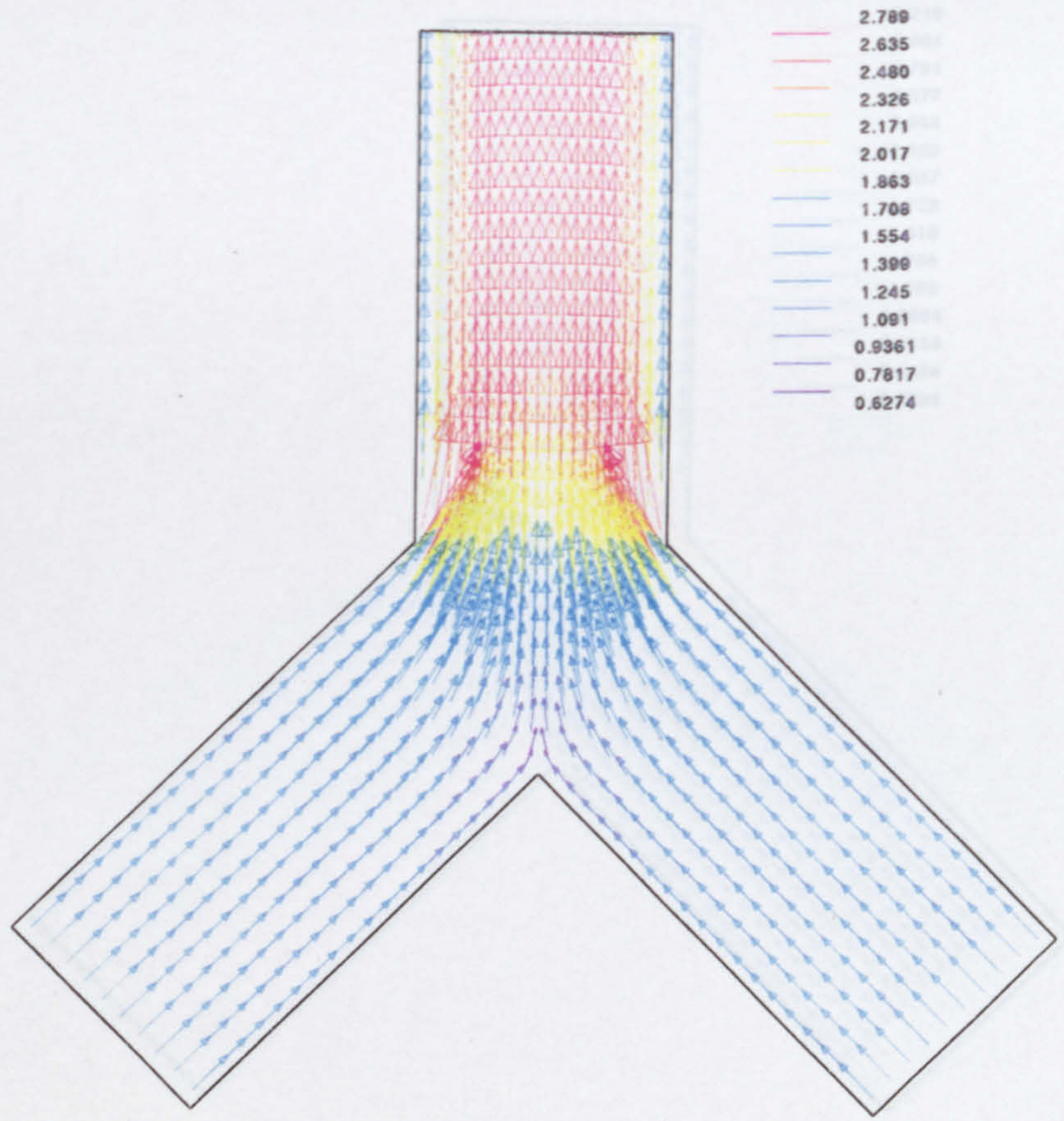

Figure 5.25a Flow Visualisation and CFD Vector Plots for 90° 'Y' Junction Flow Ratio 0.5/0.5.

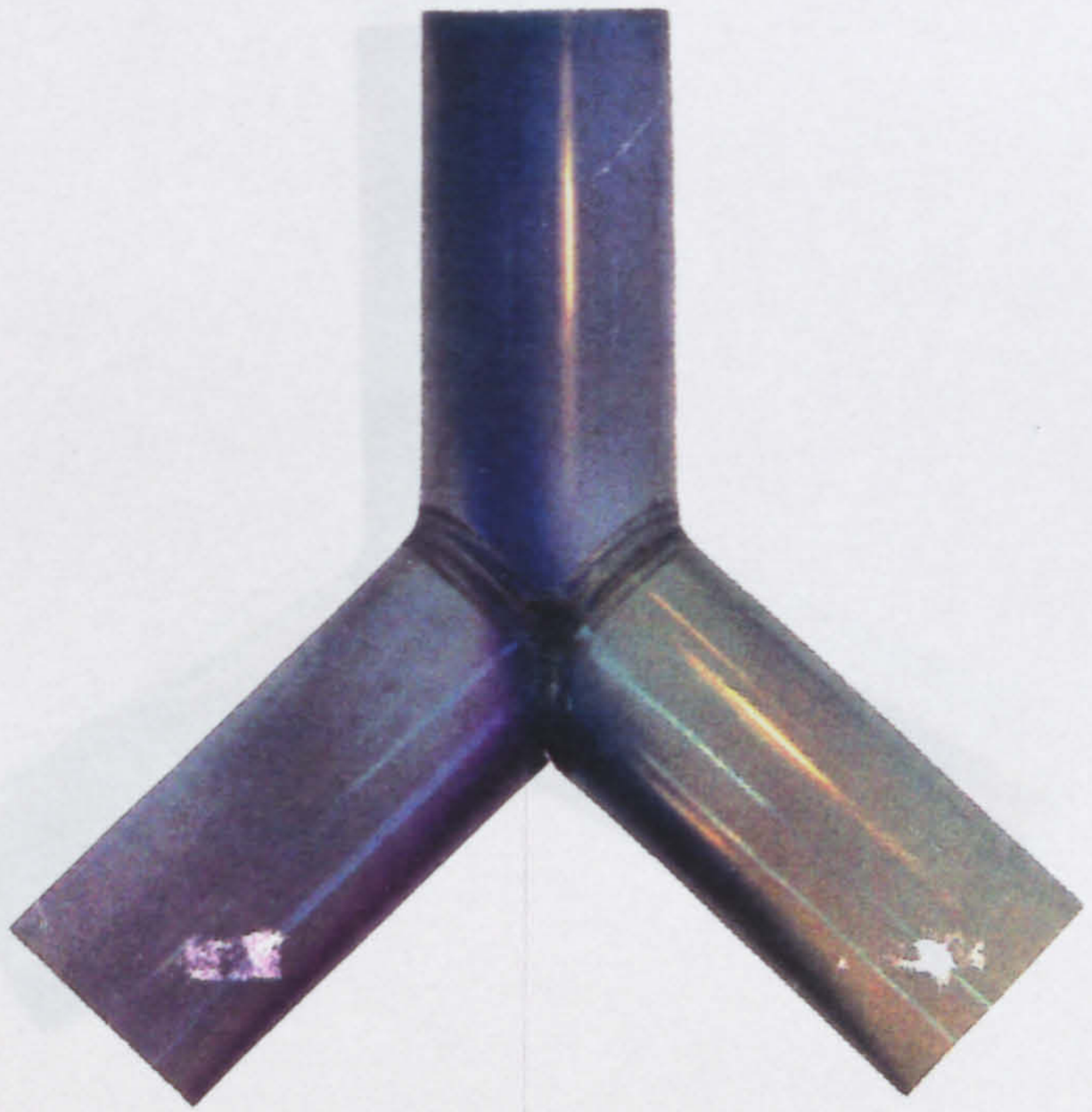

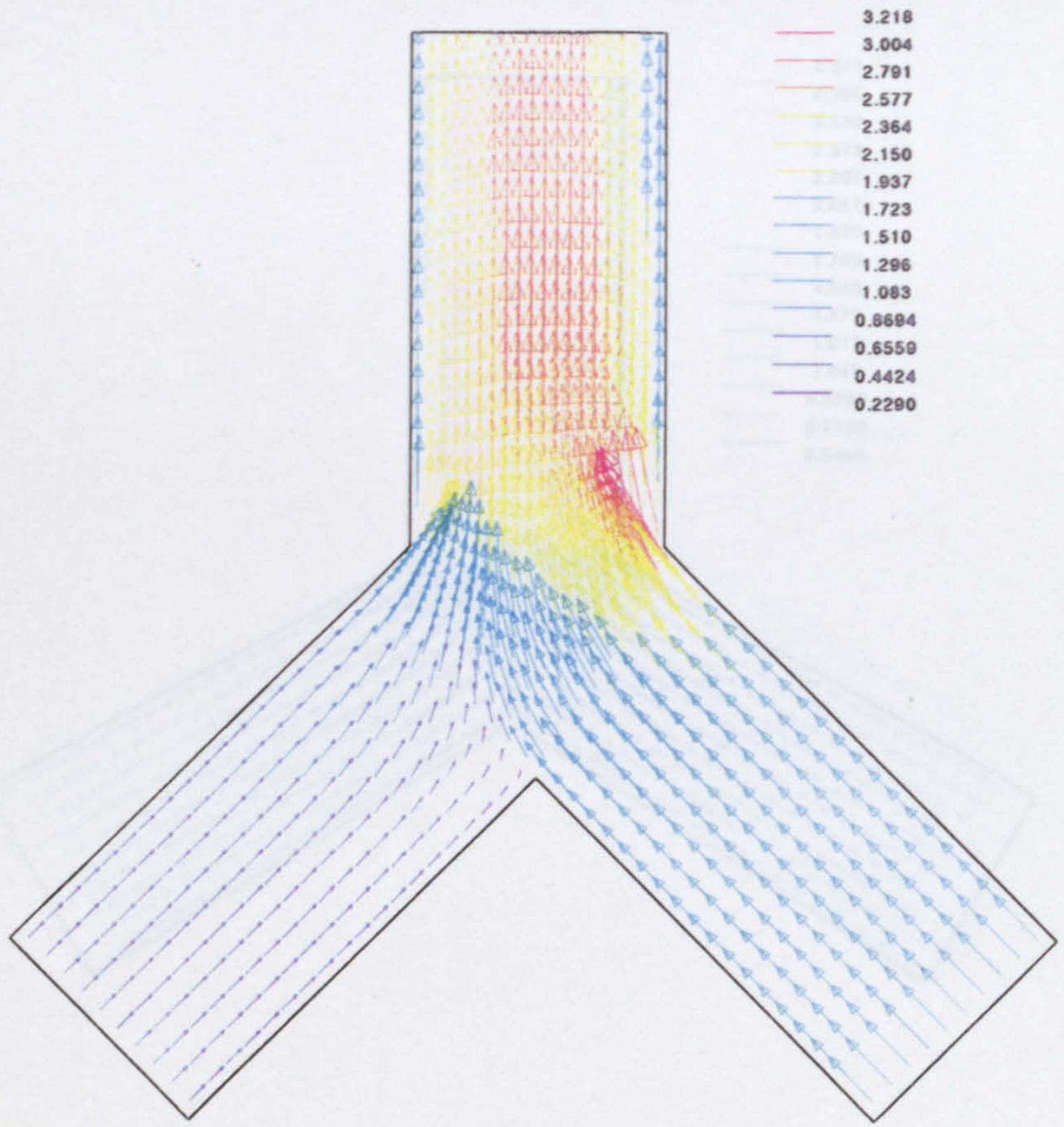

Figure 5.25b Flow Visualisation and CFD Vector Plots for 90° 'Y' Junction Flow Ratio 0.25/0.75.

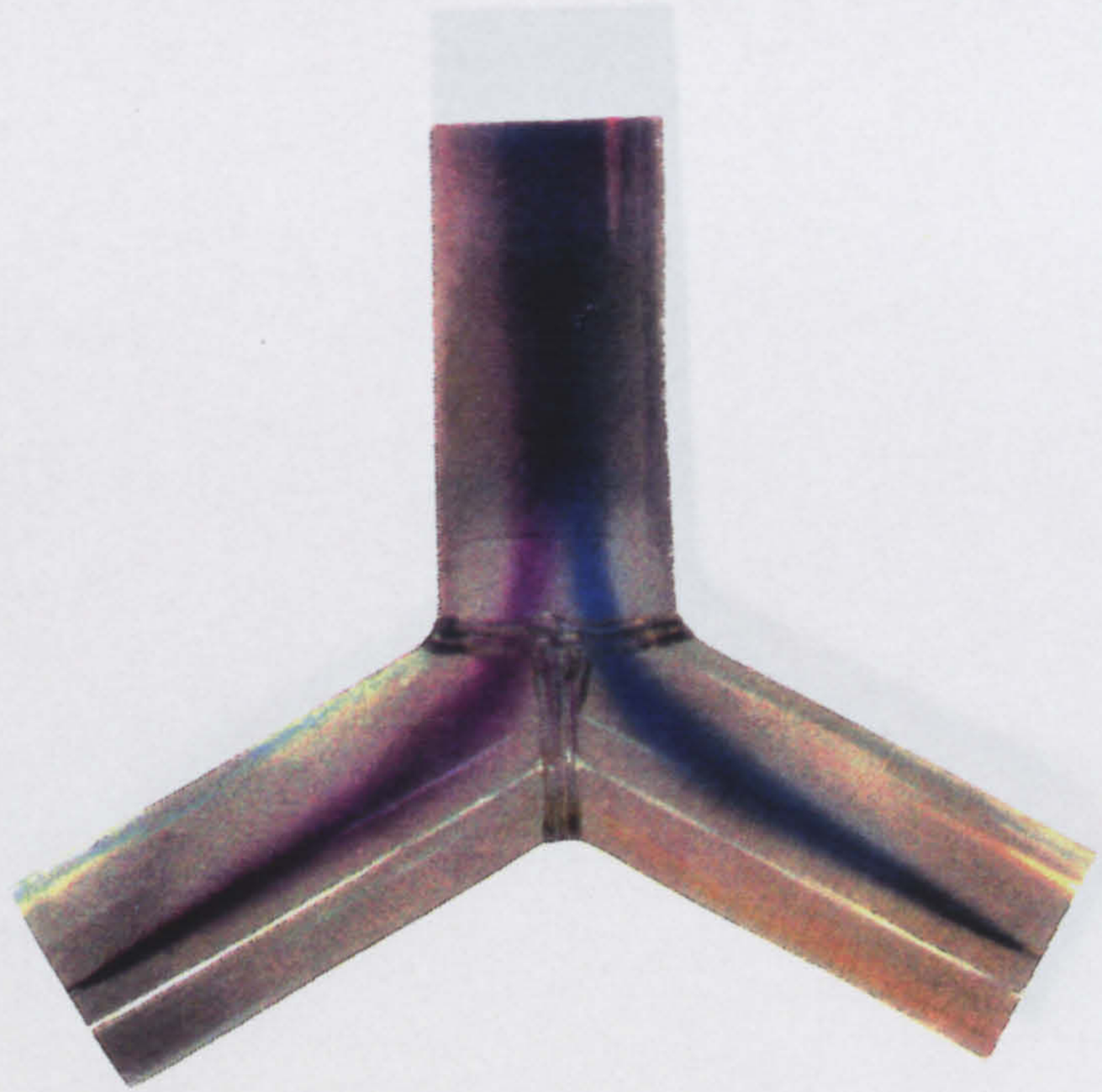

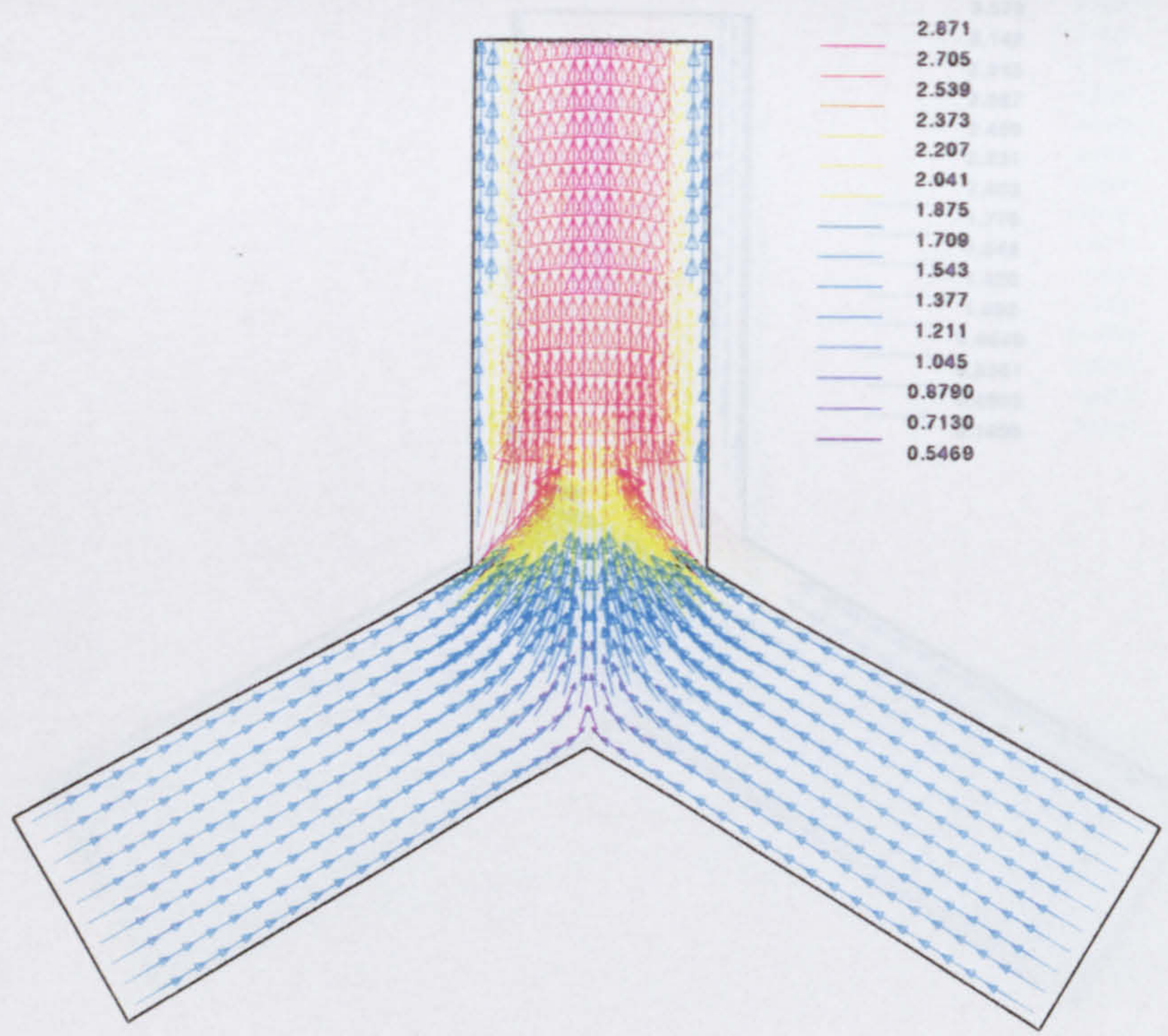

Figure 5.26a Flow Visualisation and CFD Vector Plots for 120° 'Y' Junction Flow Ratio 0.5/0.5.

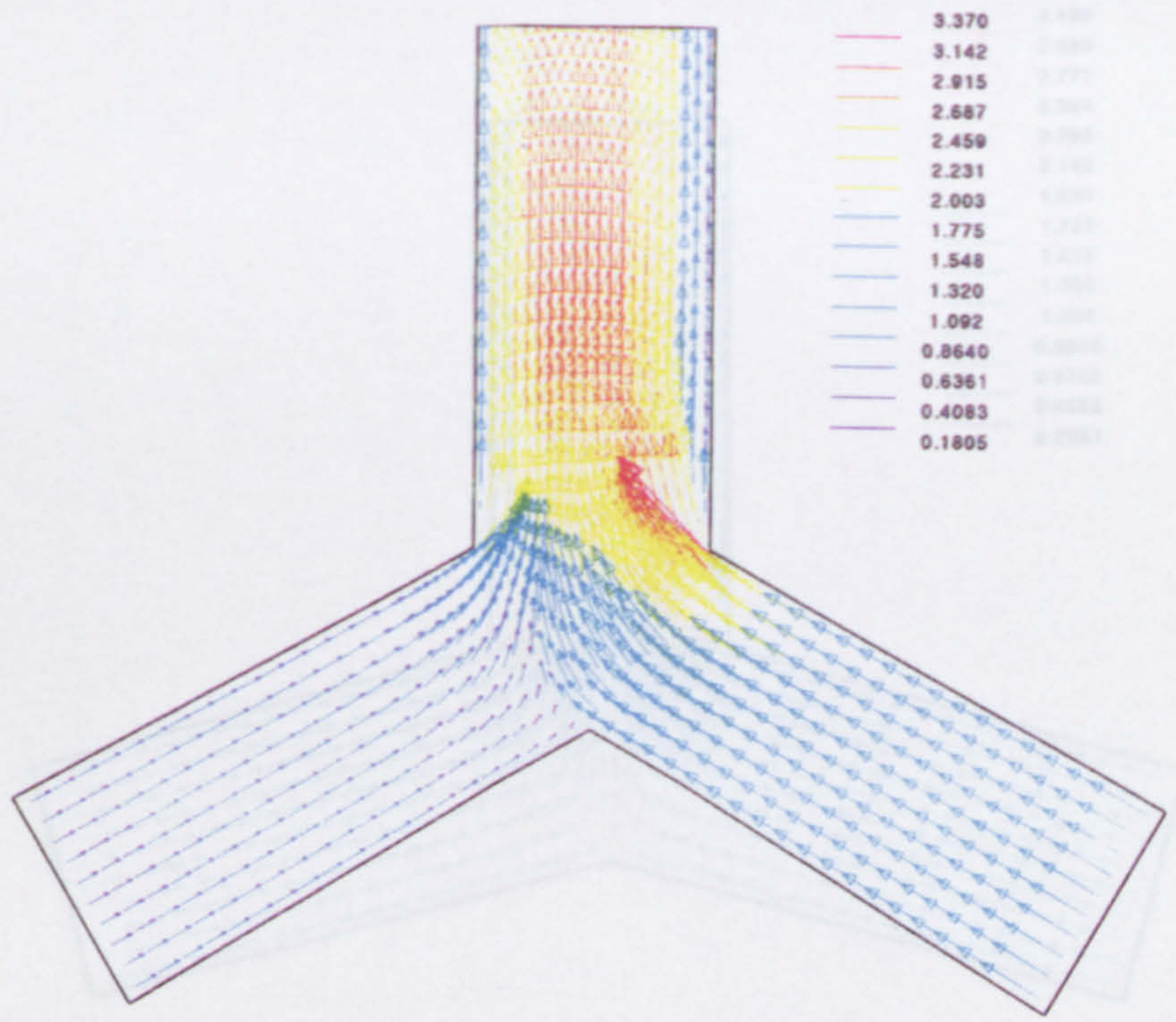

Figure 5.26b Flow Visualisation and CFD Vector Plots for 120° 'Y' Junction
Flow Ratio 0.25/0.75.

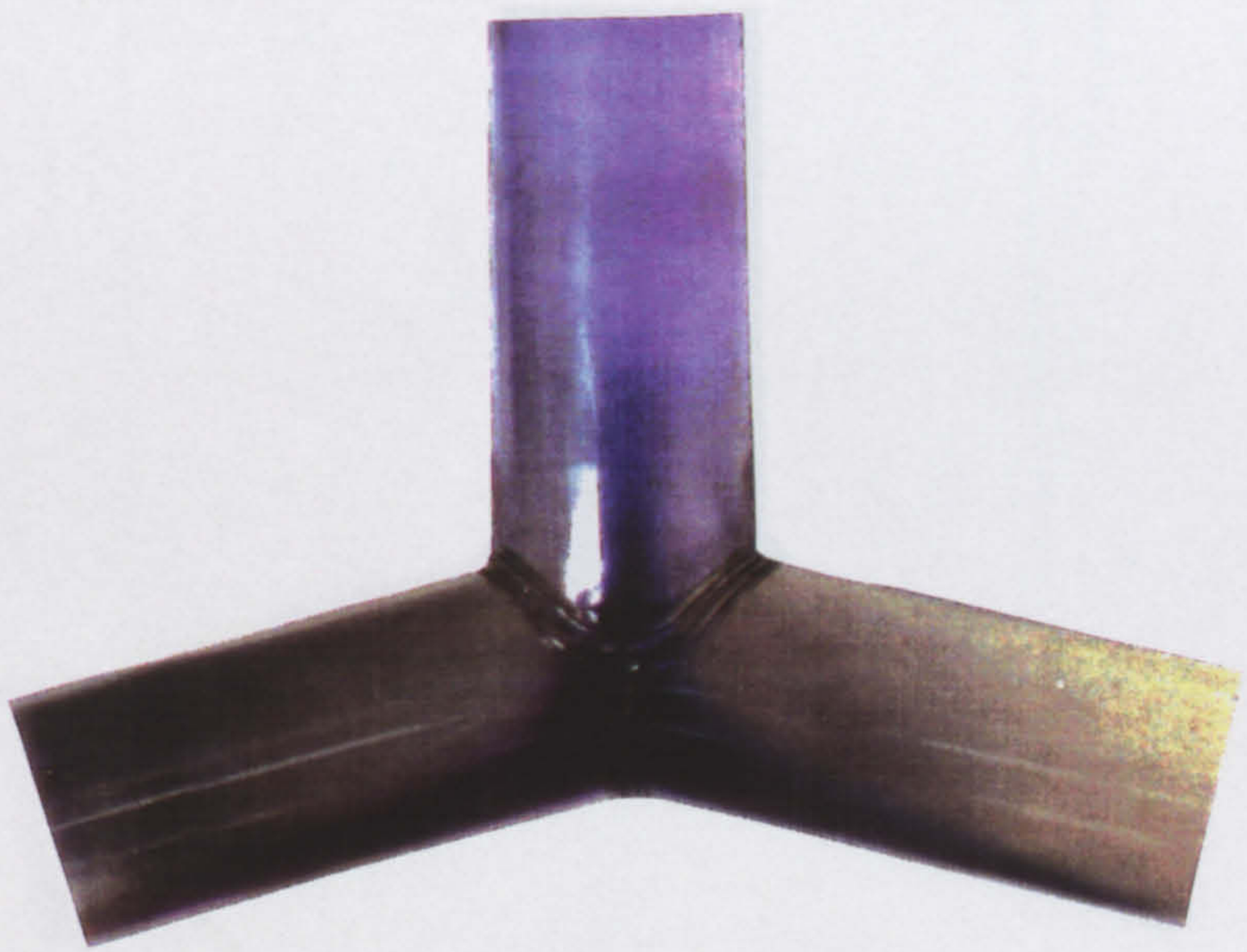

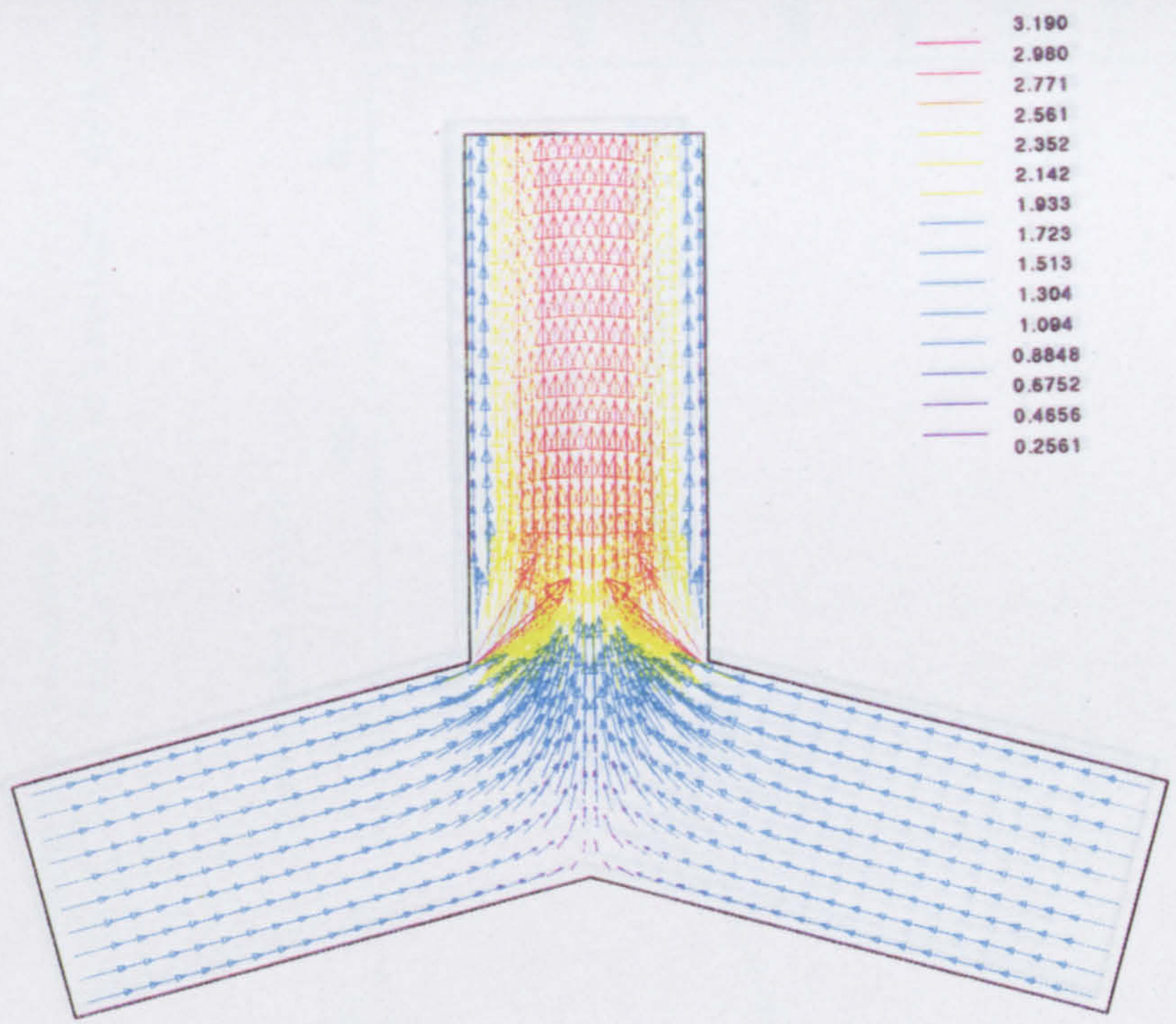

Figure 5.27a Flow Visualisation and CFD Vector Plots for 150° 'Y' Junction Flow Ratio 0.5/0.5.

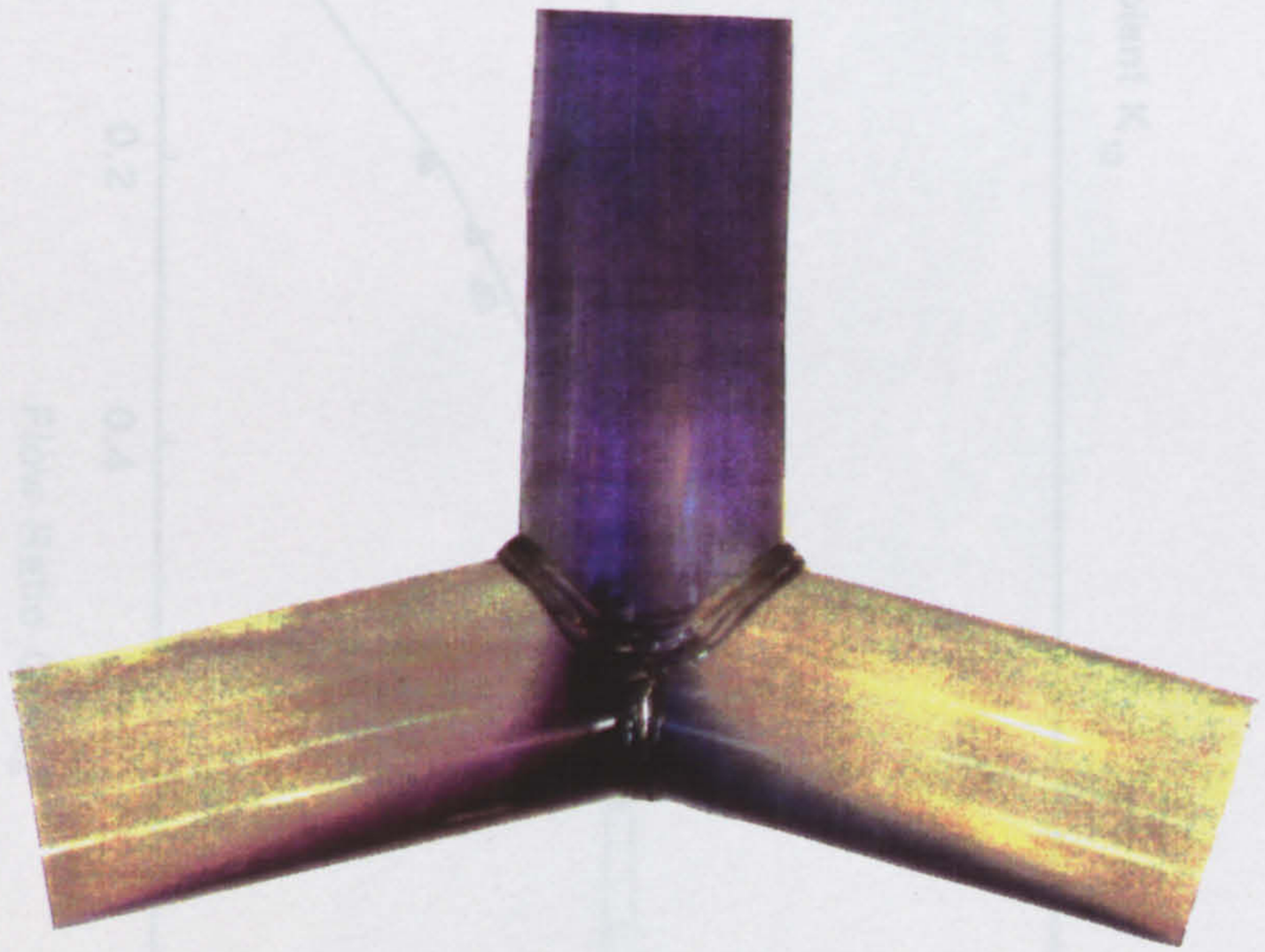

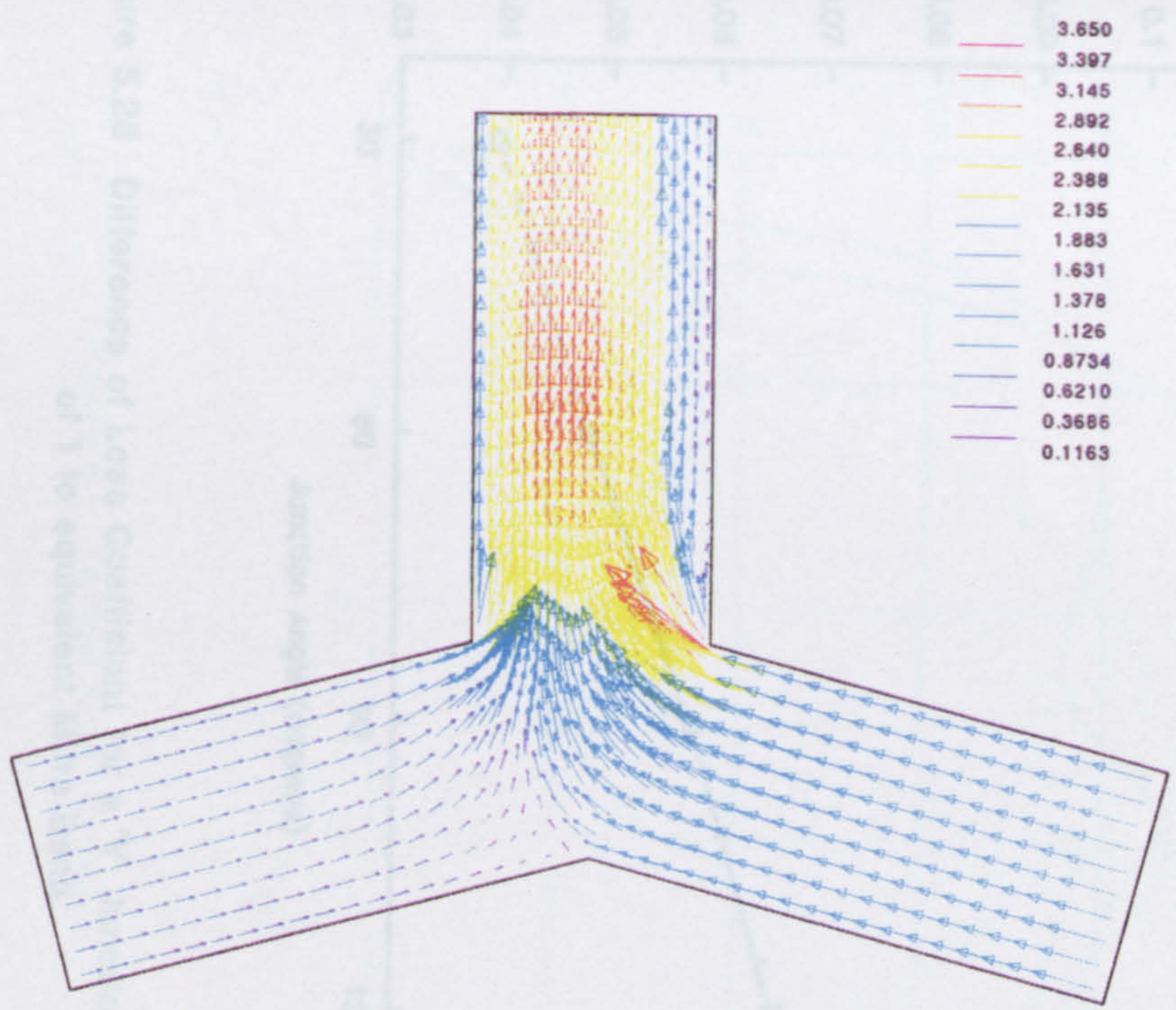

Figure 5.27b Flow Visualisation and CFD Vector Plots for 150° 'Y' Junction
Flow Ratio 0.25/0.75.

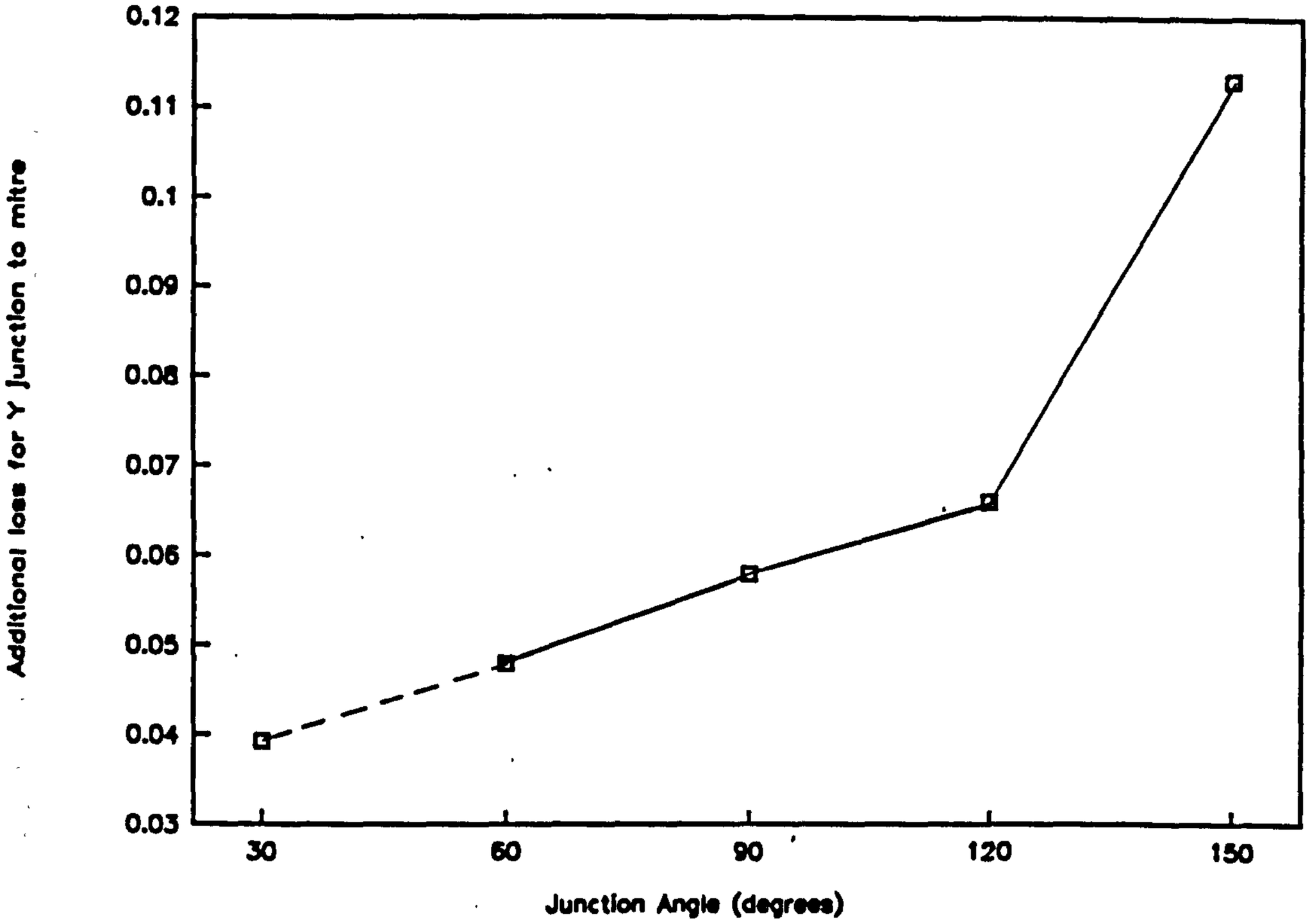

Figure 5.28 Difference of Loss Coefficient for a 'Y' Junction with a Flow Ratio of 1 to equivalent Mitre Bend.

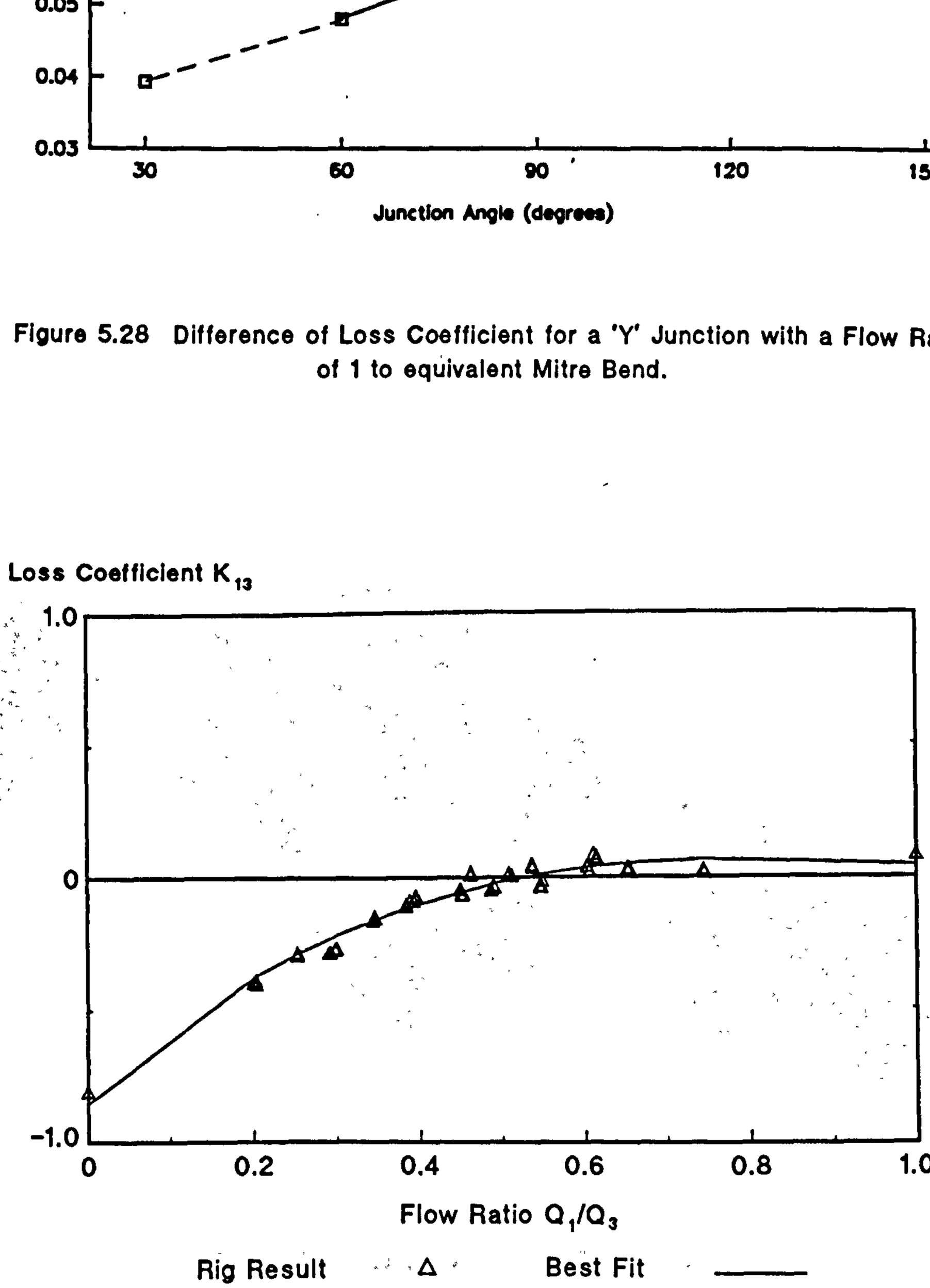

Figure 5.29 Loss Coefficient Curve for a Symmetrical Combining 30° 'Y' Junction

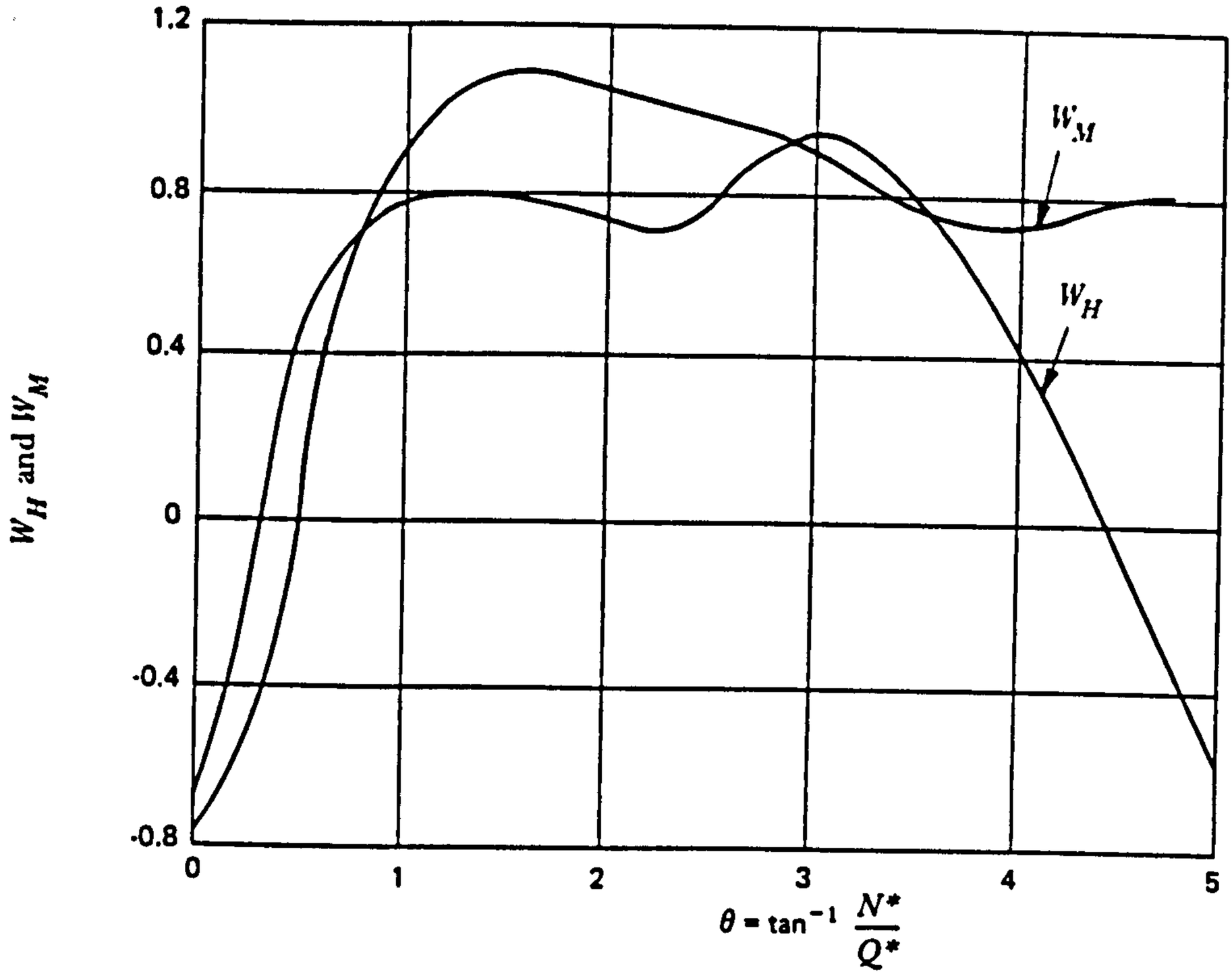

Figure 6.1 Typical Suter Curves

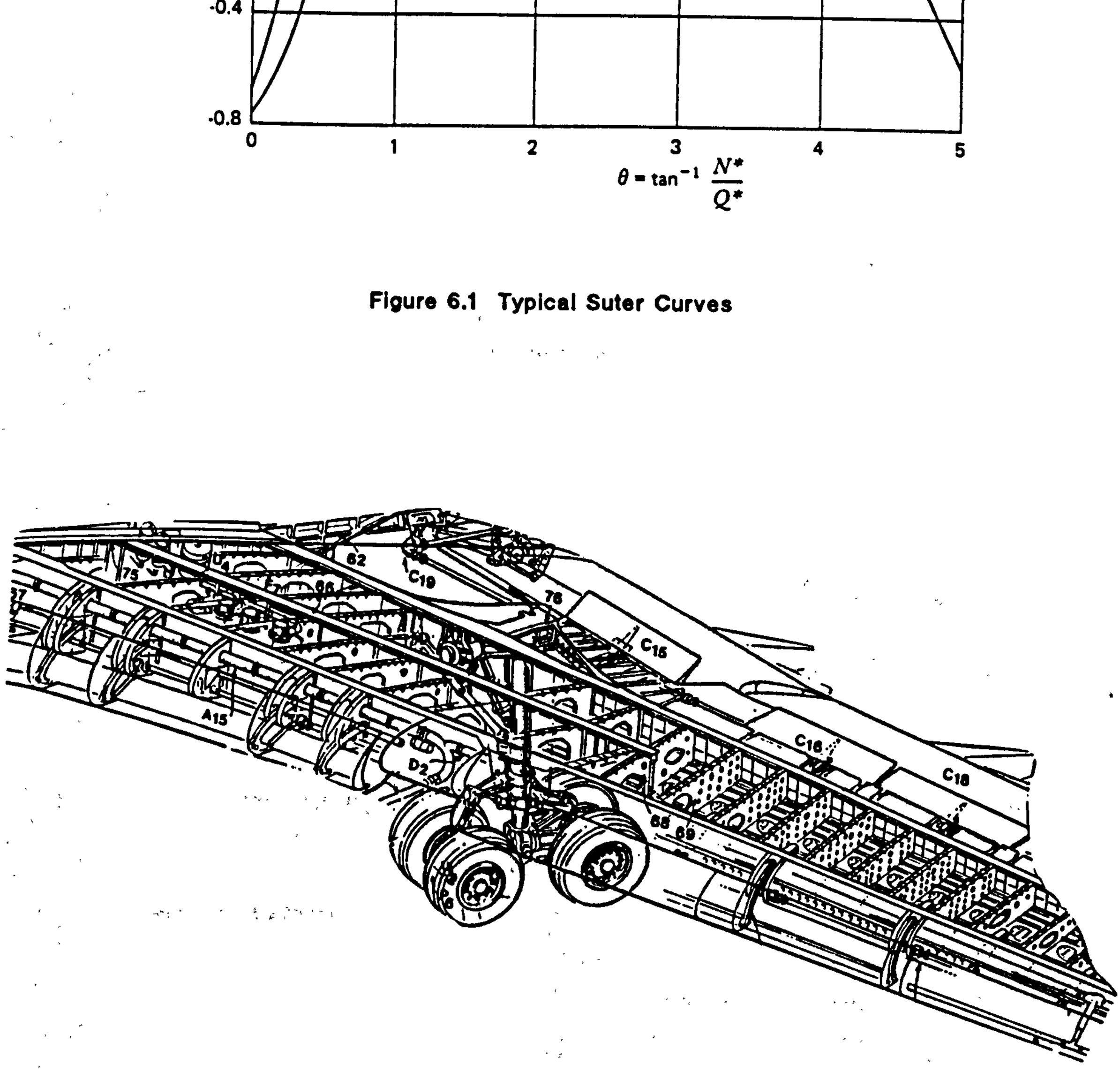

Figure 6.2 Typical Wing Tank Structure

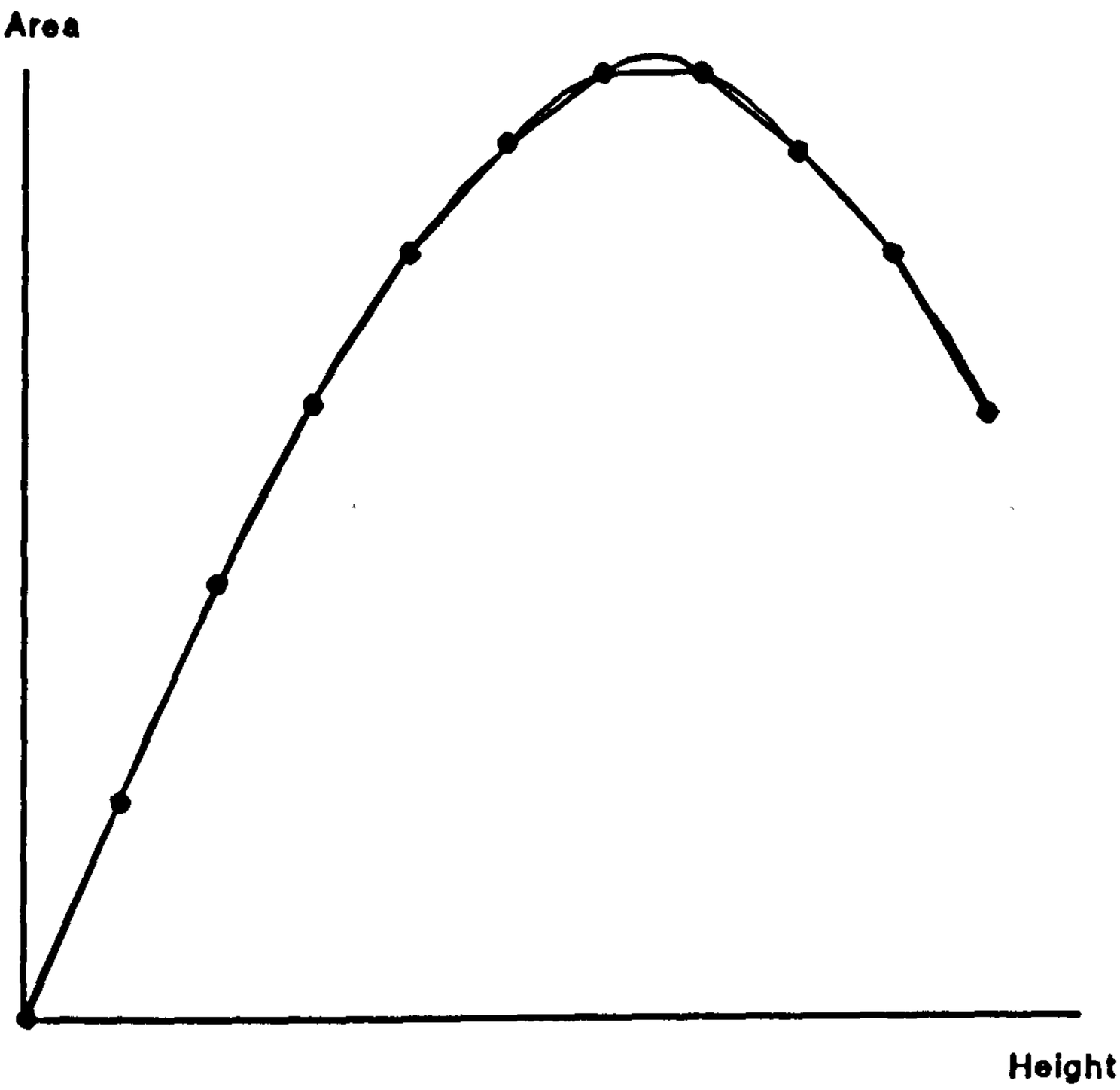

Figure 6.3 Typical Area Height Curve With Integration Spacing Superimposed

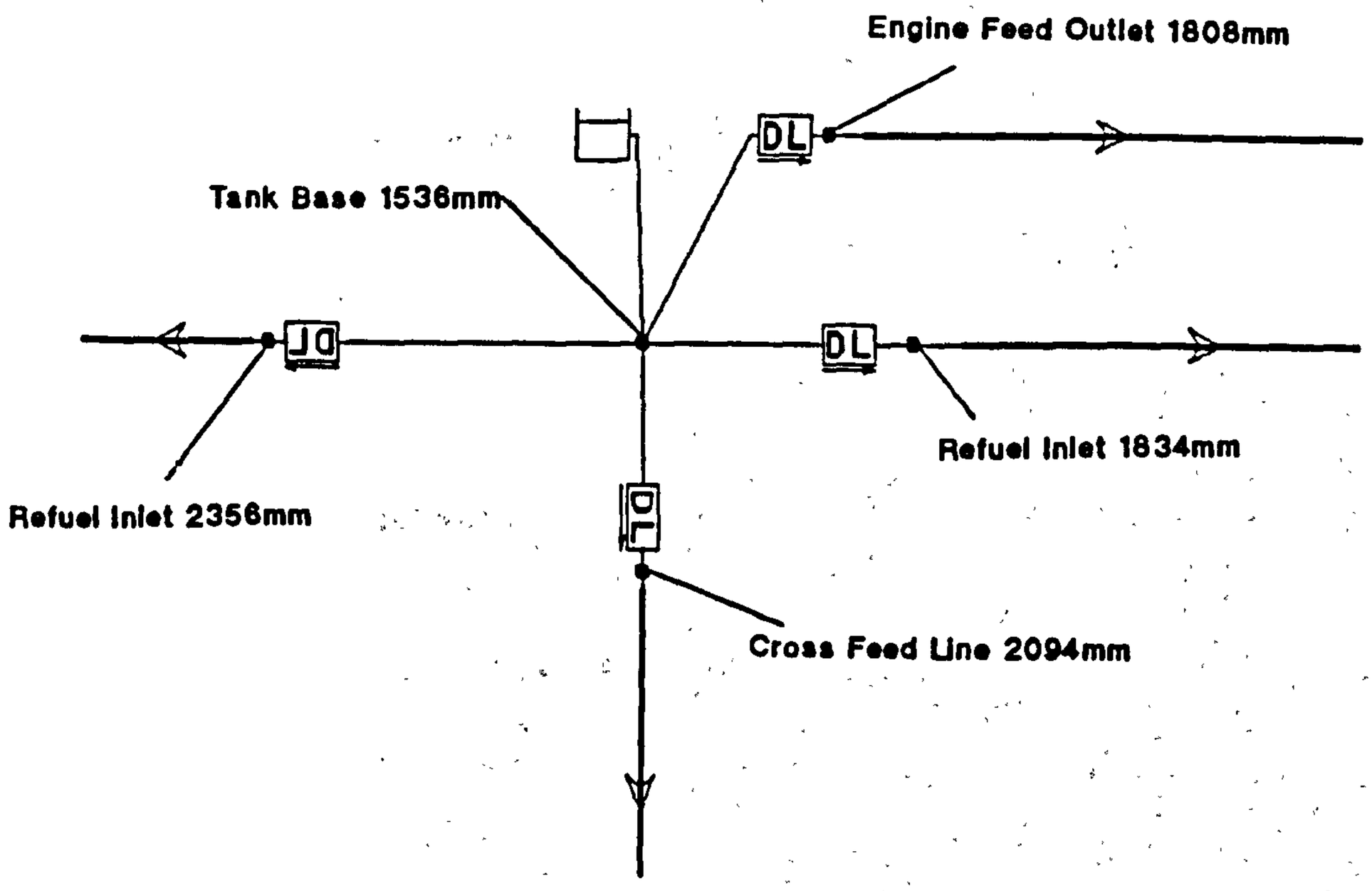

Figure 6.4 Modelling of Multiple Inlets and Outlets on a Flowmaster Tank Model.

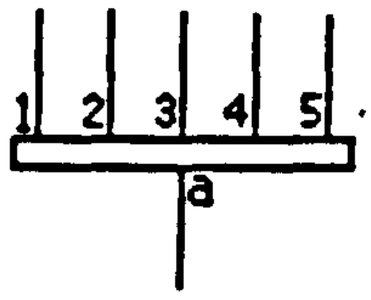

Figure 6.5 Six Port Tank Inlet/Outlet Model.

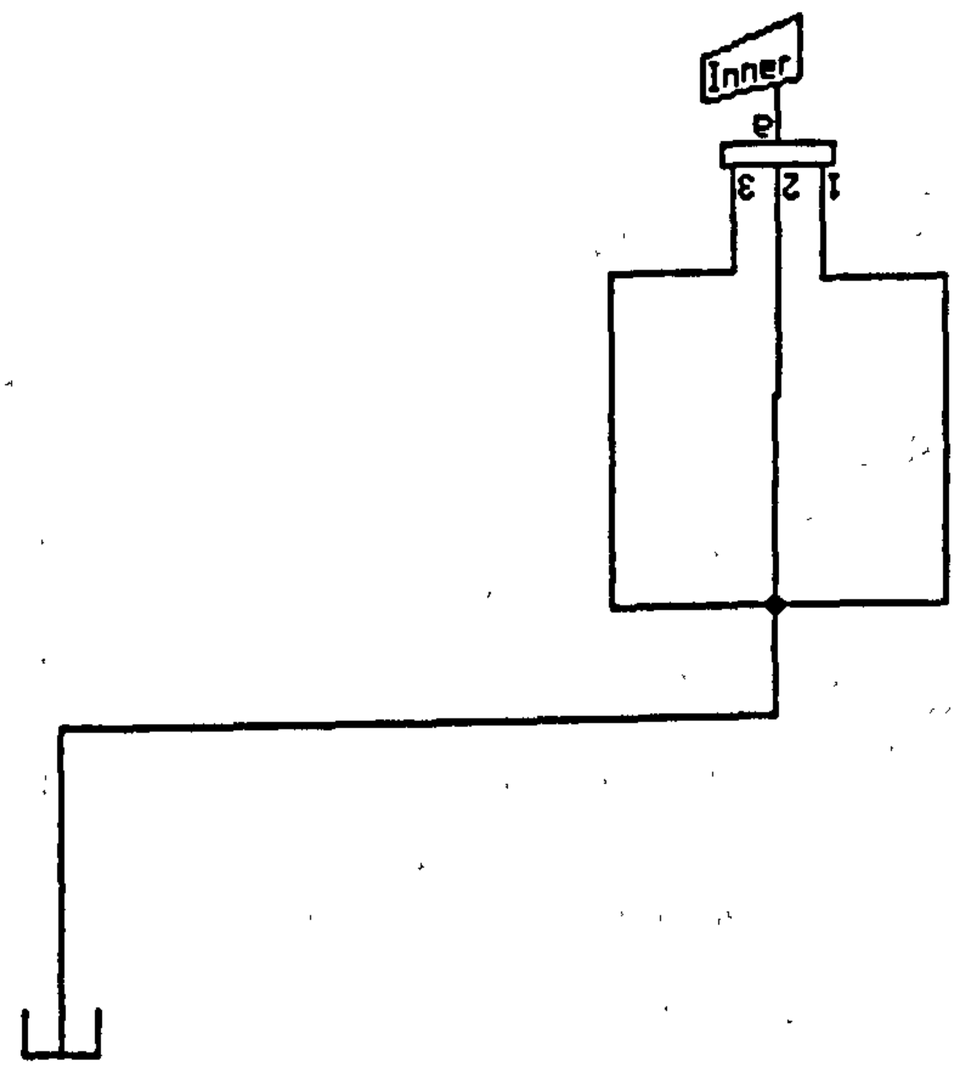

Figure 6.6 Network to Determine Effects of Diffuser Models.

a. Discrete Loss Model.

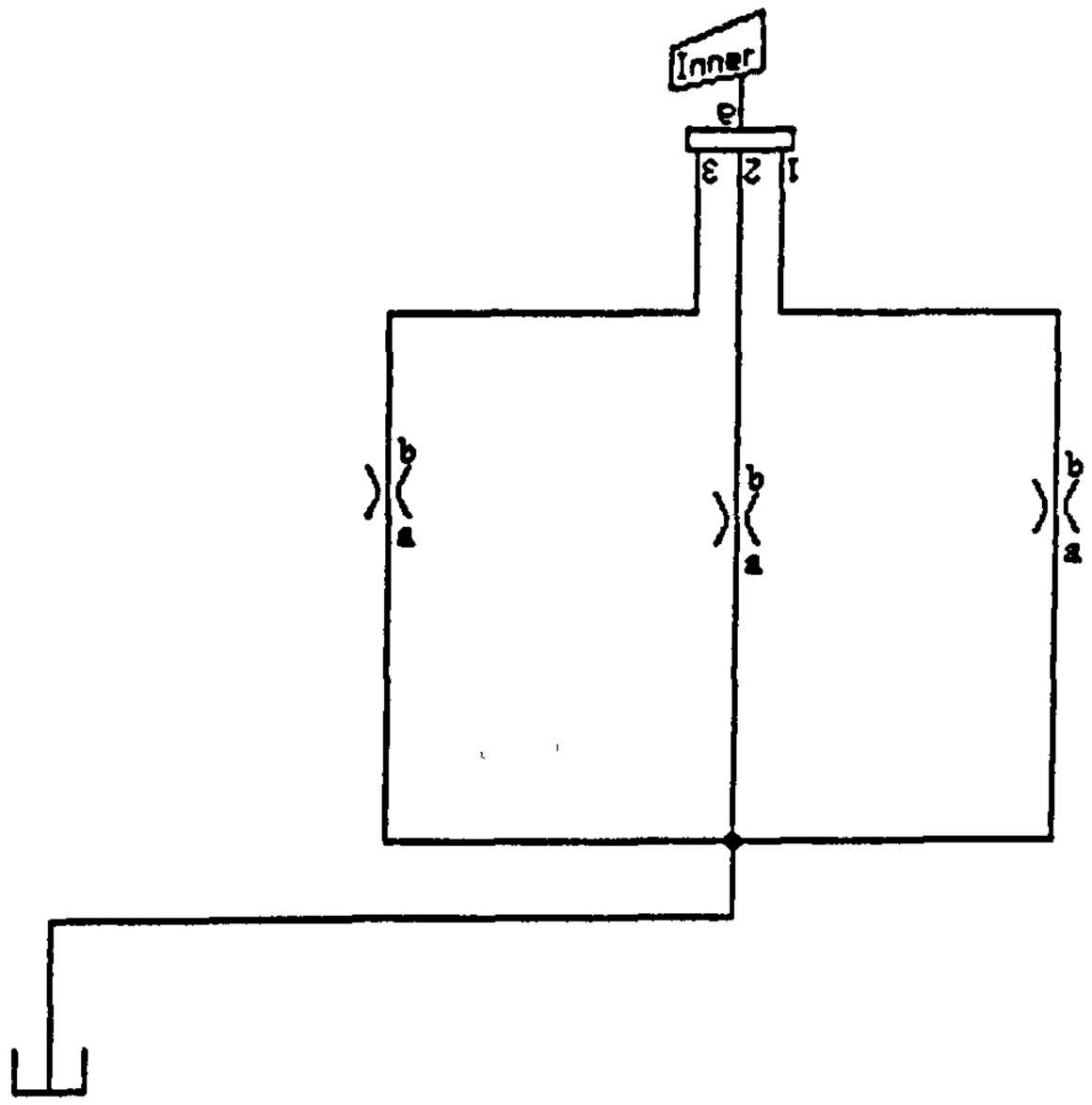

Figure 6.6 Network to Determine Effects of Diffuser Models.

b. Orifice Model.

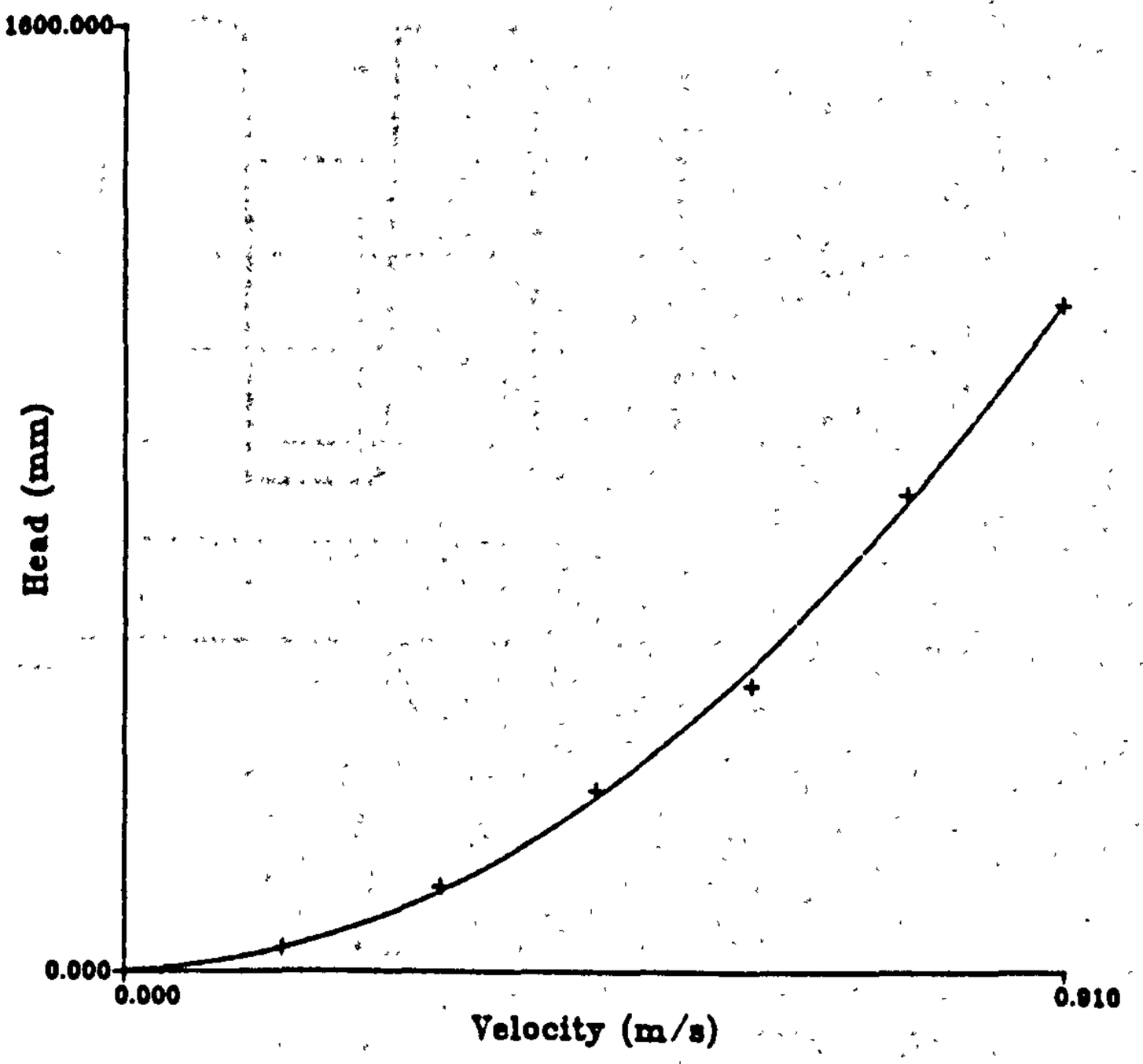

Figure 6.7 NACA Intake and Surge Tank Inlet Loss Characteristic.

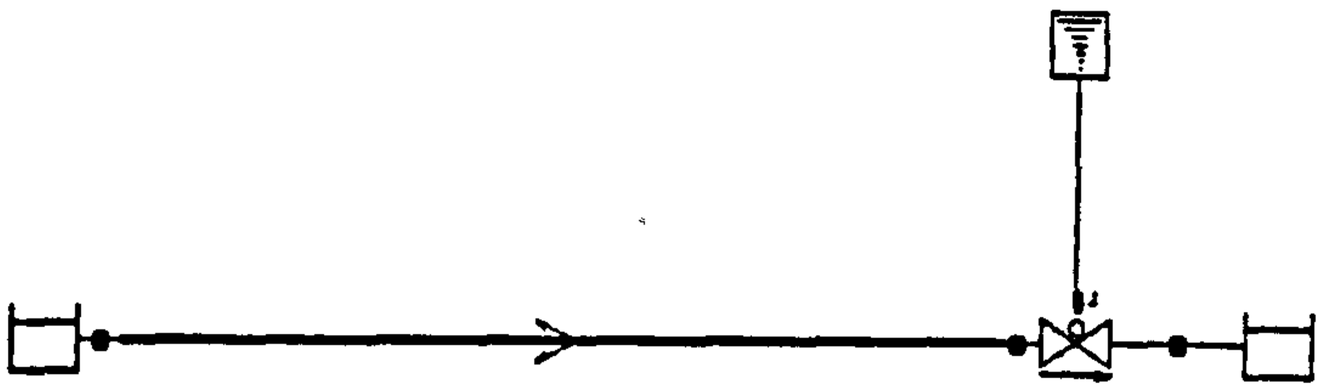

a. Network.

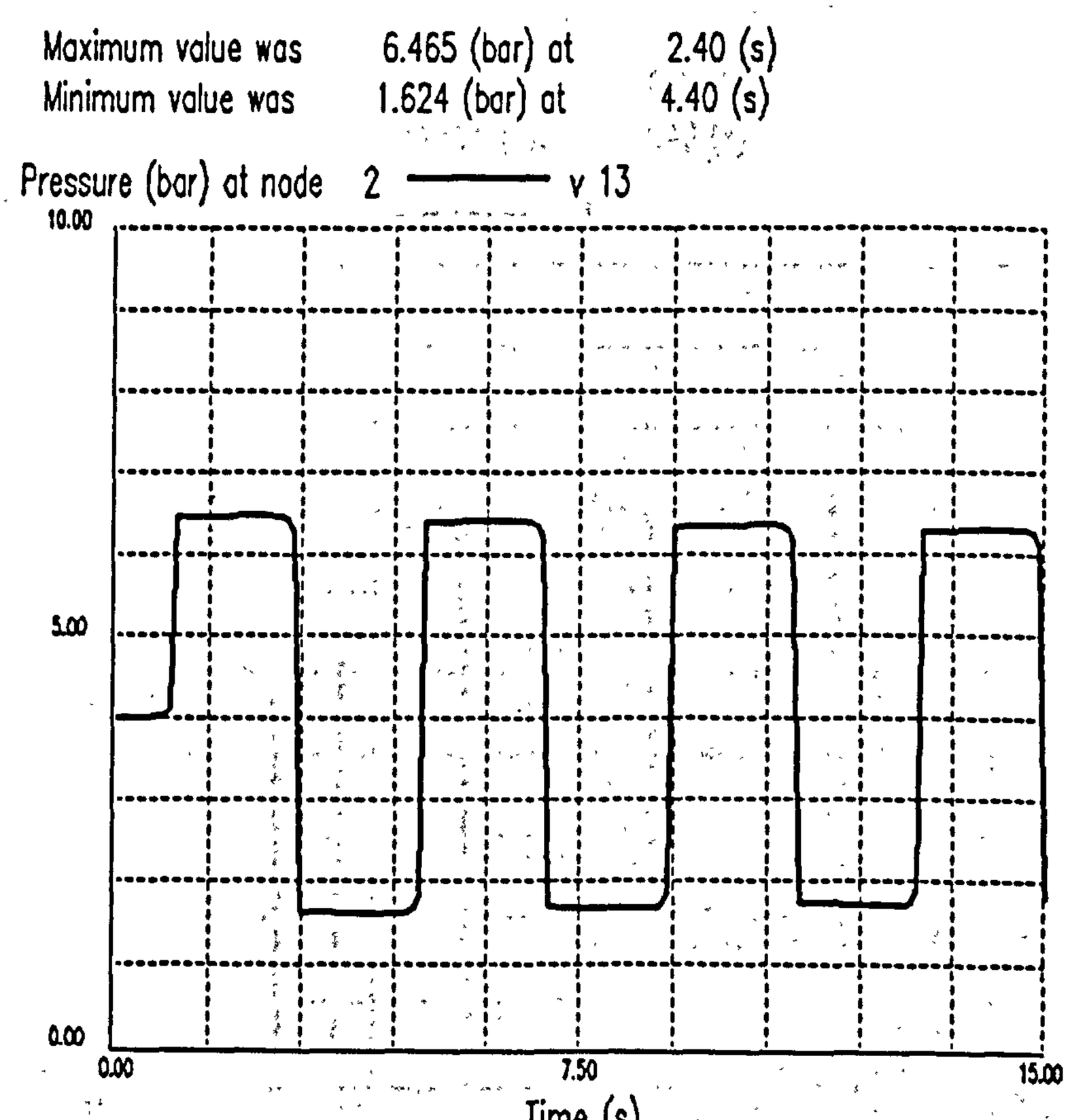

b. Resultant Pressure Surge at Valve Face.

Figure 7.1 Pressure Surge in a Straight Pipe.

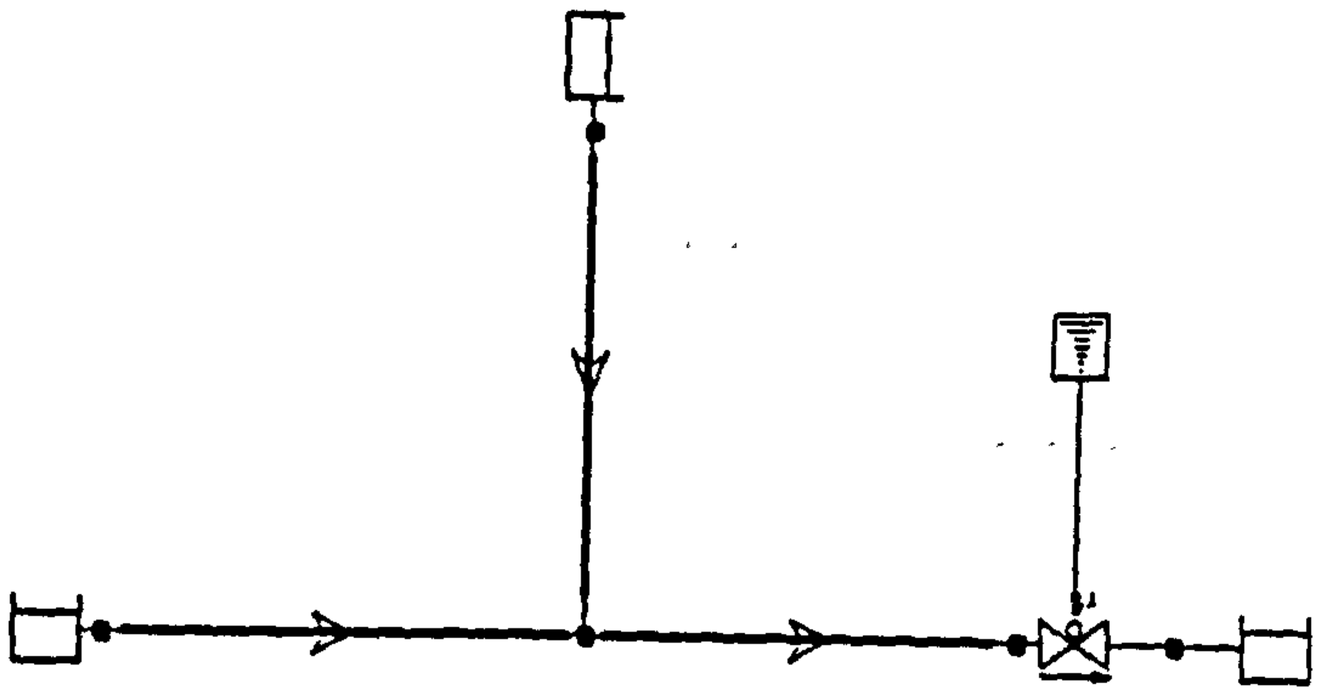

a. Network

Maximum value was 7.600 (bar) at 8.40 (s)
Minimum value was 0.303 (bar) at 3.40 (s)

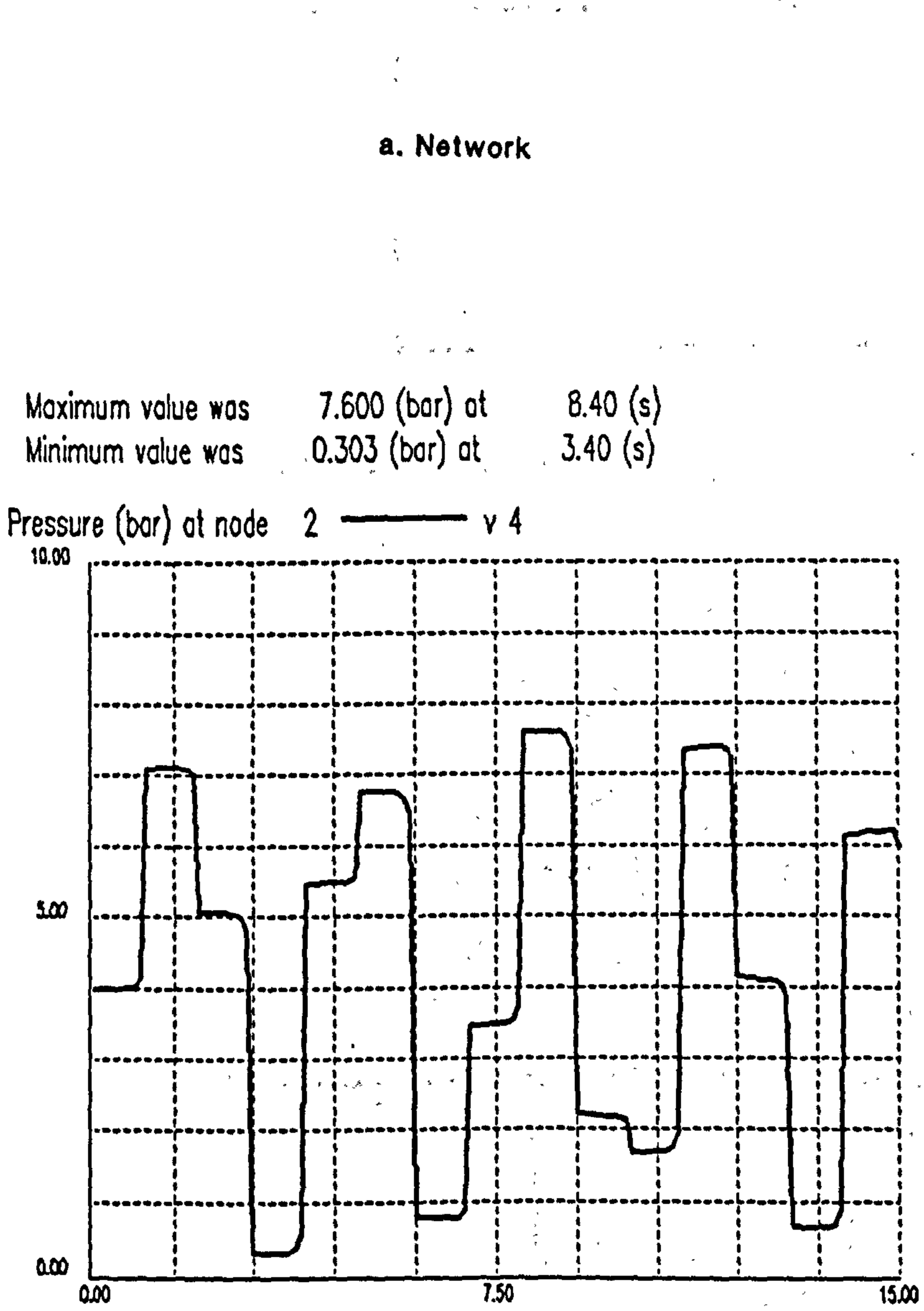

b. Resultant Pressure Surge at Valve Face.

Figure 7.2 Pressure Surge in a Branched Network.

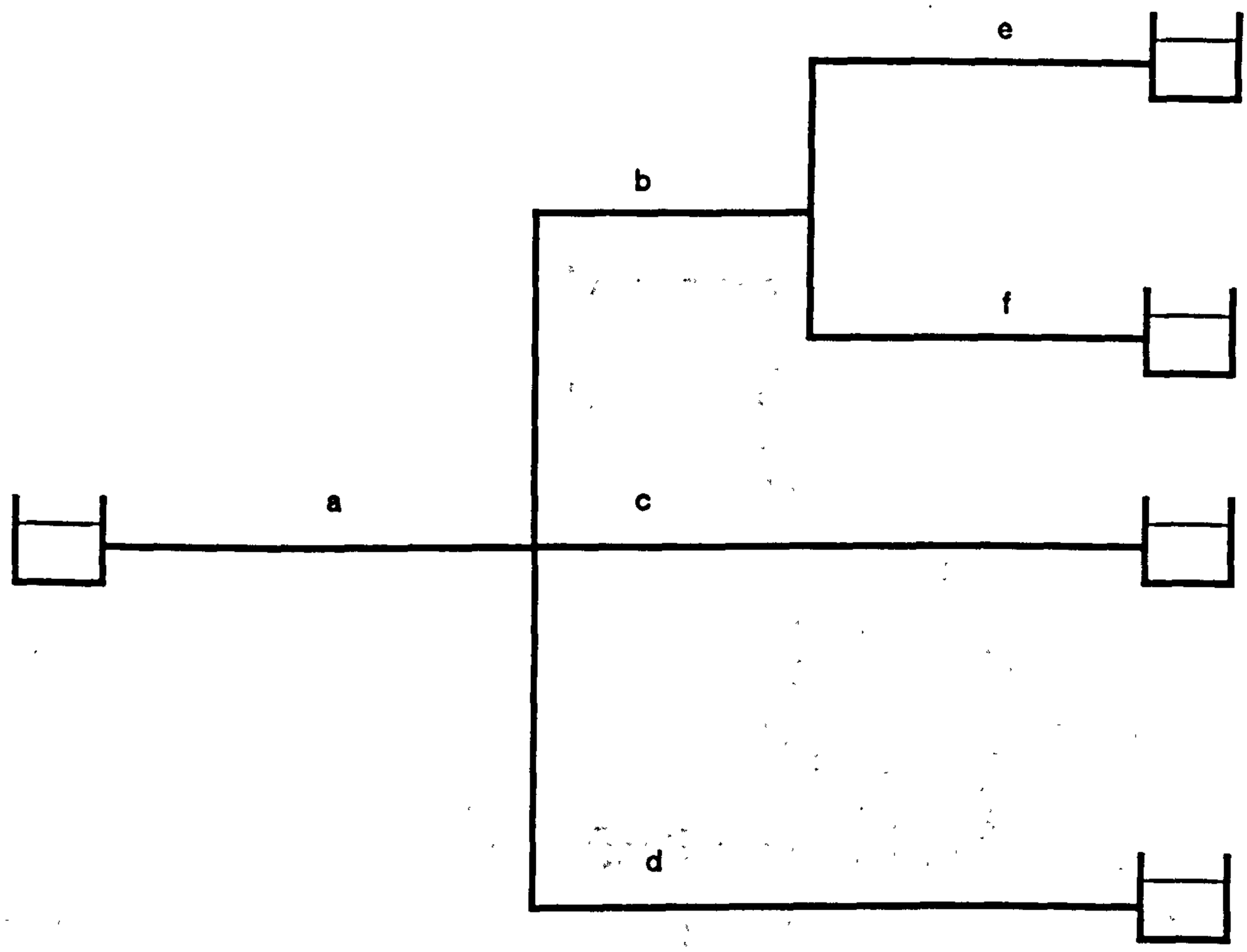

Figure 7.3 Loop Specification in a Branched Network.

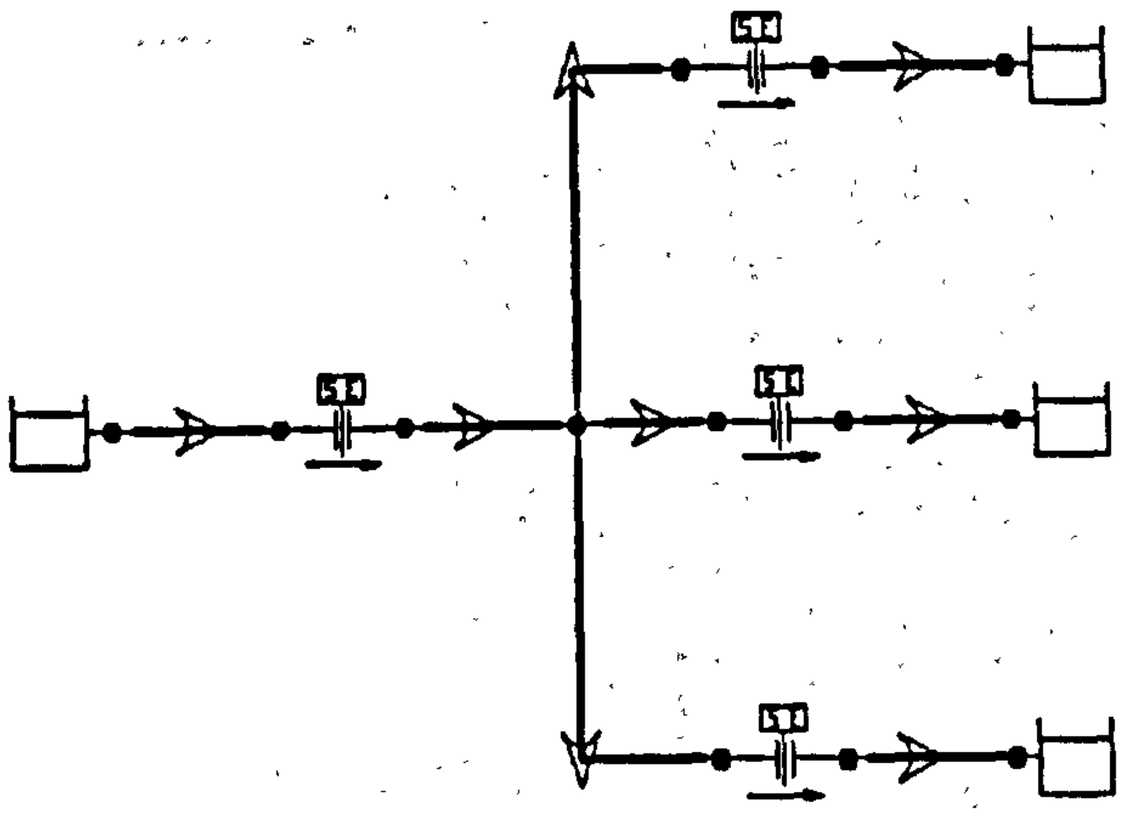

Figure 7.4 Illustrative Branched Network.

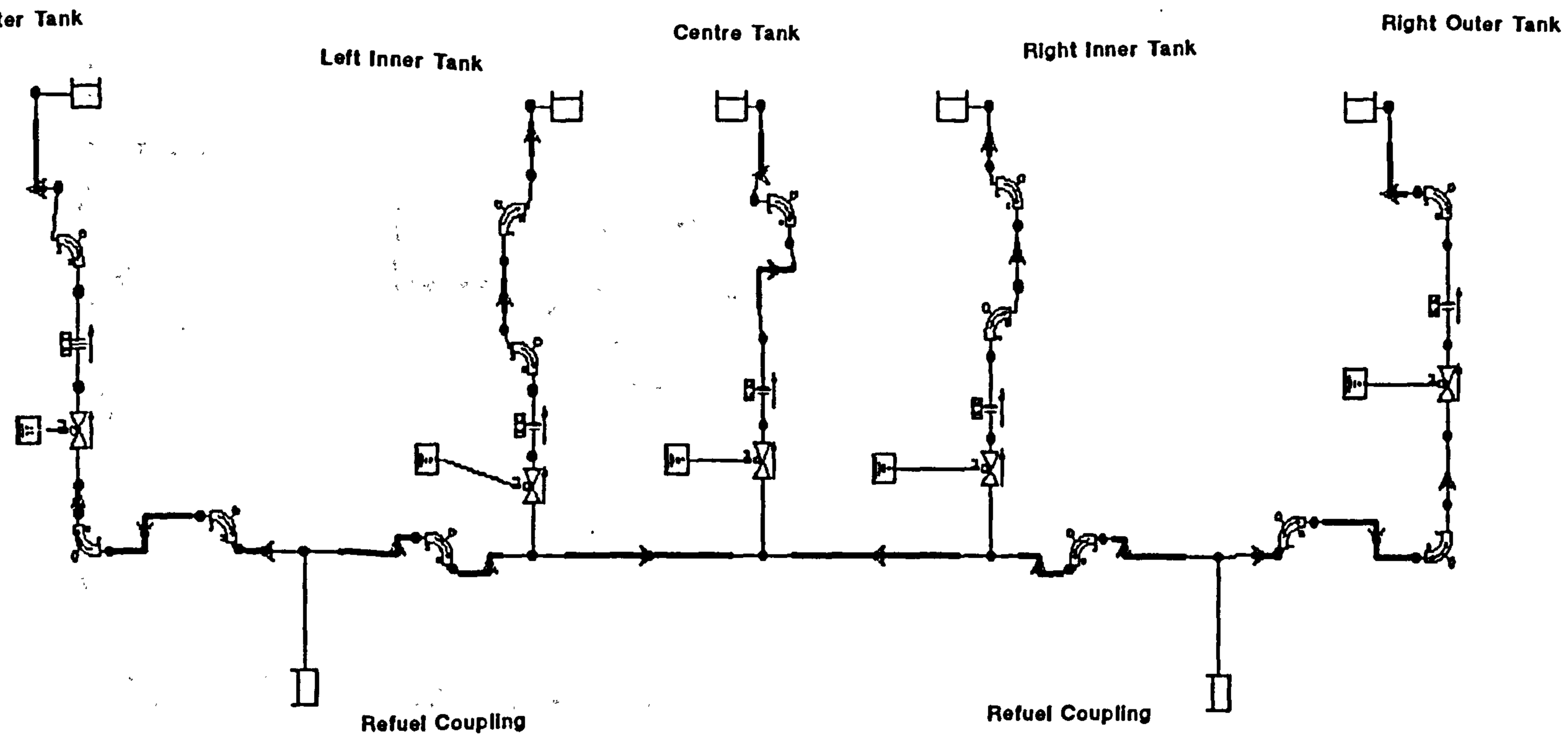

Figure 7.5 Typical Refuel Simulation Network.

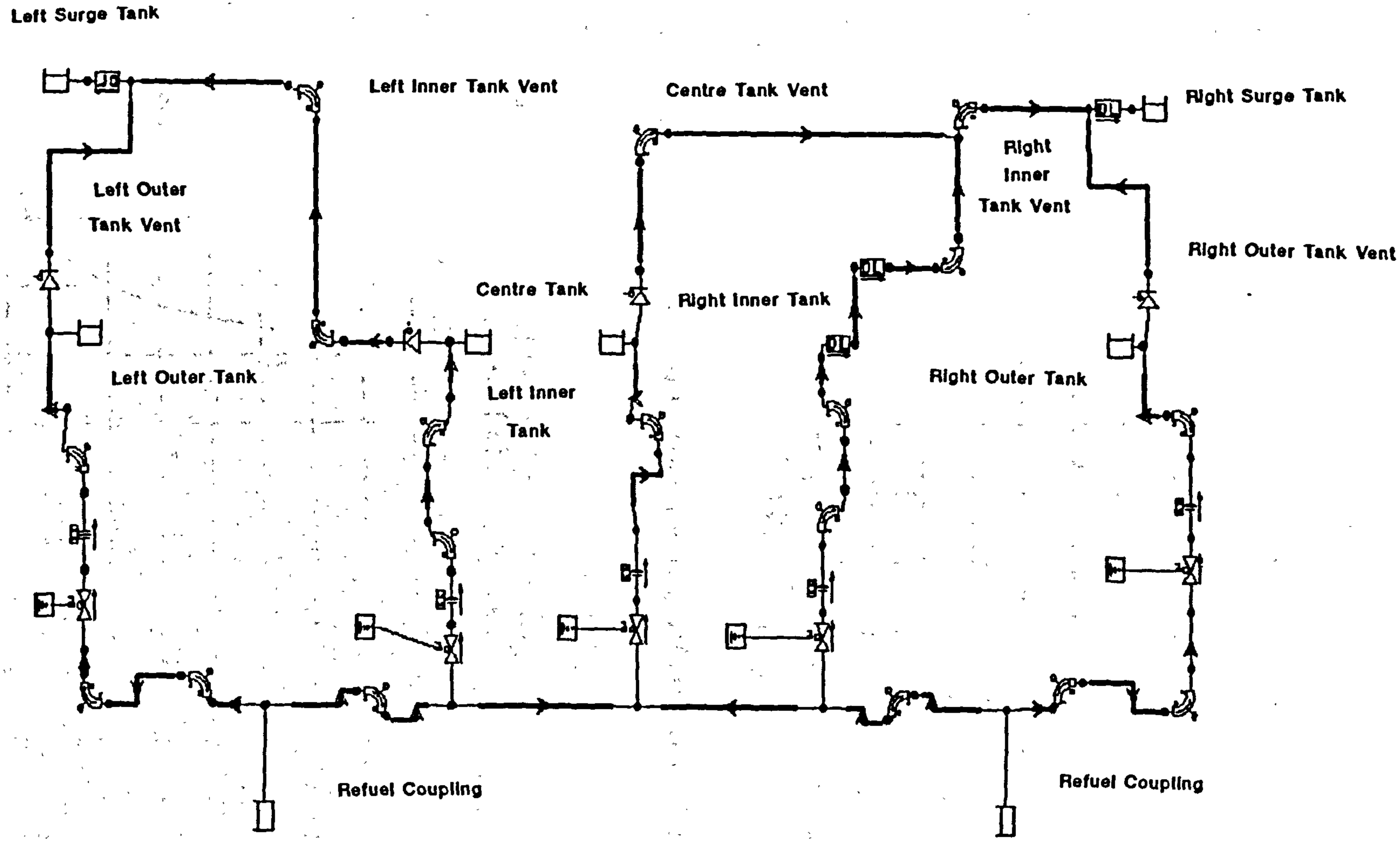

Figure 7.6 Typical Refuel Simulation Network, with Addition of Vent System to Model Right Inner Tank at Refuel Overflow.

Maximum value was 9.56E+01 (psi) at 1.156 (s)
Minimum value was 2.20E+01 (psi) at 0.002 (s)

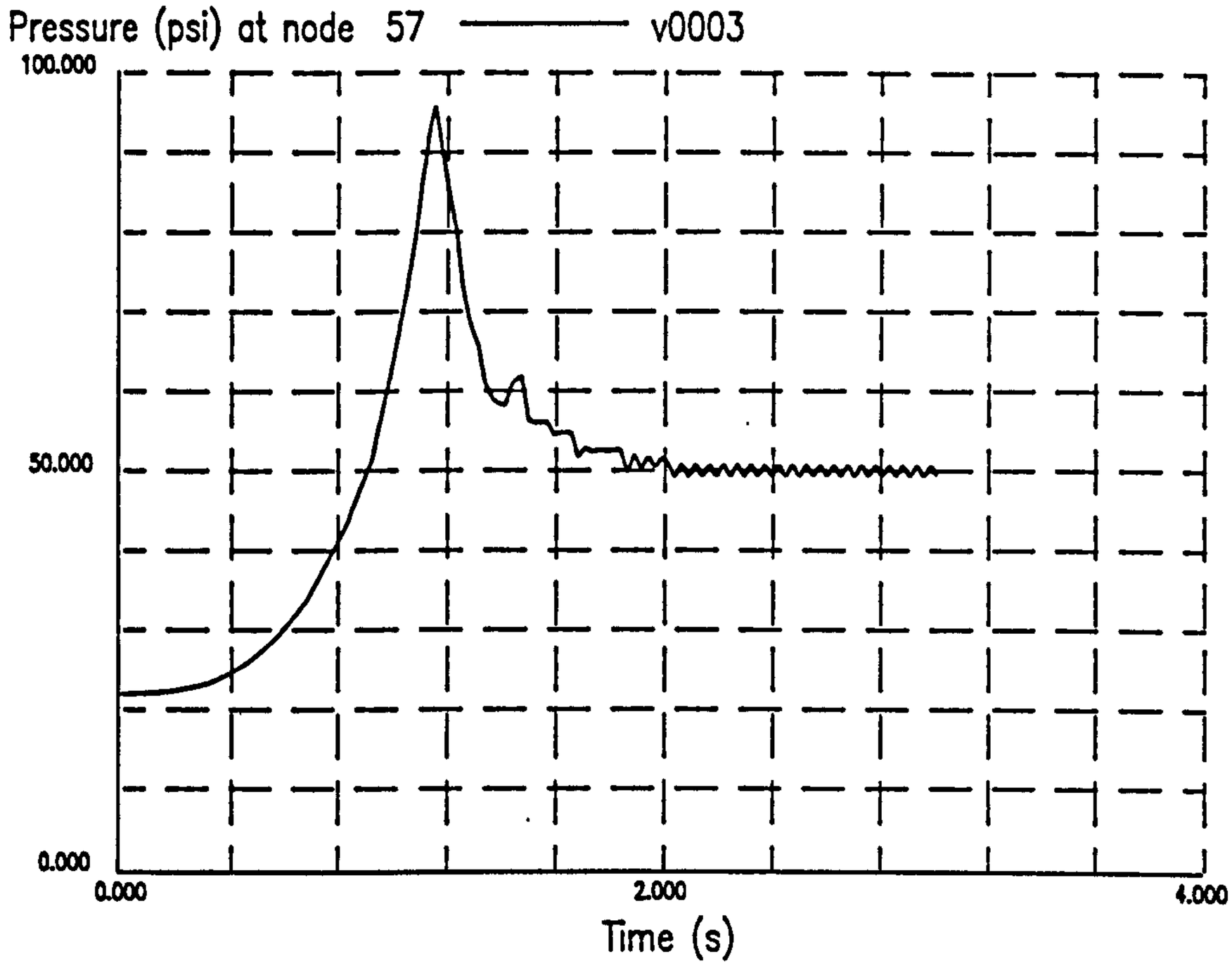

Figure 7.7 Pressure Surge Modelled with the Method of Characteristics.

Maximum value was 9.37E+01 (psi) at 1.160 (s)
Minimum value was 2.20E+01 (psi) at 0.000 (s)

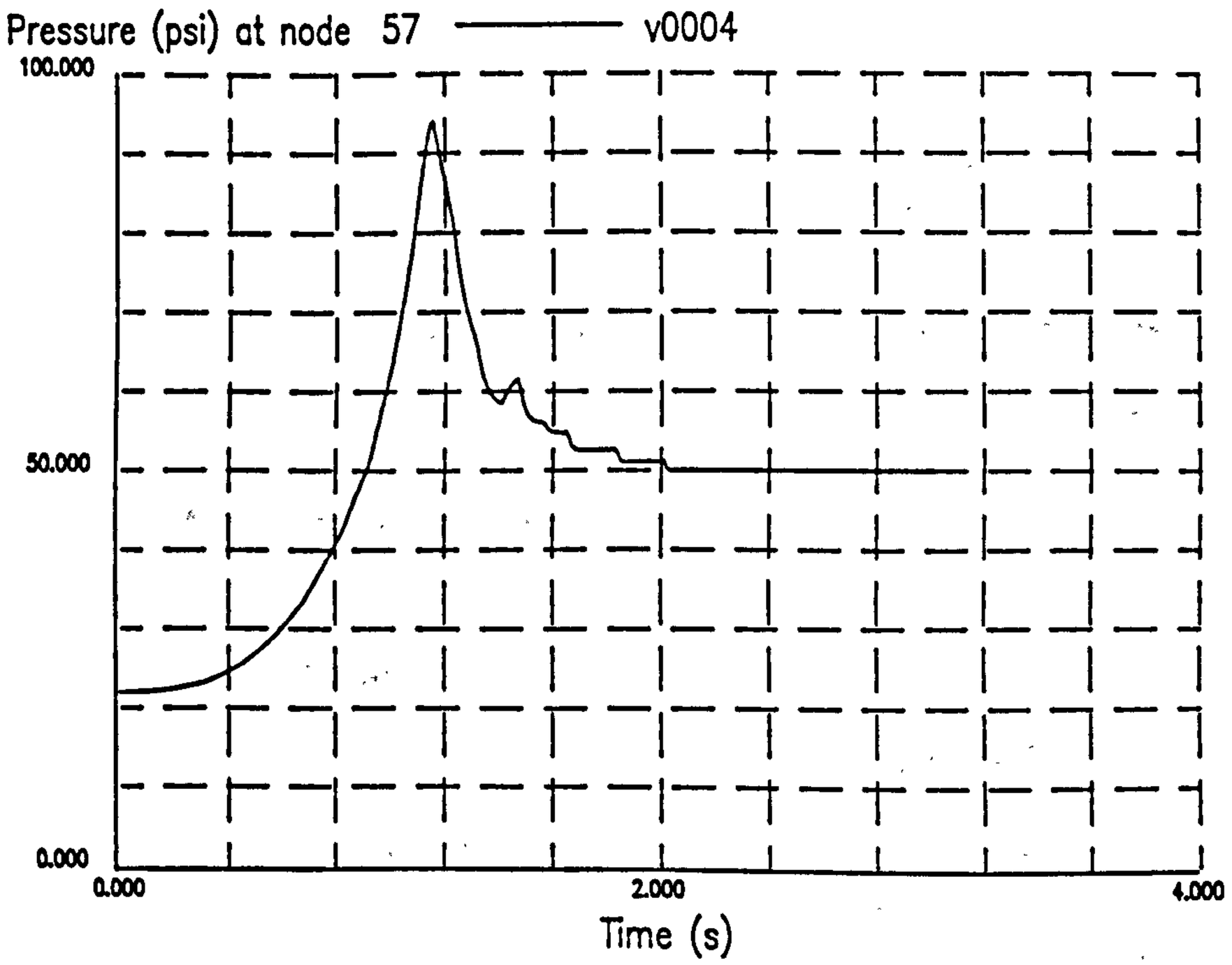

Figure 7.8 Pressure Surge Modelled with Standard Pipe Model.

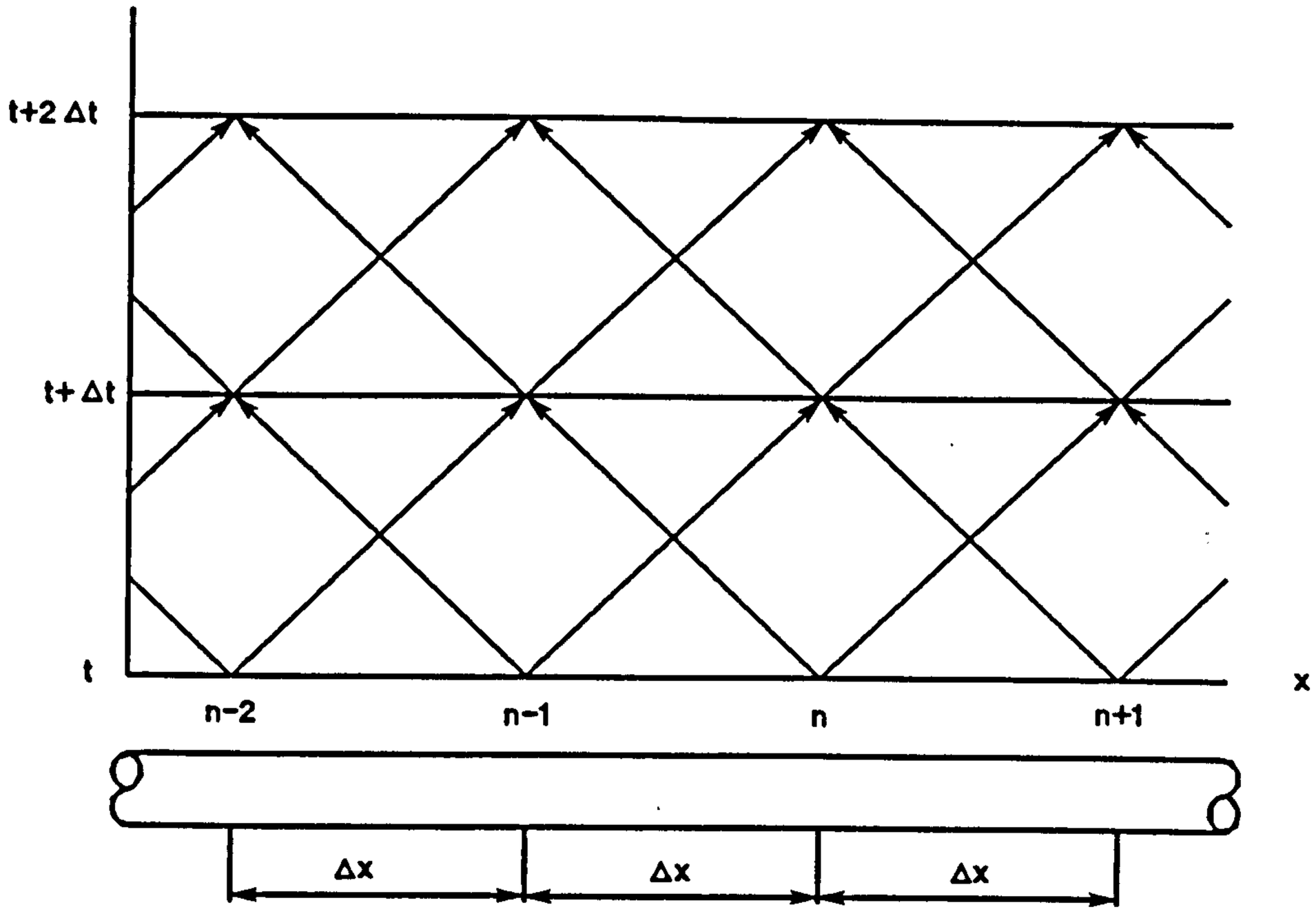

Figure 7.9 x,t Plot of Method of Characteristic Solution.

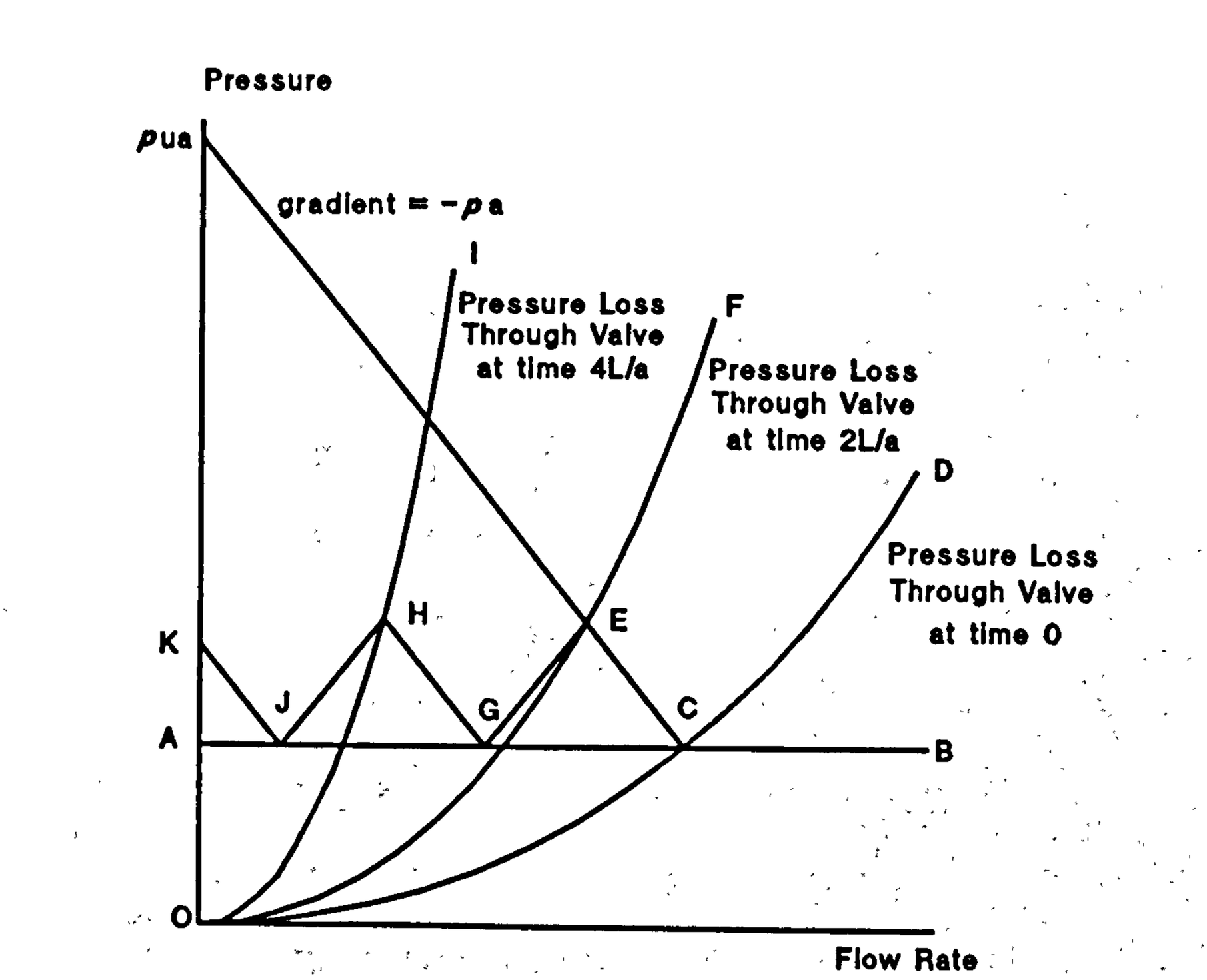

Figure 7.10 Simplified Graphical Pressure Surge Analysis

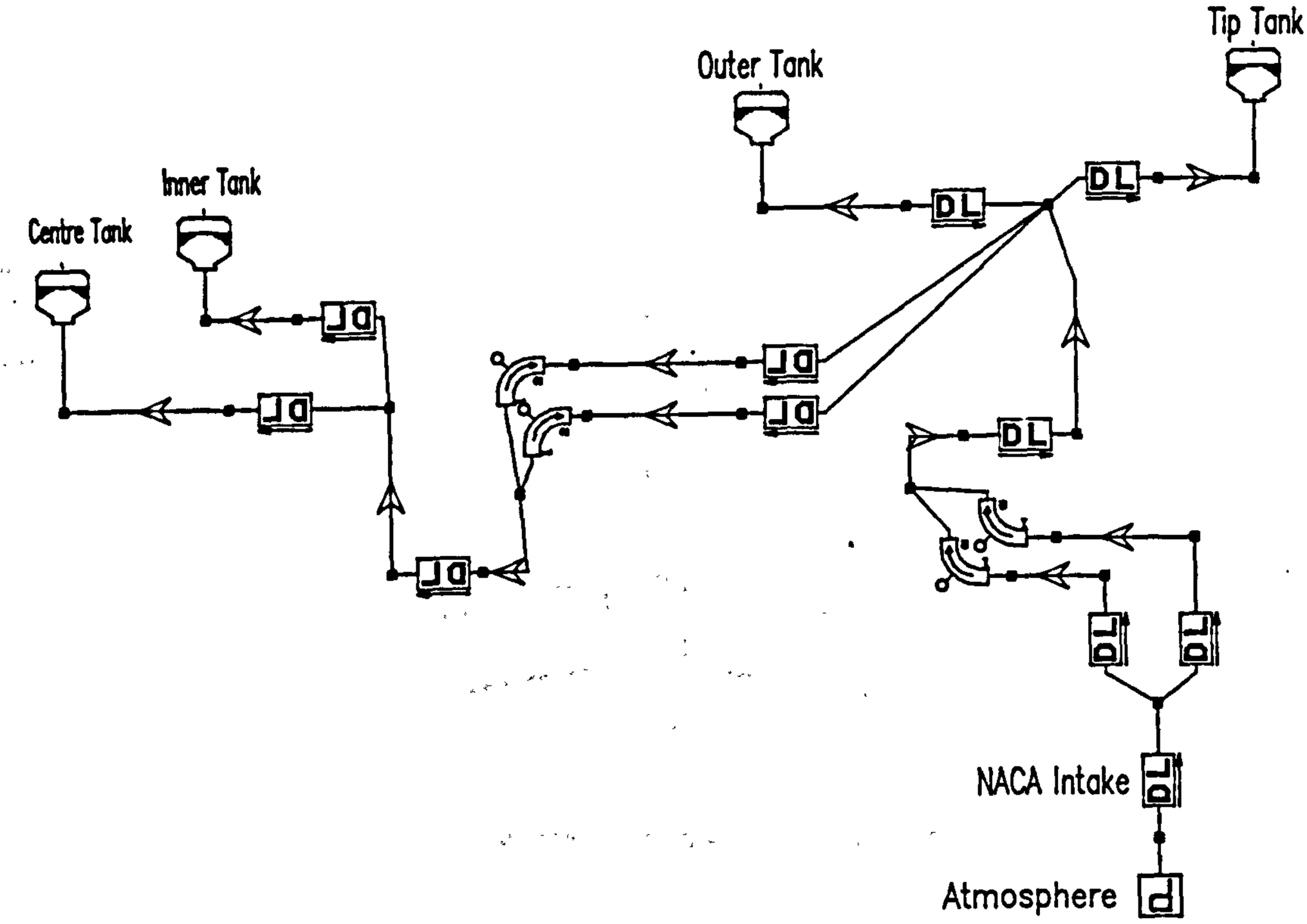

Figure 7.11 Typical Simulation Network for Modelling Emergency Descent.

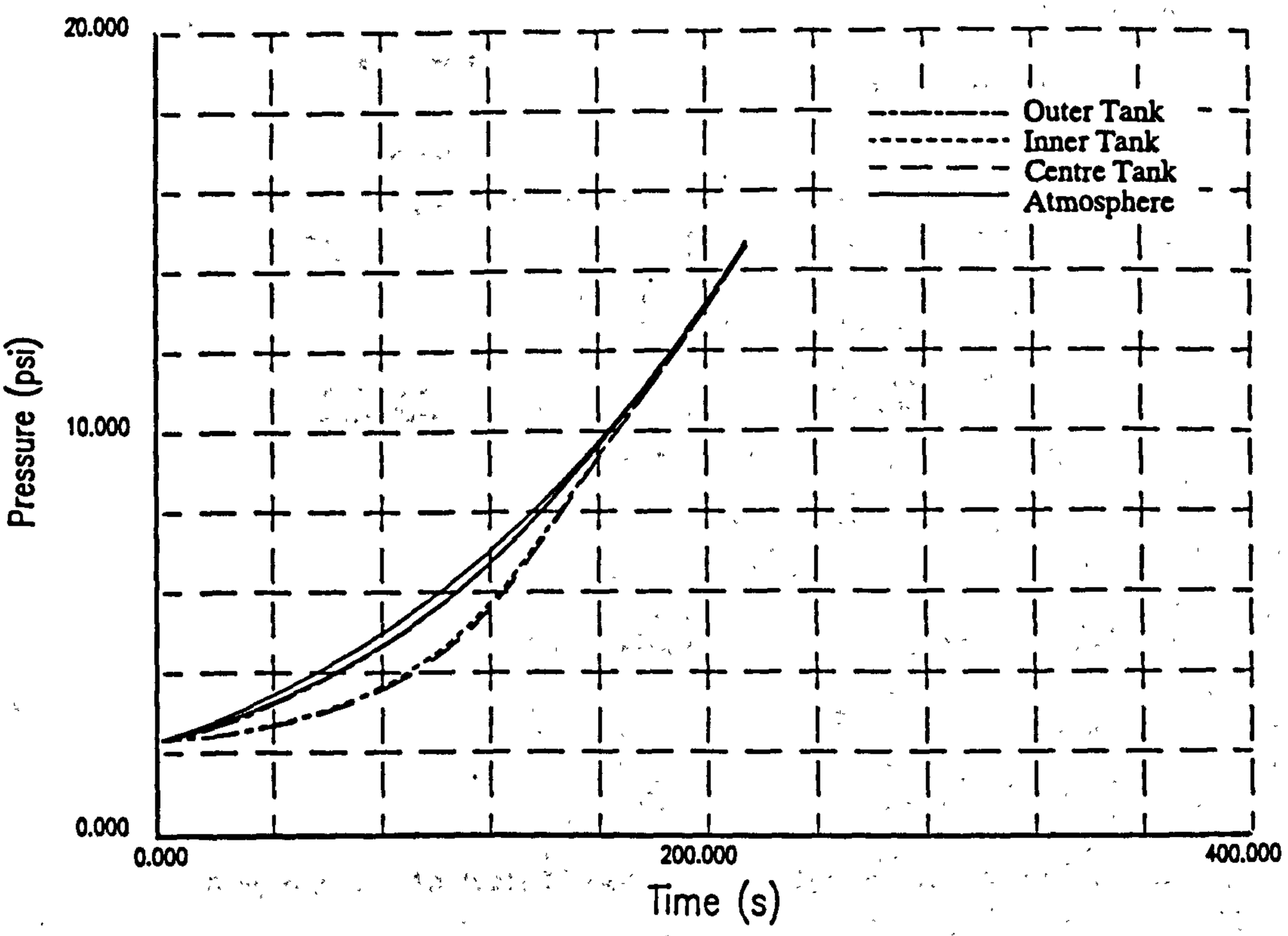

Figure 7.12 Typical Pressure Differentials due to an Emergency Descent.

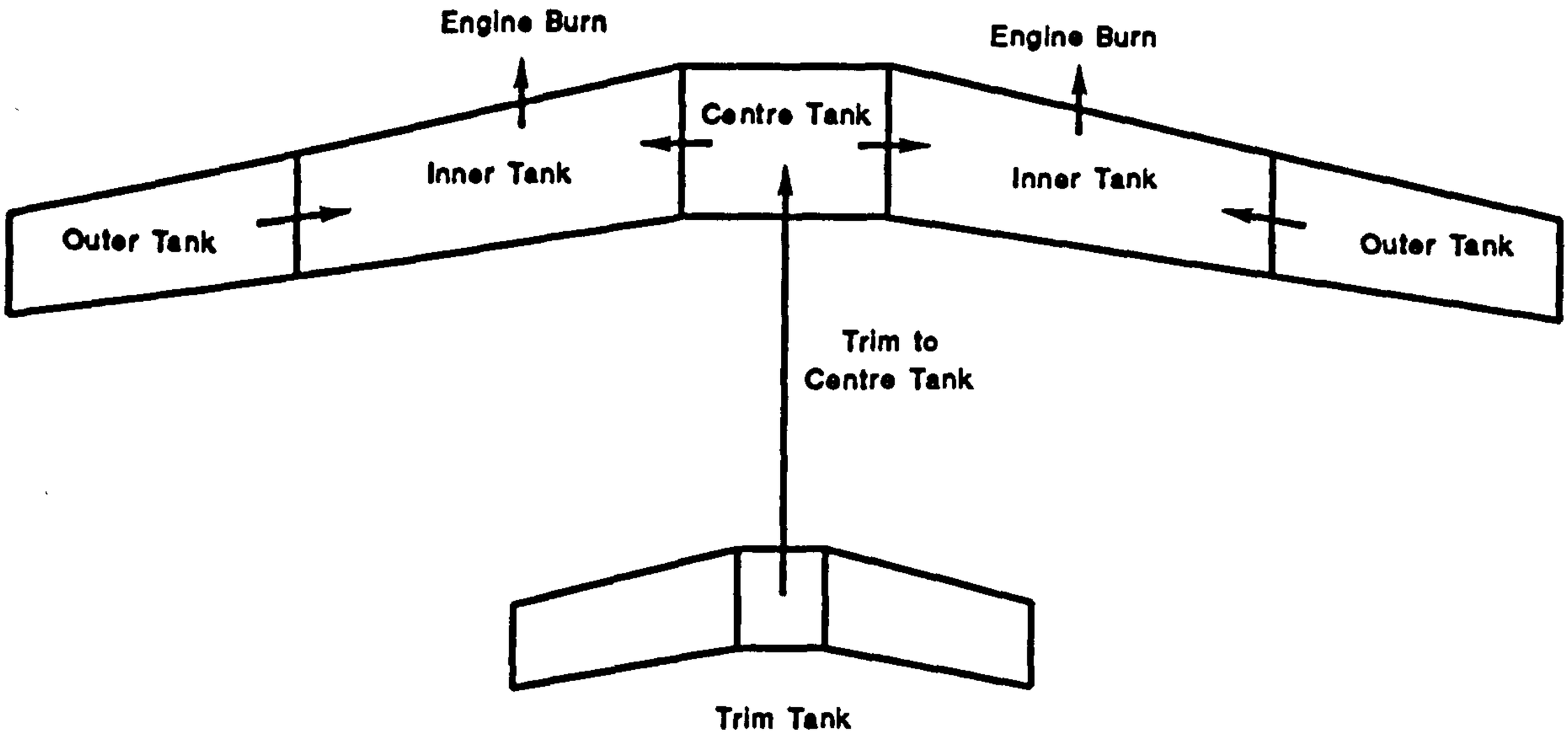

Figure 7.13 Fuel Transfers for a Six Fuel Tank Arrangement

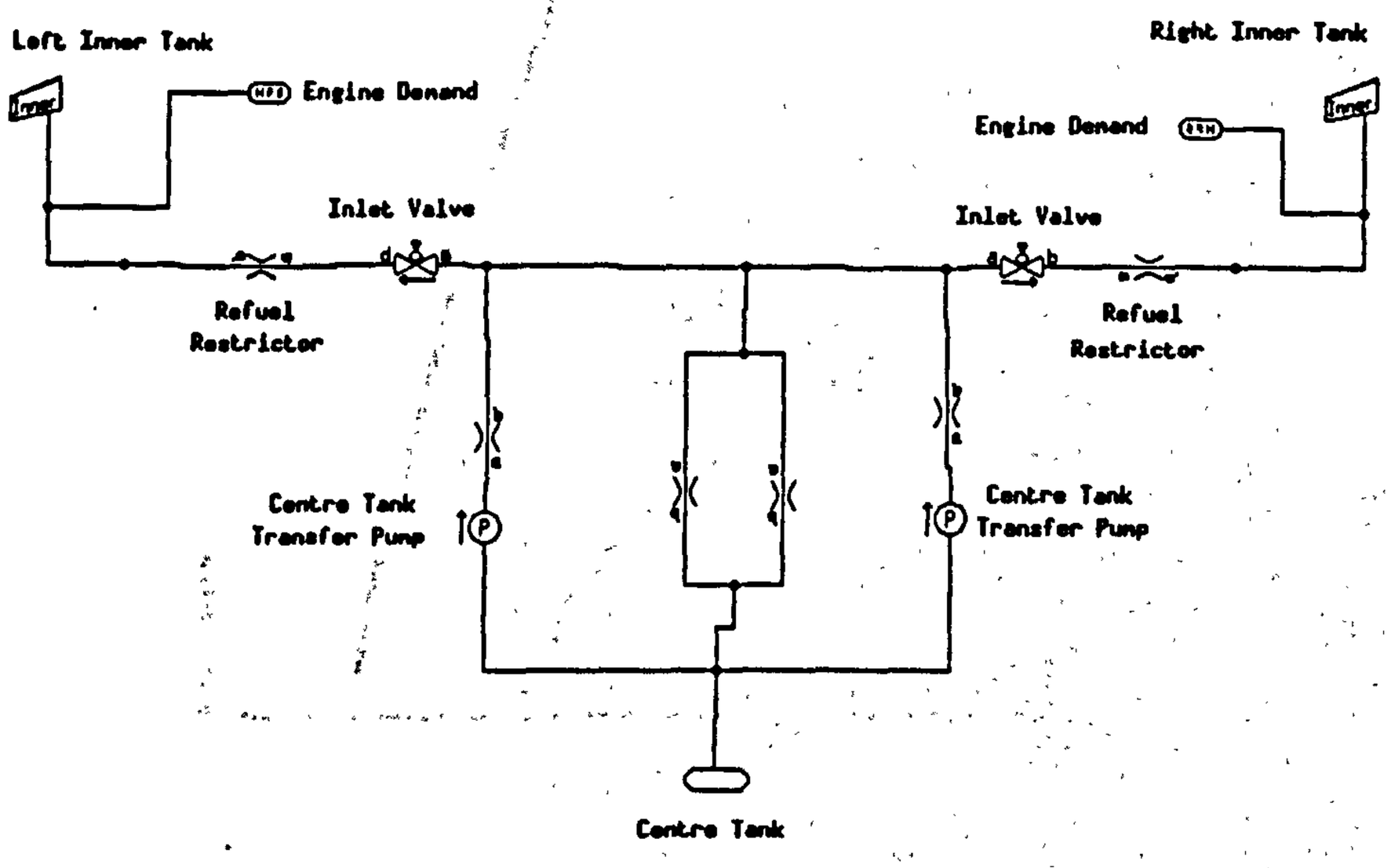

Figure 7.14 Analysis Network for Centre to Inner Tank Transfer.

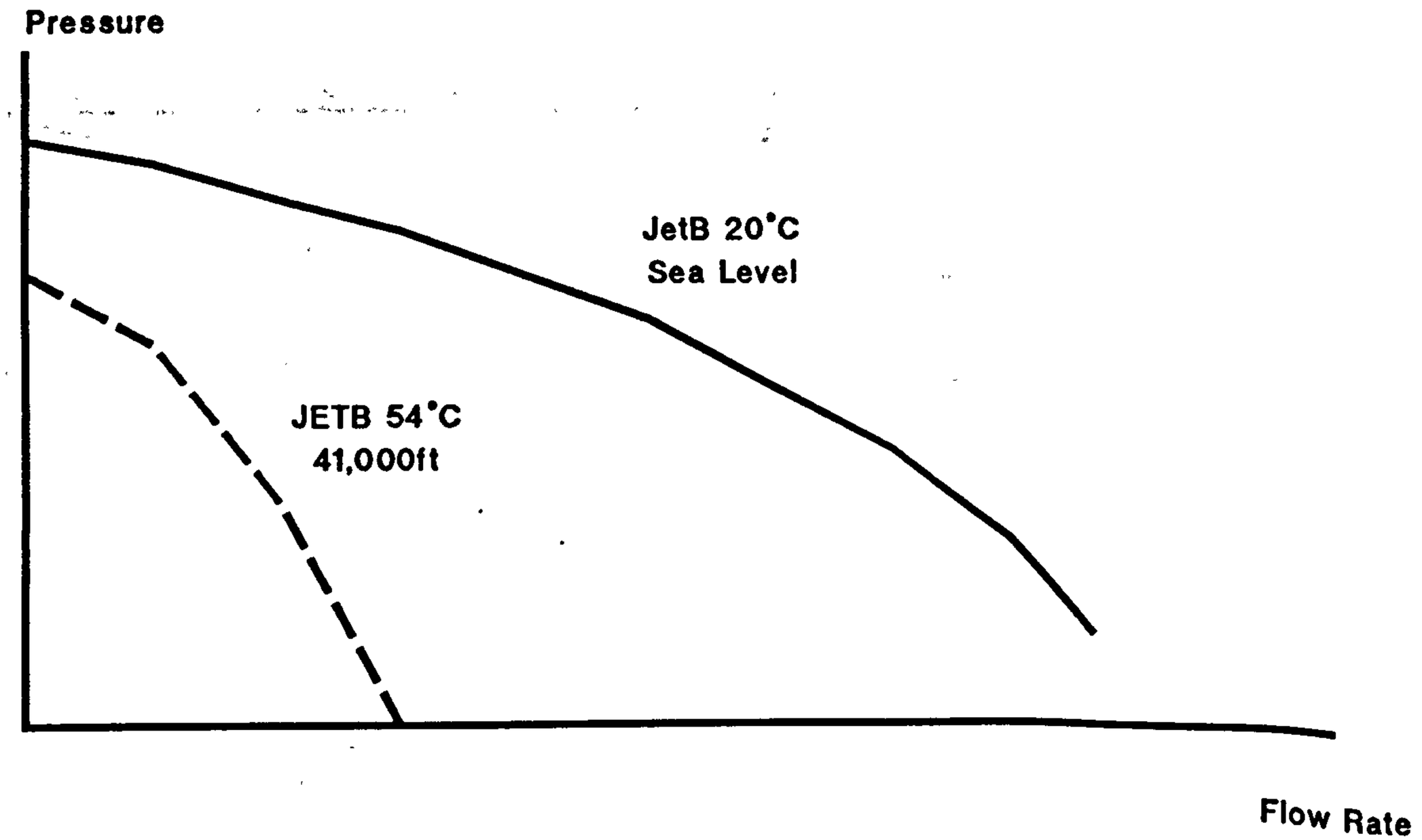

Figure 7.15 Centre Tank Pump Performance Characteristic

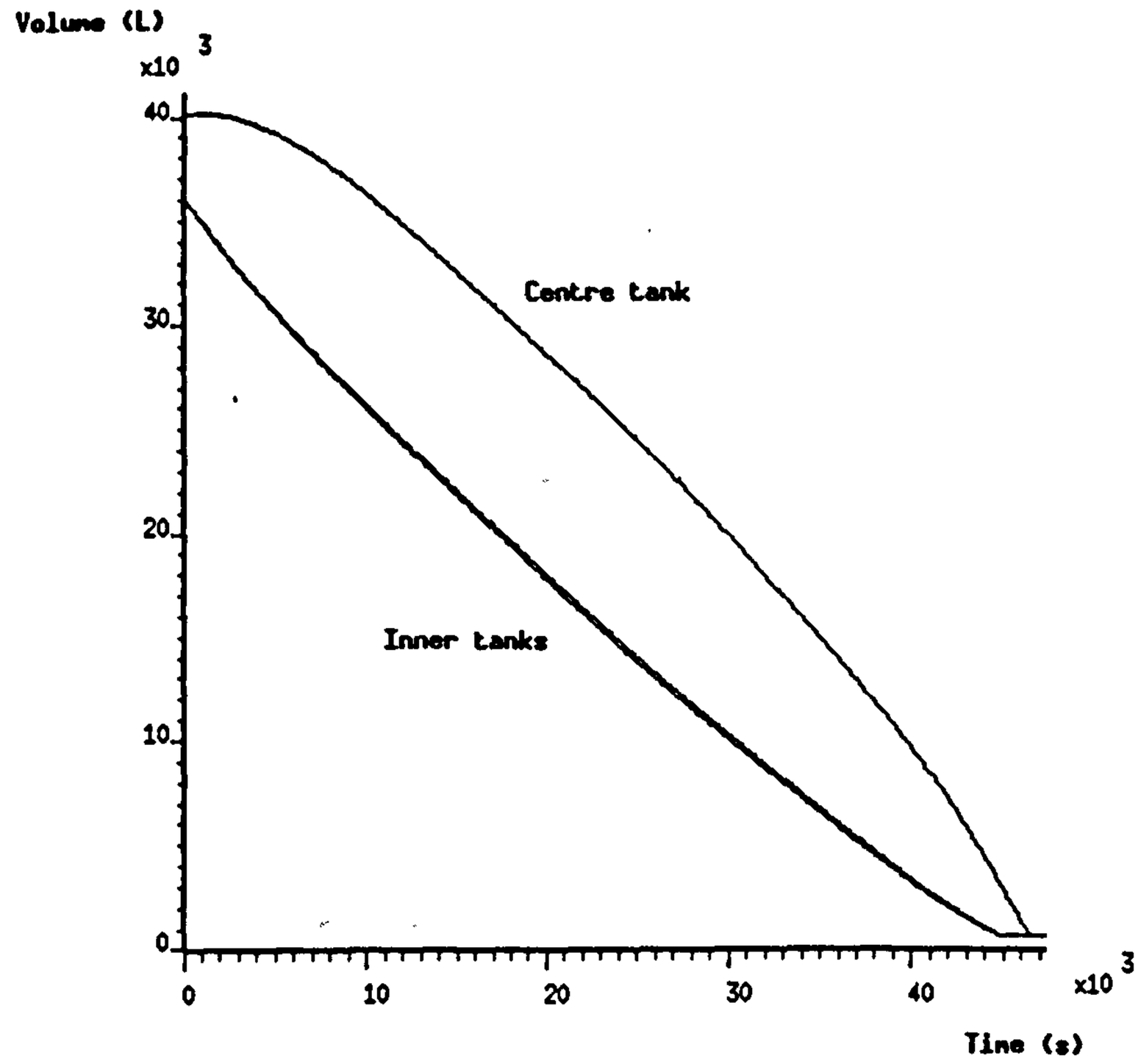

a. Volume of Fuel in Tanks.

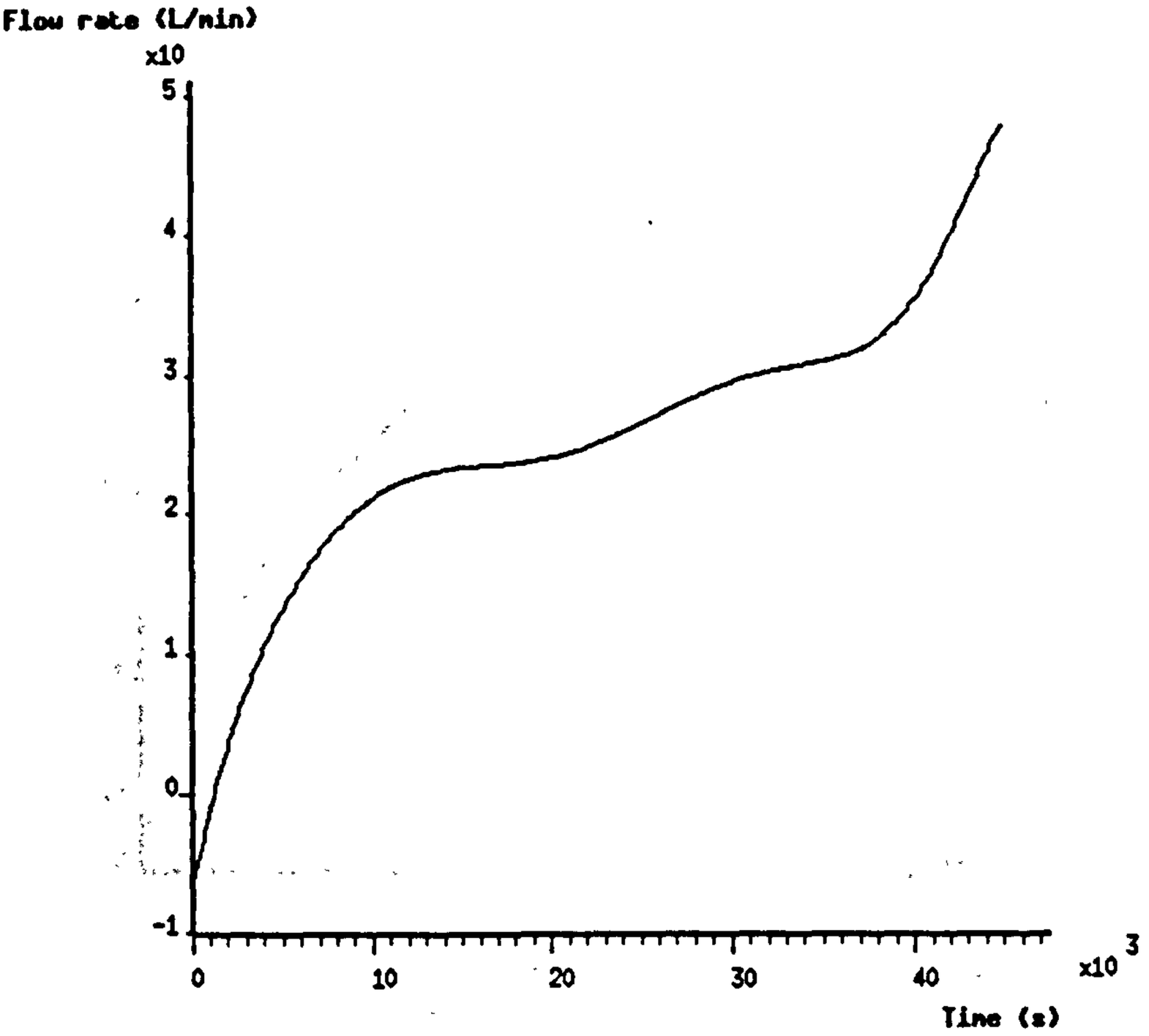

b. Flow Rate Through Inlet Valve.

Figure 7.16 Centre to Inner Tank Transfer, Both Tanks Full at Start of Analysis

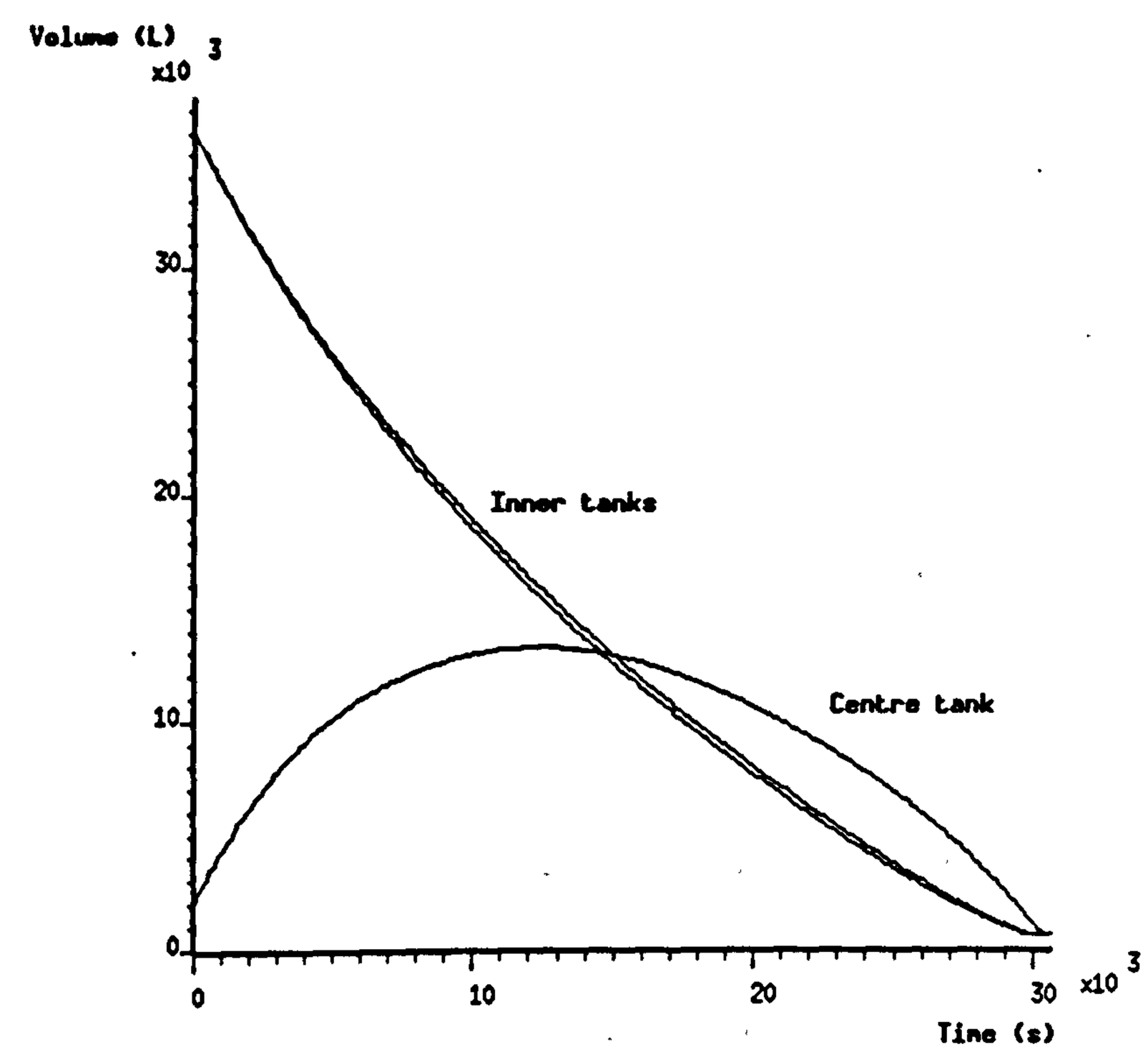

a. Volume of Fuel in the Tanks.

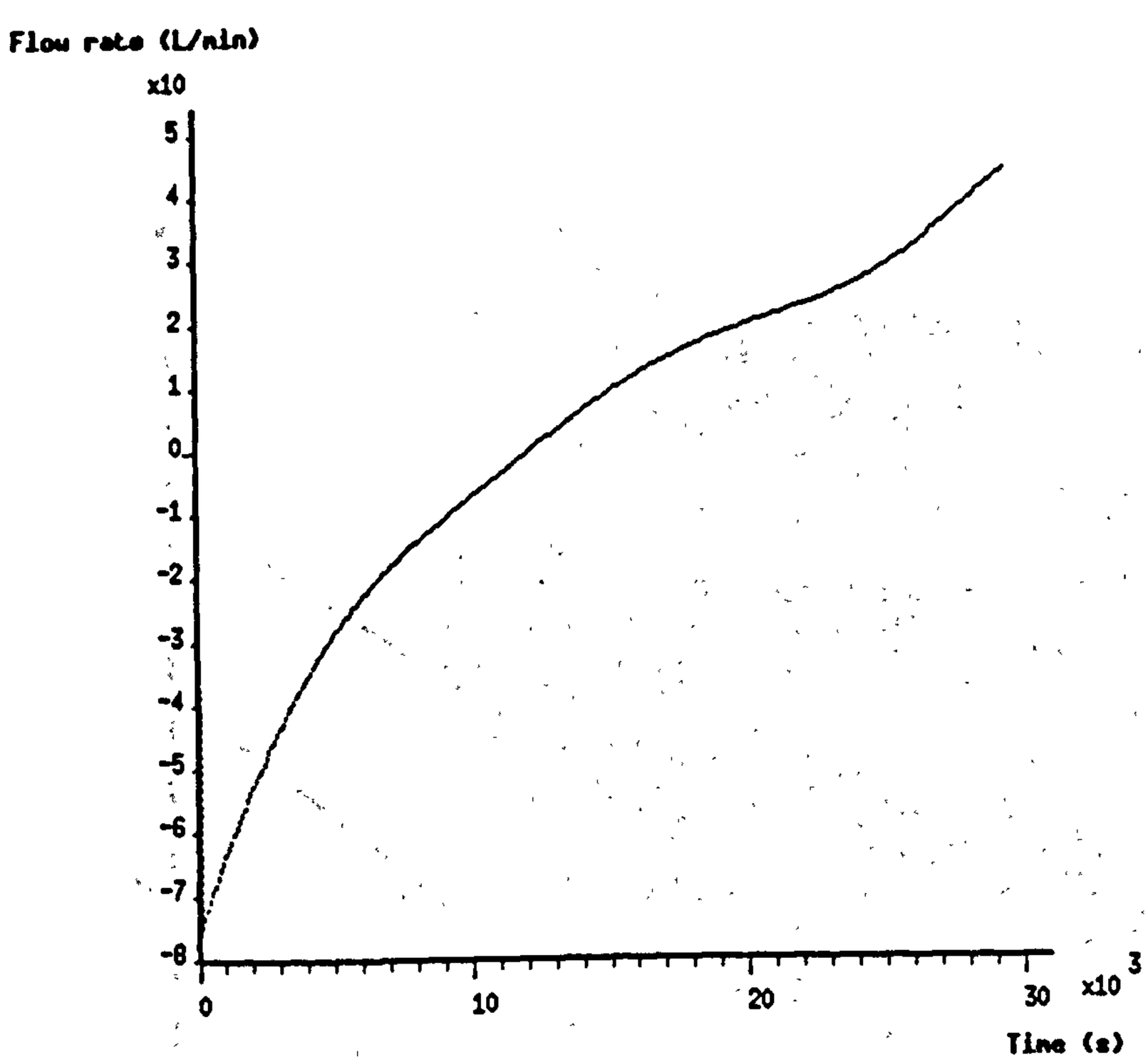

b. Flow rate Through Isolation Valve.

Figure 7.17 Centre to Inner Tank Transfer, Centre Tank Empty Inner Tank Full at Start of Analysis.

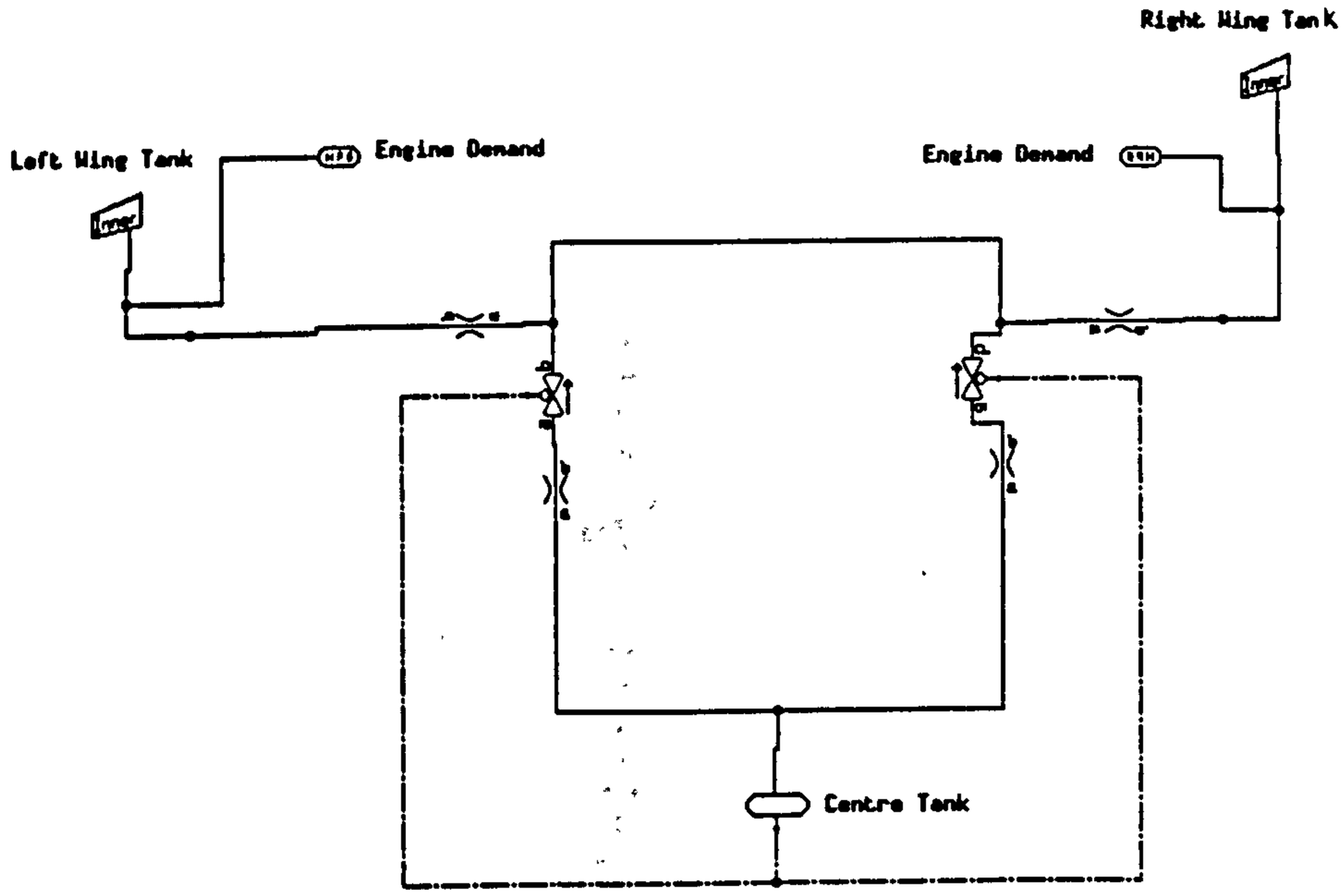

Figure 7.18 Typical Flight Profile Simulation for a Meduim Capacity Civil Aircraft.

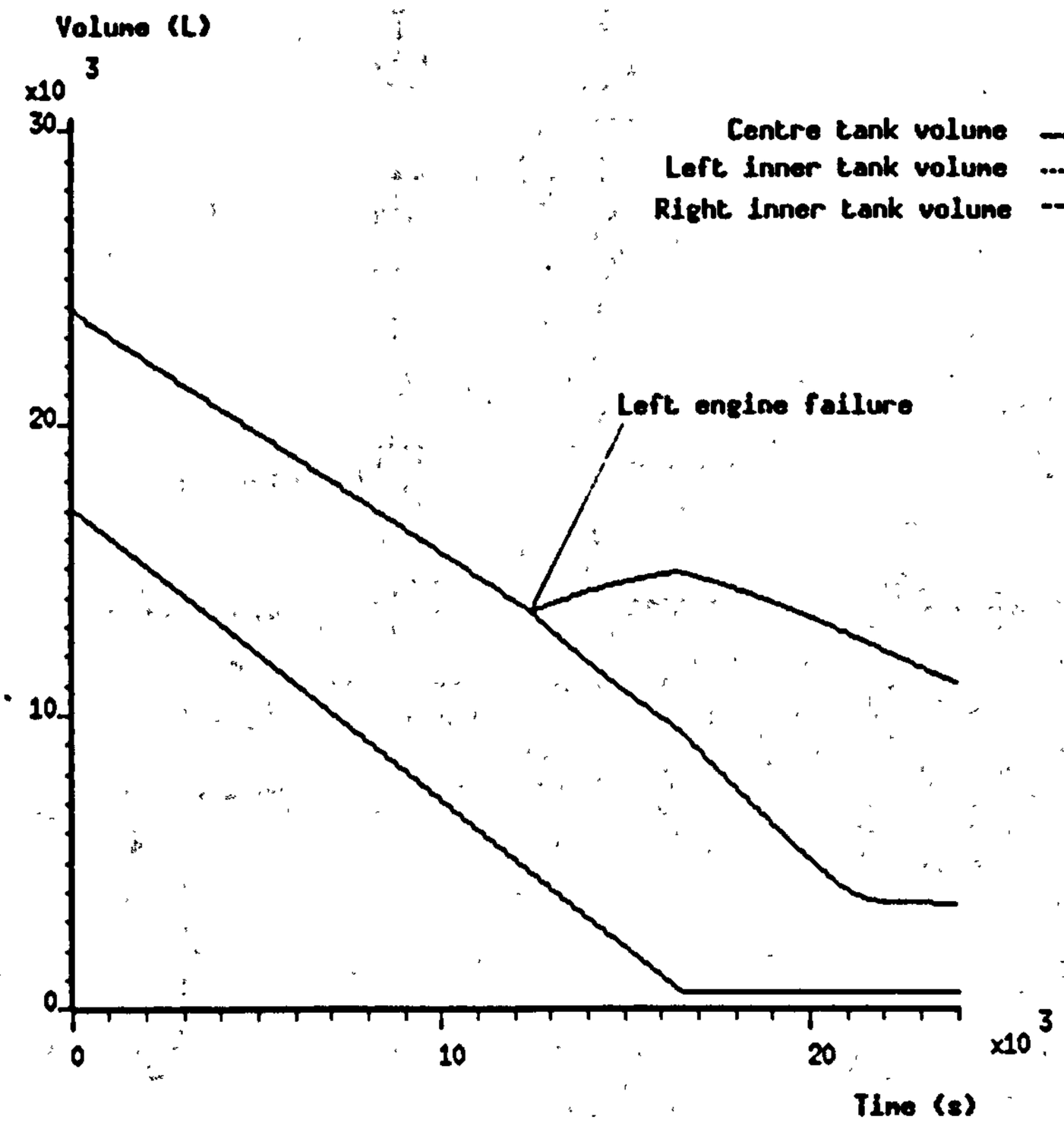

Figure 7.19 Typical Transfers for an Engine Failure.

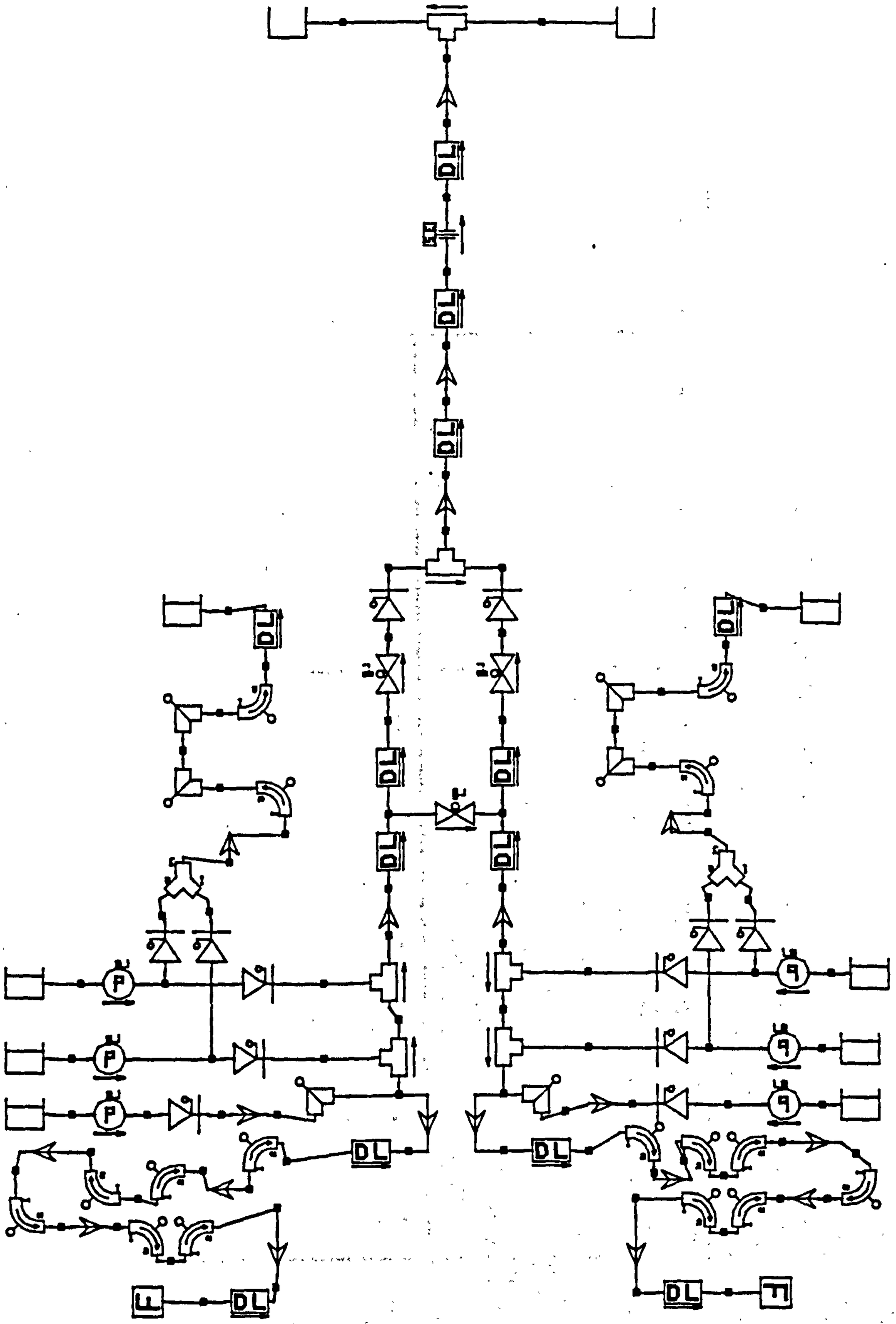

Figure 7.20 Typical Engine Feed Analysis Simulation Network for a Large Civil Aircraft.

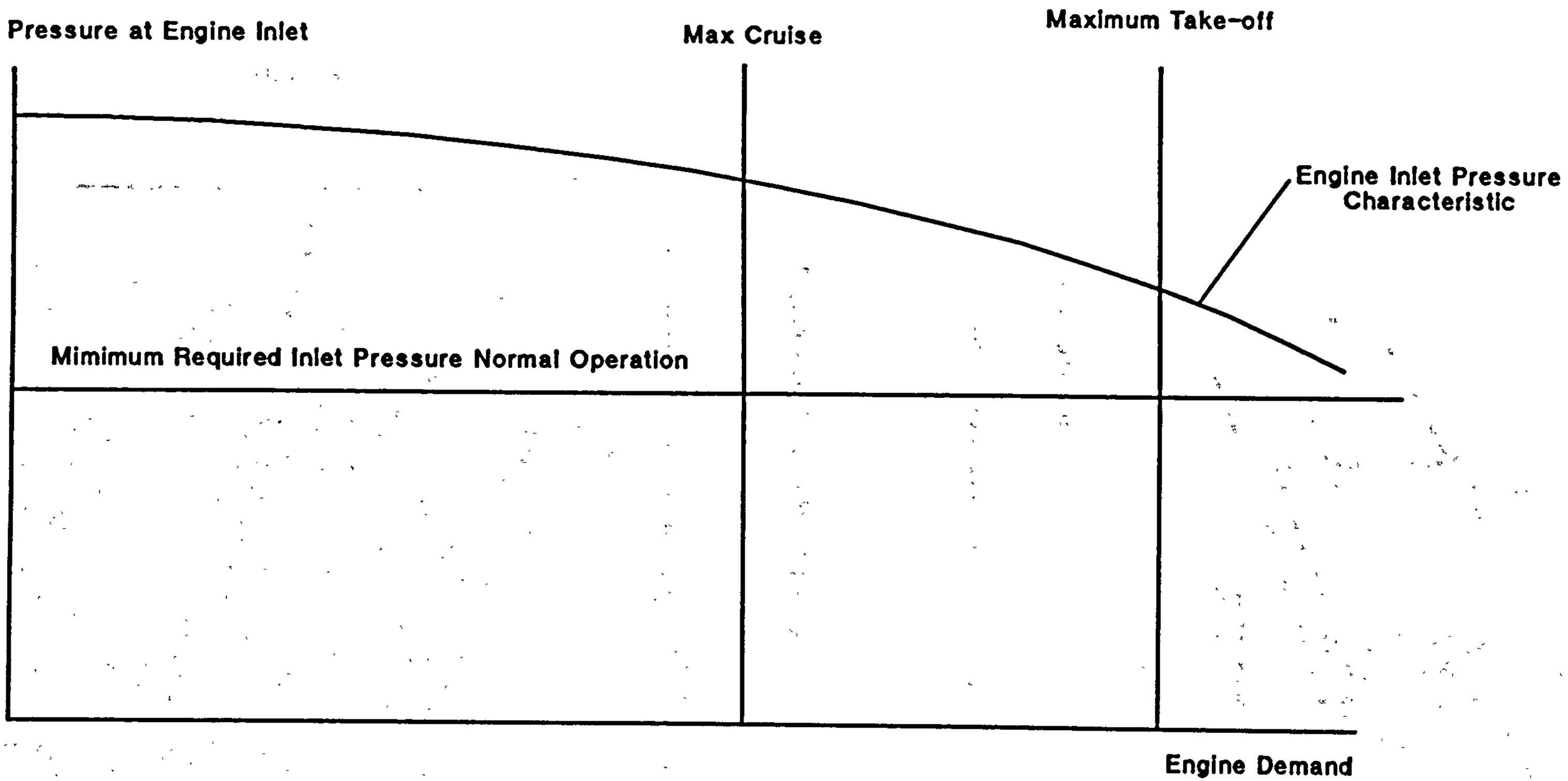

Figure 7.21 Typical Engine Feed Performance Curve.

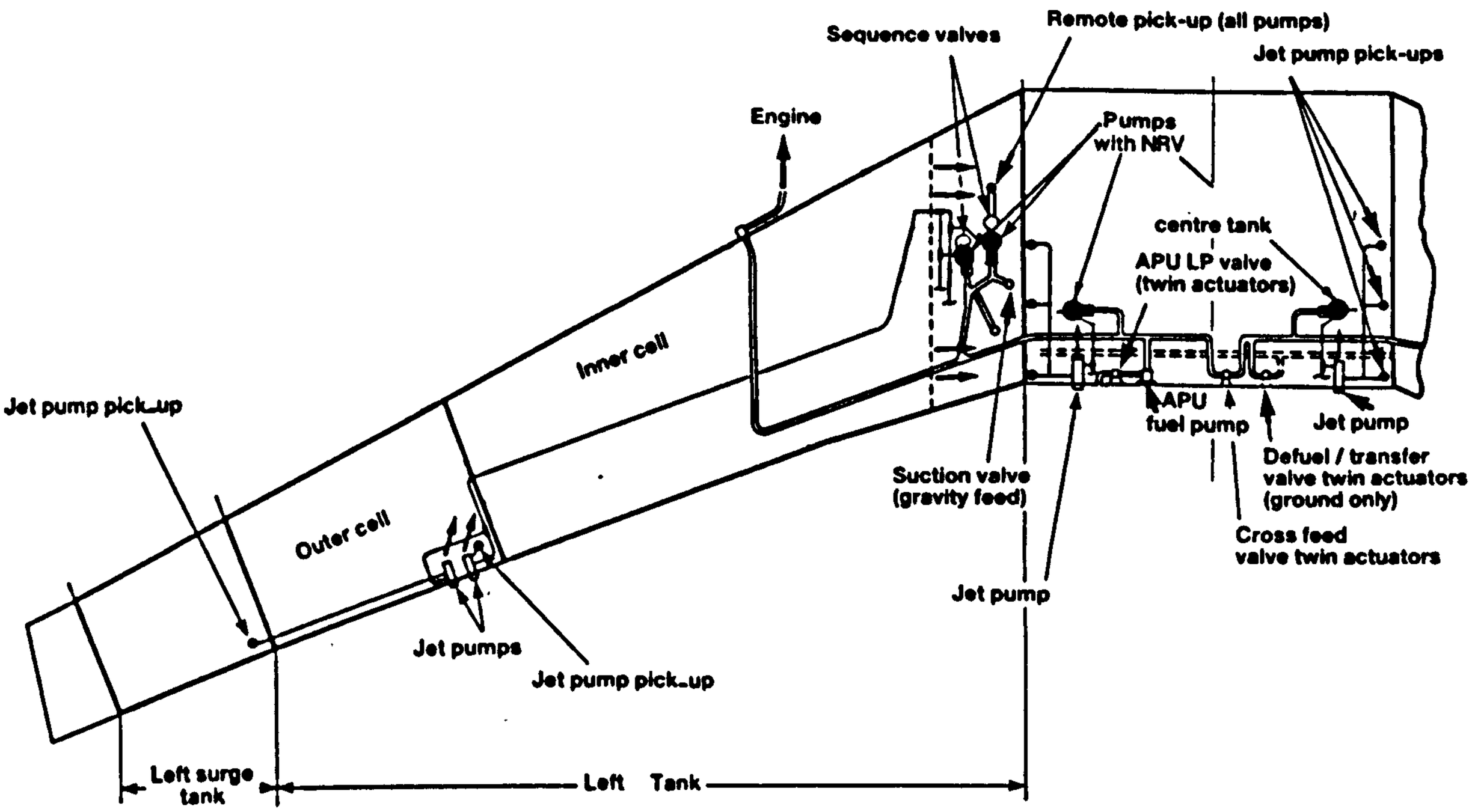

Figure 8.1 Engine Feed System.

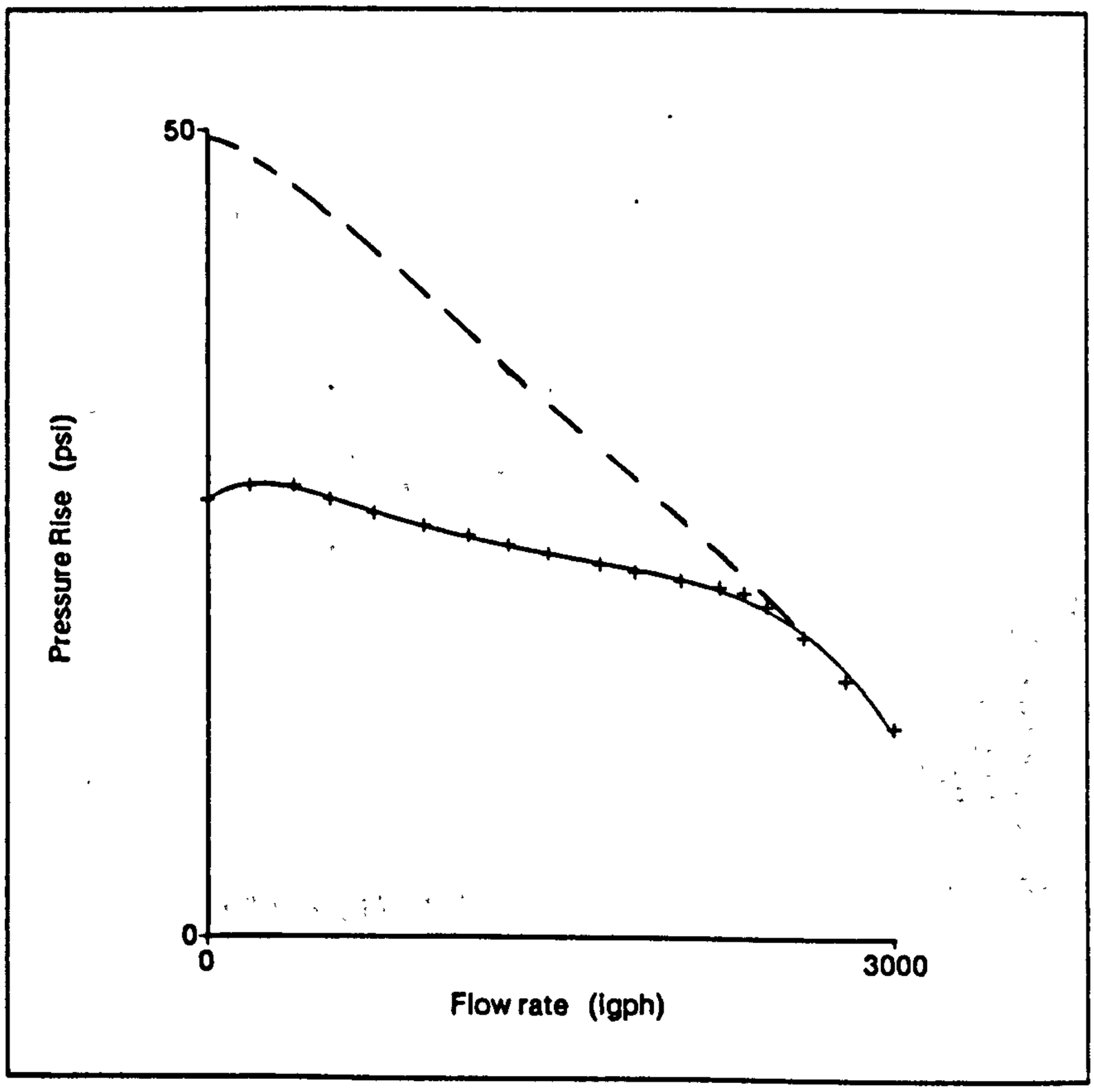

Figure 8.2 Combined Boost Pump and Sequence Valve Characteristic.

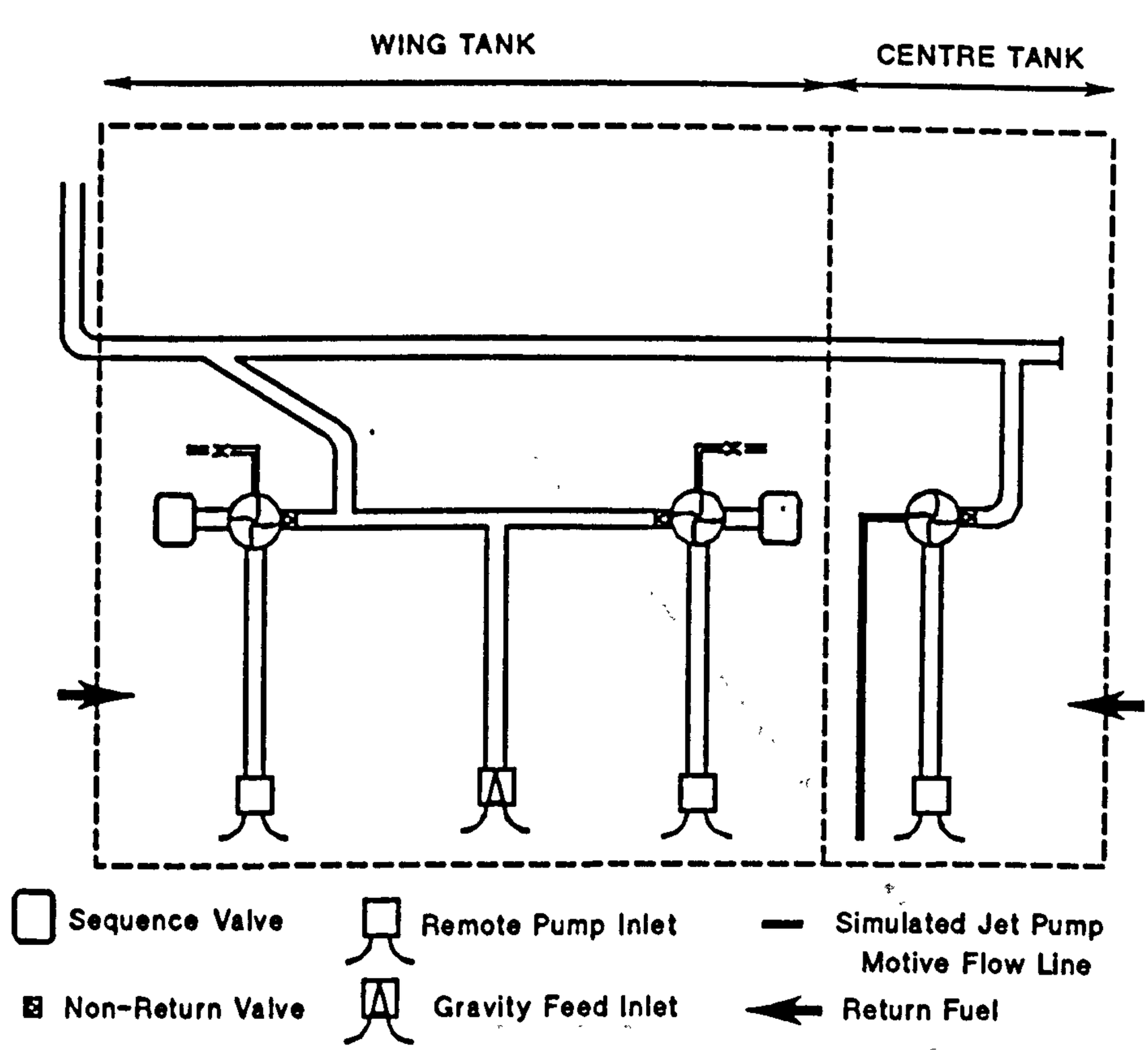

Figure 8.3 Engine Feed System Test Rig.

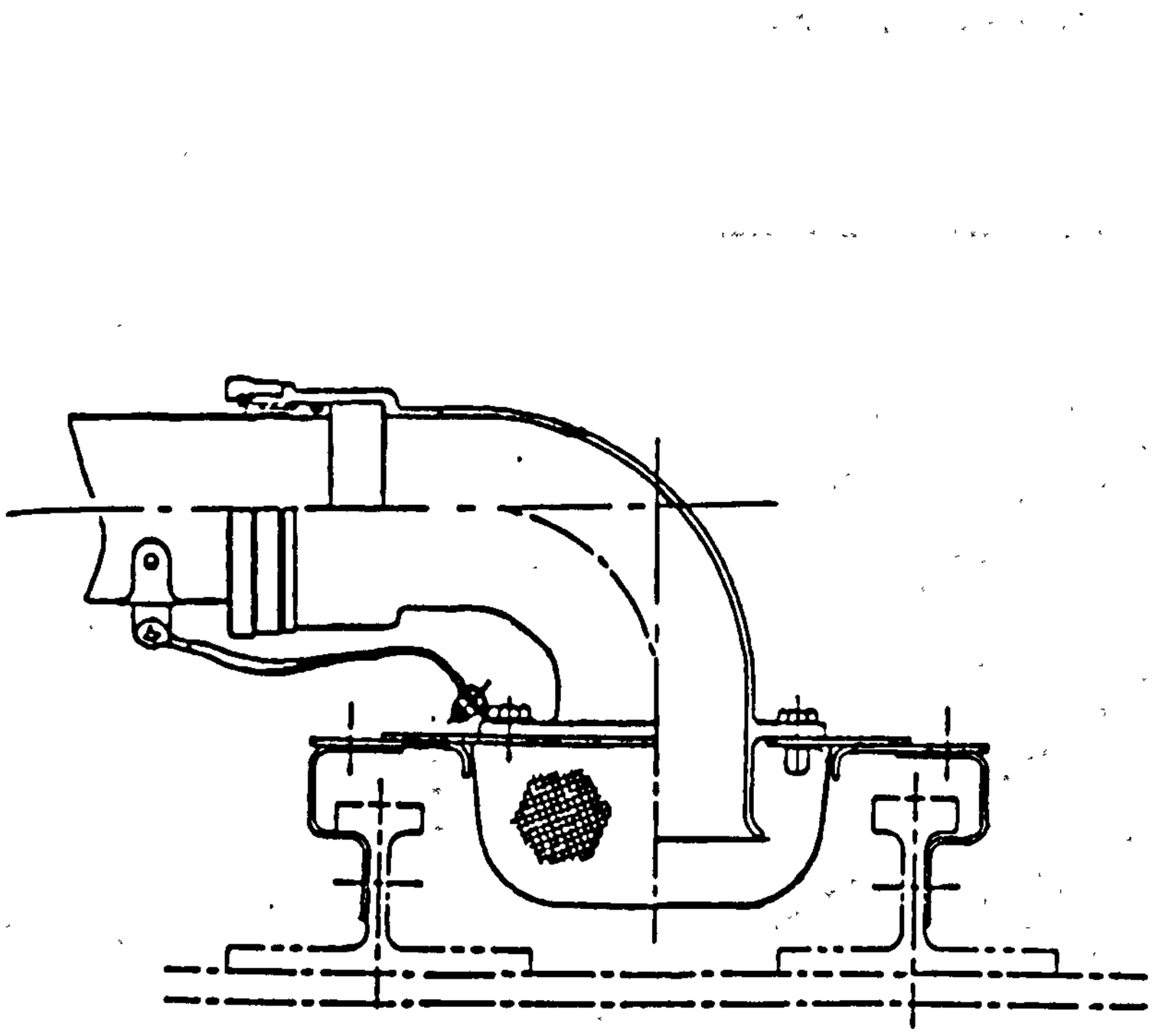

Figure 8.4 Engine Feed Remote Inlet.

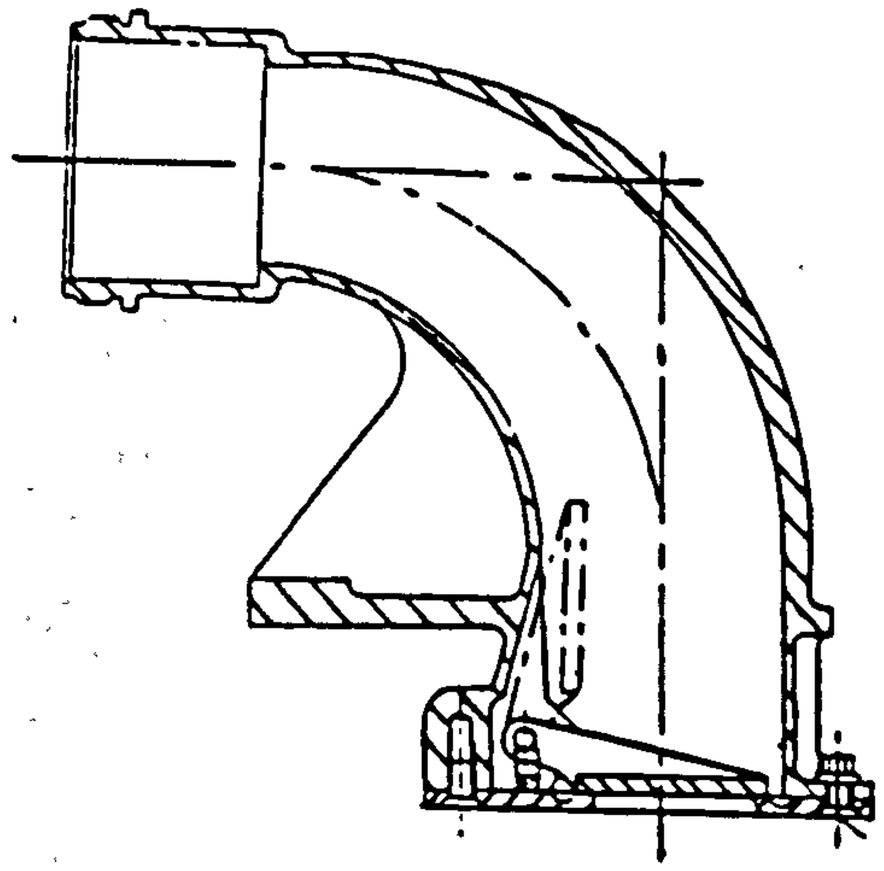

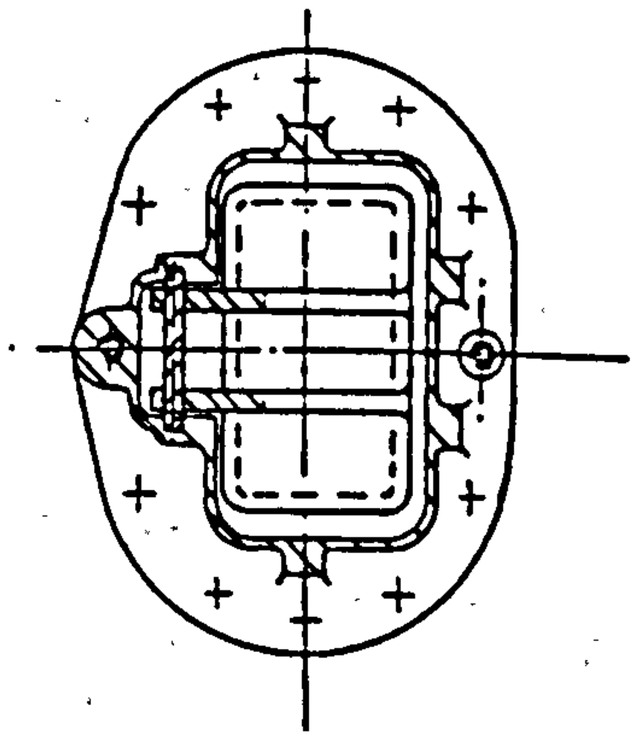

Figure 8.5 Gravity Feed Inlet.

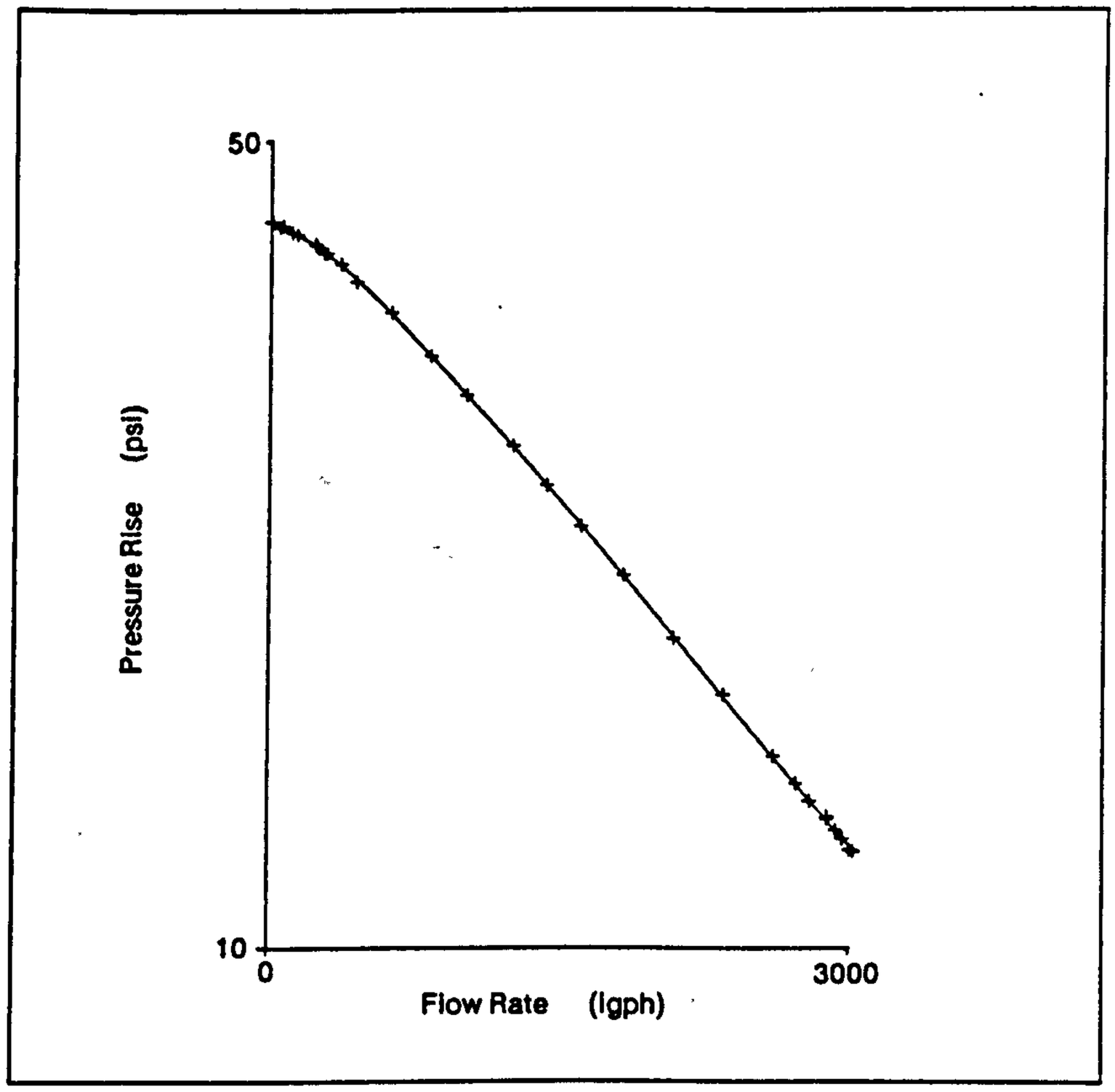

Figure 8.6 Engine Feed Boost Pump Characteristic.

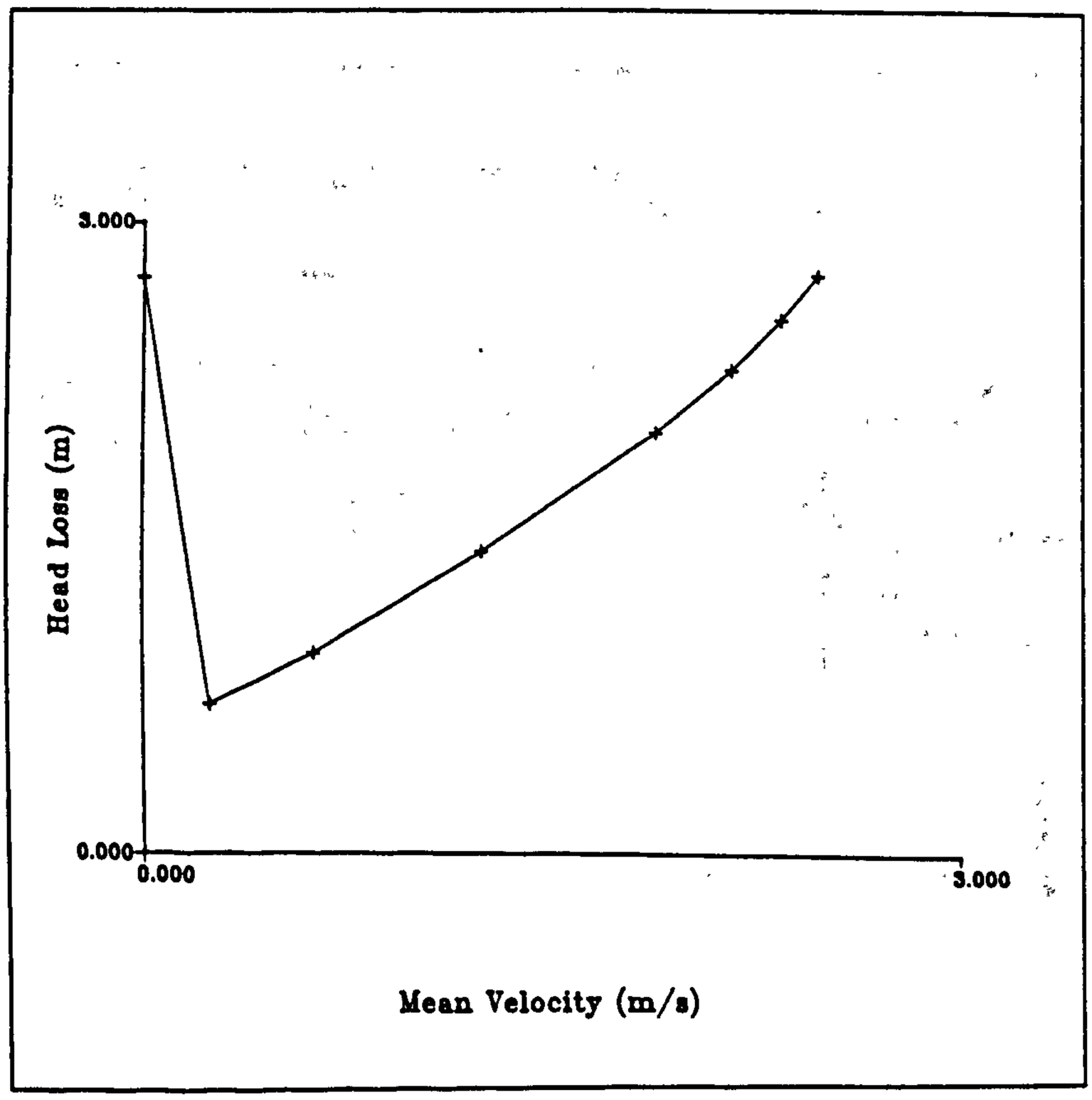

Figure 8.7 Engine Feed Boost Pump Outlet Non-Return Valve Characteristic.

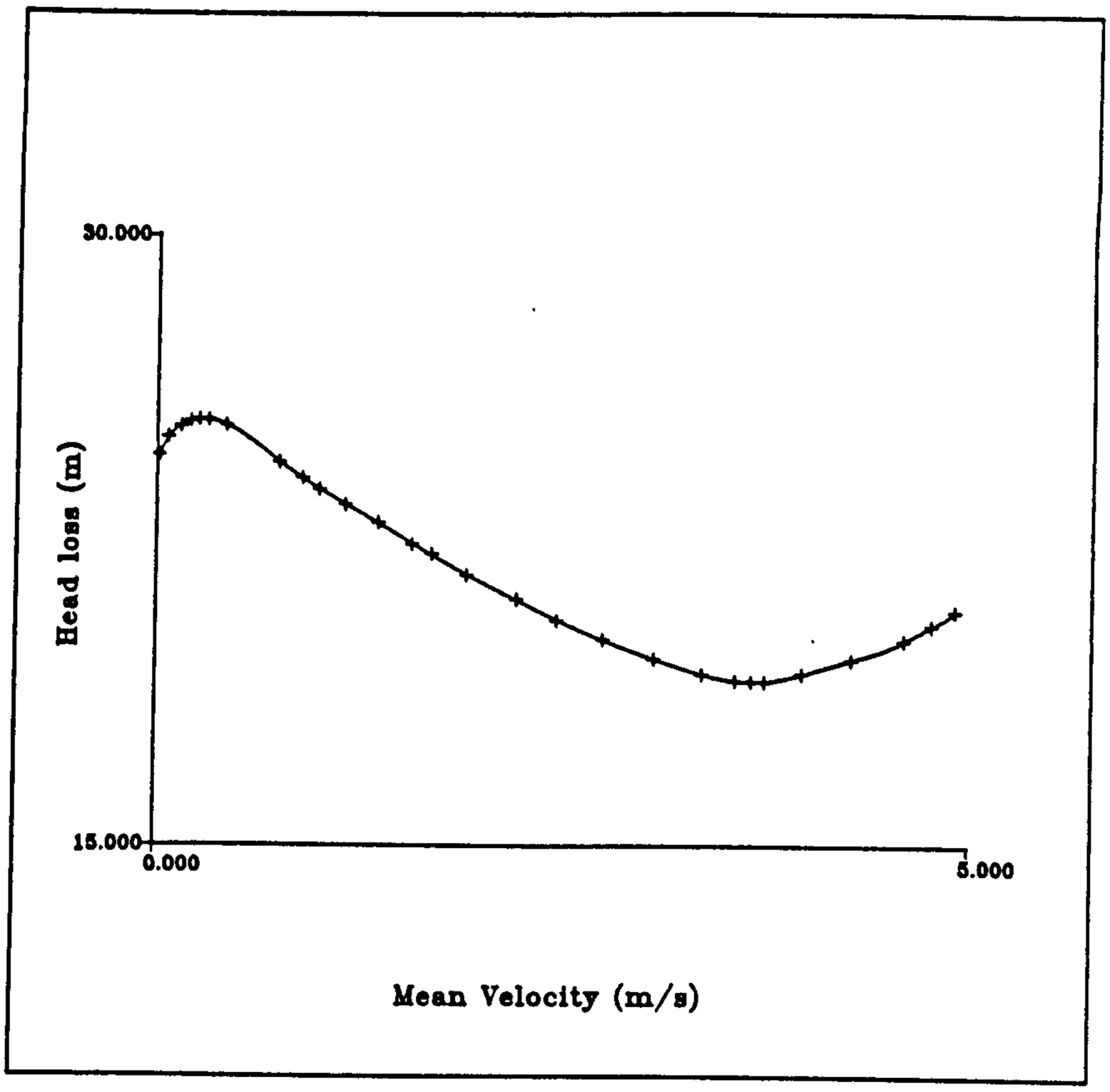

Figure 8.8 Engine Feed Sequence Valve Characteristic.

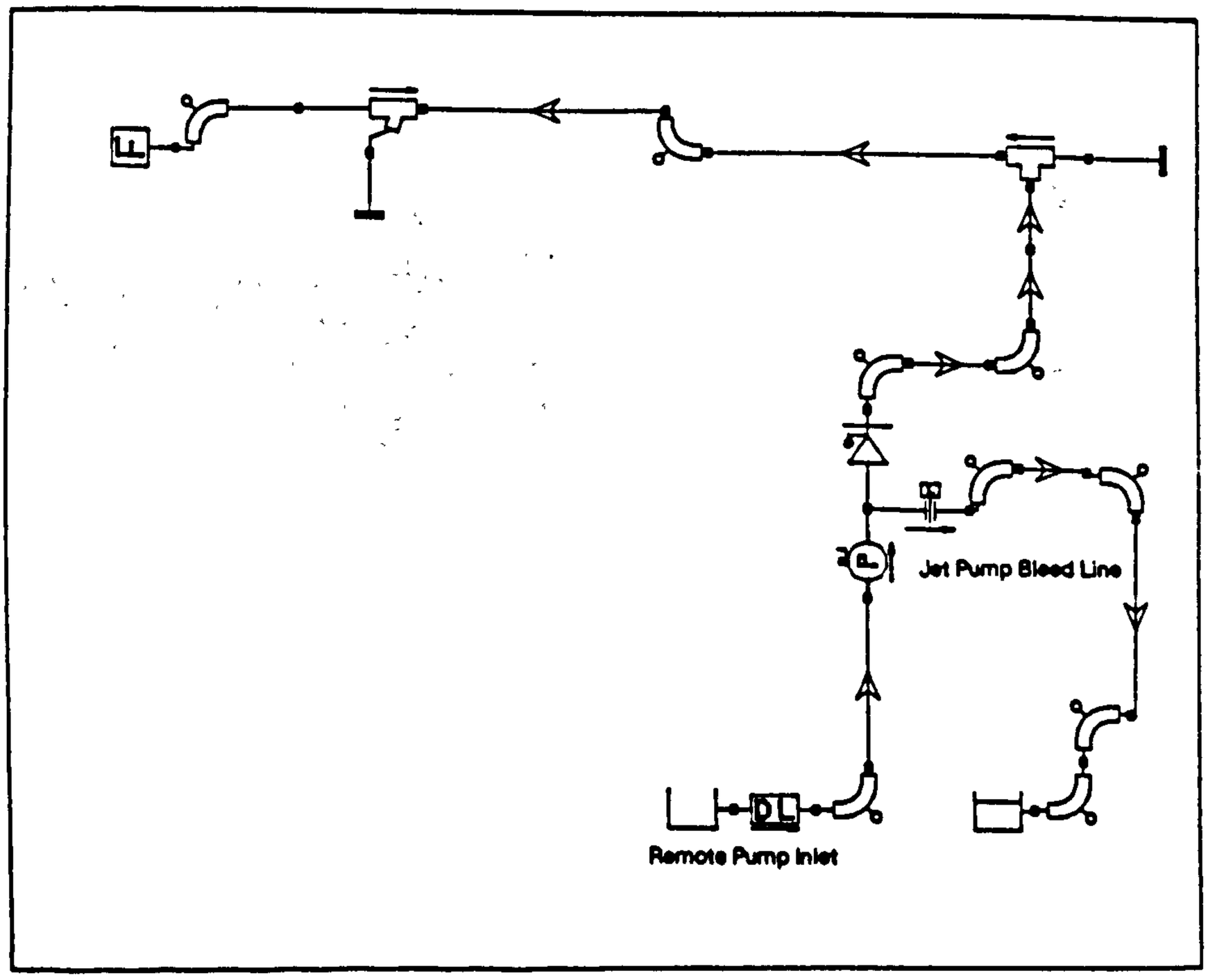

Figure 8.9 Simulation Network for Centre Tank Engine Feed System.

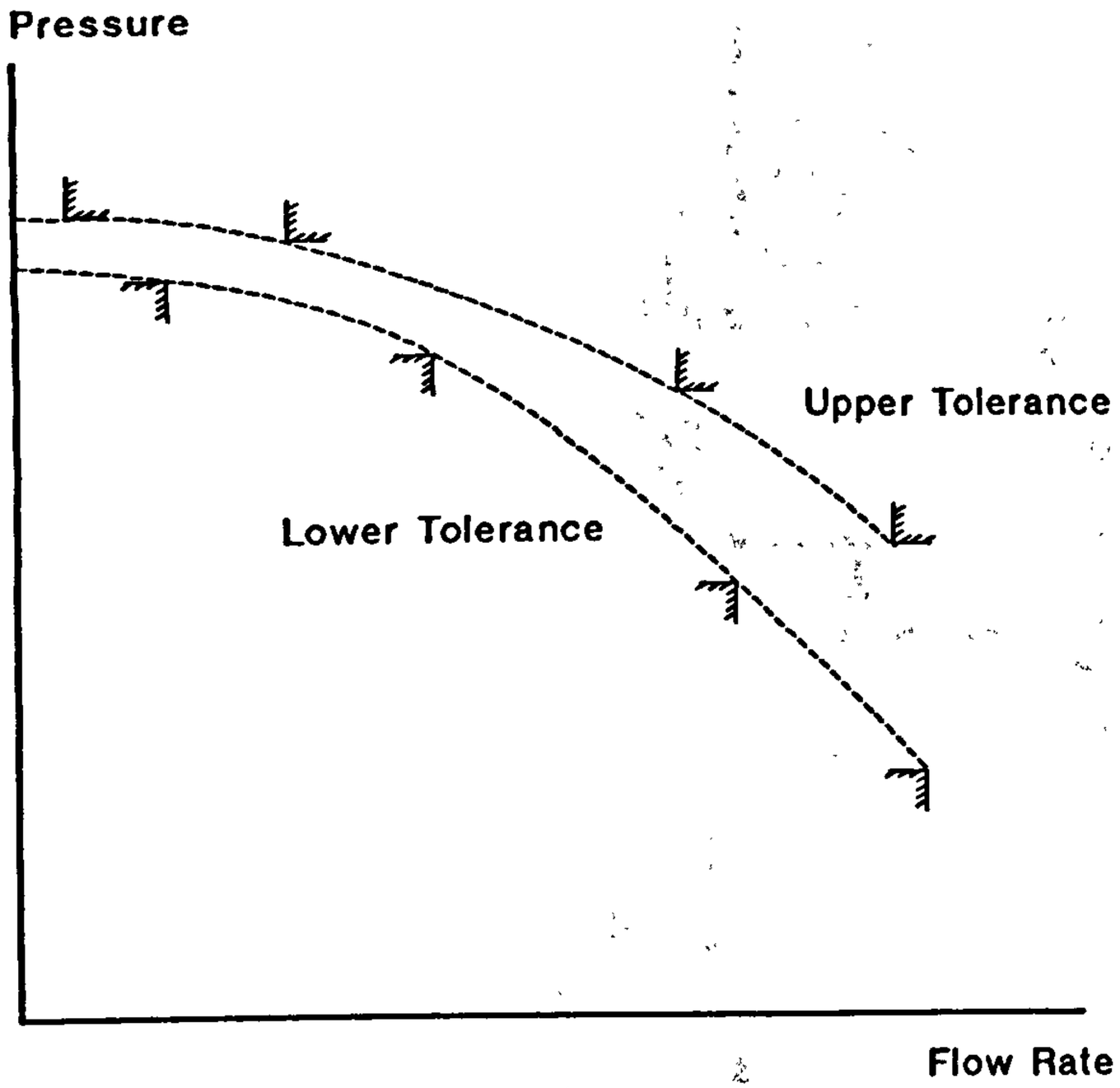

Figure 8.10 Typical Pump Specification

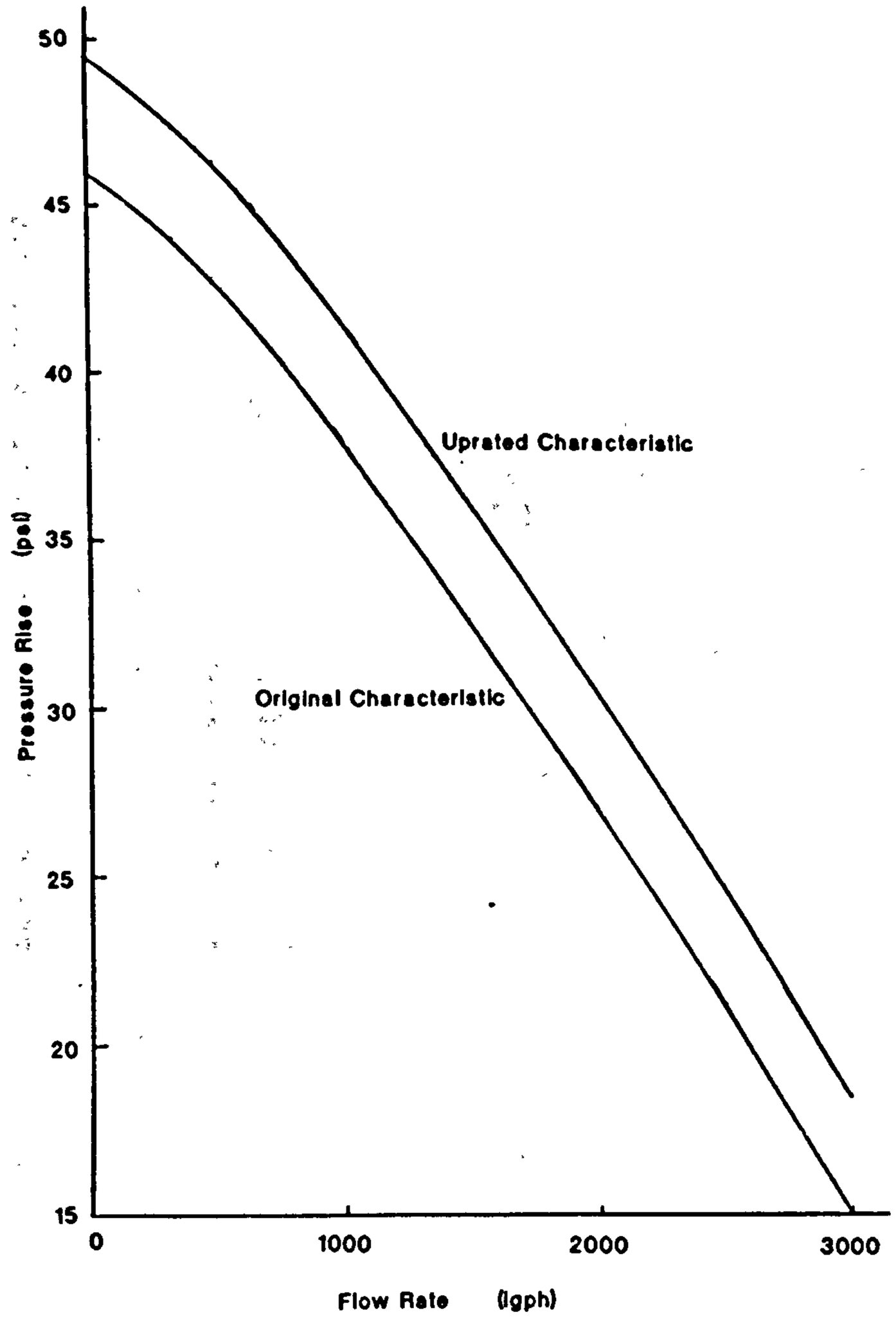

Figure 8.11 Uprated Pump Characteristic.

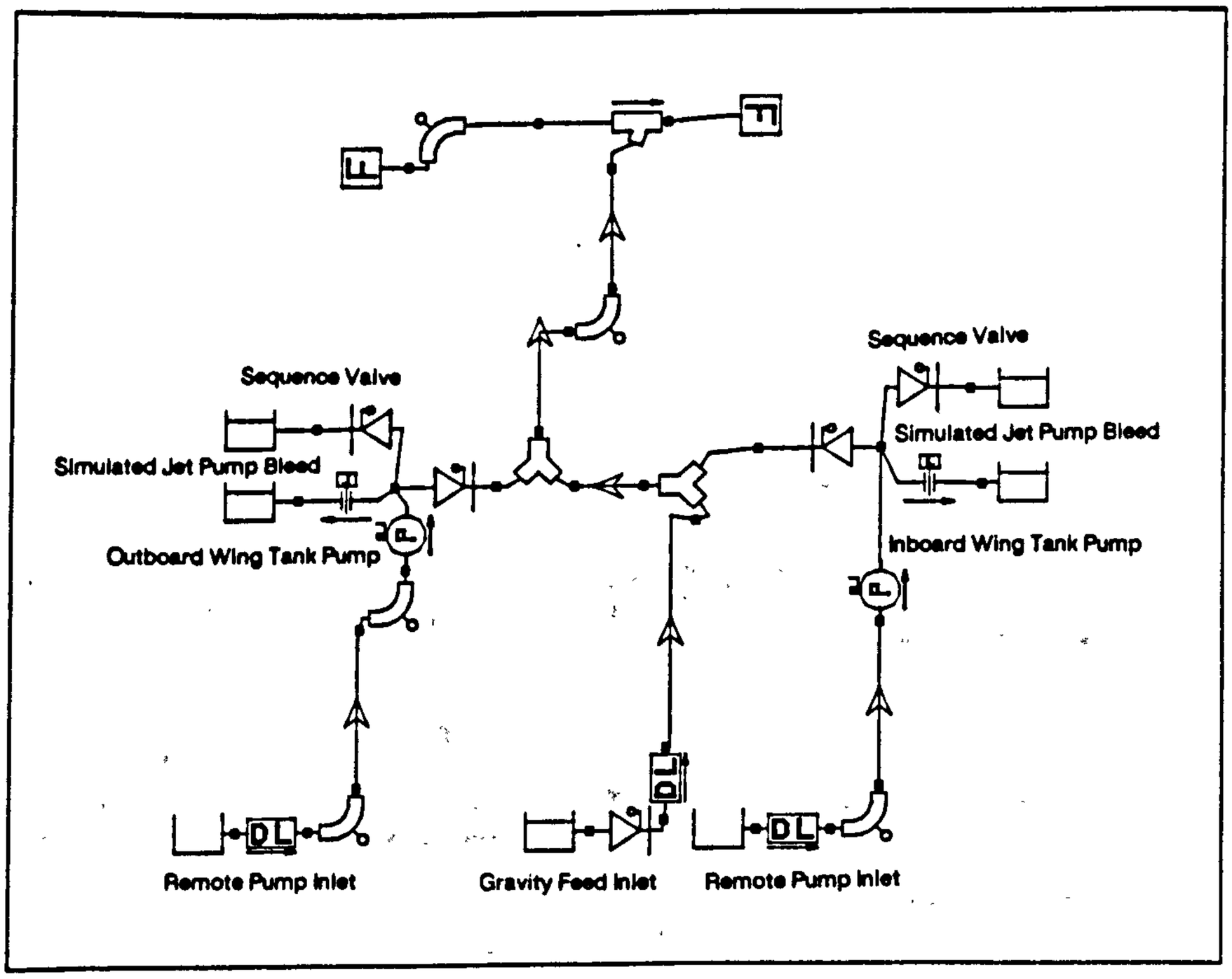

Figure 8.12 Simulation Network for Wing Tank Engine Feed System.

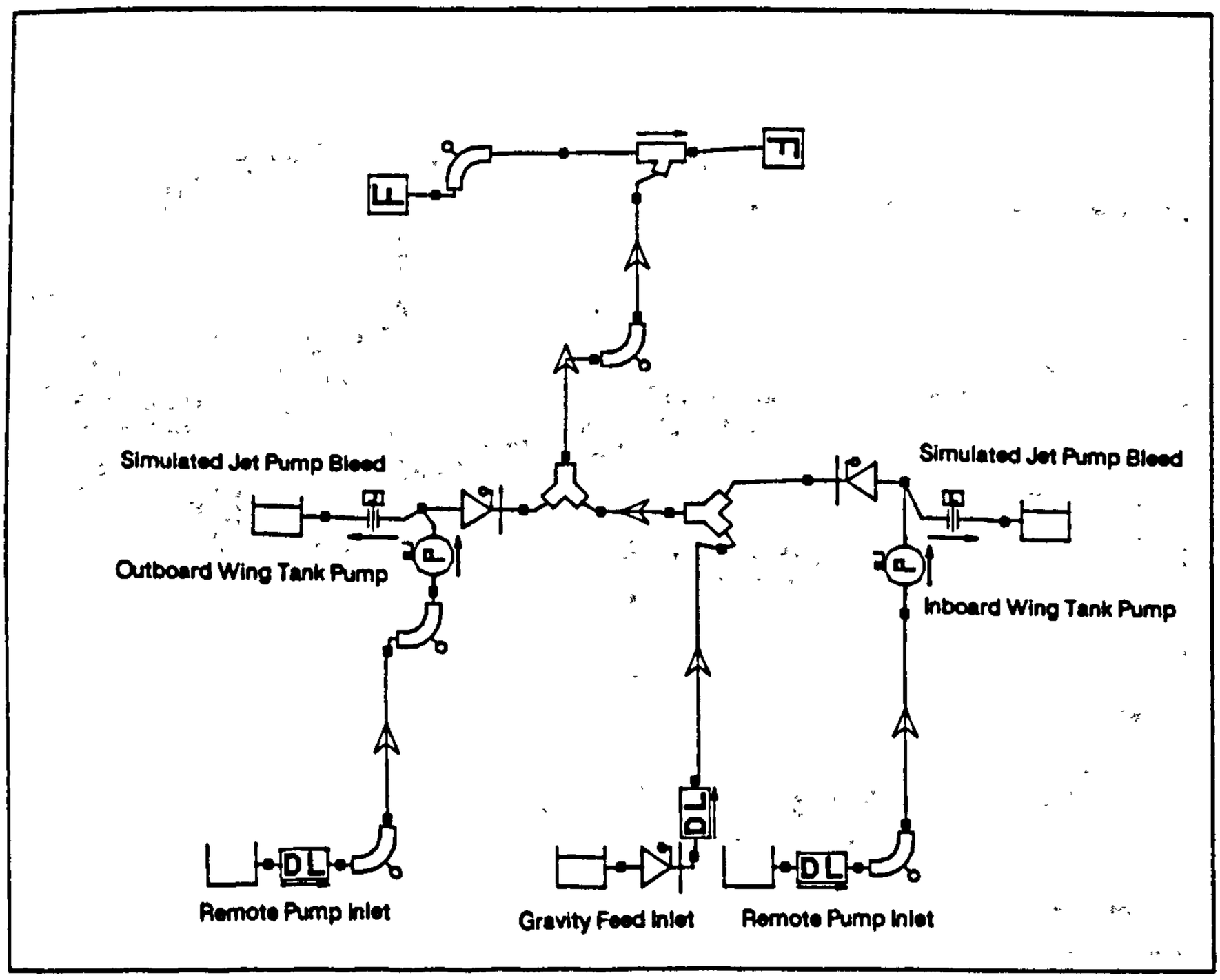

Figure 8.13 Simulation Network for Wing Tank Engine Feed System Without Sequence Valve.

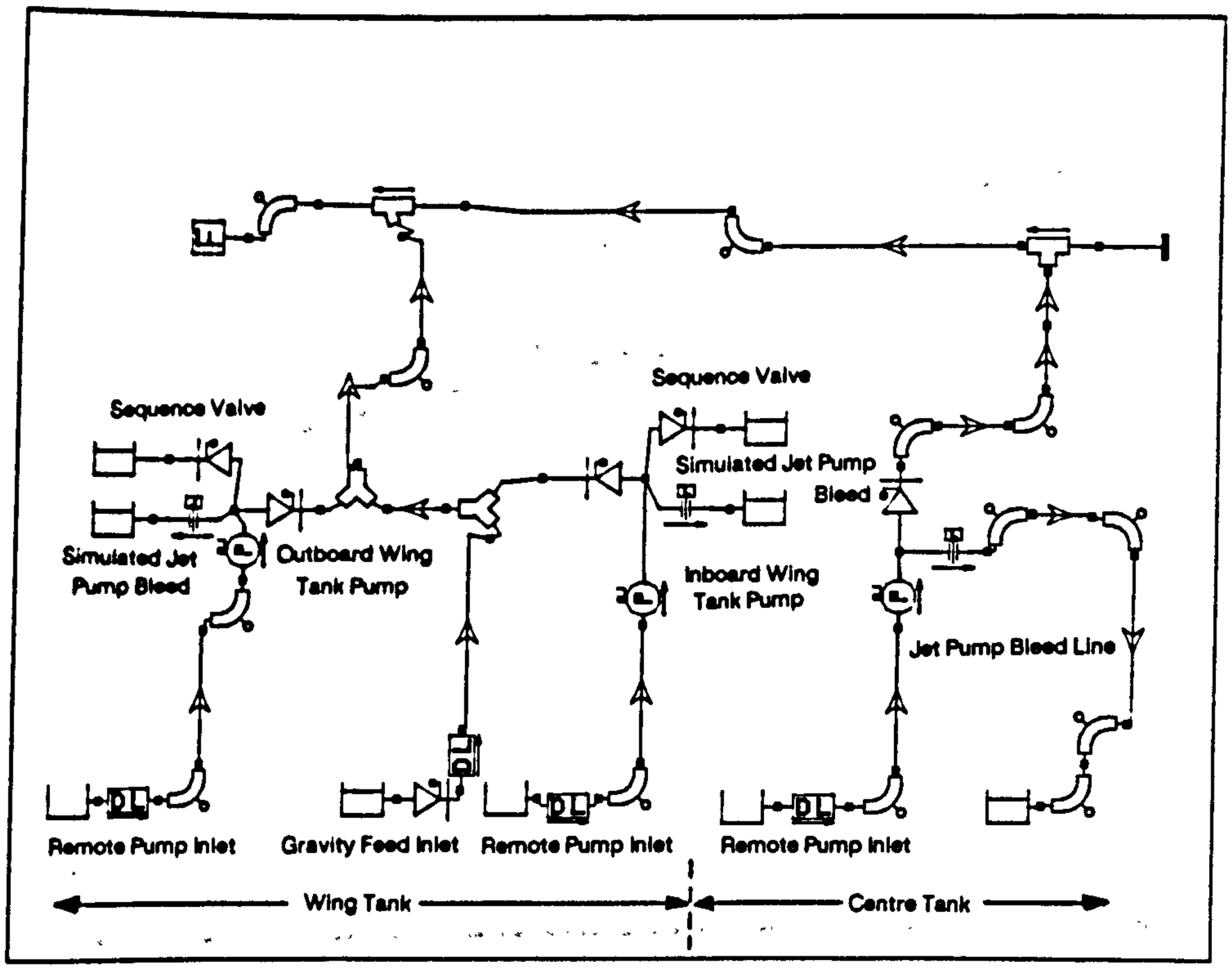

Figure 8.14 Simulation Network for Engine Feed System.

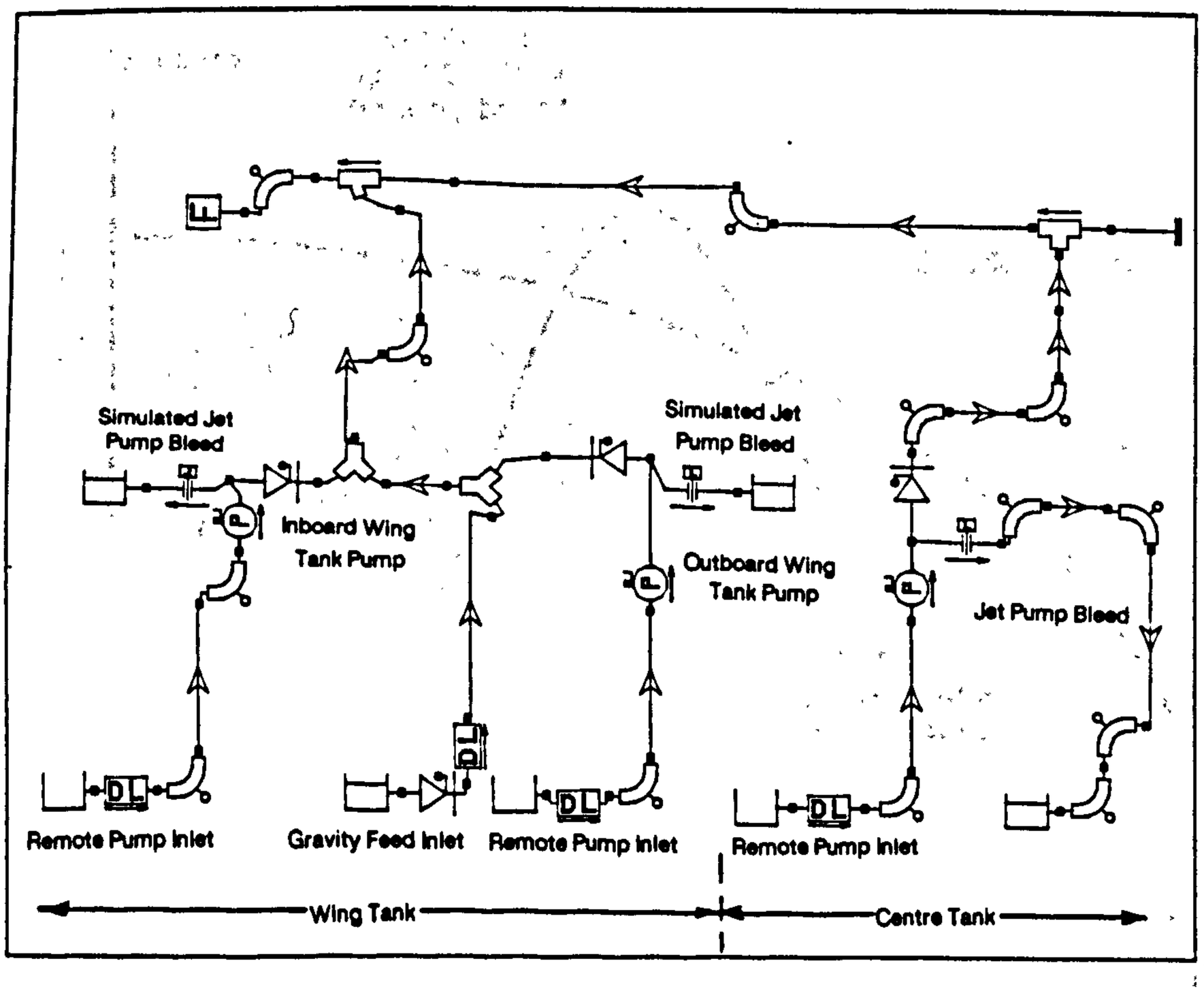

Figure 8.15 Simulation Network for Engine Feed System, Without Sequence Valve.

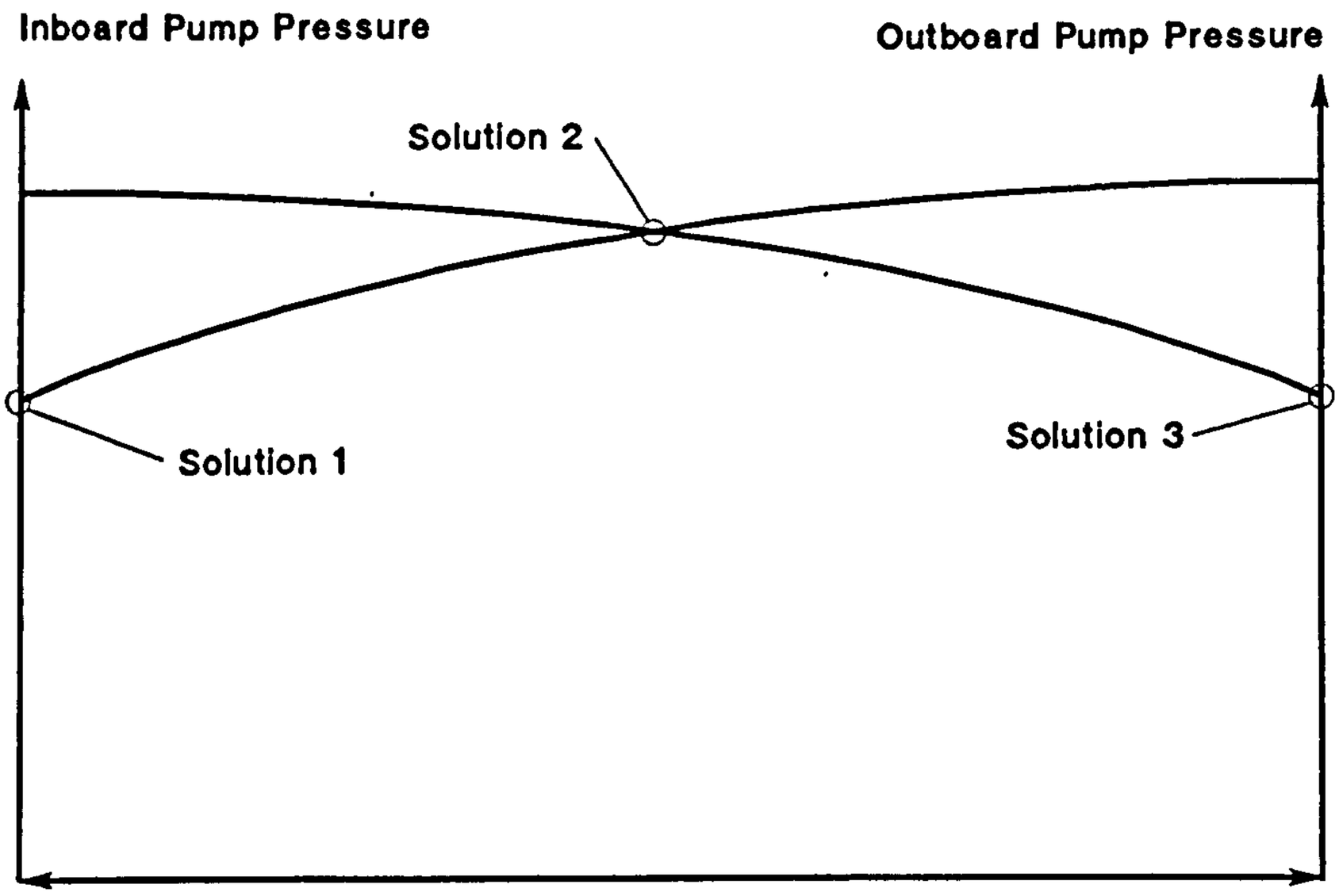

Figure 8.16 Constant Flow Rate Characteristic of Inboard and Outboard Pumps

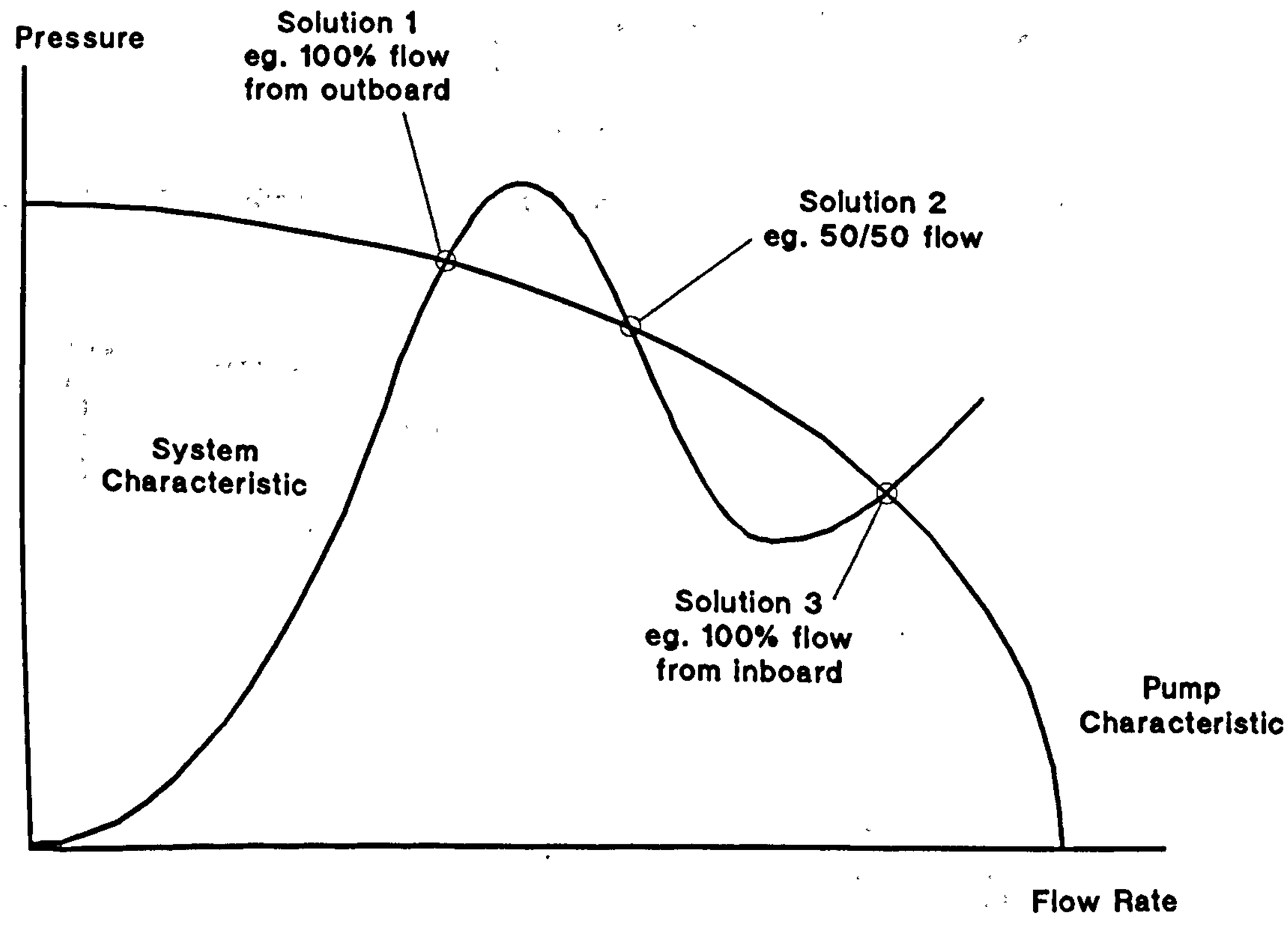

Figure 8.17 Illustrative Tri-Stable System Curve and Single Pump Curve

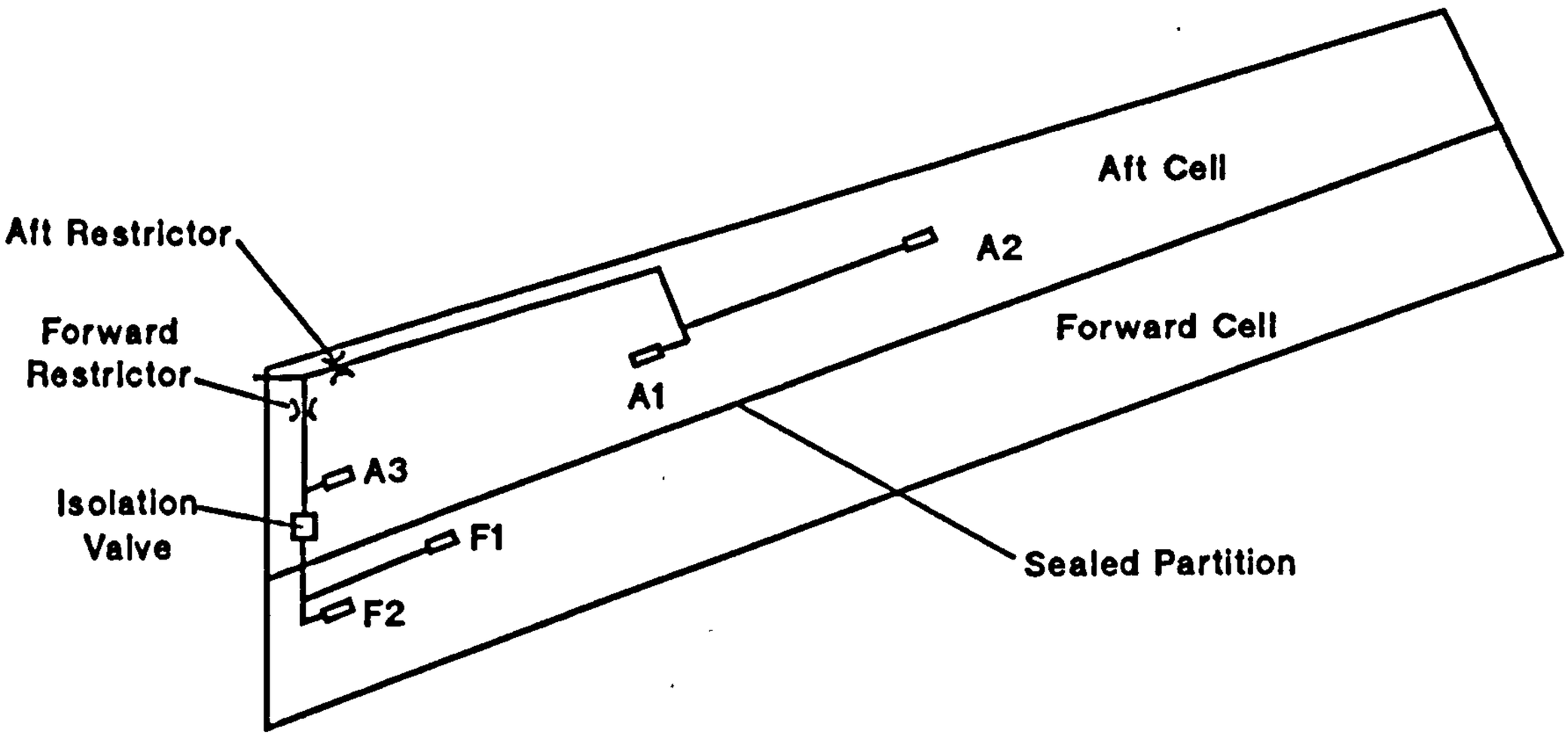

Figure 8.18 Refuel System for a Partioned Tank.

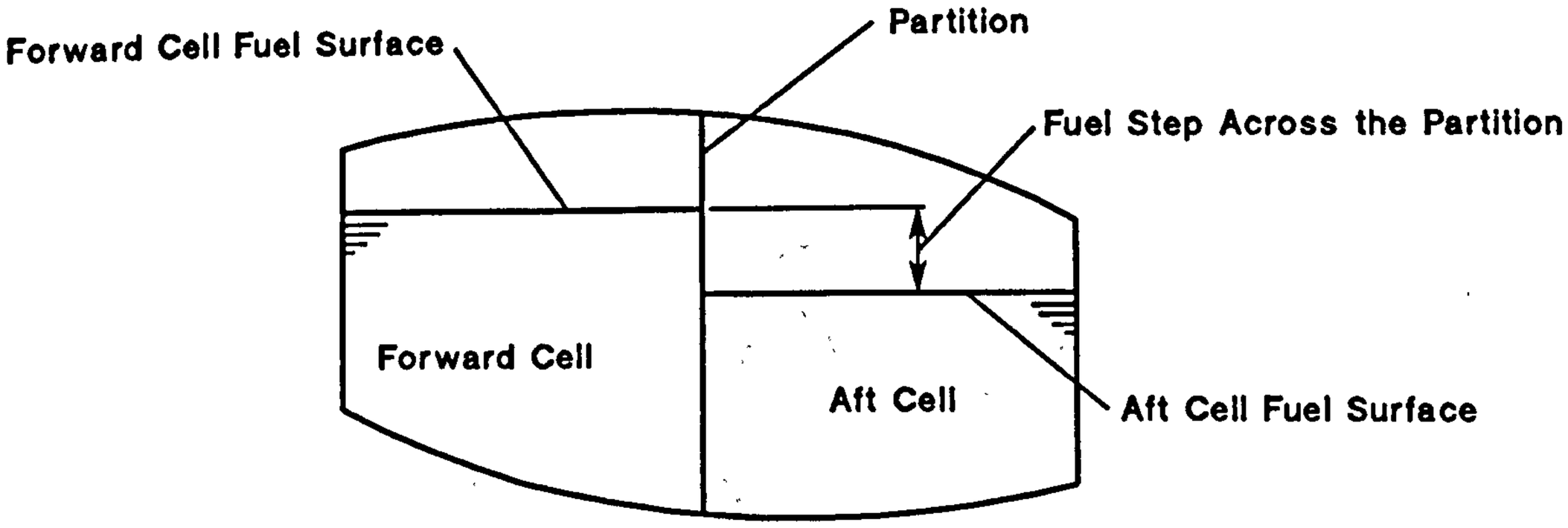

Figure 8.19 View From Wing Root Outboard Showing Fuel Step Across the Partition

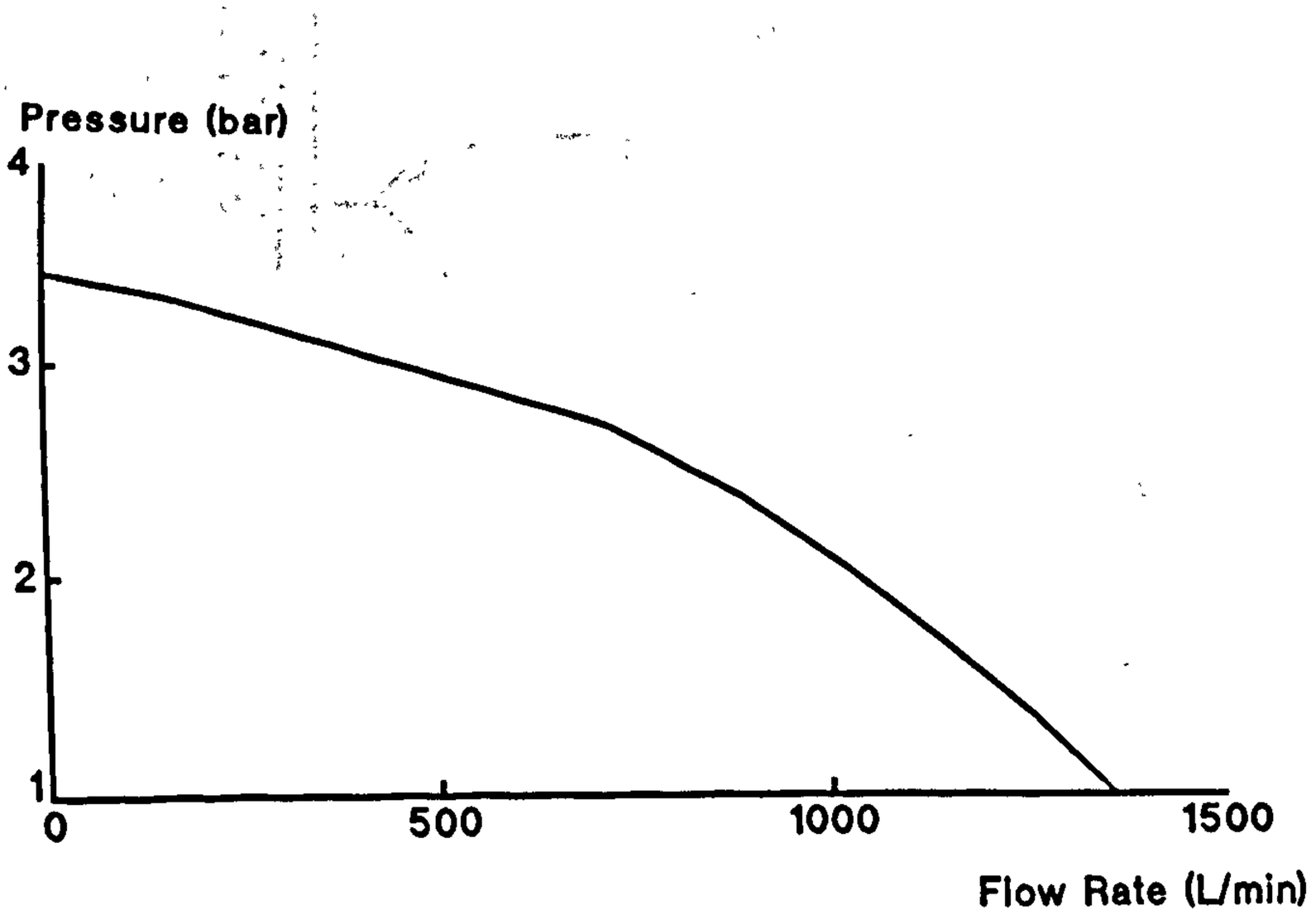

Figure 8.20 Presure, Flow Rate Characteristic of Refuel Supply.

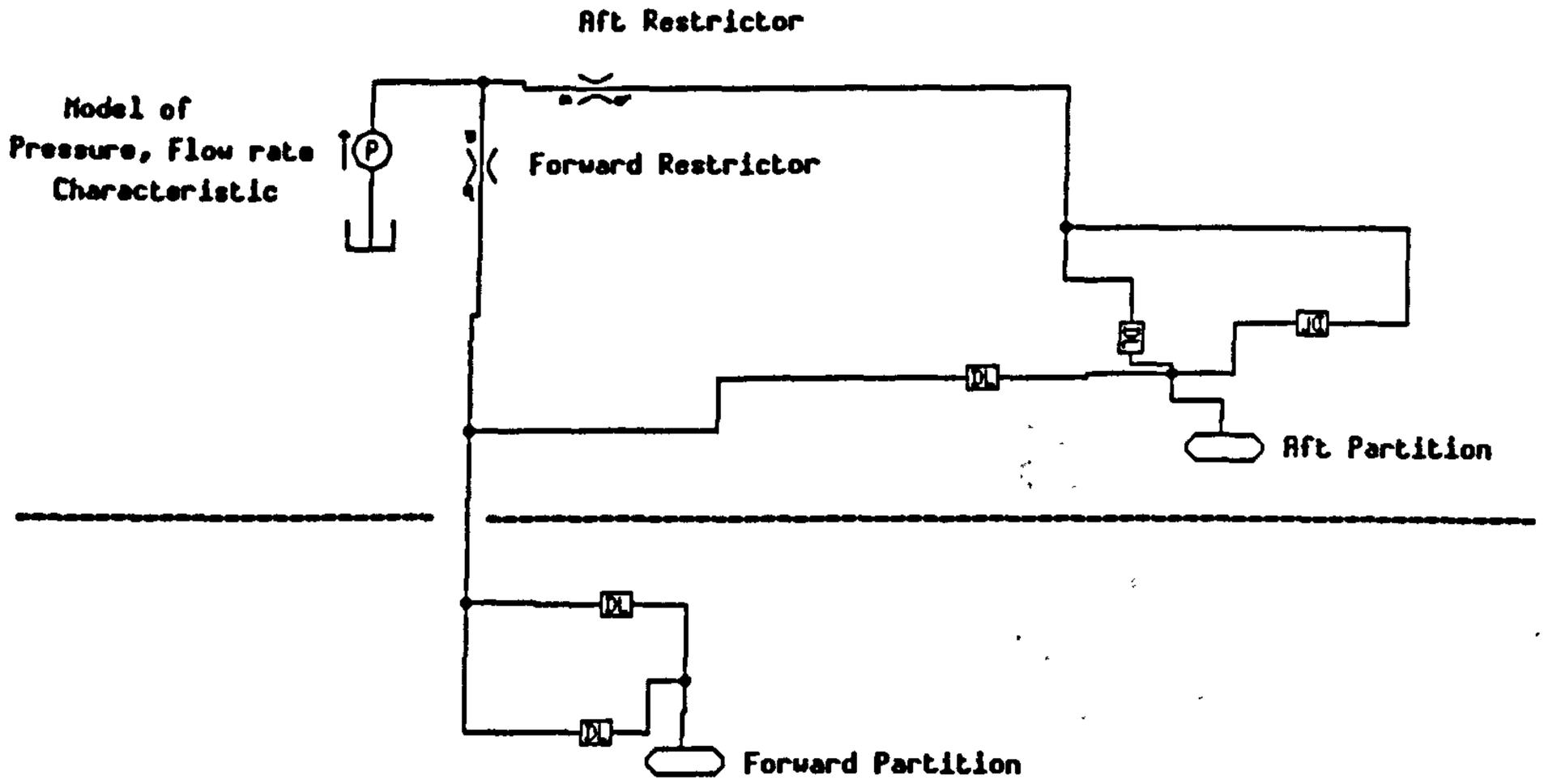

Figure 8.21 Simulation Network for Refuel System of a Partitioned Tank.

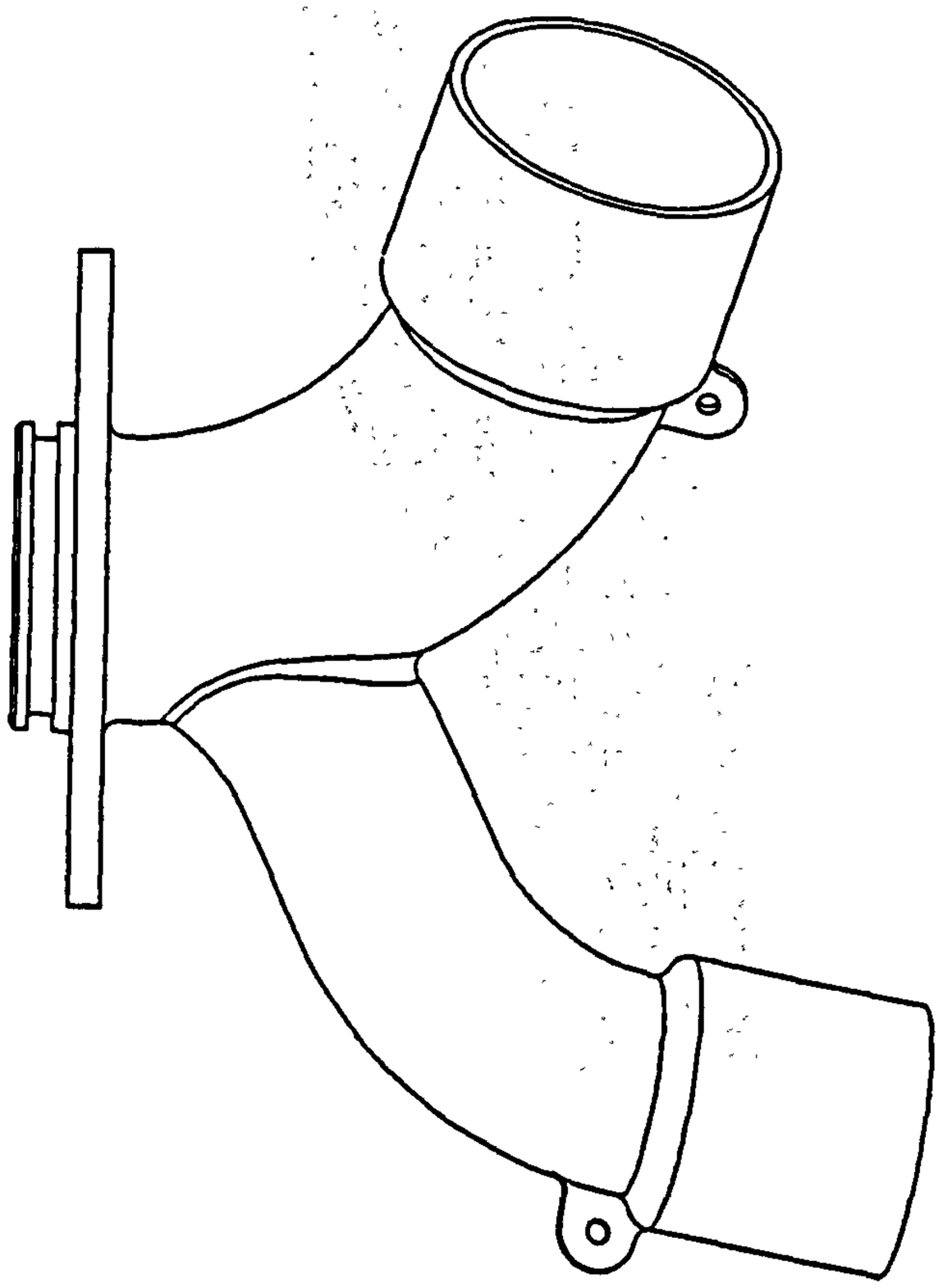

Figure 8.22 Original Junction of Forward Diffusers.

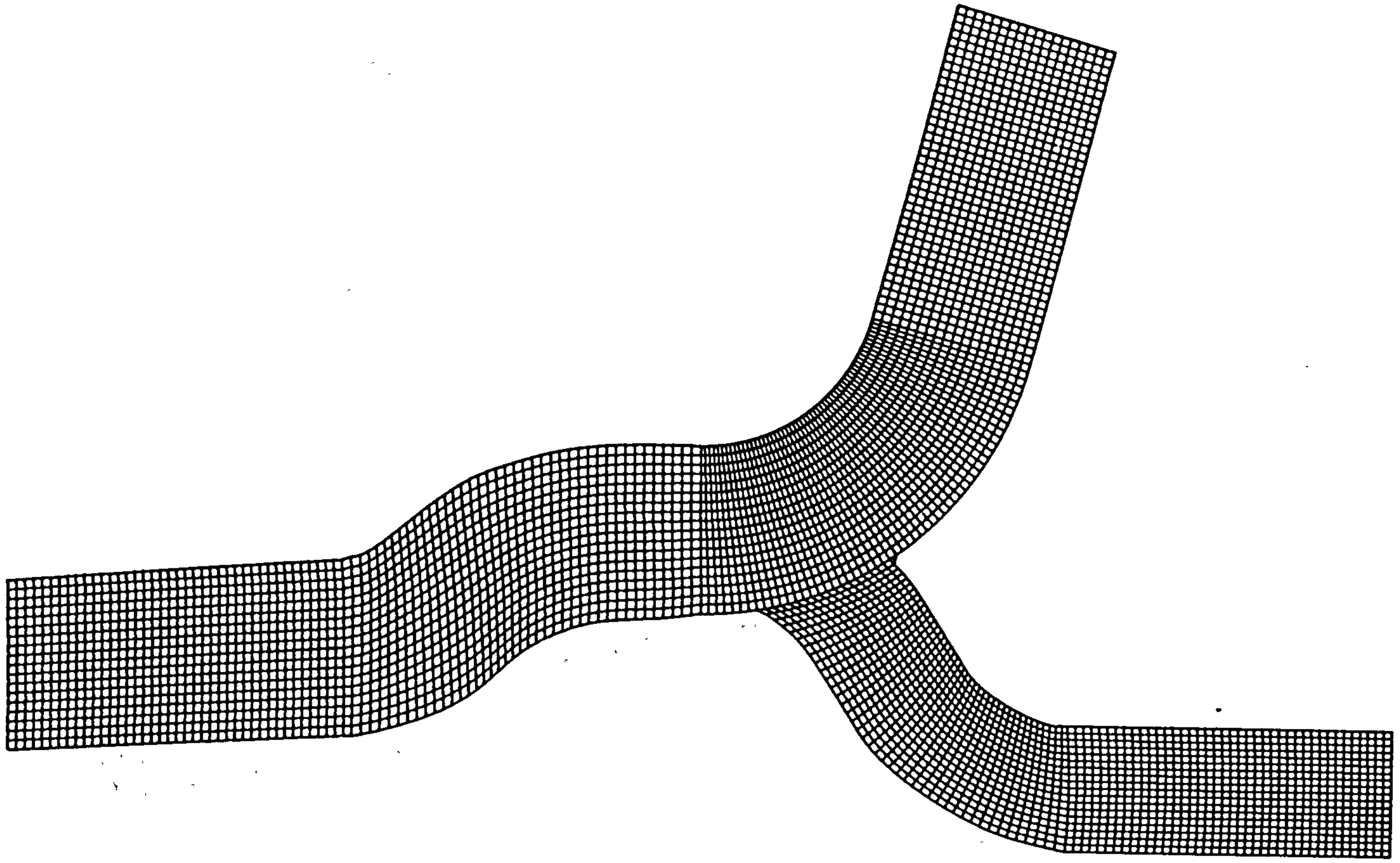

Figure 8.23 Two-Dimensional CFD Model of Original Junction.

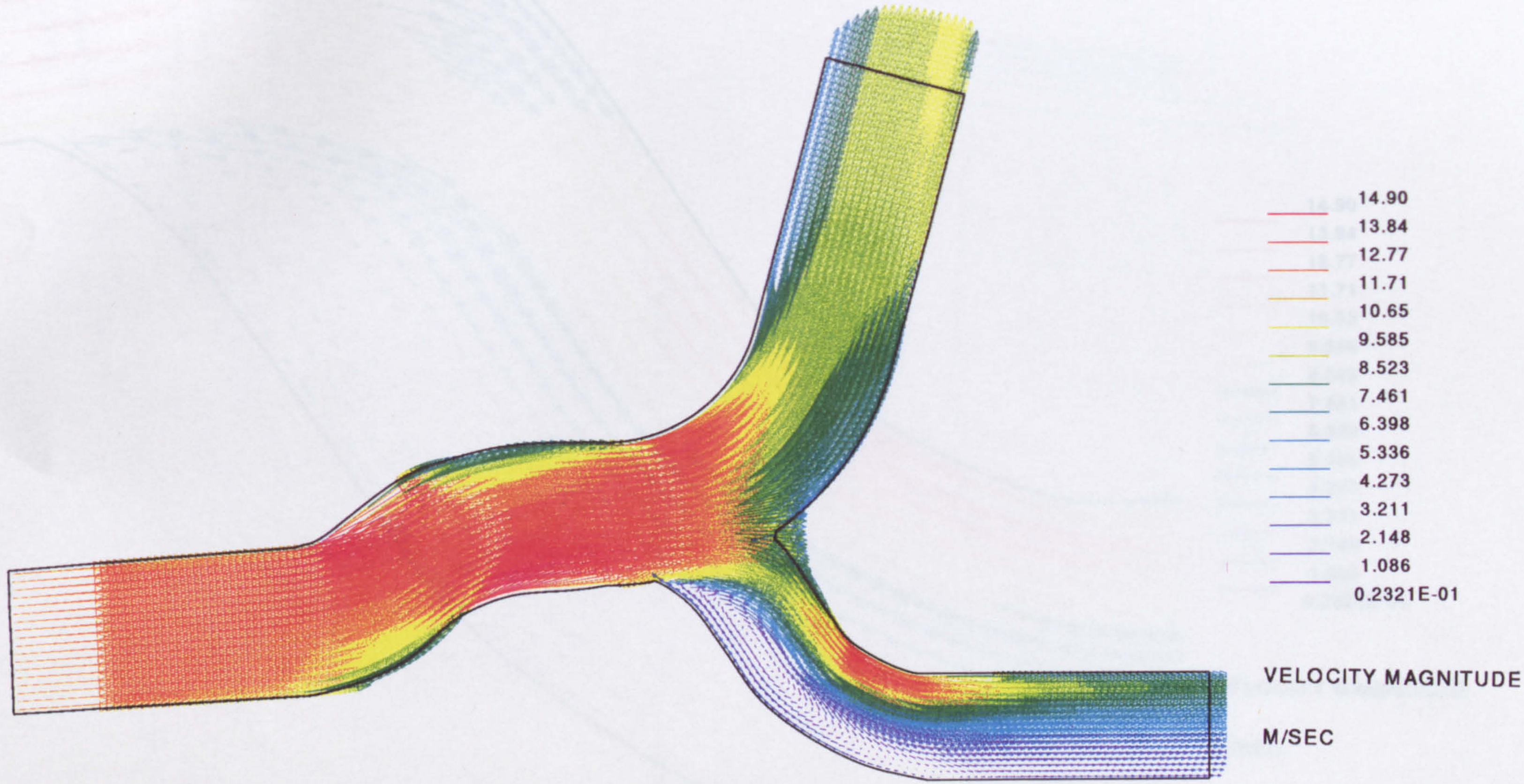

Figure 8.24 CFD Prediction of Flow Rates Through Original Junction.

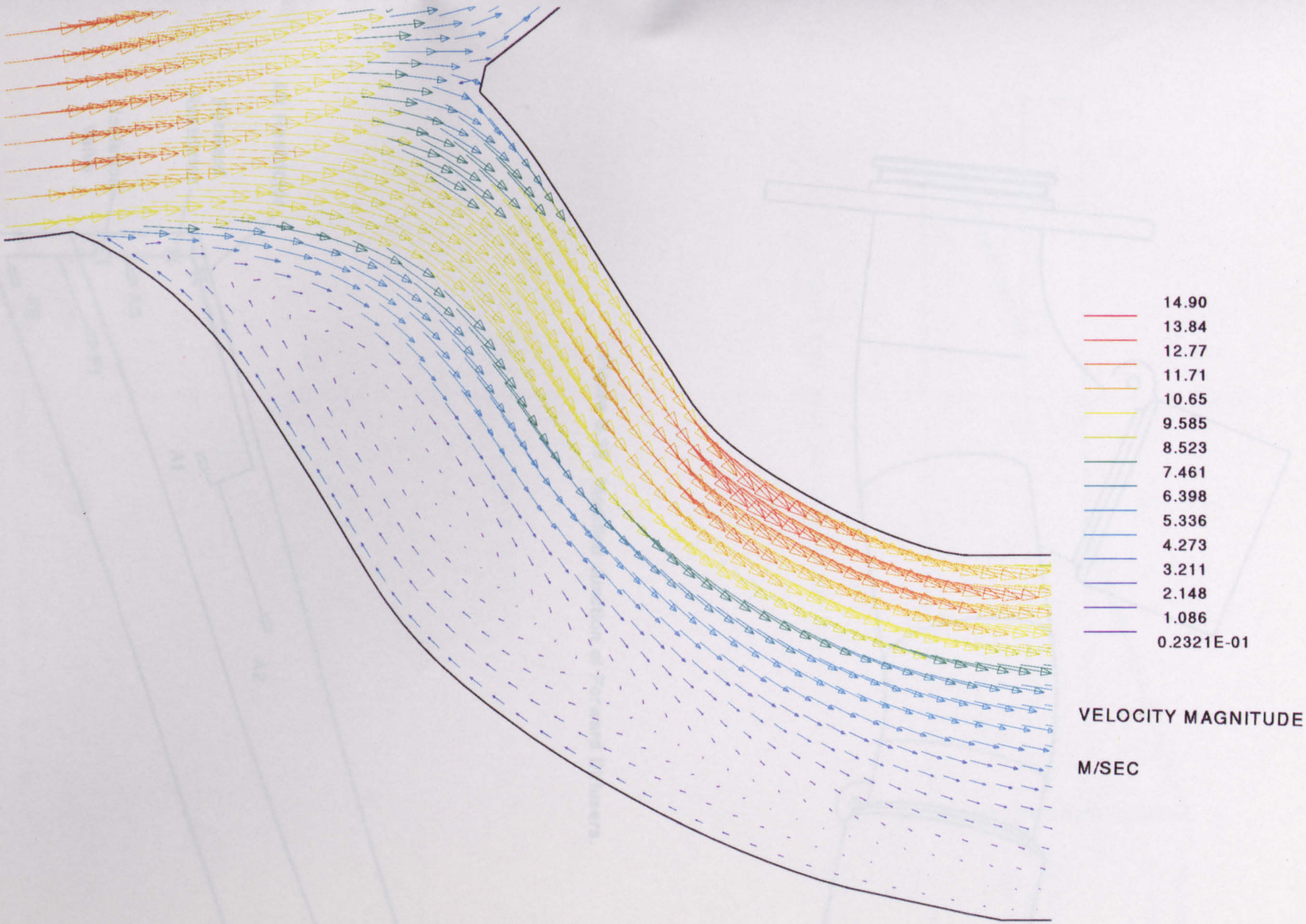

Figure 8.25 Detailed View of Recirculation Zone Predicted by CFD.

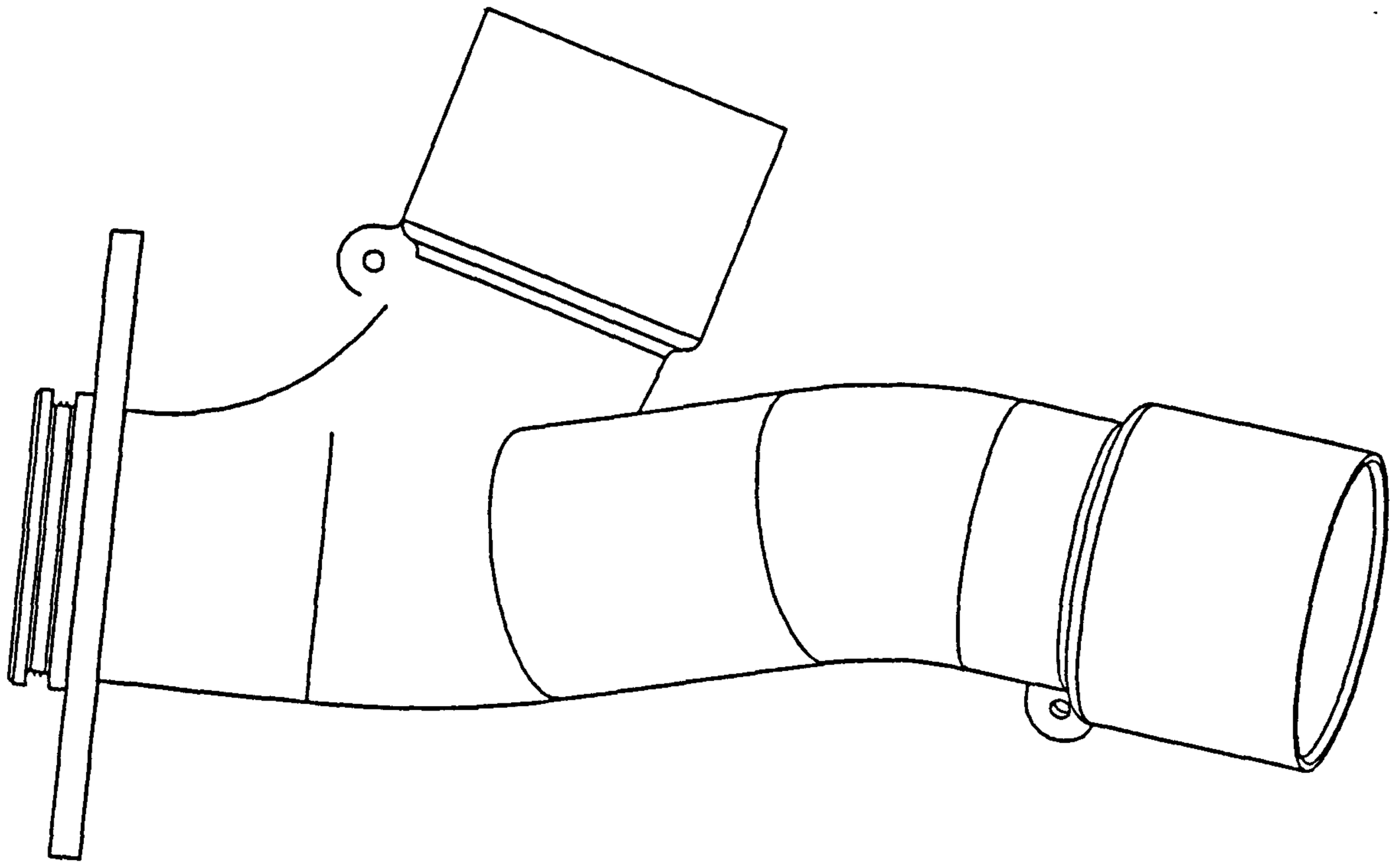

Figure 8.26 Modified Junction of Forward Diffusers.

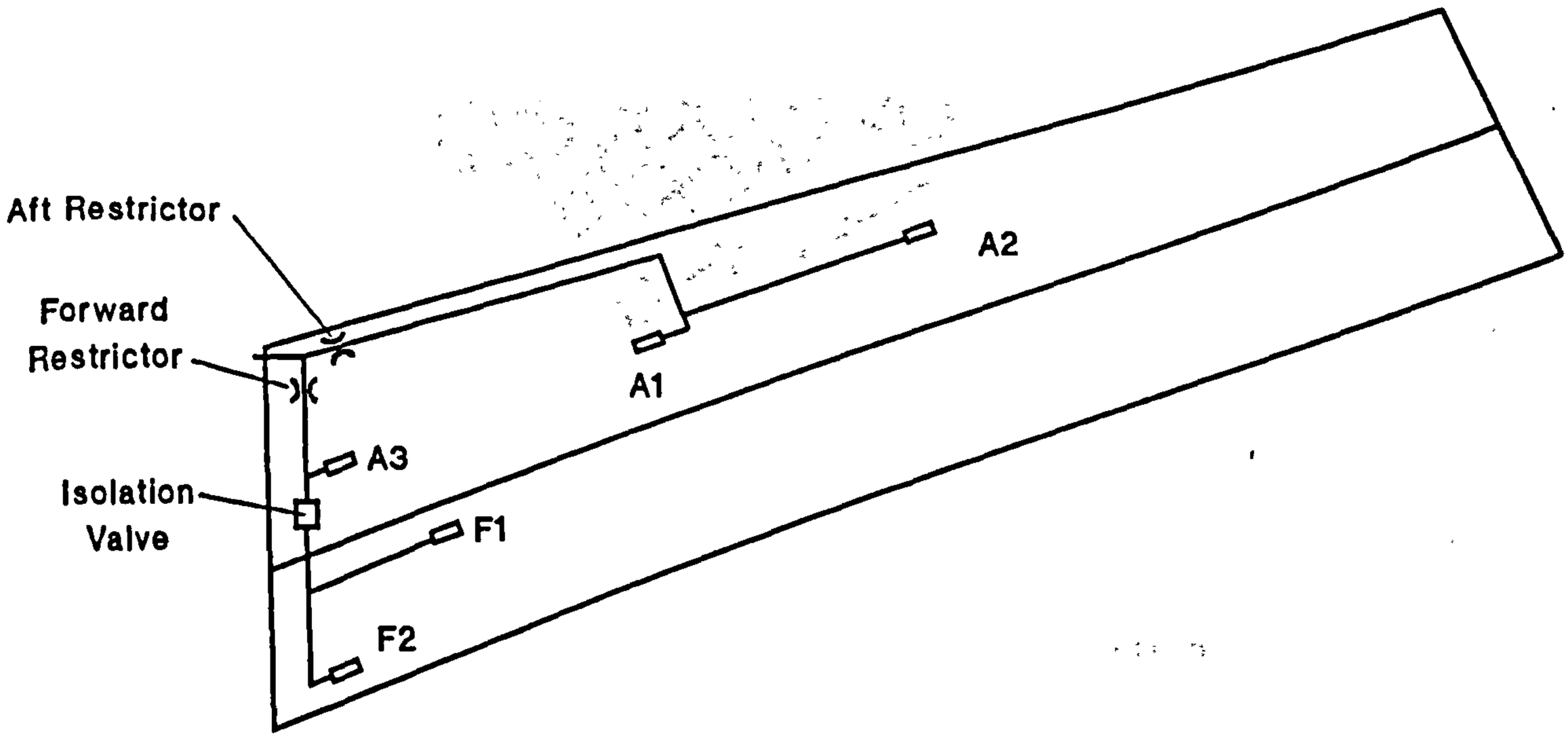

Figure 8.27 Modification to Refuel System.

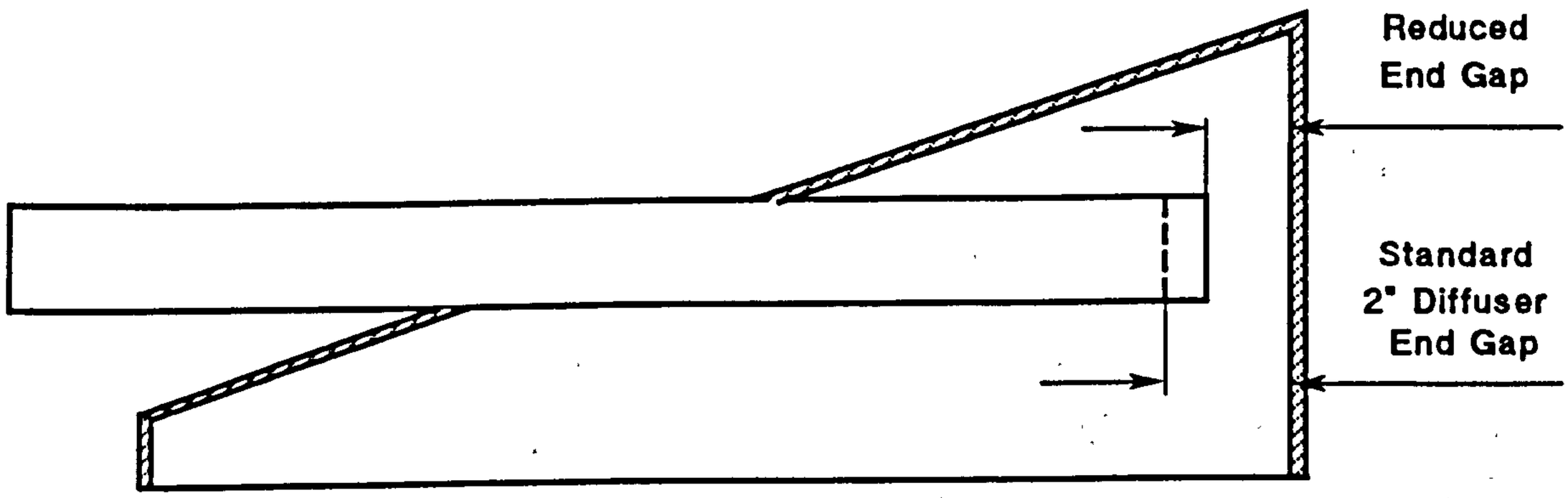

Figure 8.28 Modification to Diffuser End Gap.

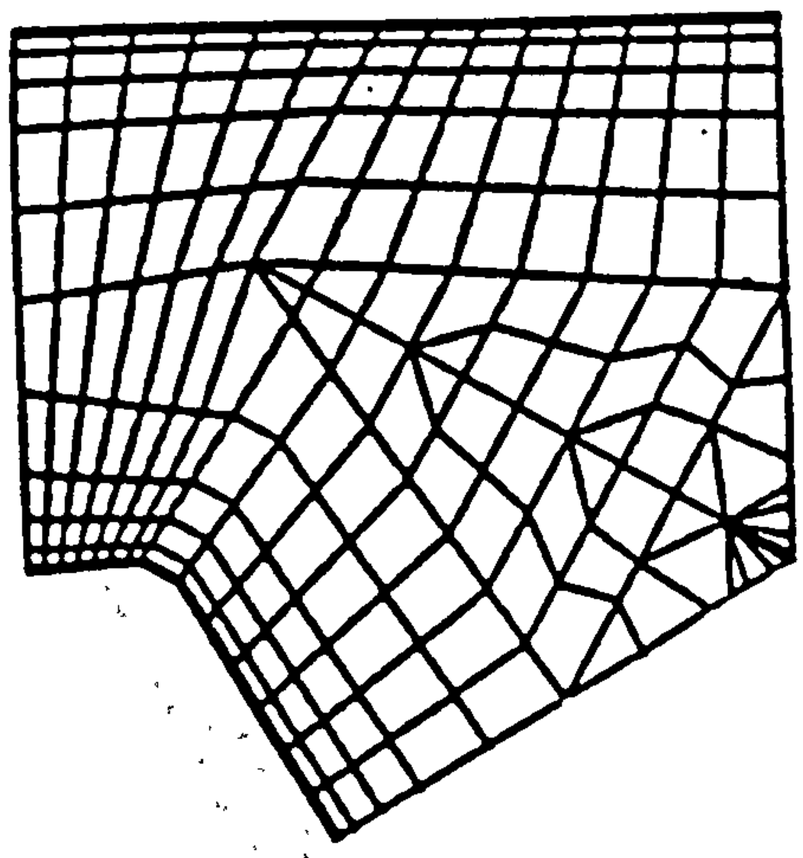

Figure 8.29 Modification of Three-Dimensional 'Y' Junction to Represent a Straight Through Branch.

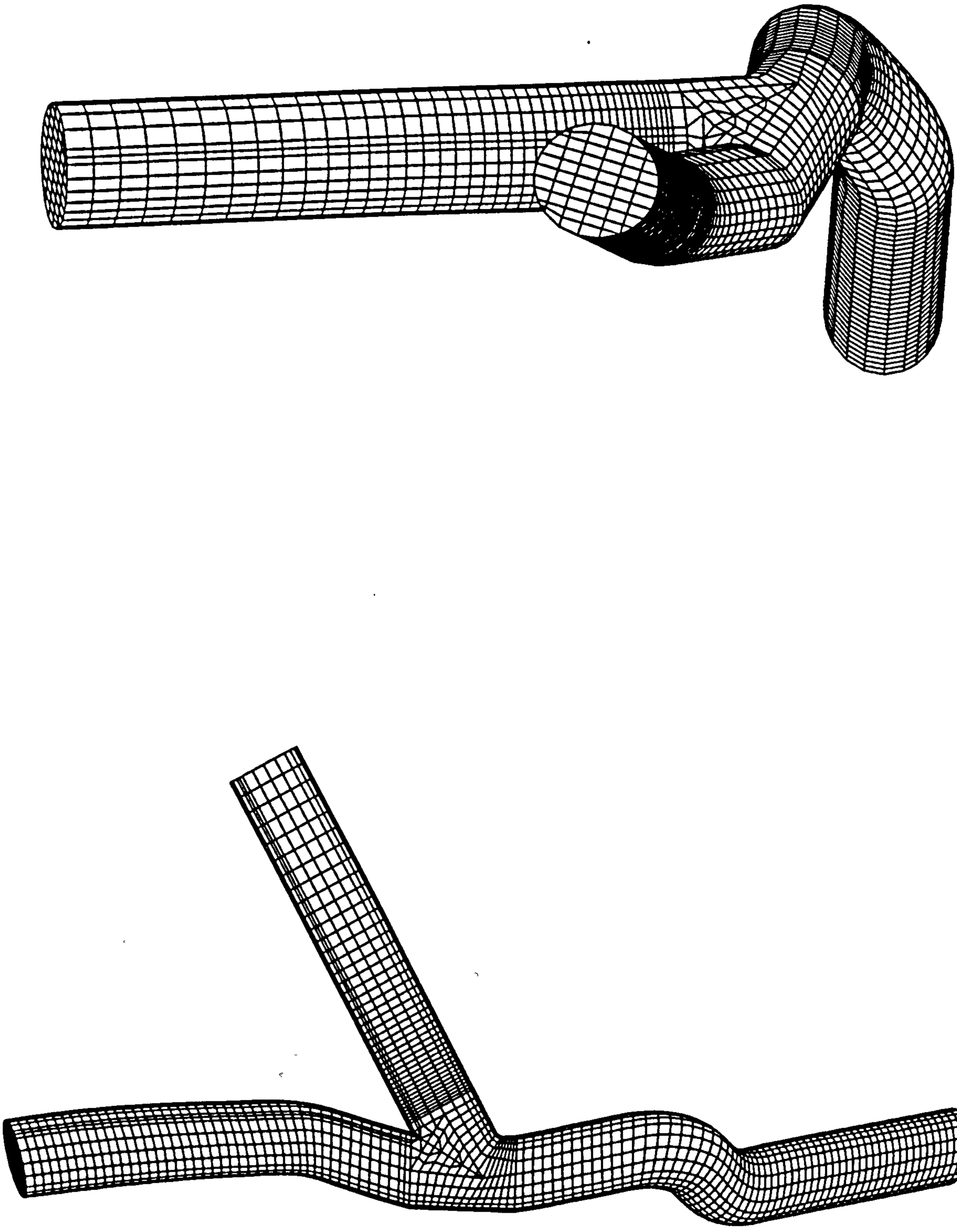

Figure 8.30 Three-Dimensional CFD Model of Modified Junction.

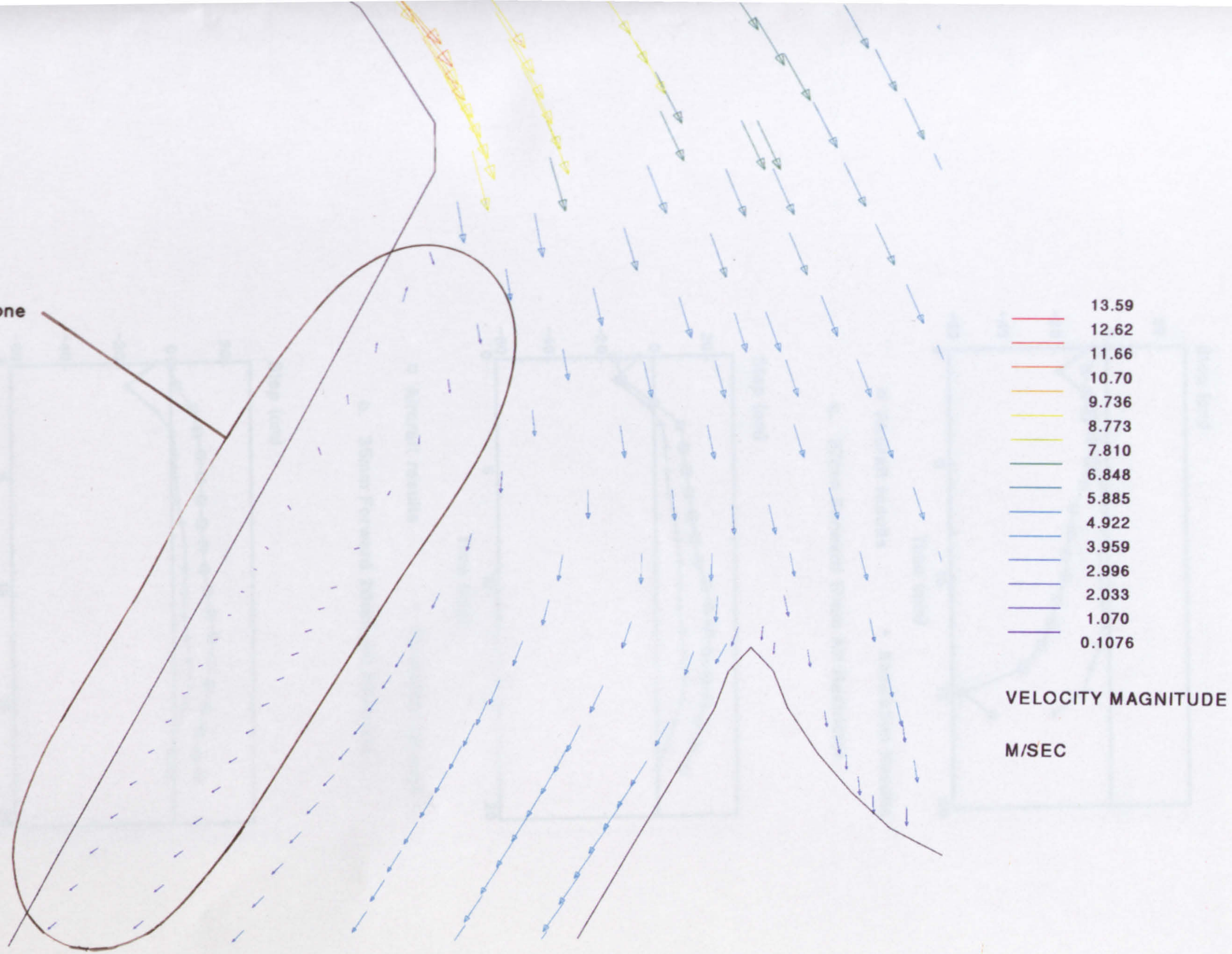

Figure 8.31 CFD Prediction of Recirculation in Modified Junction. Section Plot at 10% Diameter.

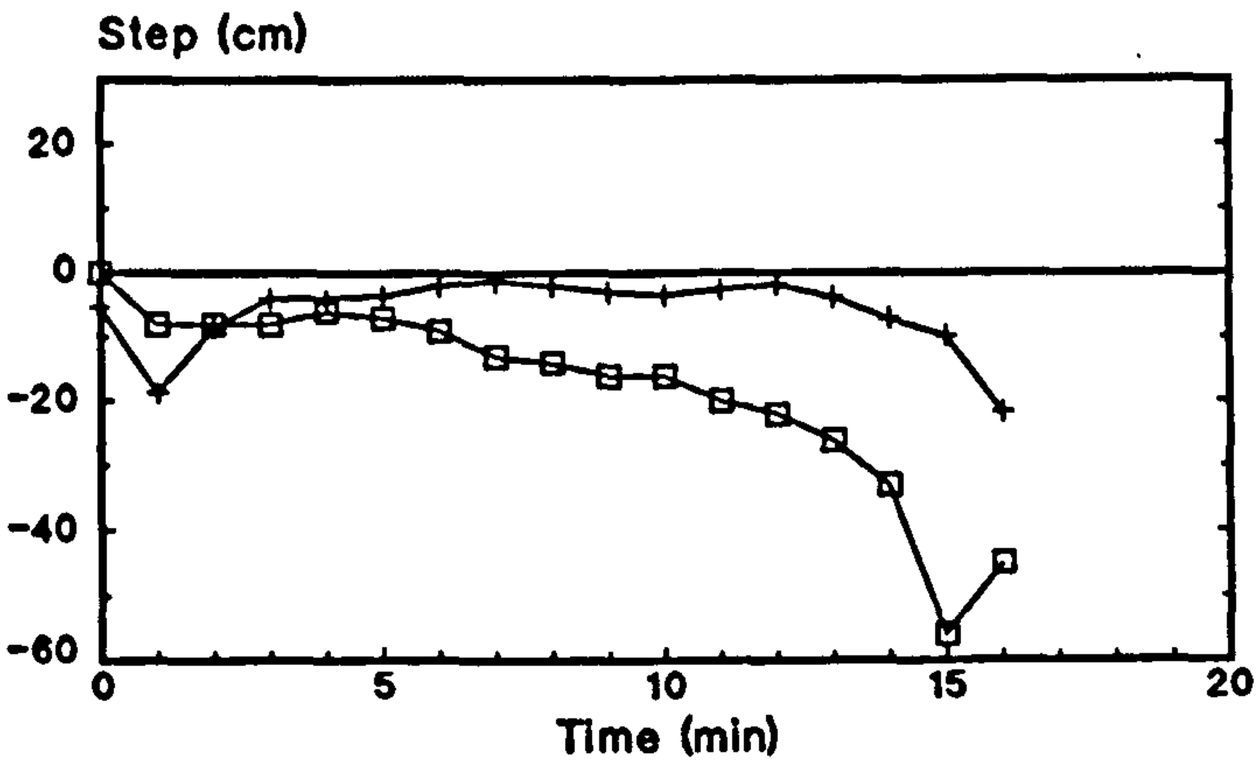

□ Aircraft results + Simulation Results

a. 37mm Forward 17mm Aft Restrictor.

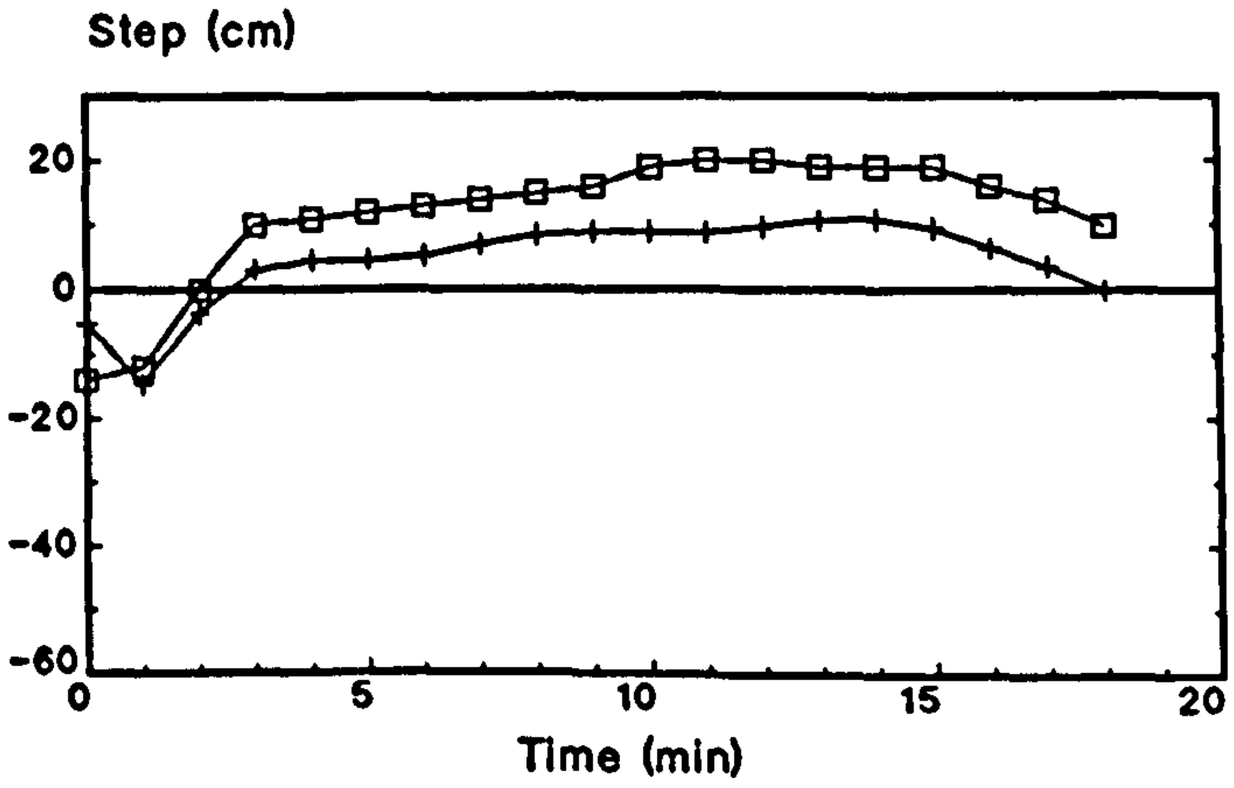

□ Aircraft results + Simulation Results

b. 35mm Forward 20mm Aft Restrictor.

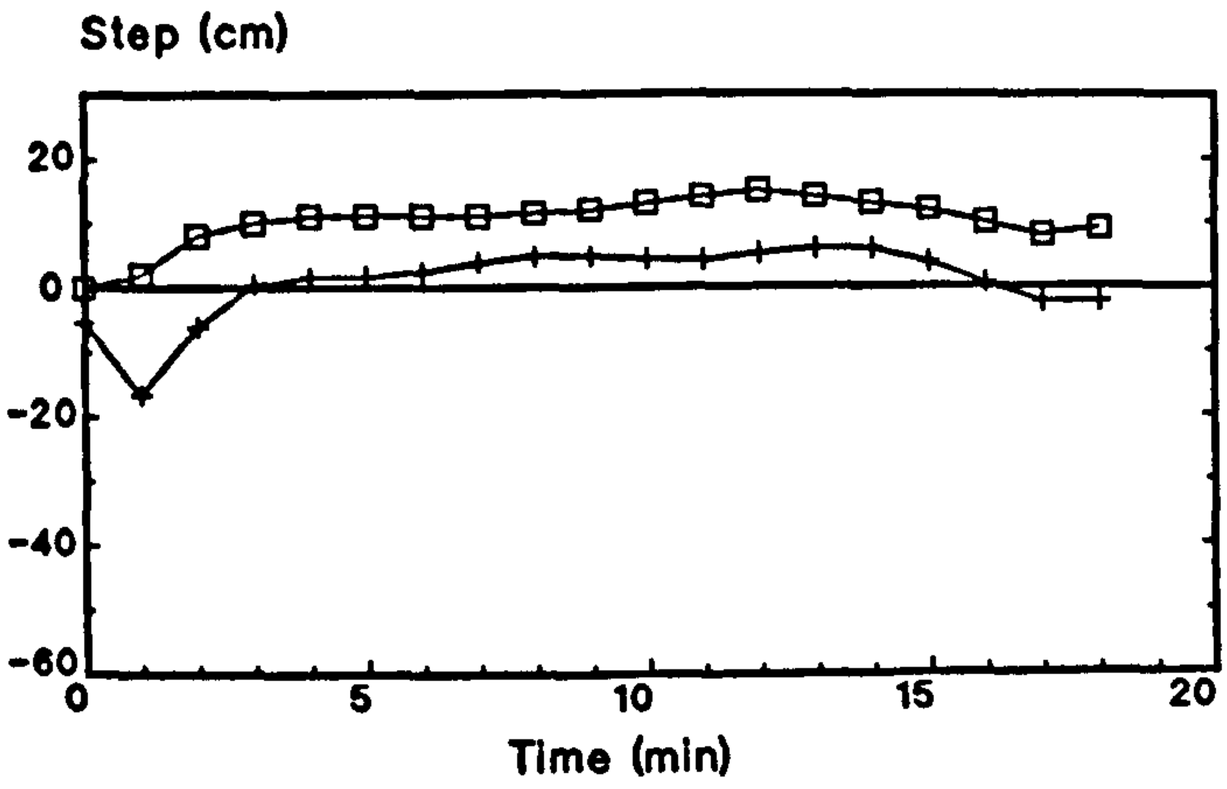

□ Aircraft results + Simulation Results

c. 36mm Forward, 19mm Aft Restrictor.

Figure 8.32 Fuel Steps Across the Partition

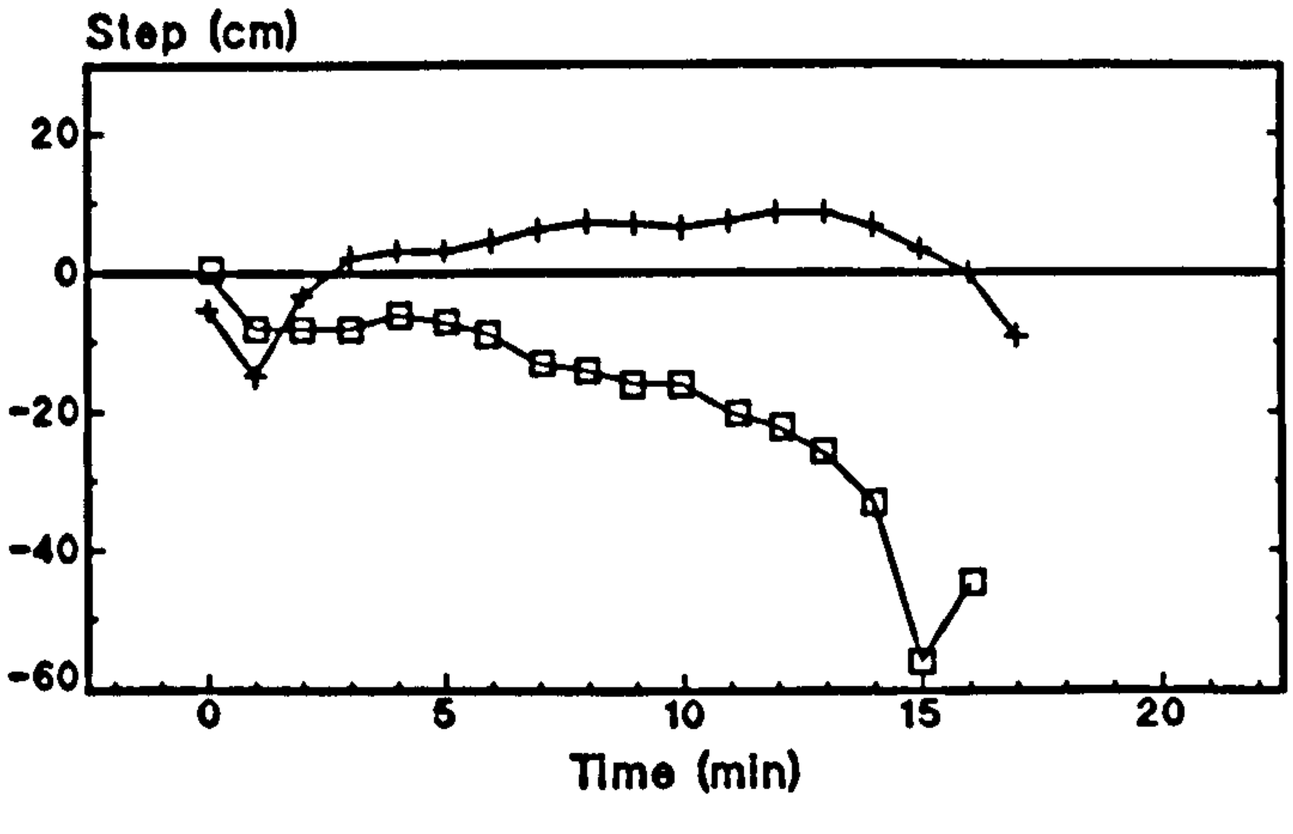

□ Aircraft Results + Simulation Results

a. 37mm Forward, 17mm Aft Restrictor

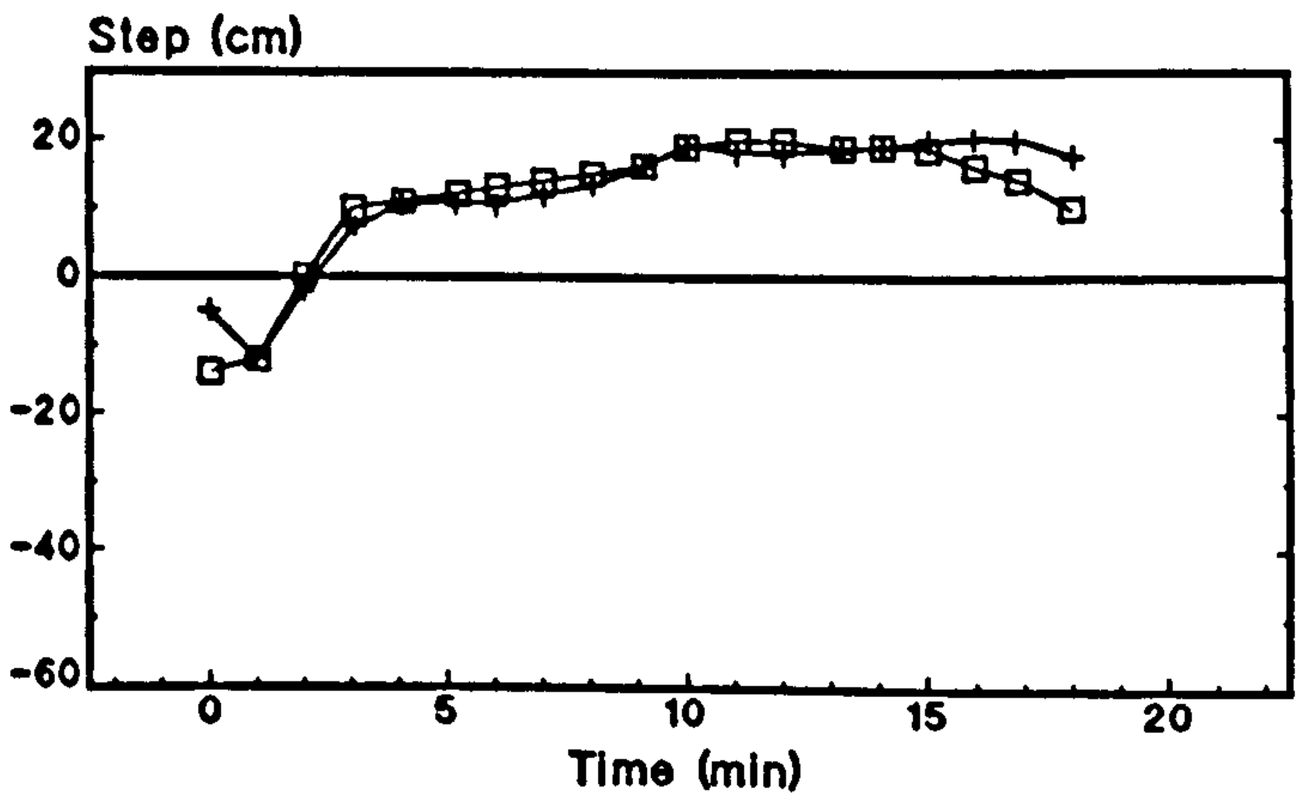

□ Aircraft Results + Simulation Results

b. 35mm Forward, 20mm Aft Restritor.

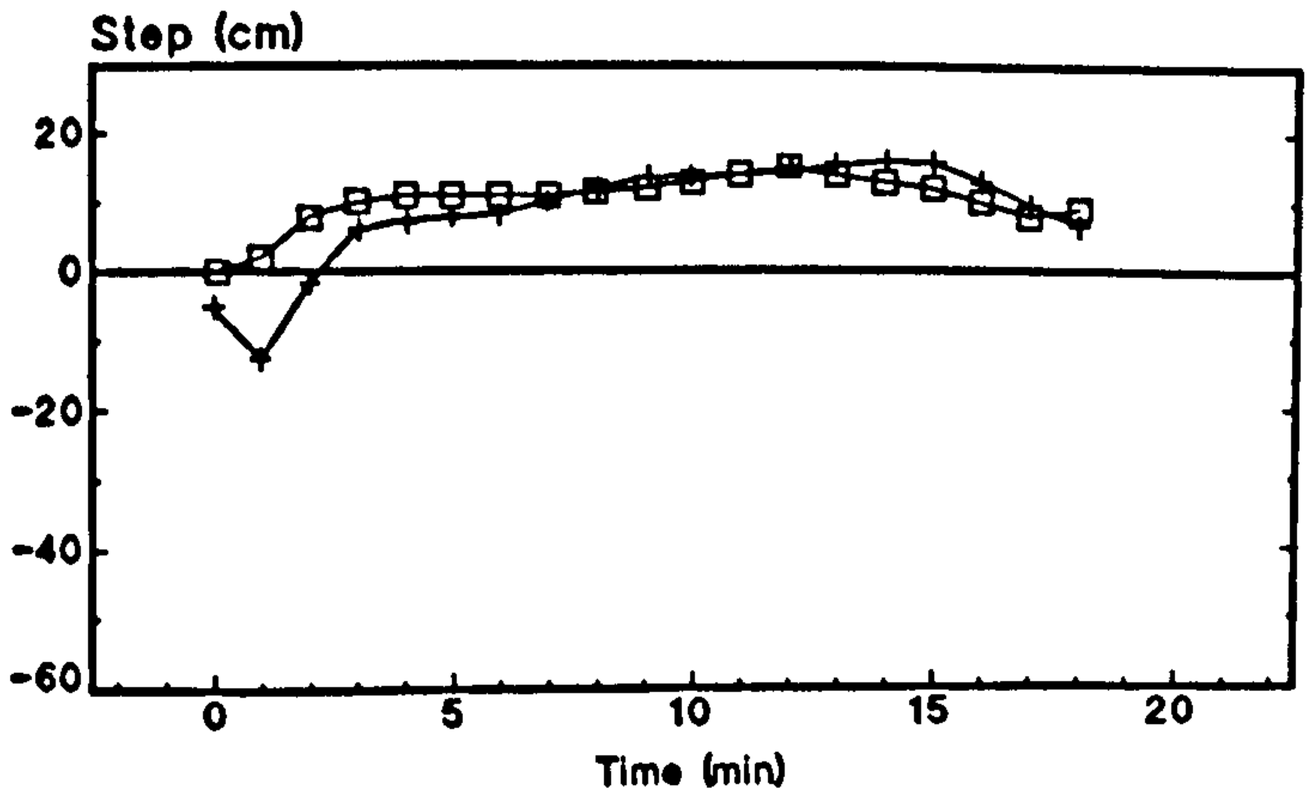

□ Aircraft Results + Simulation Results

c. 36mm Forward, 19mm Aft Restrictor

Figure 8.33 Fuel Steps Across the Partition with the Modified Loss Coefficient